UNCLASSIFIED

AD 442879

DEFENSE DOCUMENTATION CENTER

FOR

SCIENTIFIC AND TECHNICAL INFORMATION

CAMERON STATION ALEXANDRIA, VIRGINIA

UNCLASSIFIED

This Document
Reproduced From
Best Available Copy

REPRODUCTION QUALITY NOTICE

This document is the best quality available. The copy furnished to DTIC contained pages that may have the following quality problems:

- Pages smaller or larger than normal.
- Pages with background color or light colored printing.
- Pages with small type or poor printing; and or
- Pages with continuous tone material or color photographs.

Due to various output media available these conditions may or may not cause poor legibility in the microfiche or hardcopy output you receive.

☐ If this block is checked, the copy furnished to DTIC contained pages with color printing, that when reproduced in Black and White, may change detail of the original copy.

NOTICE: When government or other drawings, specifications or other data are used for any purpose other than in connection with a definitely related government procurement operation, the U. S. Government thereby incurs no responsibility, nor any obligation whatsoever; and the fact that the Government may have formulated, furnished, or in any way supplied the said drawings, specifications, or other data is not to be regarded by implication or otherwise as in any manner licensing the holder or any other person or corporation, or conveying any rights or permission to manufacture, use or sell any patented invention that may in any way be related thereto.

442879
AD No. ___
DDC FILE COPY

ELECTROMAGNETIC HARMONIC DRIVE LOW INERTIA SERVO ACTUATOR.

TECHNICAL DOCUMENTARY REPORT NO. ASD-TDR-63-466

December 1963

Final rept. Jan 62 - Feb 63

Flight Control Laboratory
Aeronautical Systems Division
Air Force Systems Command
Wright-Patterson Air Force Base, Ohio

Project 8225, Task 822503

DDC
JUL 23 1964
DDC-IRA A

Contract AF33(657)-7731

D. F. Herdeg, H. W. Proctor,
W. B. Spring, G. C. Newton, Jr.

NOTICES

When Government drawings, specifications, or other data are used for any purpose other than in connection with a definitely related Government procurement operation, the United States Government thereby incurs no responsibility nor any obligation whatsoever; and the fact that the Government may have formulated, furnished, or in any way supplied the said drawings, specifications, or other data, is not to be regarded by implication or otherwise as in any manner licensing the holder or any other person or corporation, or conveying any rights or permission to manufacture, use, or sell any patented invention that may in any way be related thereto.

ASTIA release to OTS not authorized.

Qualified requesters may obtain copies of this report from the Armed Services Technical Information Agency, (ASTIA), Arlington Hall Station, Arlington 12, Virginia.

Copies of this report should not be returned to the Aeronautical Systems Division unless return is required by security considerations, contractual obligations, or notice on a specific document.

AD 603 101

FOREWORD

This report summarizes the results of Project No. 8225, Task No. 822503, accomplished under Air Force Contract No. AF33(657)-7731 under cognizance of Mr. Morris Ostgaard of ASD. Principle contributors to the project were Messrs. W. B. Spring, Project Manager, D. F. Herdeg, Project Engineer and H. W. Proctor, G. P. Scott and J. F. Shaw, Jr., all of the Harmonic Drive Division of United Shoe Machinery Corporation and Dr. G. C. Newton, Jr. of Newton Associates. Dr. Newton served as a consultant throughout the project as well as contributing to this report. His aid and encouragement are gratefully acknowledged.

The Project covered the period from January, 1962 to February, 1963. This is the final report.

ABSTRACT

In this research and development project the feasibility of a new type of low inertia electrical servo actuator, designated Electromagnetic Harmonic Drive, is demonstrated. Drastic reduction in inertia, compared to conventional electrical devices, provides for increased power rate, power rate to weight, and power rate to electrical loss characteristics, which are shown to best determine the usefulness of an actuator for fast response, light weight, efficient servo systems. A fundamental analysis is made of the requirements for optimizing these parameters. The relative feasibilities of various electromagnetic configurations for meeting these requirements are discussed in depth.

It is shown that two forms of the electromagnetic Harmonic Drive concept offer the most promise. The first is a stepping device which offers all the advantages of digital control systems. It has the higher response capability and is therefore the primary type. The second form is a synchronous device with constant torque output but a somewhat lower response capability.

Following detailed analyses of both types, models were designed, manufactured, tested and evaluated in comparison with conventional devices. Experimental results correlate well with the analyses. Examples of applications are given, typical of aeronautical systems as well as other fields. Mathematical expressions for scaling the models to other sizes are developed. Advanced concepts are presented for obtaining improved mechanization, more versatile operation, and packaging for field environments. Implications upon electrical control systems, resulting from the advance in performance provided by the new device, are discussed.

PUBLICATION REVIEW

This report has been reviewed and is approved.

FOR THE DIRECTOR:

Lawrence C. Wright

LAWRENCE C. WRIGHT
Lt. Colonel, USAF
Chief, Flight Control Division
AF Flight Dynamics Laboratory

Preceding Page Blank

This Document
Reproduced From
Best Available Copy

TABLE OF CONTENTS

TABLE OF CONTENTS
(Continued)

TABLE OF CONTENTS
(Continued)

LIST OF ILLUSTRATIONS

LIST OF ILLUSTRATIONS
(Continued)

LIST OF ILLUSTRATIONS
(Continued)

LIST OF TABLES

LIST OF TABLES
(Continued)

LIST OF SYMBOLS, UNITS AND ABBREVIATIONS

General

The same symbols are employed throughout the report for the same type of quantities, and these are defined herein, together with a few generally-used subscripts. However, many subscripts are necessary to represent various parts of the devices. It is felt best to explain the use of specifically used ones in each section or appendix, wherever they appear.

In general, unless otherwise noted, the rationalized MKS system of units is used throughout because of greater convenience in making magnetic, inertia, and other calculations. However, for the benefit of many readers not familiar with this system, results are often transformed into English units. Power rate is given in kilowatts/sec.

Standard electrical symbols are used on schematics and in accompanying discussions.

LIST OF SYMBOLS
(Continued)

Symbol	Quantity	Unit	Abbreviation
A	Area	meter^2	m^2
a	Constant dimension	meter	m
b	Constant dimension	meter	m
C	A constant		
c	Constant dimension	meter	m
D	Diameter	meter	m
D_p	Harmonic Drive pitch diameter	meter	m
d^p	(By itself) Harmonic Drive deflection; (with another function) Differential operator		
E	Voltage, effective or rms	volt	v
E_y	Young's modulus of elasticity		
e	Voltage, instantaneous	volt	v
EHD	Electromagnetic Harmonic Drive		
EHD-1*	Rotating Field, powder and core armature, with cup shape, plastic flexspline, no teeth.		
EHD-2	Rotating Field, powder and core armature, with bell shape, metal flexspline, with teeth.		
EHD-3	Stepping Actuator Type		
EHD-4	Rotating Field, Link Armature, with bell shape, metal flexspline, with teeth.		
F	Force	Newtons	n
Fa	Average magnetic force produced by one magnet.	Newtons	n
F_C	Centrifugal force	Newtons	n
F_D	Deflection force	Newtons	n
F_I	Inertia force	Newtons	n
F_L	Radial force due to the external torque load.	Newtons	n
F_M	Total radial force produced at both air gaps of a "U" shape magnet, or by all acting stator teeth, referred to the plane of the teeth.	Newtons	n
F_N	Tooth separating force	Newtons	n
F_Q	Magnetic force produced at one of the two air gaps of a "U" shaped magnet or by one "tooth" of a stator.	Newtons	n
F_R	Radial force produced at the major axis due to all magnetic forces acting together.	Newtons	n

* Serialized in order of manufacture of model

LIST OF SYMBOLS
(Continued)

Symbol	Quantity	Unit	Abbreviation
F_T	Tangential force produced at the major axis due to all magnetic forces acting together.	Newtons	n
f	Frequency	cycles/sec.	cps
f ( )	Function of		
f_f	Coefficient of friction		
g	Constant gap length dimension	meter	m
H	Magnetic field intensity	ampere-turn/meter	a-t/m
h	Heat transfer coefficient	watt/inch^2-deg. C	w/in.^{2}-C
I	Current, effective or rms	ampere	a
i	Current, instantaneous	ampere	a
J	Inertia	kilogram-meter^2	kg-m^2
J_a	Effective inertia of the armature due to harmonic motion.	kilogram-meter^2	kg-m^2
J_f	Effective inertia of the flexspline due to harmonic motion.	kilogram-meter^2	kg-m^2
J_M	Total inertia of the actuator	kilogram-meter^2	kg-m^2
J_r	Inertia of the armatures due to output-speed rotary motion.	kilogram-meter^2	kg-m^2
J_s	Inertia due to output speed rotation of the output shaft and attached elements.	kilogram-meter^2	kg-m^2
j	$\sqrt{-1}$		
K	A constant		
K_{ma}	Mechanical advantage		
L	Inductance	henry	h
l	Constant axial length dimension.	meter	m
M	Mass	kilograms	kg.
M_a	Mass of the armatures associated with a single magnet.	kilograms	kg.
MMF	Magnetomotive force	ampere-turn	a-t
N	No. of turns of a coil or in general a coil	turns	t
N_C	No. of teeth on the circular spline		
N_F	No. of teeth on the flexspline		

LIST OF SYMBOLS
(Continued)

Symbol	Quantity	Unit	Abbreviation
n_M	No. of magnets		
n	Symbol for an integer		
P	Power	watt	w
P_C	Average power dissipated in a coil	watt	w
P_D	Diametral pitch		
$\dot{P}_L$	Power rate of the external load	kilowatt/sec	kw/sec
P_M	Output power of the actuator	watt	w
$\dot{P}_M$	Power rate of the actuator	kilowatt/sec	kw/ sec
P_R^M	Mean I^2R power loss of the actuator	watt	w
Q	One leg of a magnet, or one "Tooth" of a stator		
Q	Heat	watt	w
R	Resistance	ohm	Ω
R_C	Resistance of one coil	ohm	Ω
R_g	Reduction ratio (input/output)		
RF	Rotating Field (Refers to all sinusoidal rotating field types)		
r	Radius	meter	m
S	Stacking factor		
SF	Stepping Field(refers to all stepping field types)		
s	Slip (a fraction of synchronous speed)		
T	Torque	newton-meter	n-m
T_M	Average output torque of the actuator	newton-meter	n-m
t	Time	second	sec.
t	Temperature	degrees C	C
U	Utilization factor		
u	Circumferential spacing between magnets or stator teeth	meter	m
V	Volume	$meter^3$	m^3
V_{mg}	Volume of a magnet	$meter^3$	m^3
W	Energy (or work)	Joule	Joule
W_{mg}	Work done per cycle by a magnet	Joule	Joule
Wt	Weight (kilograms and pounds used)		
w	Constant width dimension	meter	m
X	Reactance	ohm	Ω
x	Variable distance	meter	m
y	Variable distance	meter	m
Z	Impedance	ohm	Ω
z	Variable distance	meter	m

LIST OF SYMBOLS
(Continued)

Symbol	Quantity	Unit	Abbreviation
$\mathcal{F}$	Magnetic Force	ampere-turn	a-t
$\mathcal{P}$	Permeance	weber/ampere-turn	w/a-t
$\mathcal{R}$	Reluctance	ampere-turn/weber	a-t/w
$\mathcal{B}$	Magnetic flux density	weber/meter^2	w/m^2
Δ	An operator which denotes a small change in the function following		
δ	Harmonic Drive Power angle		
η_T	Harmonic Drive torque efficiency		
η_S	Shape factor representative of the distortion from the ideal harmonic shape.		
θ	Angular position of a moving element.		
θ_e	Angle between voltage and current		
θ_k	Angular position between the major axis and the center of the kth magnet		
θ_M	Angular position of the output shaft		
μ	Permeability	weber/ampere-turn-meter	w/a-t-m
μ_o	Permeability of free space = $4\pi \times 10^{-7}$		w/a-t-m
π	Universal constant 3.14159		
ρ	Mass density	kilograms/meter^3	kg/m^3
Σ	The summation of (an operator)		
τ	Time constant	second	sec
Φ	Magnetic flux(lines of force)	weber	w
Φ_a	Pressure angle	degree	o
ψ	Reference angular position, phase angle, etc.		
ω	Angular frequency = $2\pi f$	radian/second	rad/sec.

Generally-Used Subscripts

a	Refers to an armature element
c	Refers to a single coil
i	Input
o	Output
k	Refers to the generalized kth item of a quantity of similar items
L	Refers to the external load
M	Refers to the characteristics of the entire actuator by itself
m	Maximum
min	Minimum
Q	Refers to one leg of a magnet, or one tooth of a stator
t	Refers to the terminal of an electric circuit

Miscellaneous

Dots placed over or primes after a function indicate the time derivative (nth derivative for n dots or prime marks).

Numbering of Equations

Equations presented in the main text are designated by a two-part number: the first part represents the section, the second part orders the equations within the section.

Equations presented in the appendices are also designated by a two-part number. But to avoid the awkward use of roman numerals, the first part consists of an A followed by the arabic number corresponding to the roman numeral of the appendix concerned.

SECTION 1
INTRODUCTION

1.1 The Problem

High performance servomechanism systemshave benefited by rapid advances in electronic components to the point where, in many instances, the output actuator limits the reliability, duty-cycle, and weight-minimization characteristics that can be achieved in the overall control system.

The Flight Control Laboratory has recognized that the power supply compatibility, reliability, storage and life capability of electrical servo actuation techniques are considerably higher than other methods.* However, presently available electrical actuators, in the size required to meet high response requirements, are not competitive to hydraulic devices with regard to (1) weight, such as conventional low-inertia torque motors, (2) efficiency and duty cycle, such as some of the new low-inertia DC motor concepts, or (3) capability to withstand steady state loads with a resonable temperature rise.

Therefore, a need exists for an electrical power servo actuator capable of fast bi-directional response and steady-state holding torque, with minimum weight and temperature rise, and not requiring separate clutching or braking mechanisms.

Low weight is obviously a fundamental need. Efficiency is important because of the heavy power supplies required for low efficiency devices. Low duty cycle ratings, due to necessary temperature rise restrictions, either eliminate or lower the reliability of the actuator for many applications.

1.2 Project Objective and Approach

The purpose of this project was to investigate the feasibility of a new concept for achieving the required high response without unattractive weight, efficiency, duty cycle, or temperature rise characteristics.

This new concept involves combining the principles of Harmonic Drive** with a rotating electromagnetic field, in a manner whereby the combination produces high output torques without the rotation of the electromagnetic elements, rotors, bearings or any other masses at speeds corresponding to the electrical frequency, thereby drastically reducing the device's inertia.

*Exhibit "A" dated 18 May 1961, Contract No.AF33(657)-7731.

**Harmonic Drive is the subject matter of U.S.patent No.2,906,143 and other U.S. and foreign patents and patent applications. All proprietary rights of United Shoe Machinery Corporation are hereby reserved.

Manuscript released by the authors March 1963 for publication as an ASD Technical Documentary Report.

This concept has been called Electromagnetic Harmonic Drive.* It is an example of how Harmonic Drive, by means of its unique elastic body mechanics principle, permits such advantageous combinations of functions, such as prime power source and torque amplifier, to be made.

The project was organized with the purpose in mind of performing a thorough analysis of alternative approaches, so that a sound technical foundation could be laid for future work in this area. In addition, experimental models were to be designed, built, and tested to confirm the validity of the analysis. A further objective was that the designs should not incorporate features which could not, by routine development engineering, lead to devices meeting the environmental requirements of military vehicles, such as aircraft and missiles.

Other specific objectives of the research model actuator were:

- -Bi-directional operation
- -Variable speed
- -25 lbs. maximum weight
- -Maximum dimensional envelope of a 10" diameter and 16" long
- -Operable from 400 $\pm$ 5% cps, 115/200 volts, single or three-phase
- -1000 hours life

The project was organized into phases:

- -Basic Studies and Analyses
- -Design, Fabrication and Test
- -Evaluation

These phases, in turn were subdivided into a number of specific tasks.

This report generally follows that organization, and the succeeding sections present objectives and significant results. Overall results and conclusions for the project are presented in Section 13, and recommendations for future work in Section 14.

Test results are given within the same sections as the analyses of predicted performance, Sections 4 and 5 for the two basic types of actuators. This was done, first, to integrate theory and experimental results and, second, because it was found that some major characteristics, such as power rate and inertia, could not be measured directly and had to be derived.

---

*Abbreviated to EHD in this report.

SECTION 2

THE RATING OF SERVO ACTUATORS

2.1 General

The purpose of this section is to explain that power rate, or torque squared to inertia, is the significant parameter determining the capability of a servo actuator to meet a fast response requirement. Therefore, if one is to advance the state-of-the-art in servo actuators, primary effort should be given to optimizing the power rate. This parameter is explained. Examples of how it is used are given in Section 6.

The primary method by which large advances in power rate can be made without requiring severe pulse currents, is to lower an actuator's inertia.

In selecting or designing actuators for servo systems it is necessary to know what key rating or ratings of the actuators are most meaningful in determining their capability to drive the load. The answer to this question depends, first of all, upon the significance of the load. The majority of applications, particularly within the Air Force, are power servos and the load is significant. The other category is instrument type servos where the load is insignificant. In this latter case the key rating is the motor time constant, τ_M.

Assuming an actuator with inertia J_M, which can be operated at peak torque T_M during the accelerating period, as is most common, velocity is a ramp function and so

$$\tau_M = \frac{\dot{\theta}_M J_M}{T_M} \qquad (2\text{-}1)$$

where $\dot{\theta}_M$ is the peak velocity.

The time required to effect step changes in position or velocity, and the bandwidth of frequencies that can be handled with acceptable attenuation and phase shift, are intimately related to τ_M. Since this is not of primary interest here, it will not be discussed; other than to point out the EHD provides greatly reduced τ_M values and hence potential for improved performance from instrument servos.

For power servos, the requirement is for actuators with high peak power outputs as well as the capability of applying this power to the load quickly. Therefore, the concept of power rate, the time rate of change of motor output, appears logical as the major parameter defining the usefulness of servo actuators. One of its advantages is that, when gearing is required between the actuator and the load, the actuator's power rate, reflected to the load through the gearing, is not changed. Other parameters that are sometimes used by systems designer, such as actuator torque to inertia, are modified by the transmission gear ratio. The power rate and peak power output ratings required of an actuator are interrelated and depend upon the ratio of two so-called time constants, one characteristic of the load, τ_L, and the other of the actuator, τ_M.

τ_L can vary widely with the nature of the application, and in general is related to the required bandwidth and damping characteristics of the system. τ_M can also vary widely for different types of actuators (such as, induction motors, torquers and hydraulic motors).

The basic research into these concepts, by Dr. G. C. Newton, Jr., is fundamental to the discussion and has been used throughout. As part of the project scope he has analyzed electromagnetic Harmonic Drive and its possible applications, using these techniques. Certain parts of his analyses appear as Appendix I.

2.2 Power Rate and Peak Power Output

Motor power alone is obviously insufficient to characterize a servo motor since these devices must accelerate their own inertia in addition to the loads that are coupled to them. Thus, conventional electrical servo motors are required to produce instantaneous power outputs which may be 20 times or more the total external load power requirements.

The peak motor power P_M is simply the peak motor velocity times the peak motor torque T_M. The peak external load power P_L is given by the product of the peak load torque times the peak velocity $\dot{\theta}_L$

$$P_L = \dot{\theta}_L \left(J_L \ddot{\theta} + T_L\right) \qquad (2\text{-}2)$$

where J_L is the load inertia, T_L the load frictional torque and $\ddot{\theta}_L$ the peak load acceleration. The relationship of P_M/P_L is developed from the torque and the velocity conditions that have to be satisfied in order that a realizable actuator speed with or without gearing can be found for matching the motor to the load.

Newton shows how the peak motor P_M is related to the peak load power P_L and the two time constants characteristic of the motor (τ_M) and the load (τ_L).* These time constants are simply the ratios of peak velocity to peak acceleration. The motor time constant is given by Equation 2-1. The load time constant is defined as

$$\tau_L = \frac{\dot{\theta}_L}{\ddot{\theta}_L} \qquad (2\text{-}3)$$

In terms of these parameters Newton shows that the actual peak motor output power required to drive a particular load is related

*Reference 7. The references are listed following Section 14.

to the peak power by the following ratios:

$$\frac{P_M}{P_L} \geq \frac{1}{1 - \frac{\tau_M}{\tau_L}}, \qquad \frac{\tau_M}{\tau_L} < \frac{1}{2} \quad \text{(Case 1)} \qquad (2\text{-}4)$$

$$\frac{P_M}{P_L} \geq 4\,\frac{\tau_M}{\tau_L}, \qquad \frac{\tau_M}{\tau_L} \geq \frac{1}{2} \quad \text{(Case 2)} \qquad (2\text{-}5)$$

These relationships have fundamental significance to this report, but their meaning requires some explanation. First it must be understood that each and every servo actuator is characterized by a particular motor time constant τ_M which is representative of the time required to reach rated speed. This actuator may be applied in a variety of applications, which are characterized by the load time constant τ_L. Low τ_L results from high acceleration requirements relative to peak speeds, and high τ_L the converse. The dimensionless ratio of τ_M to τ_L is then computed. Whenever this ratio is more than 1/2, which most often occurs with conventional electrical servo actuators, the required motor output power, compared to the external load power, must be at least four times the time constant ratio. For example, if τ_M = .010 sec, $\dot{\theta}_L$ = 20 rpm = 2.1 rad/sec., and $\ddot{\theta}_L$ = 500 rad/sec^2, then τ_L = .0042 sec., τ_M/τ_L = 2.4 and $P_M/P_L \geq 4(2.4) = 9.6$; and this actuator would have to be capable of producing 9.6 times the particular peak external load requirement considered above. All combinations of actuators and applications which have a τ_M/τ_L ratio which is $\gg 1/2$ are required to produce relatively large amounts of "excessive" power, over and above the external load, according to Equation 2-5. If the time constant ratio is less than 1/2, Newton has shown that the peak motor output power need not be much greater than the external load power requirement according to Equation 2-4. In other words, the torque required to accelerate the actuator's own inertia is relatively insignificant. Obviously this situation would result from either a relatively low load acceleration requirement or a low actuator inertia. Since load acceleration is normally not alterable, the only alternative is to select an actuator with lower inertia. All combinations of actuators and loads resulting in $\tau_M/\tau_L < 1/2$ need produce but little "excessive" power, according to Equation 2-4 The words "Case 1 and Case 2" are used for convenience in ensuing discussions to designate the two possible situations which have been explained above. It is evident that the same value of P_M/P_L results from both equations when $\tau_M/\tau_L = 1/2$, so that the separation into two cases introduces no discontinuity.

With Case 1, Equation 2-4 shows that P_M/P_L has a maximum value of 2 and approaches unity as τ_M/τ_L approaches zero. This represents the area of "power-matching" the actuator to the load, and so the actuator's power output P_M is very important, in relation to weight and I^2R loss. It is very desirable to be able to use the actuator in this region, because the lower the peak power requirement, in general, the lower is the weight and I^2R loss.

Also the actuator can operate at very high, if not full, duty cycle and be more versatile in providing a variety of responses. To operate in this region the requirement is for low τ_M, or high $1/\tau_M$. But this can be expressed as

$$\frac{1}{\tau_M} = \frac{T_M}{J_M\dot{\theta}_M} \times \frac{T_M}{T_M} = \frac{T_M^2}{J_M T_M \dot{\theta}_M} = \frac{T_M^2/J_M}{P_M} \qquad (2\text{-}6)$$

The grouping T_M^2/J_M is, by definition, the power rate of the actuator, i.e.:

$$\dot{P}_M = T_M^2/J_M \qquad (2\text{-}7)$$

It has the dimensions of power/time and is usually expressed in units of kilowatts/sec. because watts/sec. requires awkward 4 to 7 place figures. Since both high P_M and high $1/\tau_M$ are desired, the requirement is for the product of these two factors, giving

$$P_M \times \frac{\dot{P}_M}{P_M} = \dot{P}_M \qquad (2\text{-}8)$$

This is then the key rating for Case 1.

With Case 2, Equation 2-5 shows that P_M/P_L varies from 2 upwards, being directly proportional to the time constant ratio. So, again, low τ_M is important and the same result as with Case 1 is obtained: the actuator's power rate is the key rating.

The cases that apply for particular applications are best summarized by a chart such as Table I.

For Case 1, by substituting the definitions of τ_L and τ_M into the expression for P_M, and separating actuator and load factors, there is obtained

$$\frac{T_M^2}{J_M} = \dot{P}_M \geq 4(J_L\ddot{\theta}_L + T_L)\ddot{\theta}_L \qquad (2\text{-}9)$$

Motor Time Constant τ_M	Load Time Constant τ_L and Type of Application		
	LARGE τ_L	MEDIUM τ_L	SMALL τ_L
	Low Performance Servos	High Performance Servos	Extreme Performance Servos
Large (Conventional Servo Actuators	Power Match Case 1	Power Rate Match Case 2	Power Rate Match Case 2
Small (Low Inertia Servo Actuators)	Power Match Case 1	Power Match Case 1	Power Rate Match Case 2

TABLE I - IDENTIFICATION OF COMBINATIONS OF LOAD AND MOTOR TIME CONSTANTS

which specifies the required power rate of the actuator to drive a given load.

In choosing or designing for a particular application the following rules then apply to the specification of the actuator.

For "extreme" performance servo type applications, which is representative of some advanced aeronautical, missile, and space technology uses where extremely large bandwidth and accelerations are met, Case 2 applies to all actuators and one is chosen on the basis of its ratio of power rate to weight, cost, I^2R (electrical) loss, or whatever is important. Of course, there are other considerations that must be fulfilled. The velocity rating of the actuator must equal or exceed the load requirement, using gearing if necessary. The accuracy, resolution, repeatability, environmental characteristics, life and reliability requirements must also be met.

For "low" performance servo type applications, Case 1 applies to all actuators and one is chosen on the basis of its ratio of power output to the other important characteristics. In general EHD would not be used for these applications unless it were advantageous for some of its characteristics other than fast response, such as digital characteristics (also see Conclusions-Section 13).

For "high" performance servo type applications, which are most common, Case 2 applies to conventional actuators, resulting in a calculation of P_M/P_L which will generally be of the order of 4 to 20 or more. Case 1 applies to low inertia actuators such as EHD, and P_M/P_L, which lies between 1 and 2, is thereby calculated. Then the required peak powers are compared, as was done with low performance servo type applications. Of course the boundaries drawn here between levels of performance are artificial and there is no discontinuity at these points. They are used for convenience only.

SECTION 3

LOW INERTIA HARMONIC DRIVE CONCEPTS

3.1 General

Conventional Harmonic Drive has been used with various prime movers to provide torque multiplication and speed reduction. For servo applications, the inertia contributed by the Harmonic Drive mechanism in relation to the torque when properly designed and applied, can be made negligible compared to many types of electric motors. But the inertia of the motor armature still remains as the factor limiting speed of response. At the time that the original Harmonic Drive concepts were first tried out, it was recognized that Harmonic Drive provided opportunities for devising unique actuator concepts in which the conventional prime mover stage could be eliminated. One advantage of this is that the inertia of the complete actuator can be made substantially lower, thereby greatly increasing its power rate. One of the ways by which this can be done, and still retain the advantageous characteristics of an electric system, is to use electromagnetic wave generation.

The purpose of this section is to explain how a Harmonic Drive actuator produces torque from short stroke radial forces, to explore and define the desired distribution of forces within the actuator, to consider the necessary limitations in torque in relation to shape distortion of flexible elements, to survey the available electromagnetic or electrical methods of producing such forces, to highlight the new flexible armature concepts required for practical devices, and to derive mathematical expressions for torque and inertia. The expressions are used in succeeding sections for making fundamental analyses of the two basic types of electromagnetic Harmonic Drive considered most feasible. A discussion of other characteristics, common to both types, but which are of lesser significance than torque and inertia, are presented in a latter section.

3.2 Combination of Short Radial Forces and Harmonic Drive

In its usual form, Harmonic Drive consists of a flexible cylindrical element containing fine pitch spline teeth which is deflected into an elliptoidal shape so that at the ends of the major axis a number of such teeth are in mesh with teeth of the same pitch on a rigid circular spline element. Since they are the same pitch, the number of teeth on the elements must be different by two or some multiple thereof. Now if the forces that deflect the flexspline into the elliptoid rotate, so will the points of tooth contact. When this rotation makes one full revolution, assuming that the circular spline is constrained from rotating, the rotation of the flexspline will be equal to

$$\frac{\theta_F}{\theta_i} = \frac{N_C - N_F}{N_F} = -\frac{\Delta N}{N_F} \qquad (3\text{-}1)$$

where the N's are the number of teeth on the elements. The negative sign indicates a reversal of direction. Thus the reduction ratio (defined as input over output) is

$$R_{g_F} = - \frac{N_F}{\Delta N} \tag{3-2}$$

If the flexspline is constrained from rotating there is no reversal and

$$R_{g_c} = + \frac{N_c}{\Delta N} \tag{3-3}$$

Since the number of teeth are proportional to the pitch diameter of the two elements, one can also write

$$R_{g_F} = - \frac{D_{p_F}}{\Delta D} \tag{3-4}$$

$$R_{g_c} = + \frac{D_{p_c}}{\Delta D} \tag{3-5}$$

for the two cases.
ΔD, the difference in diameters, is defined as

$$\Delta D = d \tag{3-6}$$

so that

$$D_p = R_g d \tag{3-7}$$

It should be pointed out that the teeth are not necessary to obtain a motion reduction. Without teeth, so long as there is a suitable difference in diameters, frictional anchoring occurs to couple the tangential velocity of the flexible member to the rigid member at contact. However, the torque rating must be much lower due to slipping, and the accuracy resulting from the positive ratio of spline-anchored units is lost.

Based upon the above ratio formulas, with a fixed circular spline (employed in all of the EHD models) if the output is to be clockwise, the input forces that deflect the shape must rotate counterclockwise. It is seen that, as they do, the radius of the flexspline becomes progressively shorter, changing from

$$r = \frac{D_p}{2} + \frac{d}{2} \tag{3-8}$$

at the major axis, the center of tooth contact, to

$$r = \frac{D_p}{2} - \frac{d}{2} \tag{3-9}$$

at the smallest radius.

If the shape is essentially a true elliptoid, the minimum radius occurs at the minor axis, 90° away from the major axis, and the position at any angle is given by

$$r = \frac{D_p}{2} + \frac{d}{2} \cos 2\theta_i \tag{3-10}$$

where θ_i is the angle between the major axis and the point considered.

If there is no external torque load, and for the moment neglecting any no-load frictional loss, the angle between the deflecting force and the major axis, referred to as δ, remains essentially zero. The deflecting force pushes against the flexspline at a point where its radial velocity is zero, given by the derivative of equation 3-8 where $\theta_i = \delta = 0$. Thus, input power

$$P_i = 2F\dot{r} \tag{3-11}$$

is zero (no-load frictional losses still neglected) since $\dot{r}$ is zero. The factor of two exists because two forces of F each are required, pushing in opposite directions. Now in order to produce output power, it is obviously necessary to feed in the same amount of work plus the losses. This is accomplished by having the angle increase from zero. Thereupon, it is seen that the radial deflecting force now pushes against the flexspline at a point where its radial velocity is finite, i.e.,

$$\dot{r} = d \sin 2\theta \dot{\theta}_i \tag{3-12}$$

from the derivative of equation 3-10 where $\theta = \delta$.

Therefore, the input power is

$$P_i = 2Fd \sin 2\theta_i \dot{\theta}_i \tag{3-13}$$

Now, for any device

$$P_o = P_i \eta_T \tag{3-14}$$

where η_T is the torque efficiency.

Output power can be expressed as

$$P_o = T_o \dot{\theta}_o \tag{3-15}$$

but output speed $\dot{\theta}_o$ is related to input speed by the ratio

$$\dot{\theta}_o = \dot{\theta}_i / R_g \tag{3-16}$$

so that

$$\left.\begin{aligned} T_o &= 2Fd\, R_g \eta_T \sin 2\theta_i = 2FD_p \eta_T \sin 2\theta_i \\ &= F_T\, D_p\, \eta_T \\ &\text{where} \\ F_T &= 2F \sin 2\theta_i \end{aligned}\right\} \tag{3-17}$$

The condition that theoretically produces maximum torque is, of course

$$\theta_i = 45^\circ \tag{3-18}$$

It is now shown that this represents an ideal case that is not likely to be obtained for reliable operation. There are other requirements to be met, maintaining the teeth in engagement and preventing severe shape distortions that might cause early life failure due to abnormal stresses. Hence, an analysis is made of the optimum force distribution that gives the maximum torque as well as good tooth mesh and shape control.

3.3 Force Distribution and Power Angle

The angle θ_i is now specifically defined as the power angle, σ. This angle is a major parameter for CHD. From equation 3-17 it is also seen that torque output is positive for any F positioned within the range of $0 < \sigma < 90^\circ$.

This is in agreement with intuitive expectations as the radial velocity has this variation. From a theoretical viewpoint, if F were concentrated exactly at $\sigma = 45^\circ$, the maximum torque would result. A practical embodiment of this would be a roller type wave generator, viz.:

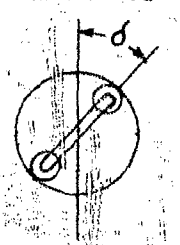

Figure 1 - Roller Type Wave Generator

Of course, if the force is the type that has a circumferential distribution, then ideally it should be centered at $\sigma = 45°$.

But another basic requirement for Harmonic Drive is that the flexible member should be maintained in contact or mesh with the circular member. Whether or not this contact need be complete at all times of operation as well as standby, depends on the nature of the application. If accuracy is not essential and life requirements not high, then some momentary loss of contact might be tolerable and σ, and hence T/F, can be greater than if positive contact must be maintained at all times with a degree of assurance. The discussion of tooth engagement will first be conducted using the assumption of a true harmonic shape, because the mathematics are much more straight forward. Then consideration will be given to the question of shape distortion, a much greater possibility when the full-supporting cam form of wave generator is eliminated. An analysis of all the radial forces acting on the flexspline was made to determine the conditions that must be met. A flexspline in Harmonic Drive with an external circular spline and with a true harmonic shape is acted upon by the following forces: (See Figure 2).

1. Spring-back deflection force due to its deflection, F_D.

2. Tooth separating force, F_N.

3. Inertia force due to acceleration of the mass which experiences harmonic motion, F_I.

4. Tangential forces due to the external torque load, which vary gradually around the mouth from "compression" to a maximum tension because of the torque "taken off" by the teeth. These forces induce radial forces, F_L, due to the curvature of the flexspline, radially inward when there is tension in the bed and radially outward where there is "compression". (The compression forces are counterbalanced by other forces and strains, such that no part of the flexspline is actually considered in compression. There is only the tendency toward compression).

5. Applied input forces, F.

It can easily be shown that centrifugal force is negligible at the speeds and rotating masses considered for this project. (See Appendix II).

Force F_N acts only where the teeth are in contact, i.e., at and around the major axis depending on the arc length of tooth contact. Also, F_N acts radially inward only. F_D and F_I act at all points around the mouth, but vary sinusoidally in accordance with position. F may act just radially outward by ball bearing

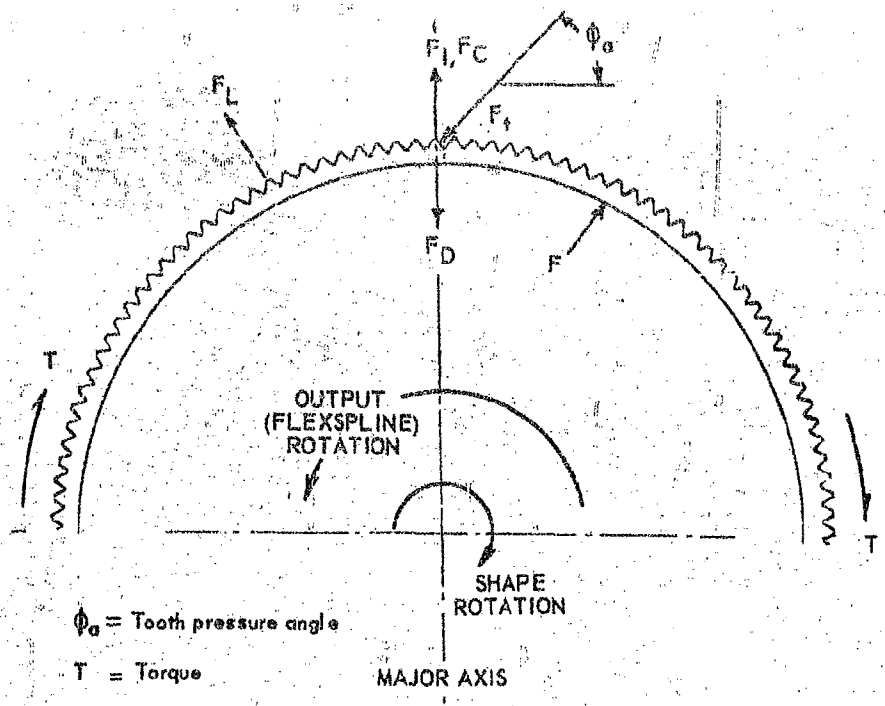

ϕ_a = Tooth pressure angle

T = Torque

F_t = Tooth normal force

F_I = Inertial force

F_C = Centrifugal force

F_D = Spring force

F = Input magnetic driving force

F_t and T can be represented by

F_N = Tooth separating force, acting collinear and the same direction as F_D

F_L = Radial reaction forces induced by the load, acting radially outward with diminishing magnitude to the left of the major axis, and radially inward with diminishing magnitude to the right of the major axis

FIGURE 2 FORCES ON THE FLEXSPLINE

forces for example, or it may act inward as well as outward, if the force source is capable of reversing its force. In this case, α must be greater than 90° when F is acting inward according to equation 3-17. But by this equation, still ignoring shape distortion at this time, the inward forces beyond 90° have the same effect as equal outward forces positioned 90° away. Hence, consider for the present only those forces acting over an angle of 45° on either side of the major axis.

Force F_D acts radially inward, varying sinusoidally with maximum value at the major axis.

Force F_N acts radially inward, but only over the tooth contact area.

Force F_I acts radially outward, ranging sinusoidally with maximum value at the major axis (for pure harmonic motion, the F_I vector is opposite to the acceleration vector, which is opposite to the displacement vector due to 180° phase shift).

Force F acts radially outward at and in advance of the axis.

F_L acts radially inward in advance of the axis, and radially outward behind the axis, hence passes through zero at the center of the tooth contact area, which is the major axis. This effect accounts for the bulge behind the axis and the hugging against the bearing (when used) in advance.

The forces must always be in equilibrium for all conditions. Expression of F_I as an inertial force permits the equations of static equilibrium to be applied. When the device is stopped and not accelerating rotationally $F_I = 0$. When the device is accelerating rotationally or at a steady speed, F_I exists.

The question arises as to how and where there are produced the required accelerating forces which are, of course, equal and opposite to the inertia force, F_I. Reference should be made to the graph of the forces. (Figure 2) It is theorized that, to a first approximation, the flexspline can withstand internal shear and bending forces to the degree necessary for equilibrium as shown, while still retaining a shape adequate for Harmonic Drive action. This means that F is applied essentially to satisfy most of the radially inward F_L requirement, which represents useful work in the general range of 22-1/2°. Over the other parts of the flexspline an equilibrium of F_N, F_I, F_D and the unsatisfied part of F_L is assumed obtained without any additional magnetic force requirement. The reasoning is intended to provide further insight into the meaning of the basic torque formula equation.

So far as maintaining engagement at the teeth is concerned, the components of F_L cancel, and if the F_D, F_I and F_N forces are represented by resultant point forces at the major axis, the value of the required applied force F at the same location is

$$F = F_N + F_D - F_I \qquad (3\text{-}19)$$

The result is that, ideally, two locations of force application are most useful, at 0° and 45°. Because of the flexibility of the flexspline, if such forces were applied, the shape would tend to distort with high curvature near the four points of force application. Thus, this scheme is not desirable. If the input were to be only one force per side of the flexspline, such as a roller type of wave generator which is capable of continuous rotation, the power angle would be equal to that required to simultaneously fulfill the torque and tooth engagement requirements. Thus, it is now necessary to determine how forces positioned at other than the major axis contribute to the net radial force at the major axis. Consider a true elliptoidal shape superimposed over the shape when the element is not deflected. (Figure 3).

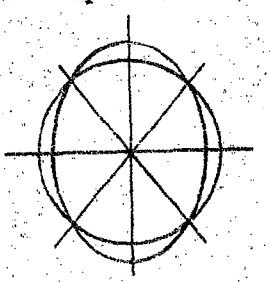

Figure 3 - Elliptoidal Shape

Consider an equally distributed force from 0° to 90°. The forces from 0° to 45° tend to increase the elliptoidal shape, their effectiveness decreasing as their position moves from 0° towards 45°; the forces from 45° to 90° tend to decrease the elliptoidal shape with their effectiveness increasing as 90° is approached, and those at 45° have no net effect. This behavior is represented by the expression

$$F_R = F \cos 2\theta \qquad (3\text{-}20)$$

Thus, F_R is positive for any F positioned within the range of

$$-45° < \delta < +45° \qquad (3\text{-}21)$$

It is seen that the mutual segment in which both T and F_R are positive is

$$0 < \delta < +45° \qquad (3\text{-}22)$$

and that for forces acting in the range of

$$+45° < \delta < +90° \qquad (3\text{-}23)$$

there is a negative F_R produced, and there must be sufficient other forces in the range of

$$-45° < \delta < +45° \tag{3-24}$$

to counterbalance this. The maximum load that could be applied would be given by the intersection of two curves, F_R and $F_N + F_D - F_I$, as shown in Figure 4.

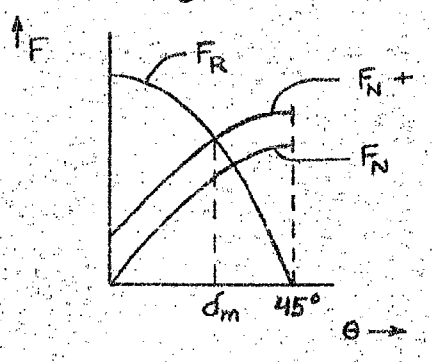

Figure 4 - Determination of Maximum Force

Now in general, the magnitude of F_D and F_I is very low in relation to F_N for the usual actuator size and load conditions. F_D (calculated in Appendix III) normally will be 3 to 10 lbs., and F_I (Appendix IV) slightly less. F_D does become important for pitch diameters below 2 inches but these are not normally encountered. If a more exact analysis involving F_D is desired, it can be taken as the following

$$F_D/F = 0.1, \qquad 1\ 5/8" \leq D_p \leq 2" \tag{3-25}$$

$$F_D/F = 0.25, \qquad D_p > 2" \tag{3-26}$$

Similar expressions could be written for F_I, but since it varies with speed, it is doubted that there is much value except for constant speed devices. Considering the counteracting direction and low magnitude of F_D and F_I, the maximum power angle can be taken, with sufficient accuracy, as the intersection of the F_R and F_N curves, giving

$$\delta_m = \frac{1}{2} \arctan \frac{1}{2 \tan \Phi a} \tag{3-27}$$

The torque at this limiting power angle would be

$$T = 2D_p \eta_T F \sin \arctan \frac{1}{2 \tan \phi_a} \qquad (3\text{-}28)$$

This is the theoretical maximum torque for a point force of value F. This indicates that the lowest practical pressure angle should be used. It has been found from many years of research with Harmonic Drive that the possibility of tooth interference increases as ϕ_a is reduced, and the nearest standard angle to the lower practical limit is 20°, the standard selection being 30°. For 20°, interference is prevented by reducing the addenda of the teeth. However, in the case where no cam type wave generator is employed, more accelerated wear due to overdeflection can raise slight burrs on the tooth tips and, together with shape distortions, the condition can be reached where the teeth will not go into proper mesh. This occured with model EHD-2 which had to have the teeth recut from 20° to 30° before proper meshing could occur. For manufacturing reasons, it is desirable to design for the standard pressure angles, 14-1/2°, 20°, and 30°. The difference in the values of the tangents between these angles is less significant for the smaller angles. Model EHD-3 performs well with 20° teeth, and although model EHD-2 was changed from 20° to 30°, it is believed that with careful tooth design 20° would work.

With magnetic deflection the flexspline is deflected until it is stopped by some rigid surface. This may conveniently be a "stop ring" such as employed in model EHD-3, a field stator as with model EHD-2, or the teeth may wedge together. The theoretical pitch lines of both gears become tangent at the point of contact and load transmittal. The unique Harmonic Drive advantage of virtually no tooth sliding results and the usual gear problems of lubrication, heat and tooth wear are greatly reduced. Under load, this ideal condition can be approached. Now, if the stopping element is designed so that the deflection is slightly greater than tangency, the teeth slide slightly while disengaging, i.e., on the way out of engagement. The friction forces, of course, act along the interface away from the flexspline, resulting in a decrease in F_N and an increase in F_T, defined above; the values being in accordance with the pressure angle and the coefficient of friction.

As derived in Figure 5, the reduced value of F_N is given as

$$F_N = \frac{F_T}{1 + f_f \tan \phi_a} (\tan \phi_a - f_f) \qquad (3\text{-}29)$$

Obviously, if the general theory of friction force is valid, it is easily shown that if there is pitch line underlap, the teeth

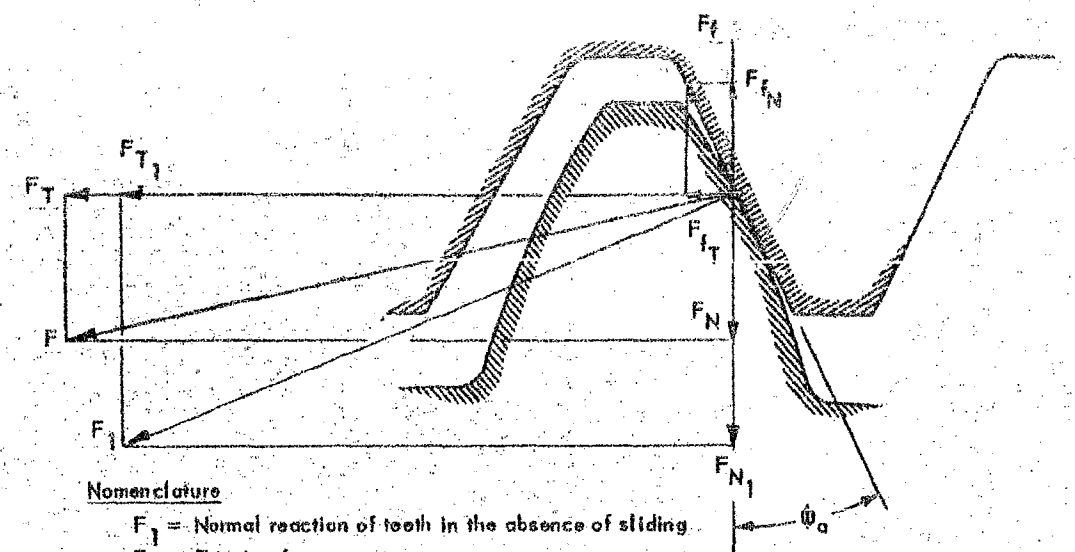

Nomenclature

F_1 = Normal reaction of tooth in the absence of sliding
F_f = Friction force
F = Resultant of F_1 and F_f
f = Coefficient of friction
ϕ_a = Pressure angle
T and N denote tangential and radial components

Derivation

$$F_f = f F_1$$

$$F_{f_T} = F_f \sin \phi_a = f F_1 \sin \phi_a$$

$$F_{f_N} = F_f \cos \phi_a = f F_1 \cos \phi_a$$

but $F_1 = F_{T_1}/\cos \phi_a = F_{N_1}/\sin \phi_a$

$$F_{f_T} = f F_{T_1} \tan \phi_a$$

$$F_{f_N} = f F_{N_1}/\tan \phi_a$$

$$F_T = F_{T_1} + F_{f_T} = F_{T_1}\left[1 + f \tan \phi_a\right]$$

$$F_N = F_{N_1} - F_{f_N} = F_{N_1}\left[1 - f/\tan \phi_a\right]$$

but $F_{N_1} = F_{T_1} \tan \phi_a$

$$F_N = F_{T_1} \tan \phi_a \left[1 - f/\tan \phi_a\right] = F_{T_1}\left[\tan \phi_a - f\right]$$

$$F_N = \frac{F_T}{1 + f \tan \phi_a}\left(\tan \phi_a - f\right)$$

FIGURE 5 EFFECT OF TOOTH SLIDING DURING DISENGAGEMENT DUE TO PITCH LINE OVERLAP

slide while engaging and the friction force vector is reversed and results in

$$F_N = \frac{F_T}{1 - f_f \tan \phi_a} (\tan \phi_a + f_f) \qquad (3\text{-}30)$$

The above analysis shows how both pitch line overlap and a smaller pressure angle decrease the radial component of the tooth reaction force. This is very important with a ball bearing wave generator as the life of the bearing, which presently limits the life of the device, varies inversely as the third power of this load. It is also important for electromagnetic deflection as this force, F_N, must be provided by the electromagnetic action or some other means.

There is, of course, a limit to increasing pitch line overlap and reducing the pressure angle. This limit is tooth wear, which increases with both of these effects because the greater the overlap, the longer the teeth are in contact; and the greater the angle, the longer is the face of the tooth over which the sliding occurs.

The theoretical values of F_N/F_T for three different pressure angles and a typical coefficient of friction of 0.15 (References 5 and 9) are summarized in Table II.

ϕ_a	Overlap	Underlap	Line to Line
30°	0.393	0.795	0.577
20°	0.202	0.542	0.363
14½°	0.104	0.425	0.258

TABLE II - THEORETICAL VALUES OF F_N/F_T

During the course of this project, a USM research study of this tooth sliding effect was completed with inconclusive results due to difficulties with devising valid measuring techniques. However, evidence being compiled through life tests of various types of wave generators (ball bearings, fluids, etc.) indicates the tooth separating loads are less than the line to line formula would predict. By basing the present design approach on neglecting the sliding effect, predicted performance, life and reliability will be conservative with regard to this factor.

The preceding analysis is based on the true harmonic shape. Now, examination will be given to the effects of shape distortion. It was forseen that forces applied at points, rather than distributed over an arc, might result in higher stresses due to localized bending and shear, which might limit the torque due to the

strength of the materials. Also, the shape might be distorted so that the relationships of torque and the supporting force F_R to the power angle might be different. This might or might not be advantageous. For example, tooth action might be affected to the degree than η_T decreased. It was desired that the laboratory models be sufficiently conservative in design to demonstrate feasibility rather than risking a negative result in pushing immediately for the ultimate, and also not require excessive time or expense for manufacturing or possibly extensive rework or modification. The philosophy adopted, then, was that in the absence of a more ideal shape-forming element, the torque loading should be limited to the degree that shape distortion was negligible. It was decided to make some experiments with models to study torque efficiency, shape distortion and maximum torque when the ball bearing is eliminated. A model (Figures 6 and 7) was prepared in which a series of push rods with curved tips were radially placed to push against the inside of a flexspline, under the teeth, when driven by a manually rotated cam. Strain gages were bonded on the sides of one push rod to permit compressive force measurement. A viewing window on the end permitted examination of the flexspline shape over a long arc. A potentiometer was attached to the cam shaft to permit measuring the distance over which the force acted. Static measurements of the peak force on one rod versus applied torque are given in Table III. From this the value of $\eta_T \sin 2\sigma$ was calculated

	CUP SHAPE		BELL SHAPE	
TORQUE LOAD (LB. IN.)	FORCE (LBS.)	$\eta_T \sin 2\sigma$	FORCE (LBS.)	$\eta_T \sin 2\sigma$
0*	18	---	14	---
240	95	0.38	76	0.47
480	160	0.45	140	0.51
720	210	0.52	190	0.57
960	280	0.51	240	0.60
1200	320	0.56	280	0.64

* Circular Spline Removed

TABLE III - POINT FORCE (CAM-DRIVEN PUSH ROD) RESEARCH MODEL TEST RESULTS

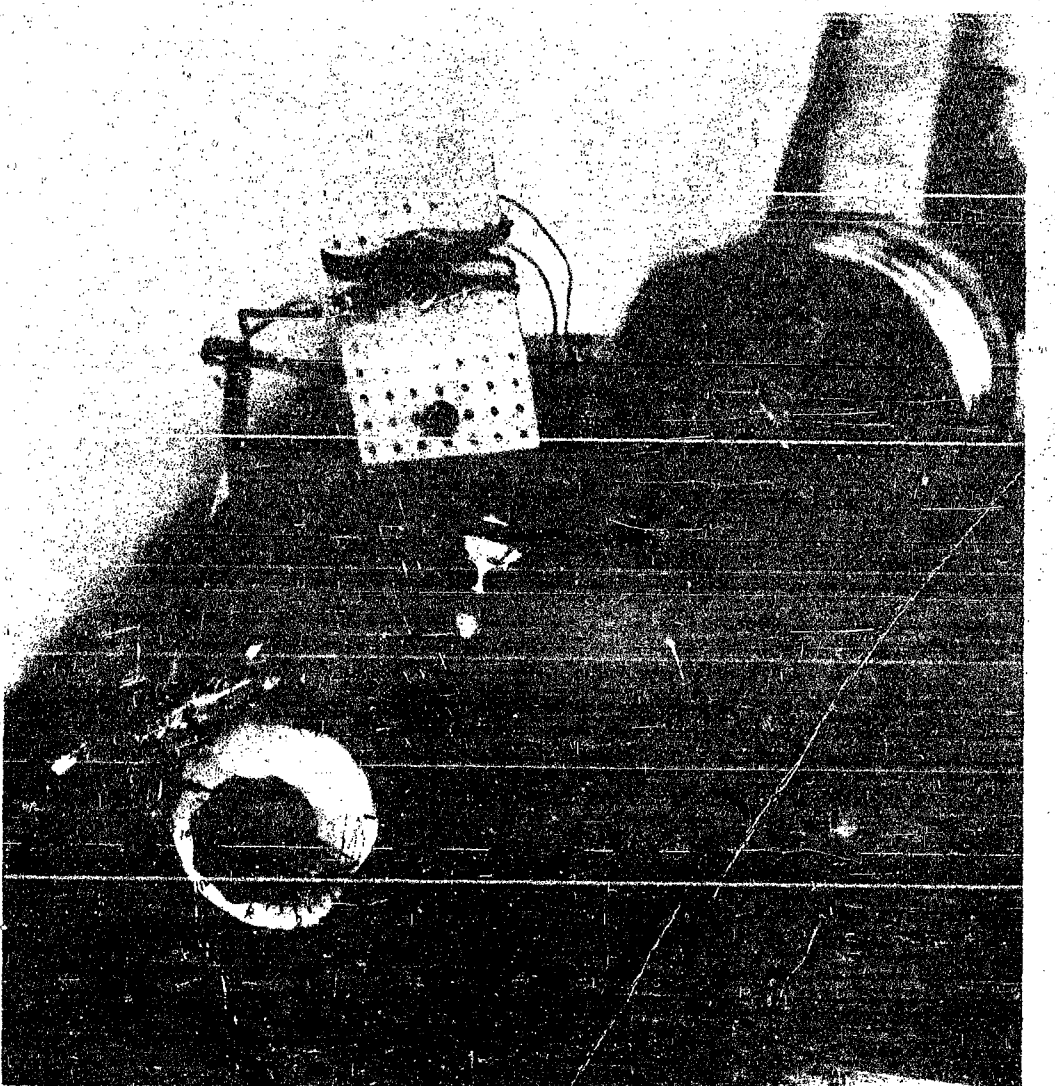

FIGURE 6 CAM-DRIVEN PUSH-ROD POINT FORCE STUDY MODEL

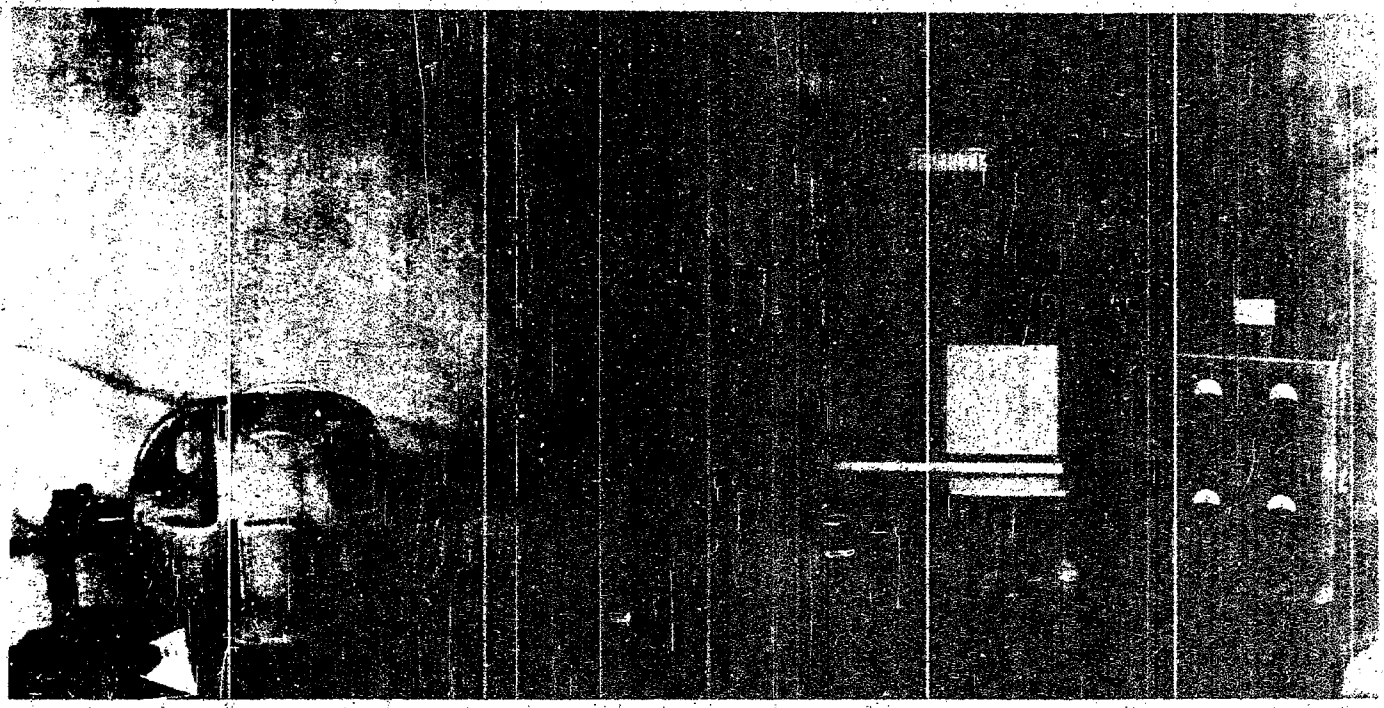

FIGURE 7 TEST SETUP FOR POINT FORCE STUDY
Showing clutch load, Harmonic Drive model, potentiometer, recorder, and strain-gage amplifier.

as shown with 16 equally spaced push rods. No shape distortion was noticeable at these torque levels. Assuming then that the shape has essentially the ideal elliptoid, the limiting value of σ is calculated as

$$\sigma_m = \frac{1}{2} \arctan \frac{1}{2 \tan \Phi_a} = 20.5^\circ \qquad (3\text{-}31)$$

for $\Phi_a = 30^\circ$ with the push rod model.

Therefore, the limiting value of $\eta_T \sin 2\sigma$ is $0.66\,\eta_T$. From this the apparent value of η_T at 1200 lb.in. torque is

$$\eta_T = \frac{0.56}{0.66} = 0.85 \qquad (3\text{-}32)$$

for the cup shape and

$$\eta_T = \frac{0.64}{0.66} = 0.97 \qquad (3\text{-}33)$$

for the bell shape.

These efficiencies appear quite high, but there are many sources of experimental and interpretative error. The factor of tooth friction is apparently very instrumental in reducing the tooth separating force, so that σ_m may be higher. (It was not measured). This would result in lower η_T values. The value of F at no load, incidently, is not a true measure of F_D, which was separately measured by the usual deflection force tests as about half that value. Side loading of the push rods introduce sizable errors at the low levels, and there was also difficulty with the electrical calibration at low levels. The potentiometer showed that when the peak force was measured, the loading on adjacent rods was zero, validating the above analysis. The study indicated a maximum torque of about 1200 lb.in. for a 3.33 inch size, beyond which the device could not be rotated, presumably due to increasing shape distortion. Harmonic Drive torque ratings are normalized to the cube of pitch diameter by the constant

$$K = \frac{T_m}{D_p^3} \qquad (3\text{-}34)$$

which, with English units, has a value of 40 lbs/in.^{2} for long life reliable operation employing a ball bearing wave generator.

The point force cam model with only 8 rods jammed and could not be rotated. This indicated that forces with this degree of separation may not be practical.

It was realized that the cam model produced contact forces like a ball bearing, not field forces which are essentially independent of small position differences, like saturated magnetic forces or fluid forces. Hence, another study model was used. An available hydraulic Harmonic Drive unit with equally spaced ports which supplied oil to push loose-fitting balls against the flexspline, was used to measure the maximum stall torque for two cases:

(1) The normal number of 24 ports.

(2) Only 8 ports, two out of every three being plugged.

For the same input line pressure of 800 psi, the comparable stall torques were:

	24 Ports	8 Ports
Stall torque (lb.in.)	165	38
Intermediate pressure (psi)	300	400
Flow to both lines (gpm)	1.10	0.70

Due to the slightly higher flow with 24 ports, the pressure at the flexspline should be slightly less than for the 8 ports. The intermediate pressure is that of the oil delivered to all of the ports positioned within an arc from 30° to 75° ahead of the port with main pressure. This works out to be 4 ports for the 24 port unit and 1 port for the 8 port unit, and could not be changed without the making of a new spool valve, which was not deemed justified. The much greater torque for the 24 port unit is partly due to the 3 extra ports acting, but their pressure was set lower than for the 8.

To overcome the problems encountered with point forces, the conventional approach has been to provide a cam, which, when rotated, provides the necessary forces acting through a ball bearing. Actually, it is found that all parts of such a wave generator between $0 < \sigma < 90^{\circ}$ produce force. Considering interaction of all the above effects the force distribution for such wave generators has the general form shown in Figure 8.

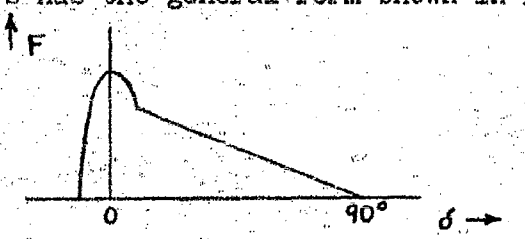

Figure 8 - Ideal Force Distribution

Producing this force distribution is much less of a problem for a ball bearing wave generator, for which the mean compressive stress under the major axis has the general level of several hundred thousand psi for high torque loads. Fort type hydraulic units might be operated at levels of several thousand psi. It is more of a problem for hydrodynamic fluid wave generators, where peak pressures run under 1000 psi in order to have the proper bearing-film thickness. But all these types require cam or valve elements rotating at input speed, which results in inertia many order of magnitude greater than is required for fast response, compact servo actuators. Electromagnetic deflection in which only the fields rotate vastly reduces the inertia. However, there are definite physical limits to the "pressure" it can produce. This depends solely on the maximum flux density, which is determined by the ferrous material used. The best saturates at about 2.4 webers/m^2 (24,000 gauss) giving a maximum "pressure" of

$$F/A = \frac{\beta_{m^2}}{2\,\mu_o} = 2.3 \times 10^6 \text{ n/m}^2 = 340 \text{ psi} \qquad (3\text{-}35)$$

Since the optimum distribution is non-symmetrical, being skewed with the peak under the major axis, if there is a limit at this point the force magnitudes ahead of the axis, for ideal distribution, would be limited even more.

The effects of shape distortion would include the possibility of higher stresses in the flexspline, which may limit the torque capability and/or shorten life, an increase in the torque produced by set magnetic forces, and an off-setting increase in inertia. In the absence of more qualitative data about the mathematical shape of the flexspline when distorted, in order to be able to make a mathematical analysis a curve is selected which is that of the second harmonic of the normal curve over certain parts of the circumference, and which has zero curvature over the other parts. This shape is shown in Figure 9. The zero-curvature, maximum-diameter portion covering 11-1/4°, and centered at the major axis, represents fairly accurately the extended tooth contact or bulge from the true harmonic shape that results with high load, even with a ball bearing wave generator. The zero-curvature, minimum-diameter portion for $\theta = 50\ 5/8°$ and greater represents the hugging against the bearing that occurs. When the method used to calculate F_T and F_R as a function of θ for the true harmonic shape is applied to this distorted shape, there are obtained the following expressions:

$$F_T = 2F \sin 4\ (\delta_m - 5\ 5/8°) \qquad (3\text{-}36)$$

$$F_R = F \cos 4\ (\delta_m - 5\ 5/8°) \qquad (3\text{-}37)$$

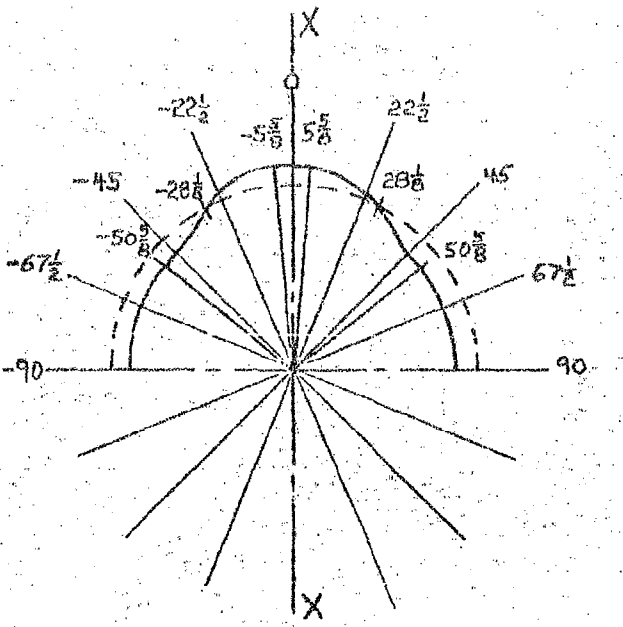

(THE BOTTOM IS A CONTINUATION OF THE TOP)
X-X MAJOR AXIS

CURVE EQUATIONS

$r = \frac{Dp}{2} - \frac{d}{2}$	$-90^\circ \geqslant \delta \geqslant -50\ 5/8^\circ$
$r = \frac{Dp}{2} + \frac{d}{2} \cos 4(\delta + 5\ 5/8^\circ)$	$-50\ 5/8^\circ > \delta > -5\ 5/8^\circ$
$r = \frac{Dp}{2} + \frac{d}{2}$	$-5\ 5/8^\circ \geqslant \delta \geqslant 5\ 5/8^\circ$
$r = \frac{Dp}{2} + \frac{d}{2} \cos 4(\delta - 5\ 5/8^\circ)$	$5\ 5/8^\circ > \delta > 50\ 5/8^\circ$
$r = \frac{Dp}{2} - \frac{d}{2}$	$50\ 5/8^\circ \geqslant \delta \geqslant 90^\circ$

FORCE EQUATIONS APPLICABLE TO THE 0° TO 90° QUADRANT

$F_T = 2F \sin 4(\delta - 5\ 5/8)$

$F_R = F \cos 4(\delta - 5\ 5/8)$

FIGURE 9 SHAPE DISTORTION ASSUMED FOR TORQUE CALCULATIONS OF SECTION 3.3

This corresponds to Figure 74 except that here the Major Axis is taken in the center of the 11 1/4° segment.

The values of peak F_T/F force ratio produced are given in Table IV and compared to those for the true harmonic shape for three cases. (20° pressure angle in all cases)

Case	True Harmonic Shape		Distributed Shape	
	σ_m	F_T/F	σ_m	F_T/F
1. Single step, no steady state load	22½°	1.414	22½°	1.85
2. Double step, no steady state load	45°	2.0	45°	2.00*
3. Single step, max. steady state load	27°	1.62	19¼°	1.95

TABLE IV - VALUES OF F_T/F

*In all cases except this one the mean torque output is approximately half to two-thirds that given by the peak value, but for this case it is considerably more, because the force begins acting when the air gap has a greater value than $\frac{d}{2}$ for which the mathematical expressions used give the maximum torque.

The maximum steady state load is that for which $F_R = F_T \tan 20°$. Therefore, theoretically, the limiting condition for maintaining tooth engagement when tooth friction effect, deflection force, and inertia force are neglected, would be exceeded.

Considering superposition of a number of applied forces, the general expressions for calculating torque and radial supporting force are

$$F_T = 2 \sum_{180°} F_K \sin 2\theta_K \qquad (3\text{-}38)$$

$$F_R = \sum_{180°} F_K \cos 2\theta_K \qquad (3\text{-}39)$$

3.4 The Pre-Stressed Ring

Besides the radial forces discussed in Section 3.3, consideration was given early in the project to another unique element that can provide radial tooth engagement force. This is called the pre-stressed ring.* However, it was determined in the

*The pre-stressed ring is the subject matter of U.S. Patent Application No. 108,600. All proprietary rights of United Shoe Machinery Corporation are hereby reserved.

analysis that, even without the pre-stressed ring, the teeth should not disengage when no electrical power was applied, due to residual magnetism. As a result, and because at the time, the element was not developed sufficiently for use with EHD, it was not utilized in the models. When they were operated, no tendency for tooth engagement was experienced, bearing out the analysis. The pre-stressed ring might warrant future investigation as a refinement, since it would assist in keeping the teeth engaged and permit a somewhat greater power angle. As discussed in Section 3.6, the pre-stressed ring significantly increases the total inertia of an EHD device, although its inertia would be negligible in relation to a conventional ball bearing wave generator. Therefore, if the increased torque it produces is permissible from a shape-control viewpoint, it would be advantageous to include the pre-stressed ring if the actuator's power rate is, thereby, increased.

3.5 Electromagnetic Wave Generation

The forces that are applied on the flexspline at equilibrium have now been defined and examined. It is quite evident that the result of all these external forces is a stress distribution within the flexspline that is very complex. There is certainly no intention to define this stress distribution here. Still, it is necessary to determine the extent to which the driving force pattern can be altered from that produced by a normal harmonic drive wave generator ball bearing, which has been proved to work properly through exhaustive life testing. The approach that might be taken is to use the design guide parameters that have been successfully developed and tested and try to duplicate the action of a ball bearing wave generator. But since magnetic forces are field forces, much poorer control of the position results, that is, already there will be an unavoidable departure from ball bearing action. To correct for this may require a force pattern or sequence different from what the bearing produces.

Therefore, it is necessary to approach the question of required force distribution in another way. The fact that magnetic forces differ from ball bearing forces must be accepted, and the characteristics of the magnetic forces adapted as required. In order to withstand the external loads discussed above, it is necessary to produce driving forces that support the two components F_T and F_N. At the same time, departure from proper shape cannot be too great or trouble might be encountered from early fatigue failure of the flexspline or from greatly increased tooth wear. Since the shape cannot be controlled as well as with the bearing, considerable care should be given to avoiding severe distortions. In general, it is the feeling of experienced Harmonic Drive personnel that gradual departures from the theoretical shape can be permitted to the extent that the torque and efficiency can be reduced. The main caution stressed by all is that reversed bending should be avoided.

At the very start of the project, a comprehensive survey was made of all the known methods of producing short stroke forces involving electrical or magnetic principles to determine the best candidates for further study. These, including the ones considered worthwhile enough for preliminary analysis, are listed in Table V, together with comments on feasibility. It was decided that two methods offered practical value for a high power rate actuator of a reasonable size, weight, and efficiency. They were:

1.1.1 Electromagnetic attraction using a soft iron armature (reluctance action)

1.1.2 Electromagnetic attraction using an armature which has a fixed magnetic polarity, either by use of a permanent magnet or a coil placed around soft iron material.

Before discussing these, brief comment should be made of the nutating armature. This is an outgrowth of a rather ancient idea, covered in many old patents (Reference 12), of a rigid rotor with a series of flats that mates with a stator which has one more than the same number of flats each with the same face area. The flats are magnetically attracted making the rotor walk around inside the stator. A flexible connection couples it to the load. Applied to flexible-body mechanics (Harmonic Drive) the rotor can be walked around, without rotating, inside a flexspline, thereby acting as a wave generator. The result is a much higher reduction ratio and torque output for the same size unit, compared to the rigid body devices. However, the inertia of such a wave generator, (often called a "swash plate") was calculated and shown to be much greater than even the rotating ball bearing wave generator (see Section 3.6).

Returning to the two feasible concepts, Figure 10 explains some of their features and variations. From the viewpoint of force produced in terms of the input to the force motor, 1.1.2 is just a special and more versatile case of 1.1.1. Hence, consider 1.1.1 first.

Reluctance type of magnetic forces result when magnetic flux of high density issues from a non-moving magnet, passes across an air gap into a movable armature assembly of sizable area perpendicular to the air gap flux. The third dimension of the armature, its depth, depends upon the type of return path of the working flux. For one basic type of force motor, in which the iron path remains constant, the flux after entering the armature turns a right angle, passes along the armature a certain distance, and then turns another right angle and recrosses another air gap similar to the first to get back to the fixed magnet. The two gaps are arranged so that the forces established at both gaps add together to provide the total output torque. An example of this type is a servo valve torque motor. For the

	FEASIBLE	NON-FEASIBLE	COMMENTS
1. Electromagnetic Field Forces			
1.1 Radial-Acting Armature			
1.1.1 Reluctance Action			Has many variations, see
1.1.1.1 Integral with Flexspline	✓		Figure 7 for comparisons.
1.1.1.2 External to Flexspline		✓	Considered marginally feasible at this time due to poorer shape control and dynamic problems - no design made.
1.1.2 Polarized Armature Action			
1.1.2.1 Integral with Flexspline		✓	Flexspline not compatible with permanent magnets or moving coils.
1.1.2.2 External to Flexspline		✓	Same comment as for 1.1.1.2
1.2 Nutating Armature (Swash Plate)		✓	Inertia several orders of magnitude higher
2. Force on current through a magnetic field			
2.1 Radial moving printed circuit cards within permanent magnets.		✓	Excessive currents required.
3. Piezoelectric Force		✓	Amplitudes too small.
4. Magnetostrictive Force		✓	Amplitudes too small.

TABLE V - METHODS OF PRODUCING HARMONIC DRIVE INPUT FORCES CONSIDERED IN THE STUDY PHASE.

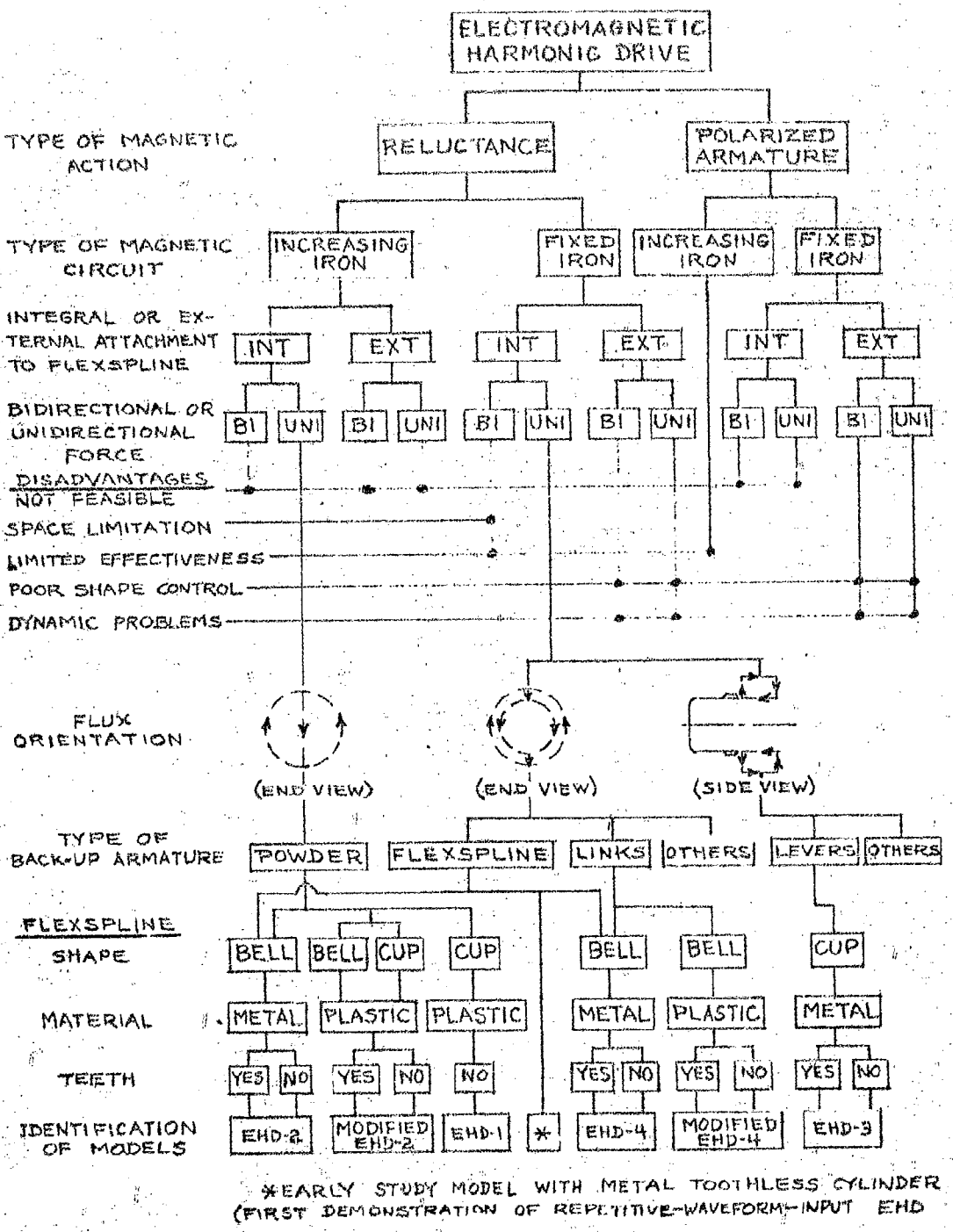

FIGURE 10 VARIATIONS OF ELECTROMAGNETIC HARMONIC DRIVE

second basic type of force motor in which the iron path changes with armature movement, part of the magnet's flux passes through the armature into another portion of the magnet on the other side, the portion of the armature lying along the flux path increasing in volume to fill the gap with high permeability material. Due to the reluctance of the added material which must be magnetized, some of the total MMF in the path is utilized, and as a result a slight loss in force occurs. If the permeability of the material is several orders of magnitude greater than air, the loss is negligible but if it is only a few times greater, the loss must be considered. An example of this latter type is a plunger magnet.

The magnetic force, in terms of the input can be expressed as

$$F = \frac{1}{2} \mathcal{F}^2 \frac{d\mathcal{P}}{dx} \qquad (3\text{-}40)$$

where $\mathcal{F}$ is the MMF drop across the air gap, $\frac{d\mathcal{P}}{dx}$ the change in permeance with change in gap. (Derived in Appendix V). When the iron portion of the magnetic path is operated below its saturation level, the MMF drop though it is negligible compared to the air gap, and $\mathcal{F}$ above can be taken as the input MMF. But for high-power tractive electromagnets, where linearity is unimportant but the highest force per unit mass of armature is desired (as with the EHD), the flux density on the iron reaches saturation and the MMF drop in the iron starts to become significant. Hence, it is more convenient to utilize an alternate expression for magnetic force

$$F = \frac{\beta_m^2 A}{2\mu_o} \qquad (3\text{-}41)$$

(also derived in Appendix V) which expresses the maximum force availablefor a flux density based upon the magnetic material's characteristics.

Return now to the second basic type of force motor to be considered. When an armature is used that has a fixed magnetic polarity in the absence of any other fields, there is a bias flux established in the air gaps and, for equal gap areas, the flux densities are equal. When a non-constant magnetic field is applied, the flux lines so producedinteract with the bias field in accordance with known physical principles to produce a combined magnetic field distribution by which the flux density is higher where they reinforce, lower where they counteract.

The major advantage of the polarized armature over the non-polarized types are that a bidirectional force can be produced upon the armature by a magnet yoke positioned on just one side of the armature. With reluctance action, bidirectional force

requires yokes on both sides. With just one yoke, the armature mass must still be accelerated during periods when no force is produced. With bidirectional forces, higher power rate results.

As the total torque may now exceed the limit based upon shape control, this may dictate a reduction in armature size, rather than a torque increase, also increasing power rate compared to the unidirectional reluctance forces.

The armature is arranged so as to apply radial forces to the flexspline deflecting it into engagement with the circular spline through the small distance required, which is a function of the reduction ratio and the basic size of the actuator. In order to obtain rotation of this deflecting action around the flexspline, a number of such magnets can be used together with proper phasing.

With the increasing-iron-path type, it can be seen that the material must of necessity be a magnetic powder, liquid or some highly elastic solid such as rubber. Because of its required elastic property, it cannot by itself be used to apply forces on the flexspline unless the flexspline is directly along the flux path. Thus, the flexspline necessarily is placed as a membrane across the path. Its material can be of two types:

1. Magnetic. - In this case it will also provide a flux path within itself of the fixed-iron-length type. The two paths would be in parallel magnetically, and the flexspline would be brought to saturation before the powder path is significantly magnetized. From the viewpoint of force, this is good as there is a no loss in force involved. But, there is a major disadvantage. The flexspline acts as an excellent electrical conductor path for eddy currents. This incurs power loss and also time delay, which may limit the speed of operation. A way around this would result from a flexspline construction that had magnetic elements directionally placed to carry flux without providing a current path at right angles. One embodiment might be a coil of wire embedded in plastic.

2. Non-magnetic. - In this case, the flexspline only acts as an increase in air gap. Obviously, a non conductor such as plastic should be used, because if non-magnetic stainless steel or aluminum were used, for example, there would be the disadvantage of eddy currents without the advantage of providing a parallel flux path.

It is desirable to avoid eddy currents in all iron portions of the path, armature or fixed.

It was seen that to obtain significant forces, the area had to be large. For the fixed-iron-length type, the cross-sectional

area of the armature must equal that of the air gap, so the armature's thickness is considerable. The problem was to devise an armature of large thickness which was essentially no less flexible than a flexspline.

In fact, this constituted the key design problem to be solved. The approach used in two of the models was to use a series of laminations or links that constitute parallel flux paths, but are not joined to each other so do not raise the deflection force. The lamination thickness should be of the order required to prevent eddy currents. For the increasing-iron-length type, the total thickness of the armature must be the thickness of the flexspline plus the Harmonic Drive deflection plus a reasonable minimum clearance for containment of that portion of the powder that does not move away when the flux is low or zero. This is an area for design optimumization.

Referring again to Figure 10, consider next how the forces are attached to the flexspline.

Distributed forces are considered much superior in their closer duplication of the ball bearing and avoidance of high localized stresses. In the push rod point force model tests when the model was operated with only 8 rods, it was not possible to rotate the unit with any torque load. Shape distortions impeded the action of the cams and push rods. Even though magnetic field forces would behave somewhat differently, an indication of shape distortion was given at higher torques with the 16 push rod tests. Thus, integral mounting is preferable.

With the polarized armature, the fixed iron provides all the advantages and none of the disadvantages of the increasing-iron type and so would be preferred. But no way was found by which the polarized armature could be made integral with the flexspline. Permanent magnetic material has poor mechanical properties and a considerable mass is required to achieve a useful field strength. The continuous shape of the flexspline does not lend itself to having coils placed around it. Thus the polarized armature type has to be external. This was the major reason for deciding not to design a model of the polarized armature type, employing external torque motors connected to the flexspline. If this type were to be pursued, a method of attachment that does not stiffen the flexspline must be conceived. It was also believed that this type would have lower resonances, be more affected by shock and vibration, and require more volume and weight.

Therefore a choice was made for the reluctance type. The following discussion in this report will be concerned with this type only.

It has been shown that the increasing iron type of magnetic circuit must work in conjunction with a flexspline, so this

eliminates the external attachment in favor of the integral. This becomes one of the feasible types. Although the fixed iron type of circuit could be made either integral or external, for the reasons given integral is chosen. This is the other feasible type.

Figure 10 gives the disadvantages for dropping various variations that have been discussed.

The next design variable to be considered, from Figure 10, is that of flux orientation. There are three possible orientations, as shown in Figure 11. Variation (C) also has some of (B) if it has a metal flexspline, as discussed previously. A variation of (A) would be use of an E shape fixed portion, with a center leg. In order to minimize flux leakage, the windings should be placed as close to the air gap as possible. Thus all legs require the same MMF, since

$$\mathcal{F} = HL = \left(\frac{\mathcal{B}}{\mu}\right)g \qquad (3\text{-}42)$$

Hence, the E shape requires 50% more total MMF. Also the E shape has more armature mass per force produced. The E shape is essential with many types of polarized armature motors.

The flux orientations (B) and (C), if they utilize a sufficient number of stator pole teeth, can conveniently be made to have a nearly sinusoidal distribution of flux, as with an AC motor. This results in a constant-magnitude, traveling wave of force (the same result produced by the external polarized magnet motor with sinusoidal input.) Provided that the load is suitably limited, the Harmonic Drive shape will rotate in synchronism at a frequency equal to the excitation frequency. Furthermore, when operated with a suitably matched external load, the device will produce constant output torque and tooth supporting force.

Orientation (B) has the disadvantage that all the flux is focussed through the links so that the maximum flux density at the gap is less than with (A) or (C). In fact, peak air gap flux density is given by

$$\mathcal{B} = \frac{r_l}{w_Q \sum_{90^\circ} \mathcal{B}/\mathcal{B}_m}\,\mathcal{B}_l \qquad (3\text{-}43)$$

where $\mathcal{B}_l$ is the flux density in the most highly magnetized link, r_l is the link's radial thickness, w_Q is the arc length of a stator pole tooth, and $\sum_{90^\circ} \mathcal{B}/\mathcal{B}_m$ represents the summation of

(A) SINGLE MAGNET TYPE – FIXED IRON PATH

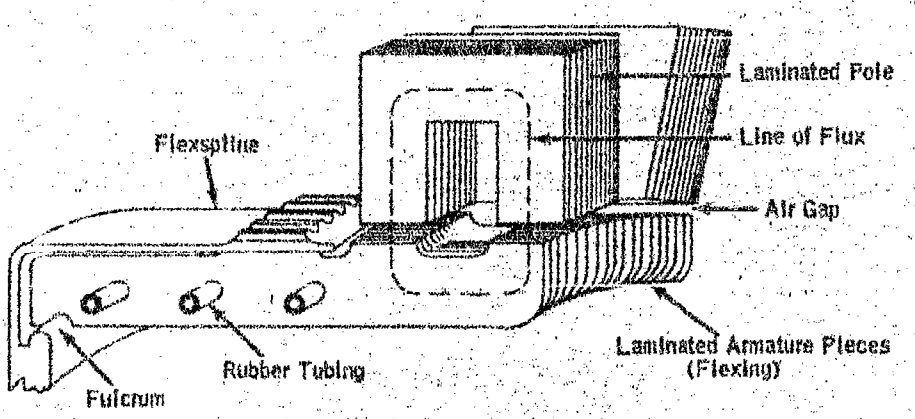

(B) CIRCUMFERENTIAL FLUX
SINUSOIDALLY WOUND TYPE – FIXED IRON PATH LINK OR SHEET ARMATURE

(C) RADIAL FLUX
SINUSOIDALLY WOUND TYPE – INCREASING IRON PATH POWDER & CORE ARMATURE

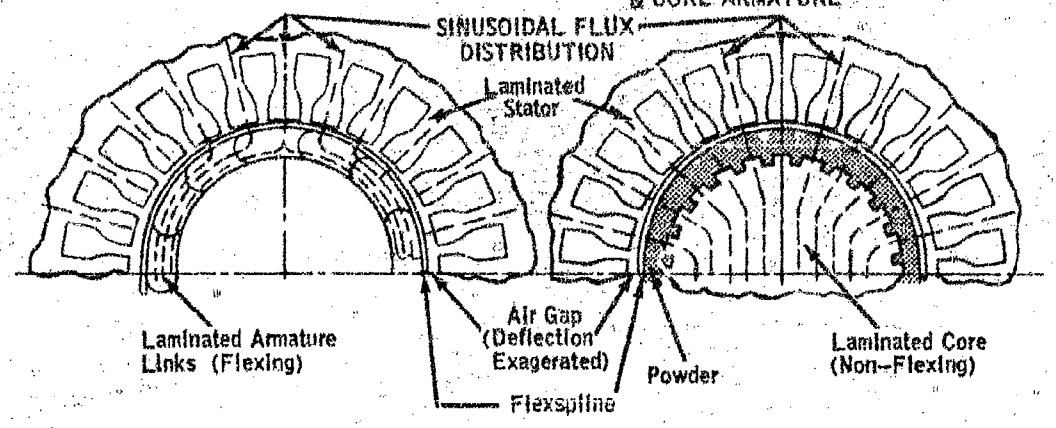

FIGURE 11 FLUX ORIENTATIONS OF THE RELUCTANCE TYPE ACTUATOR

flux from various stator teeth which equals 3.8 for model EHD-2. For typical values of r_i to w_Q of about 1.3 (model EHD-4), $\mathcal{P}$ is reduced by about 1/3. Another disadvantage of (B) is the air gaps between each of the links. The flux passing through produces MMF drop and frictional force which stiffens the flexspline and increases power losses, even though there is no powder path with its MMF drop. Also (A) is stiffened by the rubber tubing joining the laminations and (C) by the diaphragms that are used to confine the powder to the air gap. (C), of course, suffers from the loss of force due to the permeability of the powder. (B) and (C) can conveniently use ready-made motor field stators, or at least parts which need only minor modification. (A) has to be made as a series of individual magnets. Although it could be wound to have a sinusoidal distribution, it lends itself most readily to separate windings of each magnet. When these are sequentially driven, stepping action is achieved. The force produced by each magnet is considered essentially constant in magnitude due to saturation of the armature. It is fixed in space by the fixed position of the magnet and makes the shape step until net accelerating torque output is zero. The angle between its resultant force and the instantaneous major axis changes throughout the step.

As a result of these variations, it was believed that a number of models were worthy of detailed analysis, design, manufacture and test. Actually four were made, as identified in Figure 10. Types EHD-2 and EHD-4 are representative of flux orientation (C) and (B) respectively, which use the same bellshape flexspline, stator and housing. The flexspline is metal. Both were operated using tooth engagement as well as friction drive. Type EHD-1 was a preliminary model using a toothless plastic cup shape flexspline in the same stator and housing. Type EHD-3 is representative of flux orientation (A).

Sectional drawings of EHD-2 through 4 are shown in Figures 12 through 14. Various photographs of the complete models and some of their key elements are shown in Figures 15 through 21. Figures 22 and 23 show a demonstration model made early in the program, which has no teeth or output shaft, but proves that an A-C field will rotate a flexible ring by harmonic drive action. The capacitors produce two phases to assure starting and constant magnitude flux.

These models meet the basic requirements set forth in Section 3.3 to varying degrees. They will now be compared with regard to angular spacing between magnet poles and distribution of force produced. With the stepping field* actuator, model EHD-3, angular spacing between poles refers to the angle moved with each step. With 16 magnets, this is 22-1/2° for a single step and

*Abbreviated SF in this report.

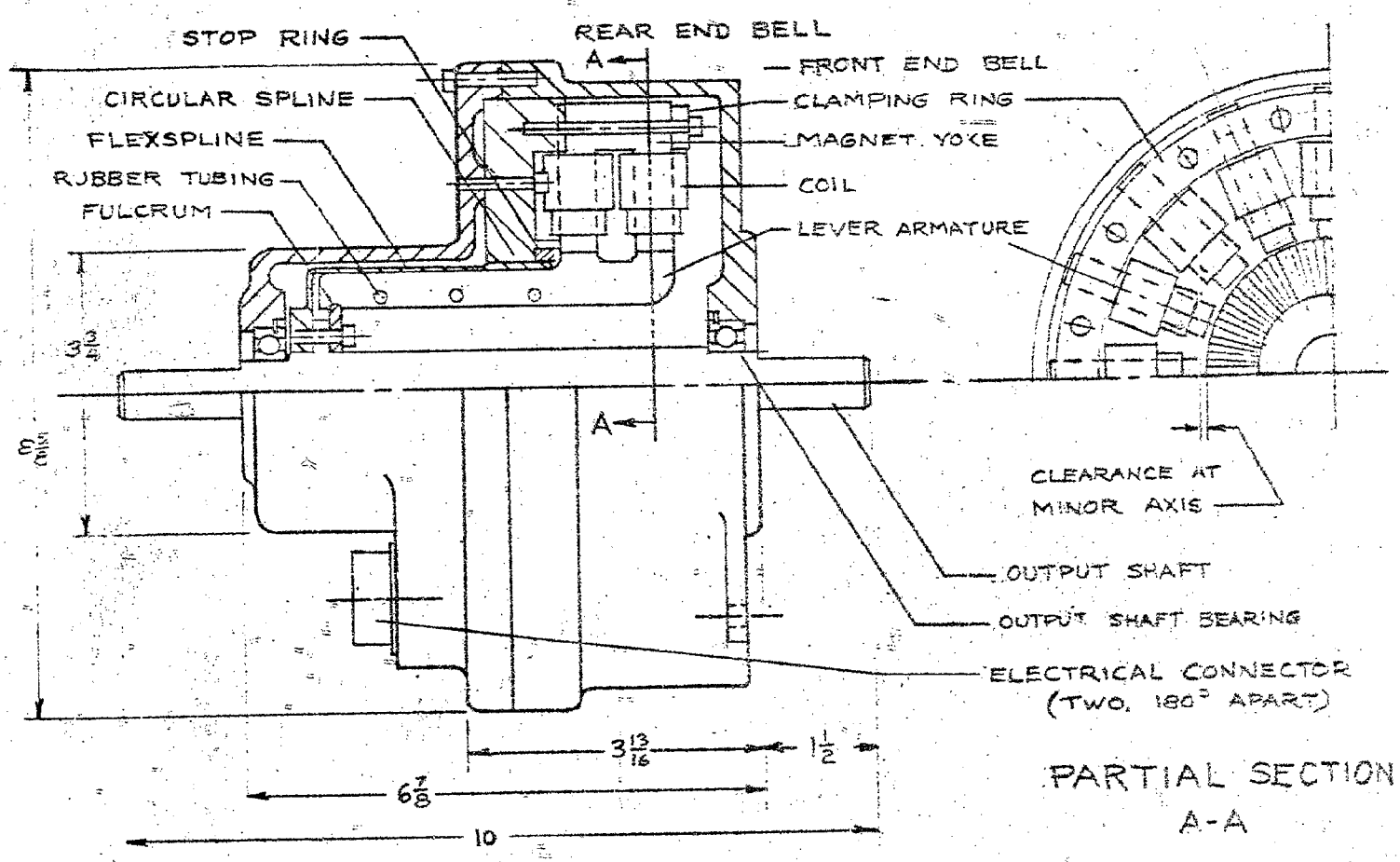

FIGURE 12 MODEL EHD-3 SECTIONAL DRAWING
WEIGHT AS BUILT 22 LBS.
PITCH DIAMETER 3 1/4"

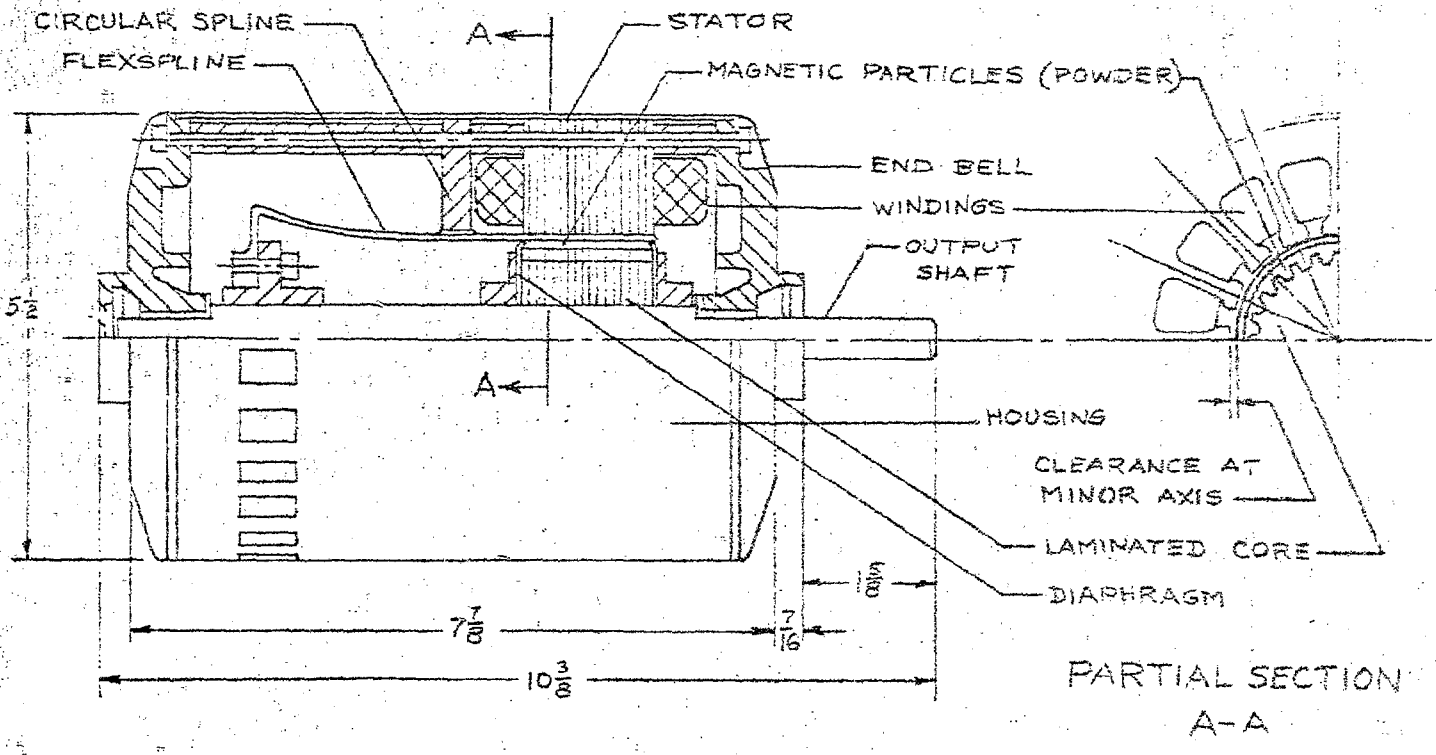

FIGURE 13 MODEL EHD-2 SECTIONAL DRAWING
WEIGHT AS BUILT 16 LBS. PITCH
DIAMETER 2.6"

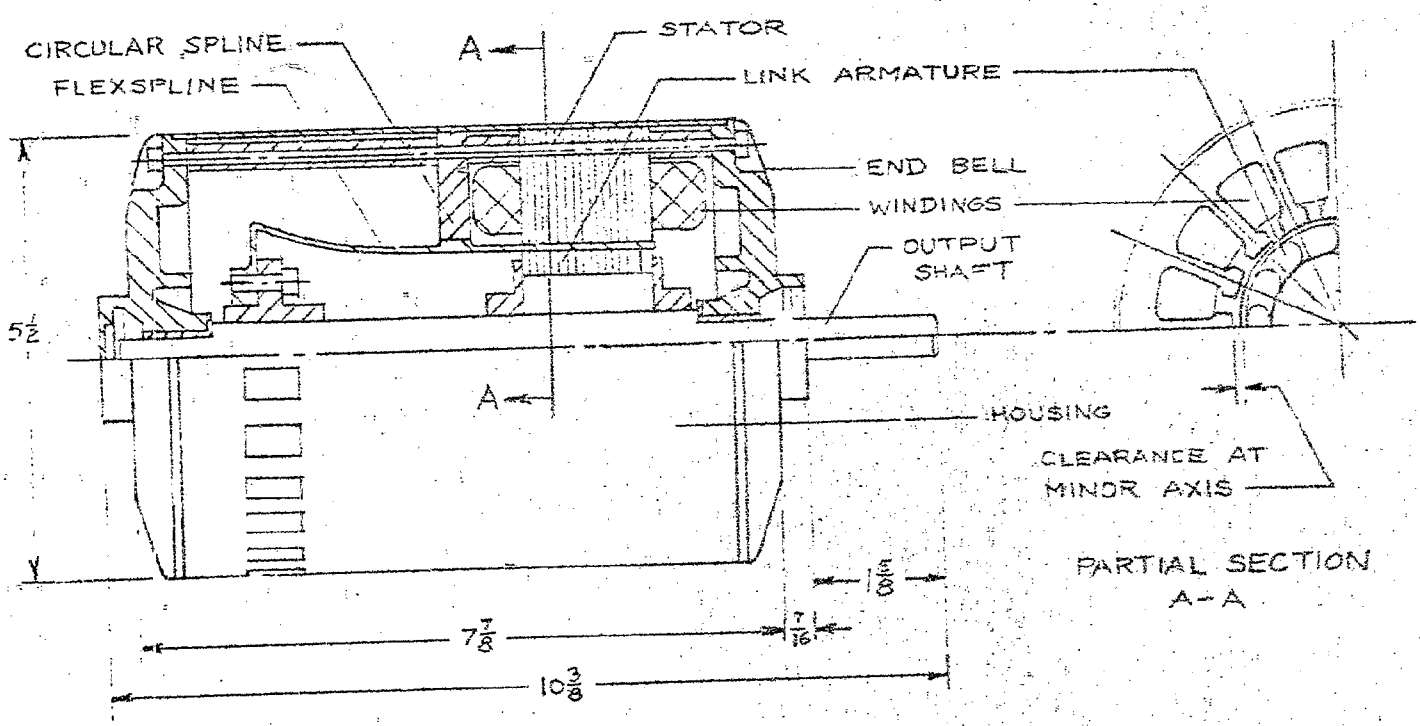

FIGURE 14 MODEL EHD-4 SECTIONAL DRAWING
WEIGHT AS BUILT 16 LBS. PITCH
DIAMETER 2.6"

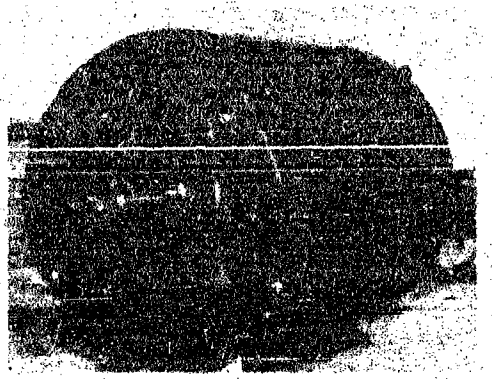

FIGURE 15 EHD-1 STUDY MODEL, END VIEW

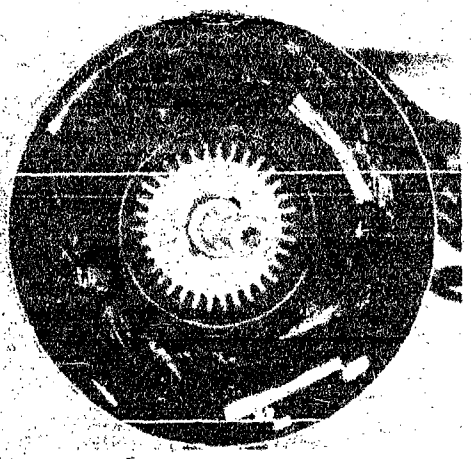

FIGURE 16 EHD-1 STUDY MODEL, END VIEW, END BELL REMOVED

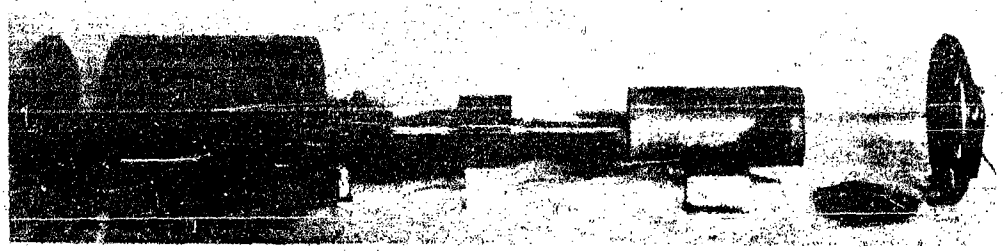

FIGURE 17 EHD-1 STUDY MODEL, EXPLODED

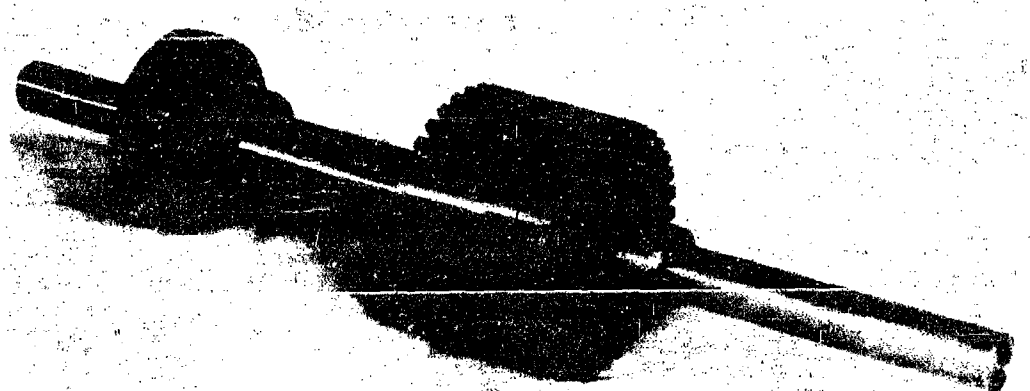

FIGURE 18 ARMATURE CORE FOR MODELS EHD-1 AND EHD-2

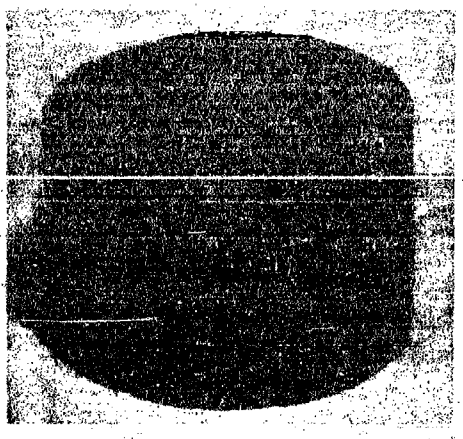

FIGURE 19 MODEL EHD-4 LINK ARMATURE

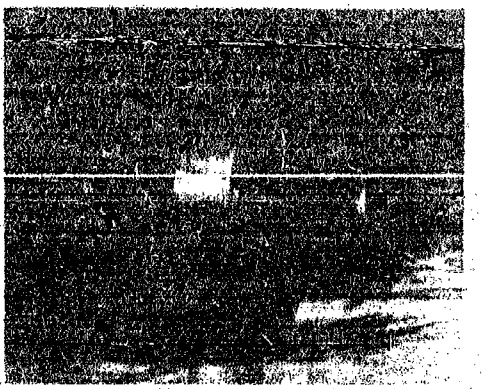

FIGURE 20 MODEL EHD-3 ASSEMBLED

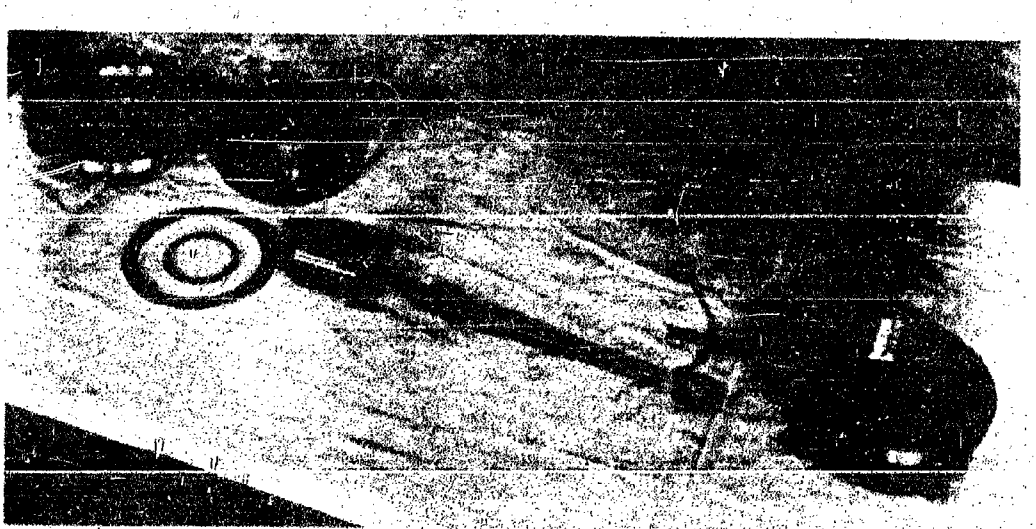

FIGURE 21 MODEL EHD-3 EXPLODED

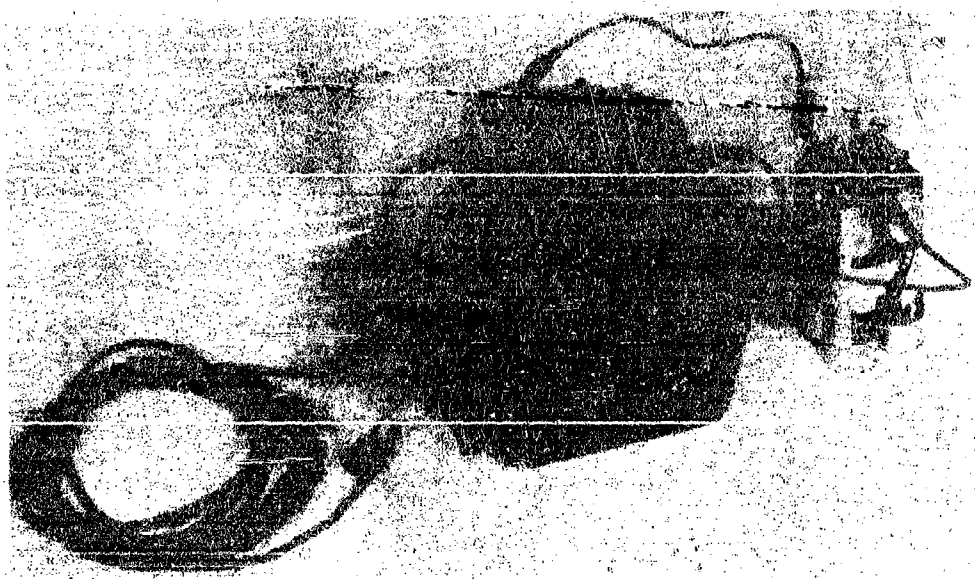

FIGURE 22 STUDY MODEL TO DEMONSTRATE ELECTROMAGNETIC HARMONIC DRIVE ACTION

FIGURE 23 STUDY MODEL TO DEMONSTRATE ELECTROMAGNETIC HARMONIC DRIVE ACTION, RING REMOVED

45° for a double step. It has been shown that the double step produces a larger peak and mean torque, but that the teeth may disengage. A single step with an 8 magnet design produces the same result. Twelve (12) magnets would offer a compromise.

Thus, the smaller the step angle, the more constant but lower the torque. Constant torque output is not obtained with most existing stepping devices, in fact it is better to have a high accelerating torque at the start of the step. The maximum step and hence the minimum allowable value of F_R is subject to interpretation. The instantaneous values of the radial components of the tooth load and the driving forces, in conjuction with the inertial resistance of the flexspline to move suddenly, will determine the instantaneous flexspline shape in the tooth contact area. The average torque loading will be lower for the electromagnetic drive than for ball bearing wave generator types, and a large value of pitch line overlap is generally to be provided at the major axis. After each new step, the flexspline is given a pulse of outward force at this point which moves the flexspline outward in the intervening arc between major axis and the new force, the portion toward which the major axis is moving. The conditions for Harmonic Drive action exist, even though there will be pulsations in the motion, possible minor local deformations as a result, and some tooth sliding. If we provide a pattern and sequence of driving forces sufficient to establish overlap at start up of the device under load, then it can be expected that overlap will exist over most of the cycle. There will be only a small portion of the cycle where F_R might be momentarily less than F_N.

With the rotating field* types, spacing between poles refers to the distance between stator pole teeth or slots. If significant, this can cause distortions in the desired sinusoidal flux distribution. But with the usual number of about 24 slots, this is not a problem.

Force distribution is studied as the length of arc segment over which the force is instantaneously applied. With the SF type, this refers to whether or not two or more adjacent poles are energized at the same time, and if there is overlap. From earlier discussion, it was said that the angle from 0° to 45° is most useful for providing both F_T and F_R forces. Thus, the SF type should be designed to have a 45° distribution, two adjacent poles acting simultaneously. With a single step, this makes the maximum power angle 22-1/2° for the combined magnets. An alternate of having three adjacent poles acting produces the same maximum power angle, for the combined magnets, but since there are three magnets acting over an angle from -11-1/4° to +56-1/4° the total F_T is increased, by the amounts shown in Table VI.

*Abbreviated RF in this report.

Normalized Force	Three Adjacent Magnets Single Step	Two Adjacent Magnets Single Step
F_T/F	1.84	1.41
F_R/F	0.71	0.71
F_N/F	0.67	0.51

TABLE VI - EFFECT OF OVERLAP UPON FORCES

Thus, an increased torque is produced. However, the increased torque loading may produce excessive stresses through distortion, the margin by which F_R exceeds F_N is very small, and 50% more total current is required by the actuator so that the heat generated is also 50% greater. Hence the gain may not be worthwhile. Two adjacent magnets were employed with the EHD-3 tests. Figure 24 shows the distribution of all the forces for this model.

For the RF type, distribution of forces refers to the angle over which a half wave of the sinusoidal force is applied. This is necessarily 180° with a sinusoidal flux distribution, since there can only be two poles to produce the elliptoidal flexspline shape. This considerably exceeds the desired angle, and is a disadvantage. (The external polarized armature type would have a 90° angle that is much superior). One possible way to get a 90° distribution from the RF type would be to apply half wave sinusoidal currents to a 4 pole stator, as shown in Figure 25. The disadvantages are torque and supporting force fluctuations to zero, and lower efficiency.

Figure 26 shows the distribution of all the forces on the RF models. A summary of the advantages and disadvantages that have been discussed is given in Table VII.

3.6 Inertia

The mass moment of inertia J_M of the EHD devices is calculated by summing the contributions of various moving elements. For elements rotating without deflecting, inertia is calculated simply by the common methods given in texts on mechanics (Reference 11). For example,

$$J = \tfrac{1}{2}M\,(r_o^2 + r_i^2) \qquad (3\text{-}44)$$

for a cylindrical element of outside and inside radii r_o and r_i and mass M.

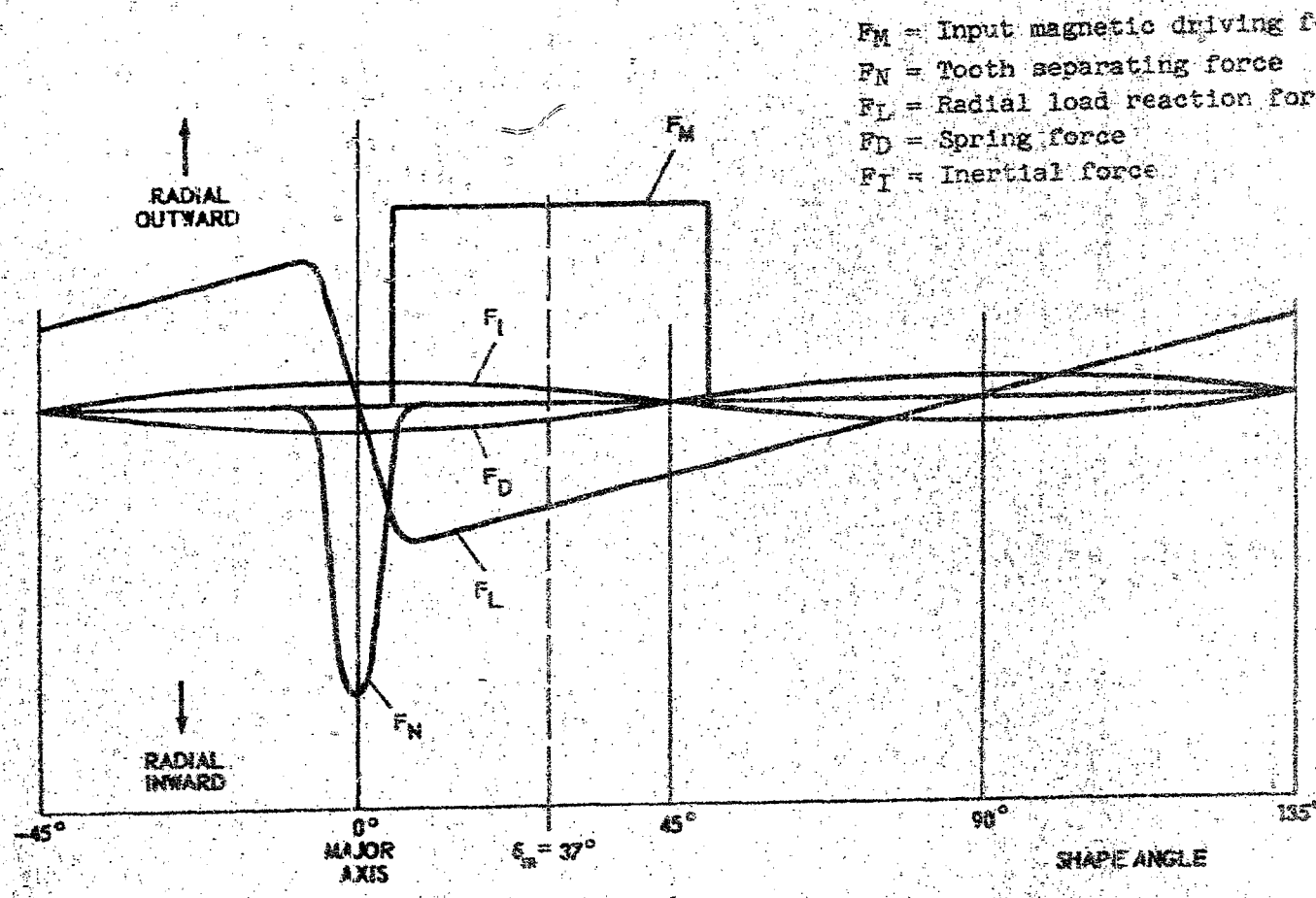

FIGURE 24 RADIAL FORCES ON THE FLEXSPLINE, MODEL EHD-3, APPROXIMATE RELATIVE MAGNITUDES, JUST AFTER SWITCHING, 27° POWER ANGLE, 20° PRESSURE ANGLE

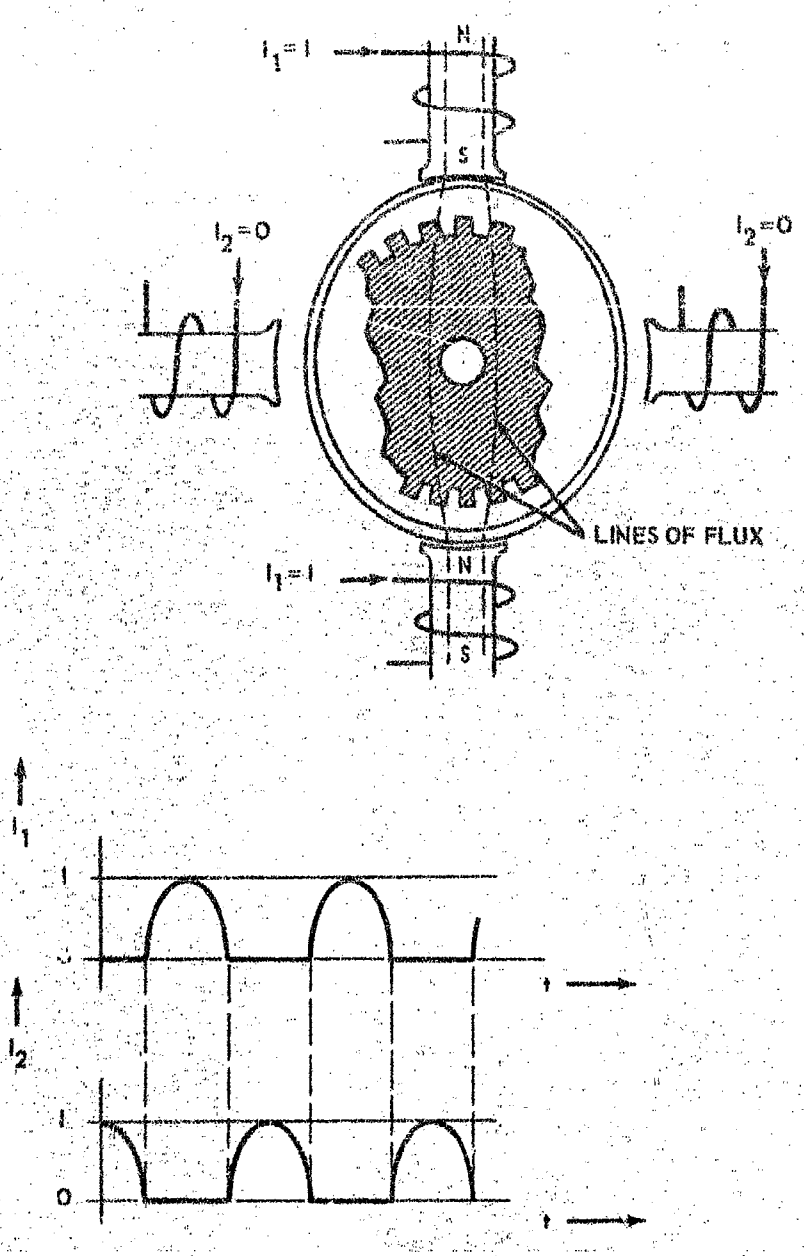

FIGURE 25 MODIFIED 4 POLE MACHINE WINDING OF ROTATING FIELD STATOR
Diametrically opposed stator poles are magnetically in series as shown. Quadrature axis current is zero due to half wave rectification.

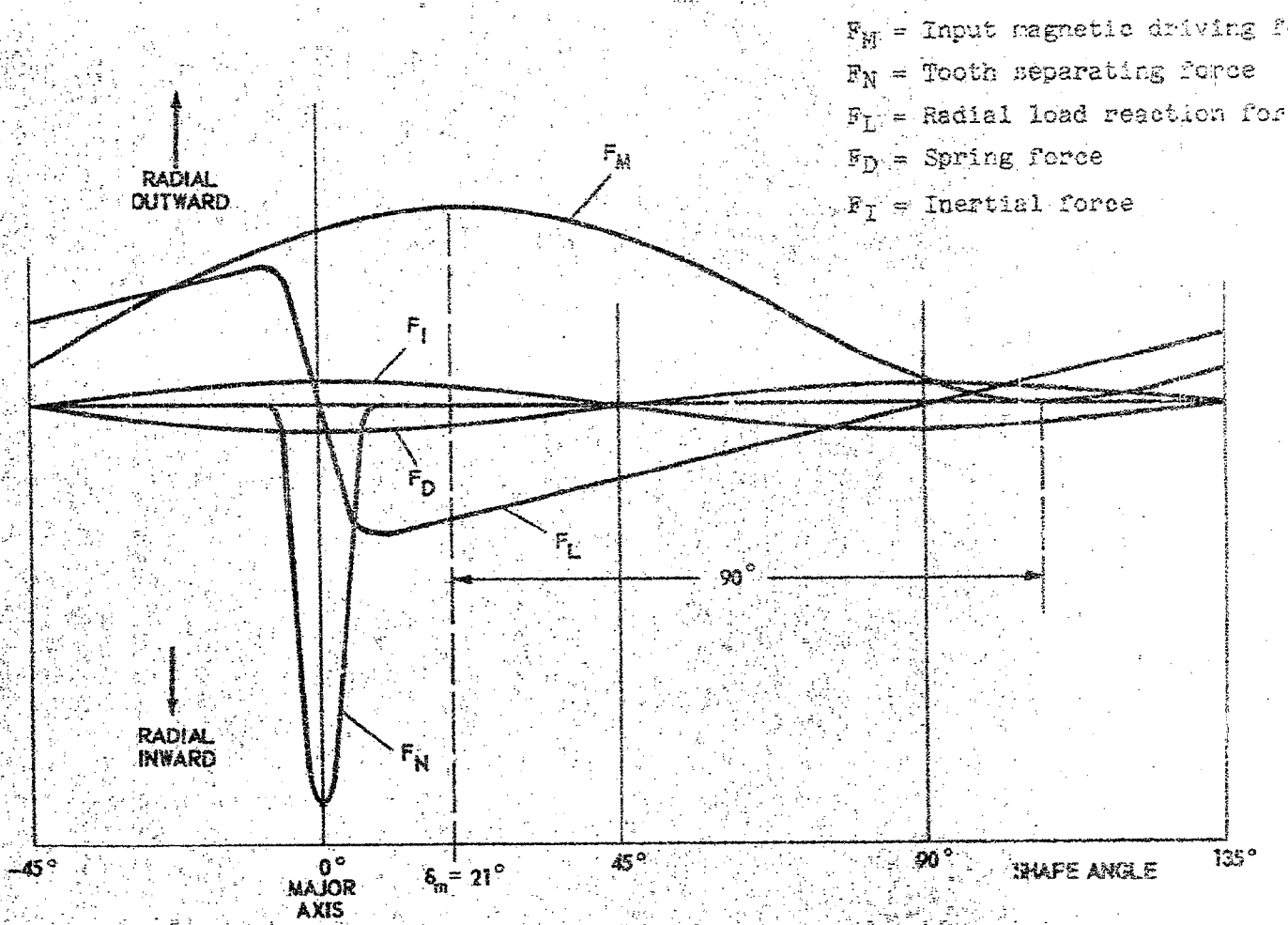

FIGURE 26 RADIAL FORCES ON THE FLEXSPLINE, ROTATING FIELD MODELS, APPROXIMATE RELATIVE MAGNITUDES, 21° POWER ANGLE, 30° PRESSURE ANGLE.

	RELUCTANCE ACTION			POLARIZED ARMATURE
	SF TYPE (EHD-3) Single Step	Double Step	RF Type	
Type and Application				
Point Force External to Flexspline				D
Distributed Forces integral with Flexspline	A	A	A	
Waveform				
Sinusoidal(Travelling)			N	N
Pulsating (Fixed in Space)	N	N		
Two-Direction Stroke				
Yes				A
No	D	D	D	
Spacing				
Size of Step	A	D*		
Waveform Distortions			A	
Distribution				
Angle Force Acting(Per Side)				
45° Square Wave	A	A		
90° $(\text{Sine})^2$ Wave				A
180° $(\text{Sine})^2$ Wave			D	

Code

A-Advantage Given
D-Disadvantage Given
N-Neutral; Advantage for that type of application

*Estimated, based upon analysis

TABLE VII - COMPARISON OF FORCE CHARACTERISTICS OF EHD CONCEPTS

For elements that deflect, their deflection contributes an effective inertia when viewed from the output shaft, which is most conveniently calculated as follows. (The following formulas are derived in Appendix VI.) The mean kinetic energy of the deflecting elements due only to the motion of such deflections, is found and equated to the expression for rotational kinetic energy at the output shaft

$$W = \frac{1}{2} J_M \dot{\theta}_M^2 \qquad (3\text{-}45)$$

This expression is solved for J_M

$$J_M = \frac{2W}{\dot{\theta}_M^2} \qquad (3\text{-}46)$$

If the deflecting elements happen to also rotate with a speed equal to some constant fraction of the output shaft, then this inertia is found as for rigid elements discussed above and added to the inertia due to deflection. One note of explanation is necessary here. If the speed is less than output speed, say the fraction R_{g_1}, then inertia, reflected to the output shaft, is equal to the inertia of the element times $R_{g_1}^2$, since inertias are reflected through gear ratios as the square of the ratio.

For the case when the flexible members have ideal harmonic shape, every element of the flexible member has an elliptoidal motion to its deflection, and the effective inertia of a continuous homogeneous flexible cylinder is

$$J = \frac{5}{8}\rho V D_p^2 = \frac{5}{8} n_M M_a D_p^2 \qquad (3\text{-}47)$$

where ρ is the density of the elements including applicable stacking factor and V is the circumscribing volume of the entire cylinder of flexible elements.

If the shape is distorted from the ideal, its inertia increases. For example, when distorted to the degree described in Section 3.3, an assumed possible shape which is convenient for calculations and considered somewhat representative of the "bulge and hug" effect, the inertia would double.

In the case of a cup-shaped flexspline, as used with Model EHD-3, the most significant part of its deflecting mass is that of the tooth bed. It is convenient to make the approximation that the inertia due to deflection is based solely on the bed and that,

for a bed of length $\frac{D_p}{8}$, to consider that it has parallel motion, i.e., that a line along the teeth always remains parallel to the axis of the flexspline. Actually, the bed rotates around a center near the outside of the diaphragm, but the result is essentially the same and the analysis is greatly simplified, particularly when the tangential component of velocity is to be taken into effect.

In the case of type EHD-3, there are a series of armature laminations that also act as levers pivoting essentially at one end. Due to their closeness and coupling by the rubber tubing and the flexspline, they will exhibit harmonic motion, or at least some degree thereof, and so tangential motion should again be considered. But the variation of mass of these levers with length is essentially constant so that a different approach is convenient. One then finds the radius of gyration of the levers, k, which is defined as the distance from the axis of inertia to the point at which the mass of the body may be assumed to be concentrated and still have the same moment of inertia as does the actual distributed mass of the body.

For the idealized shape assumed for a lever, from Appendix VI

$$k = 2.66" \qquad (3\text{-}48)$$

The amplitude of motion at this point is related to the known amplitude at the center of the teeth by the ratio

$$\frac{k}{l_2} = \frac{2.66}{2.5} \approx 1.0 \qquad (3\text{-}49)$$

Due to the proportions, then, in this case it is possible to consider that the armature elements are deflecting at the plane of the teeth with the known amplitude d.

In the case of Model EHD-2, there is a powder of small iron particles that experiences harmonic motion, or a degree thereof, as shown by high-speed movie studies. A reasonable approximation for the inertia of the powder is obtained by considering that the powder acts as a flexing cylinder the same as the tooth bed or a flexing ring of armature material, selecting a density that accounts for the porosity. Since the particles have to periodically move circumferentially to provide clearance for the inward-deflecting flexspline, the inertia may be greater than the simplifying assumption yields, but no analytical expression for the increase was obtained. Thus, the inertia calculated would represent a limiting minimum value and hence the best obtainable result.

Type EHD-2 also contains a different element, the bellshaped flexspline, in which the tooth bed and all portions that are parallel in the non-deflected state are designed to move with parallel motion. The inertia due to the deflection of such mass can, in this case, be calculated exactly. However, that inertia due to the curved shell represents another case. A satisfactory approximation is to consider that the total mass of the curved portion is equal to about $\frac{1}{2}$ the total mass of the parallel portion, and that the average velocity ratio obtained from the graphical analysis of Figure 27 is about 2/3 to 0.7. Since kinetic energy is proportional to the velocity squared, the kinetic energy, and hence the effective inertia, contributed by the curved portion is about $\frac{1}{4}$ that of the parallel portion. In the case of the cup shape, the velocity ratio is much lower so the shell portion is neglected.

With some of the types of magnetic force sources considered in the study phase, such as external polarized armature torque motors connected to the flexspline by linkages, the force is constantly varying, sinusoidally for linear operation with the ideal phasing, and the motion of the flexspline is elliptoidal or nearly so. With the RF types the force is spread out over 180° and there are departures from the ideal motion. With the SF type magnetic force is essentially constant after flux rise time and neglecting the incremental permeability of the iron above saturation, so the motion is far from elliptoidal. The forces are maximum when the armatures reach the end of their stroke and hence, they possess significant terminal velocity. This is evidenced by the noise produced by the impacting of the armatures upon the pole faces. In this case, the mean kinetic energy is greater, and it would follow that the effective inertia is also. An alternative way of viewing this effect would be that the excessive kinetic energy is transformed into heat and noise, and since it is not conserved, it does not contribute to effective inertia. But, in this case, the torque efficiency η_T would have to be adjusted and torque output would be less. From an overall viewpoint, power rate will be decreased in either case. Since no method was evolved of calculating the change in η_T, the effect was calculated as an increase in inertia, in Appendix VI. This shows that the increase is inversely proportional to operating speed. For example, at 19 rpm for model EHD-3, the inertia due to radial motion of the armature increases by 67%.

Some brief analysis was also given to the inertia of a prestressed ring. Inertia varies directly with the degree of motion, so that there is a corresponding increase in inertia as the effectiveness of the element is increased.

It should be noted that in the calculations of inertia made in Appendix VII the tangential component of the inertia due to deflection of the armatures has not been included, which has only a very slight effect upon the total.

The expression for the reflected inertia of a swash plate wave generator was calculated in Appendix VI as:

$$J = 20\ \rho \sqrt{R_g}\ D_p^5 \qquad (3\text{-}50)$$

Using the usual values of R_g (75 to 150), the inertia becomes nearly three orders of magnitude greater than the other concepts. For example, for $R_g = 156$, $D_p = 3\frac{1}{4}$" (same as model EHD-3), using a steel swash plate

$$J = 7.4\ kg\text{-}m^2 \qquad (3\text{-}51)$$

compared to

$$J_{M_1} = 1.2 \times 10^{-2}\ kg\text{-}m^2 \text{ for model EHD-3} \qquad (3\text{-}52)$$

which is calculated in Section 4.

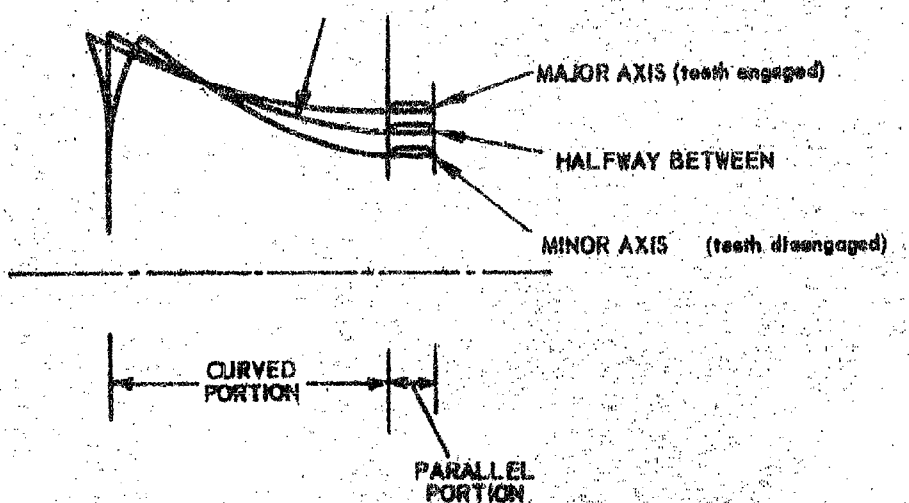

FIGURE 27 COMPARISON OF MOTION AND VELOCITY AMPLITUDES OF THE CURVED AND PARALLEL PORTIONS OF A BELL SHAPE FLEXSPLINE.
For electro-magnetic deflection the parallel portion is taken as $D_p/8$ long (Deflection exaggerated).

SECTION 4

STEPPING FIELD TYPE - DETAILED ANALYSIS AND TECHNICAL EVALUATION OF DESIGN

4.1 General

In Preceding sections the problem has been stated, the fundamentals of Electromagnetic Harmonic Drive actuators have been presented, and the various configurations have been surveyed. At this point, an intensive look will be given to the fundamental analysis of the stepping field type of EHD device that has been developed within the contract as the primary model. This analysis is correlated with the results of the testing. Following this section, the fundamental analysis of the Rotating Field Type is given (Section 5), a comparison made to competitive devices (Section 6), and some of the design and performance parameters generally common to all EHD types are discussed (Section 7).

The foremost objectives of the analysis are expressions for output torque, inertia and hence power rate, which is calculated from the other two (Section 2).

The secondary objectives include other significant characteristics: i.e., maximum speed, hence maximum power output; losses, efficiency and temperature rise; maximum speed and resolution; holding torque; accuracy (speed constancy, backlash, etc.); size and weight; repeatability, reliability and life.

Test results are combined with the analysis for reasons given in the Introduction.

Before starting the detailed analysis it will facilitate understanding to describe the model.

4.2 Description

The primary model is a stepping actuator that employs a multiplicity of solenoids. Figure 12 is an assembly drawing and Figure 21 a photograph of its key parts. Figure 20 shows the complete unit. The armature elements of all solenoids are joined in a flexible ring which, by it's motion, bears against and deflects the flexspline. There are 16 "U" shaped electromagnetic poles equally spaced around the outside of the armature ring. Each pole structure has two coils of 70 turns each, one on each leg. It is planned to energize four poles at a time, a pair of adjacent poles on each end of a diameter. This will create electromagnetic flux that crosses the air gap and completes its path within the armature pieces, there being a closed path for each pole (disregarding leakage which will be small). These armature pieces represent a significant part of the design concept. They are joined only by three flexible rubber rods that thread circumferentially through them. This allows them to move radially without increasing the required deflection force as a more rigid ring would do. The reluctance action thus deflects the flexspline outward at two diametrically opposed areas into contact with the circular spline. Due to a difference of two in the number of teeth on the mating spline, one revolution of meshing results in a backward motion of

the flexspline of two teeth, and with, for example 312 teeth on the flexspline, it thus rotates 1/156 of a revolution. The length of the flexspline integrates the hypocycloidal motion of the individual teeth into a linear rotary output. Because of the relatively small arc length covered by two adjacent poles, it is possible to drive each to saturation without incurring severe shape distortion. This results in the maximum possible torque per volume of iron and thus this device results in a very high torque squared to inertia (power rate)value. This method of coil energization explains the necessity for using digital circuitry, and the resulting stepping action. To obtain the smoothest possible output torque without using an excessive number of poles, the analysis and point force model tests showed that 16 poles represented the best approach. The number should preferably be a multiple of two, to conform with digital count-down circuits, which 16 fulfills. In operation, the circuitry steps the field around, a single pole at a time, which limits the incremental step to $22\text{-}1/2^{0}$, even though the steady state force acts over 45^{0} (on each side of the flexspline). The model uses 96 pitch teeth resulting in a .021" deflection. Considering the leverage, average air gap at the start of each armature's stroke is about .015".

4.3 Power Rate Analysis and Dynamic Performance

Besides obtaining mathematical expressions, one is interested in how power rate may be optimized in regard to necessary constraints, practical limitations, etc. It is not the purpose of this section, however, to show that power rate in general increases with the size, weight, and power rating of an actuator. This is covered in Section 10. The more significant problem is how to optimize power rate for a particular size actuator, which must properly be used in comparing against alternative types of actuators.

The power rate analysis is separated into two parts. In the first part the analysis is conducted more from a theoretical viewpoint from which the ideal upper limit on performance can be estimated. It gives insight into the fundamental understanding of the basic principles involved in the device. The second part presents the variations resulting from consideration of some of the practical aspects of the laboratory model in particular, as well as commercial models in general. Naturally, what aspects are the most important for any field application will depend on the nature of the application.

It is interesting to note that different approaches are used in the two parts to obtain output torque. However, both reside on the same fundamentals, are valid, and give the same result.

In the first approach, the mean work input of all the magnets during one output revolution is calculated. Since this, adjusted by the torque efficiency, is also equal to mean output torque times one revolution, the torque is easily calculated. In the second approach there is calculated the total tangential force induced at the ends of the major axis due to the various magnet forces. This is transposed into output torque. In this case, the instantaneous, as well as the mean torque are obtained; whereas, in the first case only the mean torque value can be obtained.

Because of the simplifying assumptions that are necessary to permit a concise, workable, mathematical analysis to be made, there are minor approximations involved in the approaches. The most significant factors producing departure from the ideal case are:

-Armature movement during MMF build-up
-Saturation limiting
-Fringing
-Distortion of the moving members from the ideal Harmonic shape

4.3.1 Theoretical Maximum Power Rate

Because of the length and detail of this analysis, it is presented as part of Appendix VII. A summary of the conclusions is presented here.

For an actuator with fixed constraints of 3½ inch pitch diameter, 100 watts total I^2R power loss, and 6 cubic inches volume per each of 16 magnets, plus others as listed in Table VIII, and a configuration given by Figure 28, the maximum power rate that might be obtained is 2700 kw/sec. This is based on the most ideal situation in which the shape is assumed ideal, and armature movement during magnetomotive force build-up, flux fringing and saturating limiting is neglected.

As the shape departs from the ideal (for which η_s is unity) the torque output can be increased slightly, but the inertia increases at a somewhat higher rate, so that taken together, the power rate will decrease slightly. The assumption that flux reaches its steady state value in times short compared to the period of a magnet cycle is increasingly valid as output speed approaches zero. Flux fringing does not constitute any large source of error in this case, as the gaps are quite short compared to the linear dimensions of the pole face. However, this analysis does not provide for specific isolation between the iron legs of the magnets which can be a source of significant leakage and distortion of the flux field. It is pointed out that if the armature laminations are made of flat stock, saturation limiting will prevent the attainment of the maximum power rate. It is suggested that tapered or wedgeshaped laminations be used, for which case the maximum power rate is estimated as 1800 kw/sec.

Emphasis is placed on the significance of the key parameter, width of magnet armature and leg (dimension b of Figure 28). For the maximum power rate, this should be 0.8 inch in the ideal case, or about 0.75 inch when saturation limiting and tapered armatures are considered.

Figure 29 is a very convenient graph of the following three parameters as a function of width b:

-Power rate for the actuator
-Magnetomotive force for a magnet available for the constraints used
-Output power for the actuator

Flexspline:	Diameter D_p = 3.25 in.
	b = 0.8 inch
	Amplitude d = 0.0208 in.(peak to peak) (Based on 128 pitch teeth)
	Ratio R_g = 156 (Based on 128 pitch teeth)
	Torque Efficiency η_T = 0.80
	Shape factor η_s = 1.00
Magnets:	Number n = 16
	Volume(each) V = 6.05 $in.^3$
	Duty Cycle--on 1/4 of time
	Saturation flux density β_m = 2.0 webers/$meter^2$
	Minimum effective gap x1 = 0.006 in.
	Effective resistivity, including insulation, ρ_c = 3.44x10-8 ohm meter
	General configuration--shown in Fig. 28
	Density of armature laminations ρ = 0.282 $lb/in.^3$(Steel)
Total Device:	I^2R power = 100 watts

TABLE VIII - MAGNET DESIGN ASSUMPTIONS FOR THEORETICAL POWER RATE ANALYSIS OF SECTION 4.3.1.

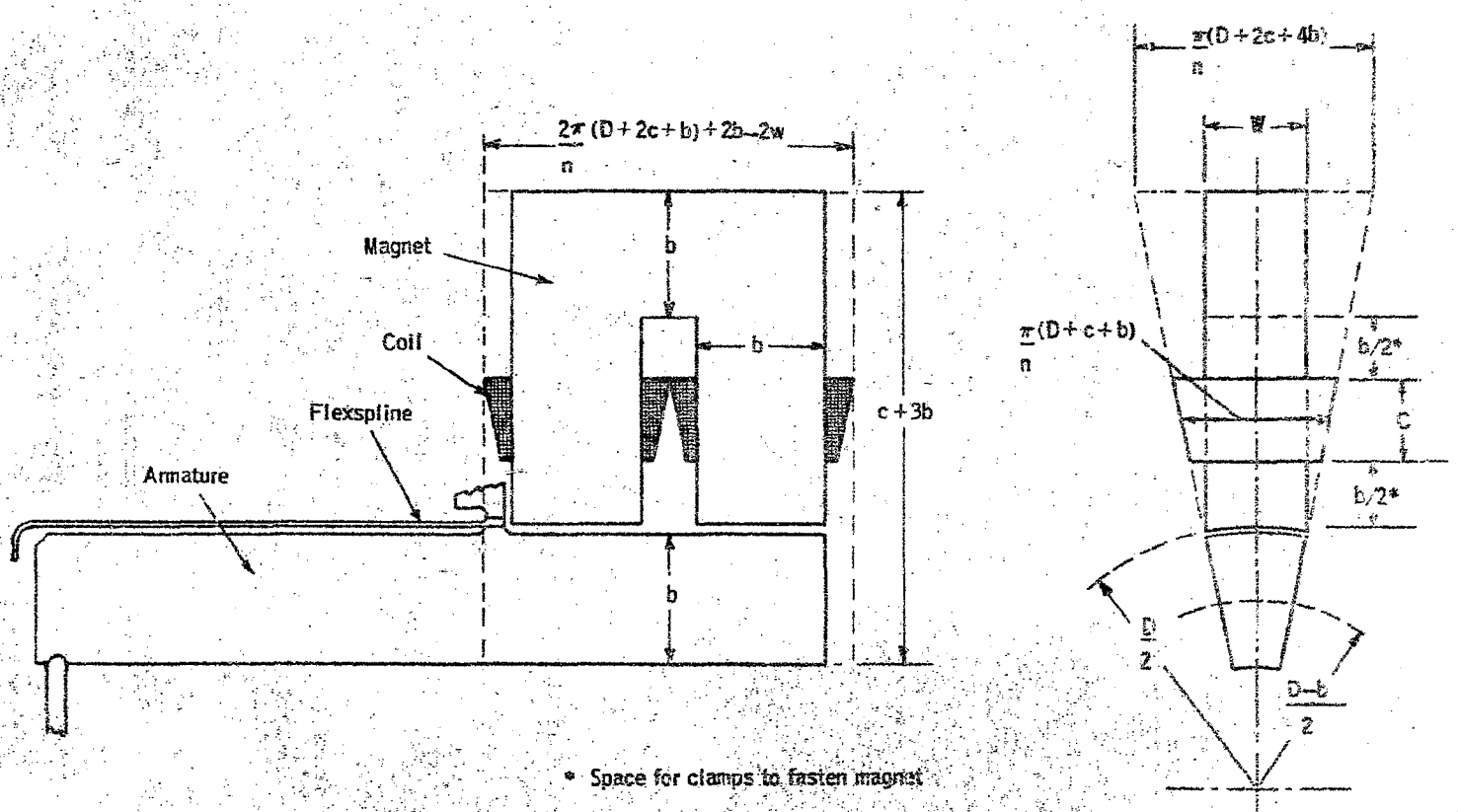

FIGURE 28 - KEY DIMENSIONS OF STEPPING FIELD MAGNET FOR THEORETICAL POWER RATE ANALYSIS (Section 4.3.1)

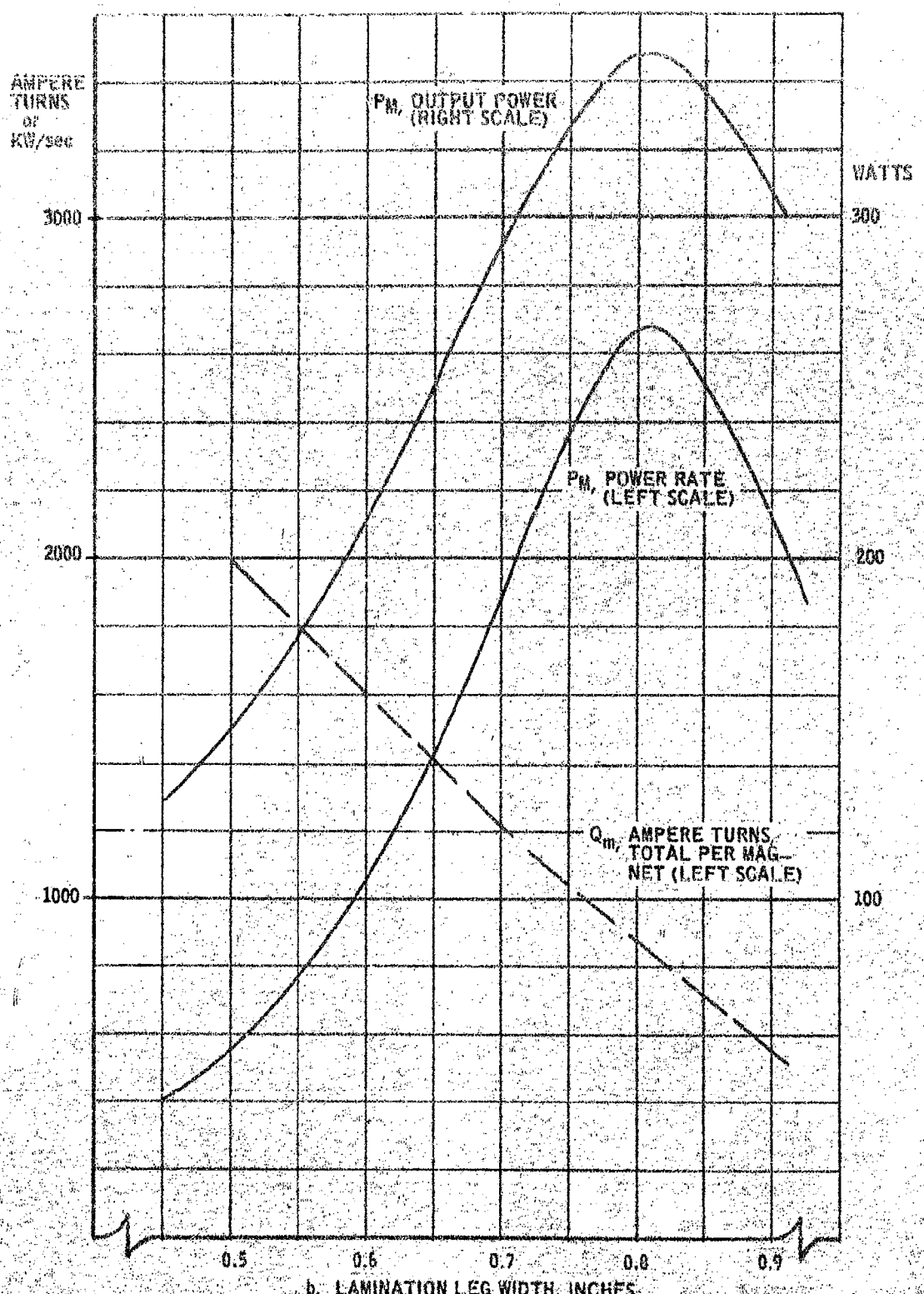

FIGURE 29 - THEORETICAL STEPPING FIELD PERFORMANCE AS A FUNCTION OF LEG WIDTH

It is shown by the analysis that at b of 0.8 inch the available magnetomotive force will produce 77% of saturation flux density when the armature is at the assumed starting position. At lesser values of b, when the ratio of copper to iron is greater, more magnetomotive force is available, and the flux density approaches or equals saturation for the material. In the analysis of 4.3.2 with smaller b, the assumption will be made that saturation is reached at the start of stroke.

4.3.2 Power Rate Analysis for Manufactured Actuators

4.3.2.1 Torque - In this analysis greater emphasis is placed on approaches which lend themselves to practical design and manufacturing as well as best performance. Therefore, somewhat different constraints are used. As with Section 4.3.1, the key dimensional parameter is the leg and armature width b. However, in this analysis its determination is essentially the starting point, not a more freely selected value.

The most significant constraint is that of limiting the torque loading to values that minimize shape distortion. This has been analyzed in Section 3.

Another constraint resulted after the basic design configuration was selected, that of levers which pivot against the flexesplines. Axial distance between the teeth and the air gaps increases with "b". It was felt that excessively large air gaps would require very high MMF and excessive flux fringing might occur as well. In regards to the size of the non-moving parts of the magnets, U-shaped poles and coils, it was not felt important to place a constraint on this as done in Section 4.3.1, but rather to design a housing for the size of magnet necessary to work with the armature width and gap selected. Another constraint results from the semiconductors used in the controls. One should consider their ratings and design for reliability. This results primarily in limiting current, which immediately determines the number of turns. As there is a maximum size wire that can be bent to fit around a specific magnet leg size, this greatly affected the size of the magnet. The relationship between thickness and height of the coil was based upon what was considered good design practice.

It was not felt important to place a firm constraint on the power dissipated in the coil, as efficiency was not the fundamental objective of the program. (Indeed it will be shown that the general level of efficiency is many times higher than competitive devices operating at peak torque). In regards to heat dissipation, if natural convective cooling of the laboratory model proved insufficient and forced air was required, this was deemed acceptable, as a reasonable degree of cooling can be worked out in design refinement.

A final and very significant reason for the selection of 0.5 inch for armature width was that this size was readily available from stock as a standard size from the supplier of the special magnetic material that was employed. The next available size was much

too large. Manufacture of a special size would have increased expense and delivery time considerably. The leg size of b = 0.5 inch used for the magnetics resulted in a moderate torque loading. A standard Harmonic Drive pitch diameter of 3-1/4" was selected as being a convenient size to assemble and work with in line with past Harmonic Drive experience. Power output of 100 watts was also an objective, and the analysis indicated this size to be about right. The comparison of the various values of the torque loading constant K1 are shown in Table IX.

In order to obtain the T_m (peak torque) values in the table, the average value T_M was doubled, based on the reasonably accurate assumption of a linear torque vs. step angle position, which is discussed later on. It is seen that for b of 0.8" K1 exceeds the long life rating for ball bearing supported types. However, the shorter life rating in such designs may be greater than this. The EHD-3 experimental model (b = 0.5") in operation showed correct dynamic operation and no early flexspline failures. Also, disassembly after several hours of operation disclosed no evidence of wear. However, until such time as life tests are run, no conclusions on the safe design value of K1 can be reached.

The overall evaluation of these points resulted in the selection of a single-step, 16 magnet configuration. The number 16 is also a preferred number for electrical reasons, being a power of two and convenient for logic circuitry.

In Section 4.3.1 it was indicated that power rate is not seriously reduced when the flexspline shape distorts. Therefore, in the calculation of torque, the assumption of an ideal harmonic shape will be made, as this greatly simplifies the analysis. From Section 3 torque is calculated from the expression

$$T_M = 2F_M D_p \eta_T \sin 2\delta \qquad (4\text{-}1)$$

The factors F_M, δ and η_T will be discussed in that order.

F_M is the total force, re erred to the tooth plane, produced by one magnet.

To find the value of F_M for this model consider how this is related to the forces produced at the two air gaps per magnet.

The expression relating the magnetic force F_Q, produced at each air gap of a "U" shape magnet in relation to the properties of the magnetic field is, from Appendix V:

$$F_Q = \frac{B_m^2 A_Q}{2\mu_0} \qquad (4\text{-}2)$$

where the assumptions are made that B_m is constant over the pole face, as well as over the working stroke; A_Q is the true area of the pole face multiplied by the stacking factor (here S_F); and that fringing is negligible, a reasonable assumption when the gap is of the order of 1/20th of a linear dimension of the pole face. Equation 4-2 is based on the assumption that armature movement is negligible during the flux build-up time. As justification of

	IDEAL ANALYSIS (SECTION 4.3.1)	INTERPOLATED FROM IDEAL ANALYSIS	END-3 DESIGN (SECTION 4.3.2) DOUBLE STEP	END-3 DESIGN (SECTION 4.3.2) SINGLE STEP
b	0.8 inch	0.5 inch	0.5 inch	0.5 inch
δ_m	45°	45°	45°	$22\frac{1}{2}$°
T_M	175 n-m(1550 lb.in.)	73 n-m(650 lb.in.)	60 n-m(530 lb.in.)	42 n-m(370 lb.in.)
T_m	350 n-m(3100 lb.in.)	146 n-m(1300 lb.in.)	120 n-m(1060 lb.in.)	84 n-m(740 lb.in.)
K_1	90 lbs/in^2	38 lbs/in^2	29 lbs/in^2	22 lbs/in^2

LEG WIDTH, b
SIZE OF STEP, δ_m
TORQUE-LOADING CONSTANT $K_1 = \frac{T_m}{D_p^3}$

TABLE IX - TORQUE AND TORQUE-LOADING CONSTANT FOR A $3\frac{1}{2}$ INCH PITCH DIAMETER END STEPPING ACTUATOR, SHOWING EFFECT OF LEG WIDTH AND SIZE OF STEP.

Assumptions:

$\mathcal{B}_m = 2.0$ webers/m^2

Steady state torque load, $T_L = 0$

$\eta_g = 0.80$

Flux rise time neglected

this for the EHD-3 consider Figure 30, the typical single-step (non-slewing) motion of the device. As position θ_M is equal to the second integral of acceleration or output torque divided by inertia, the motion must follow the approximate path shown. This approximation is true even if the torque vs. motion relationship is not linear as for the simplified form shown here. Even if t_1 approaches one half of t_p, θ_{Mt_1} is small compared to θ_{M_S} (less than 20%). In the experiments t_p has been roughly measured as the order of 1 to 2 milliseconds and t_1 less.

It is readily seen from the magnetic force formula that for a given mass of armature material, the greatest force results with the highest value of $\mathcal{B}$. Since torque is proportion to force, it is seen that highest power rate results from highest $\mathcal{B}$. This is the reason why a special search was made for magnetic materials capable of very high saturation levels with satisfactory mechanical properties for use as the lever armature elements of the device. The special material selected, vanadium permendur, is made by Allegheny Ludlum Company and fabricated by Arnold Engineering Company. The following average saturation flux density is thus obtainable:

$$\mathcal{B}_m = 2.4 \text{ webers/m}^2 \qquad (4\text{-}3)$$

The supplier reviewed the use of the material in this application and believes that at least 2.2 w/m^2 should definitely be obtainable, if not 2.4. To permit comparison with the thepretical values of Section 4.3.1, the same value of

$$\mathcal{B}_m = 2.0 \ w/m^2 \qquad (4\text{-}4)$$

will be used initially. Later the effect of an increased $\mathcal{B}$ will be presented.

The area A_Q is determined as follows:

All the iron should be laminated to minimize core losses, and a normal stacking factor of

$$S_1 = 0.90 \qquad (4\text{-}5)$$

will be employed for the yoke when insulated and bonded together. If wedge-shaped laminations are used for the armature, the same factors can be applied to them. If flat laminations are used, which is preferable from a manufacturing cost and time viewpoint, because the armature laminations are radially disposed their stacking factor must be considered differently. The device is assembled such that all these laminations essentially touch at their inside diameter. At their outside diameter adjacent to the air gap, the stacking factor from Figure 31 is given by

$$S_2 = 1 - \frac{2b}{D_p} \qquad (4\text{-}6)$$

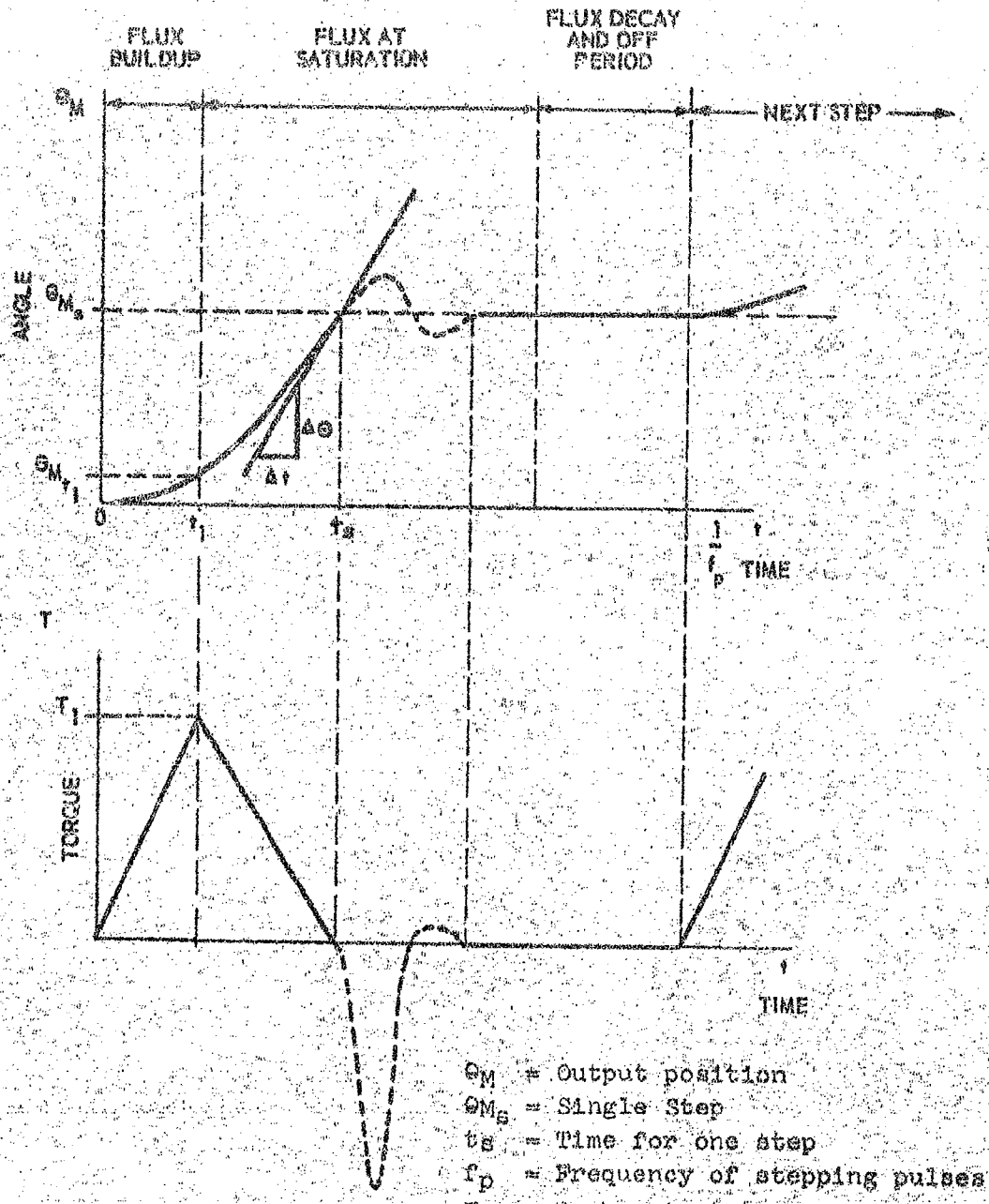

FIGURE 30 TYPICAL SINGLE STEP NON-SLEWING MOTION AND OUTPUT TORQUE OF MODEL EHD-3 WITH NEGLIGIBLE STEADY TORQUE LOADING

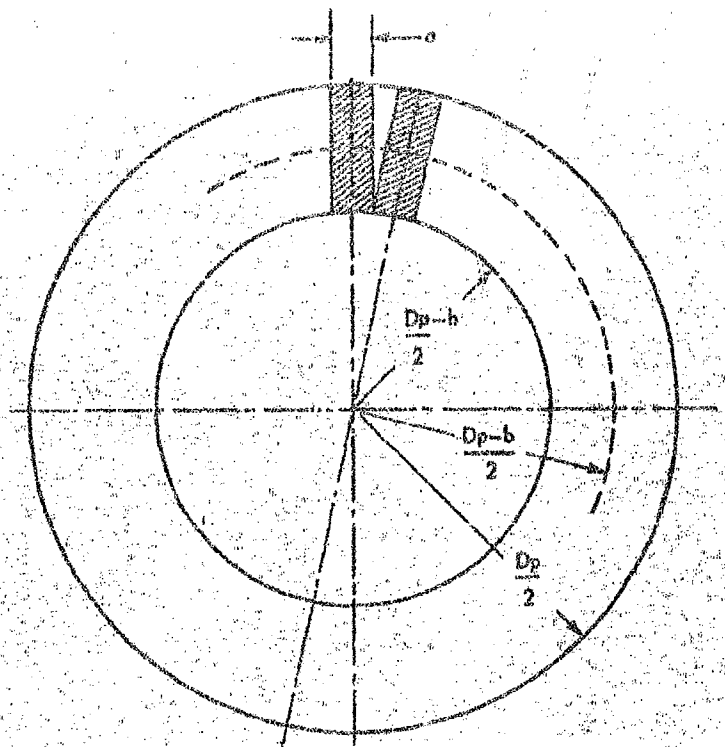

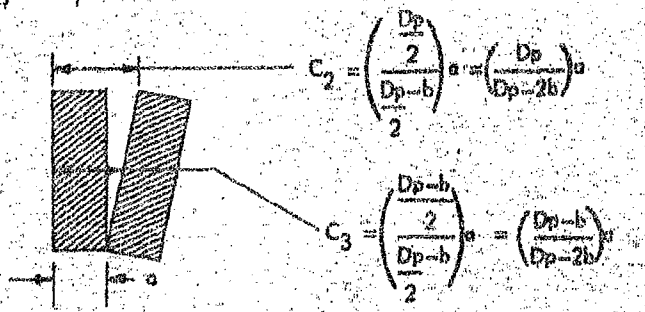

$$C_2 = \left(\frac{\frac{Dp}{2}}{\frac{Dp-b}{2}}\right)a = \left(\frac{Dp}{Dp-2b}\right)a$$

$$C_3 = \left(\frac{\frac{Dp-b}{2}}{\frac{Dp-b}{2}}\right)a = \left(\frac{Dp-b}{Dp-2b}\right)a$$

STACKING FACTOR, $S = \frac{a}{C}$

$$S_2 = \frac{a}{C_2} = \frac{a}{\left(\frac{Dp}{Dp-2b}\right)a} = \frac{Dp-2b}{Dp} = 1-\frac{2b}{Dp}$$

$$S_3 = \frac{a}{C_3} = \frac{a}{\left(\frac{Dp-b}{Dp-2b}\right)a} = \frac{Dp-2b}{Dp-b}$$

FIGURE 31 MODEL EHD-3 ARMATURE END VIEW AND STACKING FACTOR

So for the dimensions chosen for the model

$$S_2 = 0.69 \qquad (4\text{-}7)$$

However, since the ring of armature laminations is continuous, there will actually be some fringing to the laminations located between magnets, which can be looked upon as increasing the effective stacking factor. It has been decided that for good magnetic design practice a spacing of approximately

$$a = 1/4 \text{ inch} \qquad (4\text{-}8)$$

should be left between the iron of the magents at their closest points, which is at the air gap. If all of this space were utilized by fringing flux, the increase in utilization would be given by the factor

$$U_1 = \frac{\pi D_p / n_M}{\pi D_p / n_M - a} = 1.65 \qquad (4\text{-}9)$$

for 16 magnets as has been selected for the optimum configuration. The product of S_2 and U_1 is

$$S_4 = S_2 U_1 = 1.14 \qquad (4\text{-}10)$$

Since this product of two separately derived factors is greater than unity, which it obviously cannot exceed, it is reasoned that use of the same S_1 stacking factor of 0.90 might be used for calculations with the laminations as well. The problem is that the fringing lowers the flux density in the working gap, thus lowering the magnetic force. As a compromise solution to this complicated interrelationship a stacking factor of

$$S_5 = 0.80 \qquad (4\text{-}11)$$

the mean of S_1 and S_2, will be used and the assumption of no fringing made.

Also, because of the magnet clearance space, the tangential dimension of a magnet pole face is established as

$$w = \frac{\pi D_y}{n_M} - a = 0.4 \text{ in} = 1.0 \times 10^{-2} \text{ m} \qquad (4\text{-}12)$$

for 16 poles.

Thus pole area A_Q is determined as

$$A_Q = S_5 b w = 0.16 \text{in}^2 = 1.03 \times 10^{-4} \text{m}^2 \qquad (4\text{-}13)$$

Hence, from equation 4-2

$$F_Q = 165 n = 37 \text{ lbs.} \qquad (4\text{-}14)$$

To obtain the resultant force produced at the plane of the teeth F_M by the magnetic forces acting in each air gap of the "U" magnet, considering that they transmit their forces through the armatures acting as rigid levers, take

$$F_M = (K_{ma1} + K_{ma2})\, F_Q \tag{4-15}$$

The K_{ma} factors are found from Figure 9 as

$$K_{ma1}\ (\text{inboard gap}) = \frac{3.3}{2.5} = 1.32 \tag{4-16}$$

$$K_{ma2}\ (\text{outboard gap}) = \frac{4.3}{2.5} = 1.72 \tag{4-17}$$

F_M is therefore

$$F_M = 3.04\ F_Q = 500n = 100\ \text{lbs.} \tag{4-18}$$

Next consider the power angle δ . As discussed in Section 3, the study of force distribution on the flexspline showed that as the power angle increases, so also does torque up to $\delta = 45^0$, but the resultant radial force acting at the major axis to keep the teeth engaged decreases. The limiting angle at which tooth engagement is just maintained, as shown before, depends on many things, some of which are very hard to assess. If the flexspline has the ideal harmonic shape and tooth frictional forces, inertial force and deflection force are neglected, the limiting angle depends on only the pressure angle

$$\delta_m = \tfrac{1}{2} \arctan \frac{1}{2 \tan \Phi_a} \tag{4-19}$$

Φ_a being the pressure angle and δ_m the limiting power angle. It is seen that the lower the pressure angle the large is δ_m , and hence torque output. As a practical matter, a value for Φ_a of 20^0 was selected, which experiment has shown to be successful for the EHD-3. For this pressure angle, the expression for F_T, F_R and F_N are plotted in Figure 32, as a function of θ. These curves are obtained by numerical evaluation at incremental changes in θ. In order to carry out the analysis, it is useful to express F_T, F_R and F_N as a function of θ and normalized to F_M. Also, the curves are repetitive every $22\text{-}1/2^0$ due to the 16 magnets. Referring to Figure 32, it is seen that for $\delta_M = 22\text{-}1/2^0$

$$(F_R\text{-}F_N)/F_M = 1.3\text{-}0.9 = 0.4 \tag{4-20}$$

which is an expression of the safety margin by which the teeth are maintained in contact. Also, it is seen that the limiting angle for which equation 4-20 equals zero is approximately

$$\delta_M = 27^0 \tag{4-21}$$

which would represent the start of the step. At the completion of a step

$$\delta = 27^0 - 22\tfrac{1}{2}^0 = 4\tfrac{1}{2}^0 \tag{4-22}$$

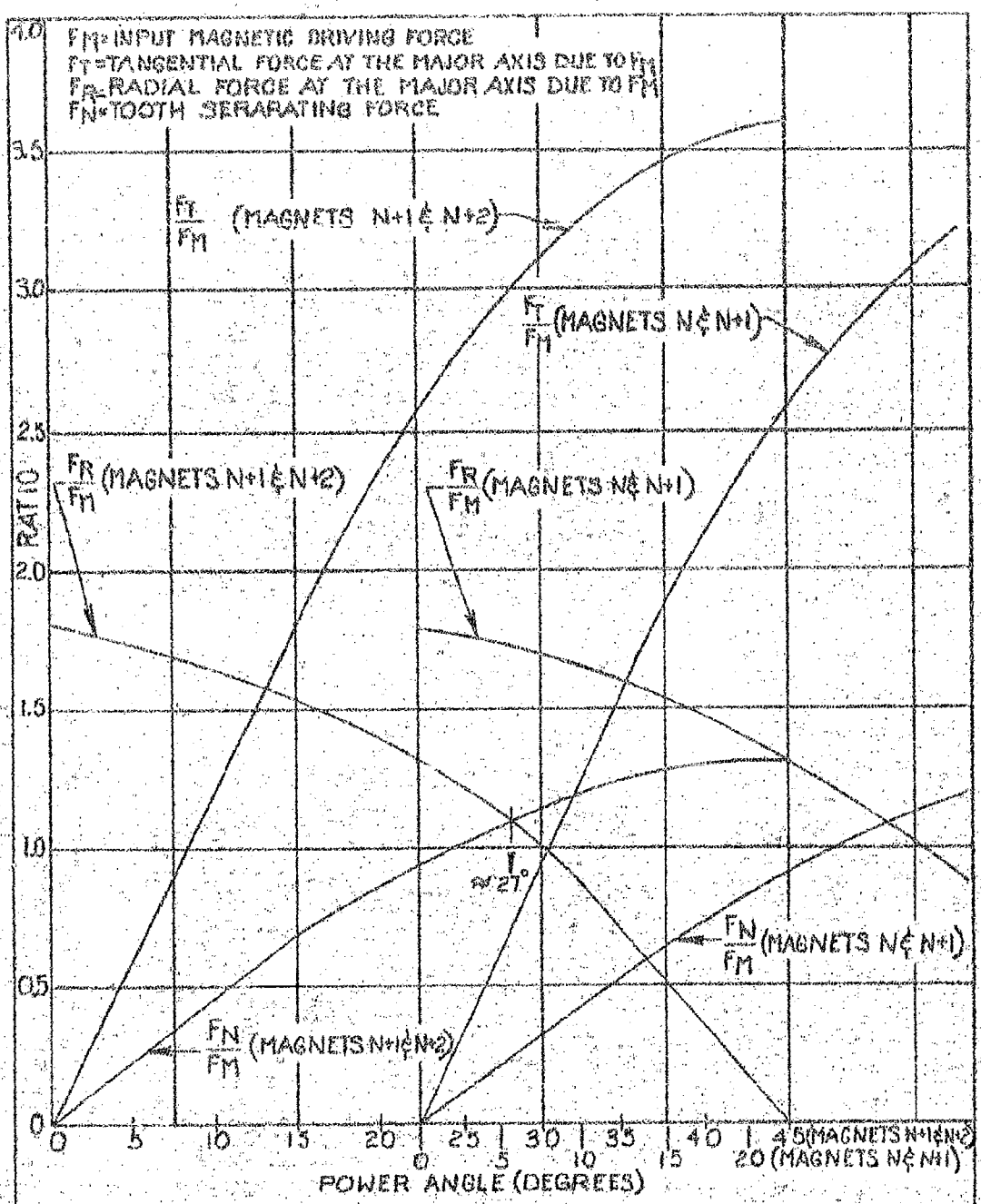

FIGURE 32 CHARACTERISTIC FORCES OF MODEL EHD-3 AS A FUNCTION OF POWER ANGLE

so that the minimum value of F_T/F_M at the end of a step would be about

$$F_T/F_M = 0.4 \qquad (4\text{-}23)$$

The value of δ_m then depends on whether or not there exists a steady torque loading. If there is none, the power angle varies between 0 and 22½° each step. If there is, the power angle operates between the angle required to produce a torque equal to the steady load and 22-½° ahead of that. Should it be shown by experiment with a double step that the teeth are maintained in engagement during the critical beginning transient part of the step, due to the pitch line overlap and inertial effects, then δ_m for zero steady torque load would be 45°. Values of performance based on this double step are calculated as well as for the more conservative single step.

Next is considered torque efficiency η_T. This factor has an average value of 80 to 90% for conventional Harmonic Drive units with normal ratios (around 100:1) based on 1/3 to full rated load and above. (It is less at lower load). However, the greatest source of the frictional loss is the wave generator ball bearing. The elimination of this major source tends to increase η_T. Counteracting this, however, are other sources of friction added when electromagnetic deflection is used. These are:

- -Greater tooth losses to the extent that the shape is distorted and abnormal pitch line overlapping occurs.
- -Sliding friction of the armature laminations against each other, the flexspline, and the fulcrum.
- -Impact of the armature laminations against the magnet pole faces.

Also, as the step is made, the torque falls so that over part of each step torque will be small compared to rating. As an overall judgement, a value of

$$\eta_T = 0.8 \qquad (4\text{-}23a)$$

will be selected. This received a fair degree of substantiation by the push rod model tests (see Section 3).

Equation 4-1 can now be applied to convert the calculated F_M values to torque for the 3-1/4 inch size model unit. For 16 poles energized four at a time, Figure 32 gives the values of

$$K_2 = 2 \sum_{180^\circ} \sin 2\theta_k \qquad (4\text{-}24)$$

$$K_3 = \sum_{180^\circ} \cos 2\theta_k \qquad (4\text{-}25)$$

as a function of the power angle δ .

The resulting torque values are given in Table X.

Characteristics	n-m	lb.in.	n-m	lb.in.
Steady torque load T_L	0	0	11	100
δ_m (degrees)	22½	22½	27	27
K_{2m} (dimensionless)	2.5	2.5	2.7	2.7
Peak torque T_m	84	740	89	790
Minimum torque T_{min}	0	0	11	100
Mean torque T_M	42	370	50	440

TABLE X - TORQUE VALUES WITH SINGLE STEP OPERATION

Again referring to Figure 32, the mean torque is taken as the numerical average because of the approximate linear slope to the curve.

If the actuator should be operated with a double-step, there would result:

Characteristics	n-m	lb.in.
Steady torque load T_L	0	0
δ_m (degrees)	45	45
K_{2m} (dimensionless)	3.6	3.6
Peak Torque T_m	120	1100
Minimum Torque T_{min}	0	0
Mean Torque T_M	60	550

TABLE XI - TORQUE VALUES WITH DOUBLE STEP OPERATION

In this case Figure 32 would indicate that T_M is more than the arithmetical average of T_m and T_{min} but this average is used here to be conservative as well as for simplification.

If saturation flux density attains the average level characteristic of vanadium permendur, these values of torque would be increased significantly. For example, at $B_m = 2.2$ w/m^2 torque would be 121% and power rate would be 146% of that based on the above torques. This value of B will be used from now on.

4.3.2.2 Inertia - Based on the formulas derived in Section 3.6 and Appendix VI, the following inertia is calculated for the constructed model. Based on harmonic motion for the armature:

$$J_a = \frac{5}{8} n_W M_a D_p^2 = 89 \times 10^{-4} \text{ kg-m}^2 \quad (4\text{-}26)$$

For the harmonic motion of the flexspline, based on the tooth bed:

$$J_f = \frac{5}{8} \rho V D_p^2 \quad (4\text{-}27)$$

Taking the total bed volume as

$$V = \frac{D_p}{8}(.030") \pi D_p = 0.125 in^3 = 2 \times 10^{-6} m^3 \quad (4\text{-}28)$$

Hence

$$J_f = 0.66 \times 10^{-4} \text{ kg-m}^2 \quad (4\text{-}29)$$

which is negligible due to its small mass.

The inertia of the shell of the flexspline rotating with output speed is

$$J_{s_1} = \rho \left[l_b W_b + (l_s - l_b) w_s \right] \pi D_p \left(\frac{D_p}{2} \right)^2 = 1.0 \times 10^{-4} \text{ kg-m}^2 \quad (4\text{-}30)$$

The inertia of the output shaft is

$$J_{s_2} = \rho l \left(\frac{D}{2} \right)^2 \pi \frac{D^2}{4} = 0.2 \times 10^{-4} \text{ kg-m}^2 \quad (4\text{-}31)$$

Hence

$$J_s = J_{s1} + J_{s2} = 1.2 \times 10^{-4} \text{ kg-m}^2 \quad (4\text{-}32)$$

When the inertia of the diaphragm, the fulcrum and the clamping ring and hardware holding the fulcrum, flexspline and shaft together are considered, the above might be increased somewhat but it is still quite insignificant.

When the armature elements rotate at output speed,

$$J_r = n_W M_a \left(\frac{D_p - b}{2} \right)^2 = 25 \times 10^{-4} \text{ kg-m}^2 \quad (4\text{-}33)$$

The total is thus

$$J_{M_1} = J_a + J_f + J_s + J_r = 1.2 \times 10^{-2} \text{ kg-m}^2 \quad (4\text{-}34)$$

For less than full speed rotation of the armature elements the total inertia is:

Half speed: $J_{M_2} = J_{M_1} - 3/4 J_r = 1.0 \times 10^{-2}$ kg-m^2 (4-35)

Zero speed: $J_{M_3} = J_{M_1} - J_r = 0.9 \times 10^{-2}$ kg-m^2 (4-36)

4.3.2.3 Power Rate Calculations - Table XII presents the evaluations of power rate. The values for the case of the distorted shape are not presented. As discussed earlier, both inertia and torque increase and so power rate would not decrease significantly.

4.3.2.4 Experimental Calculations of Torque, Inertia and Power Rate - Static measurements of torque were made and in general confirmed the anticipated values. However, it was indicated that at stall the maximum power angle δ_m may be considerably greater than the value of 27° given earlier as a safe working limit. It had been anticipated that T_m at $\delta = 27°$ would be about 800 lb.in. and require about 15 amperes per magnet, and that if δ went to the value of 45°, T_m would be about 1050 lb.in. The static tests (see Figure 33) show T_m of about 1350 lb.in. at 15 amperes per magnet. However, it was discovered in the static torque test that the different sets of magnets differ quite widely in the maximum torque produced by them, the curve of Figure 33 being based on a very good set. This is believed due to fit-up variations that affect the air gaps, which is mostly correctable with more elaborate tooling. Appendix VIII covers the static torque tests.

The difference in δ_m is considered due to either or both of two effects:

1. β_m is greater than the 2.2 w/m^2 value used. (Indeed 2.4 w/m^2 is considered a good average value for the material).

2. There is some shape distortion that increases the torque produced by the magnetic forces.

To be on the conservative side the previously selected values of torque based on β_m of 2.2 w/m^2 will continue to be used. It was decided that the difficulties associated with using a dynamic torque pickup for measuring operating torque outweighed the advantages to be gained.

Consider next methods of measuring inertia. There appear to be several methods, some more exact but correspondingly more complicated. One was selected, based on assuming a sinusoidal wave form, and is covered in detail in Appendix VI. The result was reasonably close to the prediction considering that the basic measurements obtainable with the equipment used were limited in accuracy.

Another method of measuring power rate directly is to measure the time constant when the actuator is loaded by a known inertial load.

	SINGLE STEP		DOUBLE STEP
T_L	0	11 n-m (100 lb.in.)	0
θ_m	$22\frac{1}{2}^o$	27^o	45^o
T_M	51 n-m (450 lb.in.)	60 n-m (530 lb.in.)	73 n-m (640 lb.in.)
T_m	102 n-m (900 lb.in.)	120 n-m (1060 lb.in.)	146 n-m (1280 lb.in.)
$K_1 = \frac{T_m}{D_p^3}$	26 lbs/in.^{2}	31 lbs/in.^{2}	37 lbs/in.^{2}
$\dot{P}_{M_1} = \frac{T_M^2}{J_{M_1}}$	220 kw/sec.	310 kw/sec.	440 kw/sec.
$\dot{P}_{M_2} = \frac{T_M^2}{J_{M_2}}$	260 kw/sec.	380 kw/sec.	540 kw/sec.
$\dot{P}_{M_3} = \frac{T_M^2}{J_{M_3}}$	280 kw/sec.	410 kw/sec.	590 kw/sec.

TABLE XII - TORQUE, TORQUE-LOADING CONSTANT, AND POWER RATE, MODEL EHD-3, SHOWING EFFECT OF STEP SIZE AND STEADY-STATE LOAD.

Based on Section 4.3.2 Analysis, b = 0.5 inch.

Assumptions: $\mathcal{B}_m = 2.2$ webers/m^2

$\eta_T = 0.8$

$\eta_S = 1.0$

Flux rise time neglected

$J_{M_1} = 1.2 \times 10^{-2}$ kg-m^2

$J_{M_2} = 1.0 \times 10^{-2}$ kg-m^2

$J_{M_3} = 0.93 \times 10^{-2}$ kg-m^2

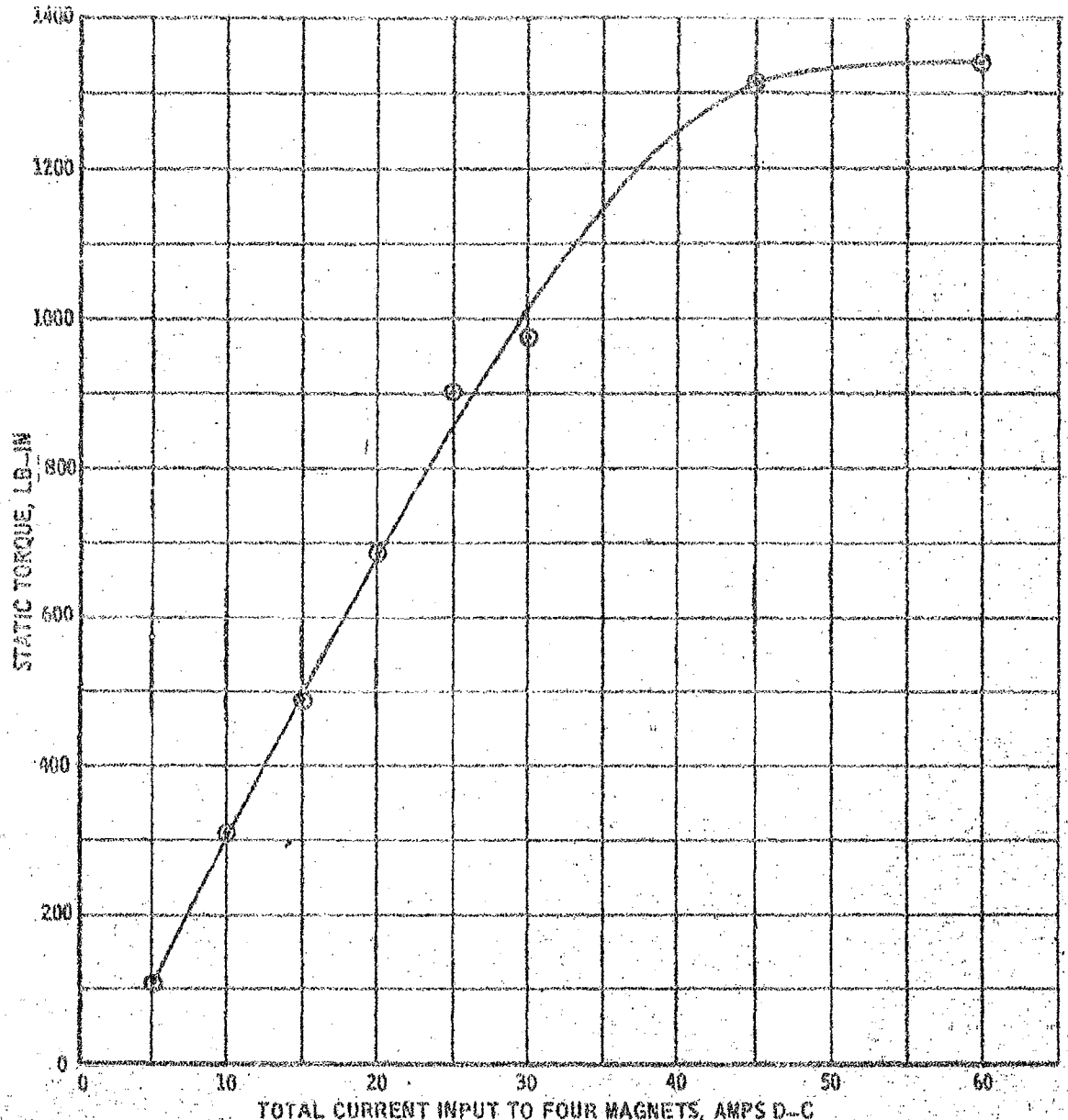

FIGURE 33 - EHD-3 STATIC TORQUE MEASUREMENTS

First the load requirement is calculated as

$$\dot{P}_L = (J_L \ddot{\theta}_M + T_L)\ddot{\theta}_M \qquad (4\text{-}37)$$

or $J_L \ddot{\theta}_M^2$ for the case where $T_L = 0$.

In general it is known (Section 2) that to drive a particular load the minimum actuator power rate required must be four times the load requirement

$$\dot{P}_M = 4\dot{P}_L = 4J_L \ddot{\theta}_M^2 \qquad (4\text{-}38)$$

Now, consider the simplifying assumption that the response is sinusoidal (see discussion of inertia measurements in Appendix VI, also Figure 30). Then:

$$\ddot{\theta}_M = (2\pi f)^2 \theta_{M_s} \sin 2\pi f t \qquad (4\text{-}39)$$

$$\ddot{\theta}_{M_m} = (2\pi f)^2 \theta_{M_s} \qquad (4\text{-}40)$$

f is the inverse of a period, which is taken as four times the step response time, t_s.

$$f = \frac{1}{4t_s} \text{ cps} \qquad (4\text{-}41)$$

$$\ddot{\theta}_{M_m} = (2\pi f)^2 \theta_{M_s} = \left(\frac{\pi}{2t_s}\right)^2 \theta_{M_s} \qquad (4\text{-}42)$$

but $\theta_{M_s} = .00252$ rad. (4-43)

$$\therefore \ddot{\theta}_{M_m} = .0062/t_s^2 \qquad (4\text{-}44)$$

It will be assumed, further, that the average acceleration during the step is 0.7 of the maximum or

$$\ddot{\theta}_M = 0.7\frac{(.0062)}{t_s^2} = \frac{.0043}{t_s^2} \qquad (4\text{-}45)$$

For the test on the model:

$$J_L = 0.10 \text{ kg-m}^2 \qquad (4\text{-}46)$$

Hence:

$$\dot{P}_M = \frac{4(0.10)(.0043)^2}{t_s^4} = \frac{7.4 \times 10^{-9}}{t_s^4} \qquad (4\text{-}47)$$

The approximate value of t_s measured was:

$$t_s \approx .002 \text{ sec} \qquad (4\text{-}48)$$

$$\therefore \dot{P}_M = 460 \text{ kw/sec} \qquad (4\text{-}49)$$

The fact that $\dot{P}_M$ varies inversely as the fourth power of t_s makes this approach of limited value for other than general confirmation of the magnitude, which it does do.

4.3.2.5 Dynamic Performance, Speed and Power Output - Figure 34 shows the model in the test stand with the adjustable-inertia load attached. Figure 35 shows it attached to the magnetic particle clutch load. Figure 36 shows the potentiometer output position transducer. Model EHD-3, wired to step one magnet for each input step (single step mode), was operated as follows.

Table XIII shows results of constant speed operation. Table XIV summarizes the frequency response test results, detailed in Table XV and Figures 37, 38 and 39.

Load Test

T_L = 196 lb-in
J_L = 0.1 kg-m^2
} Both provided by Vickers Type 6-2-5 Magneclutch and coupling

$\dot{\theta}_L$ = 12.5 rpm, no slip

I = 60 amps total(15/magnet)

e = 30 v peak

High Speed Test Conditions: $T_L = 0$, $J_L = 0$

Direction*	Steps Per Sec	<----Output Speed----> If no Slip	Measured	Slip %	Total Current amps	Armature rotation **
CCW	800	19.2	17.8	7.3	50	0
CW	730	17.6	16.6	5.7	55	1.0

* Viewing load (magnet) end
**Ratio of armature average rotation speed to output shaft speed

TABLE XIII - MODEL EHD-3, UNIDIRECTIONAL ROTATION, CONSTANT INPUT FREQUENCY TEST RESULTS

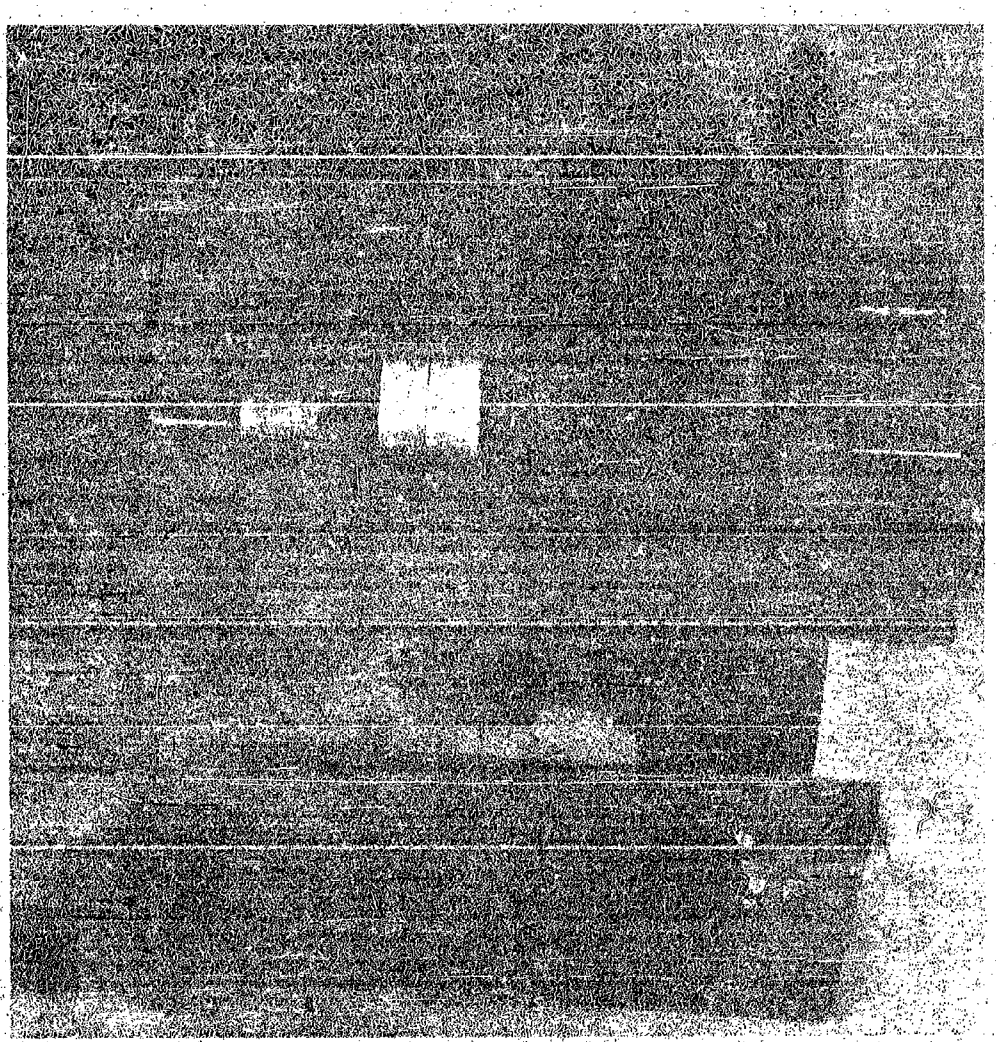

FIGURE 34 MODEL EHD-3 IN TEST STAND WITH ADJUSTABLE-INERTIA LOAD

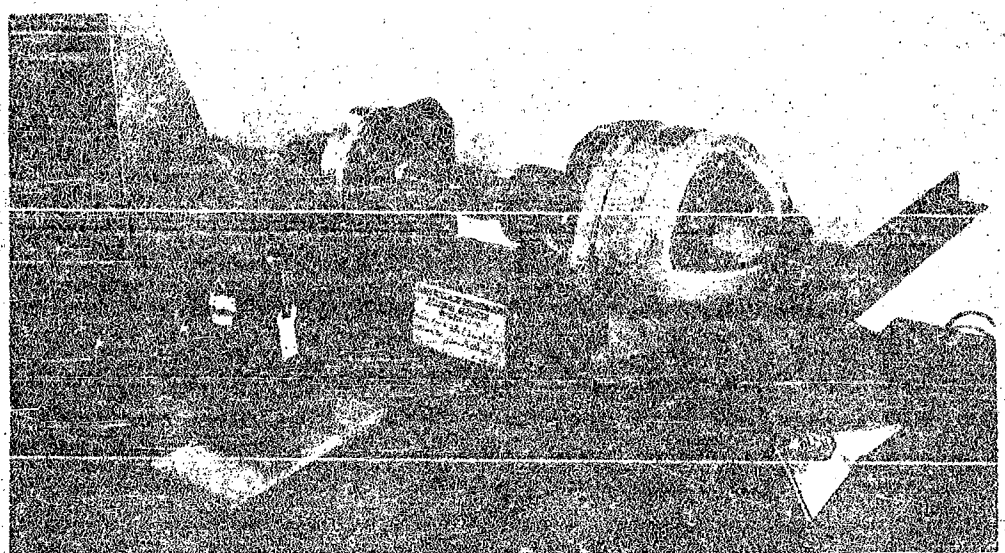

FIGURE 35 MODEL EHD-3 ATTACHED TO MAGNETIC PARTICLE CLUTCH LOAD

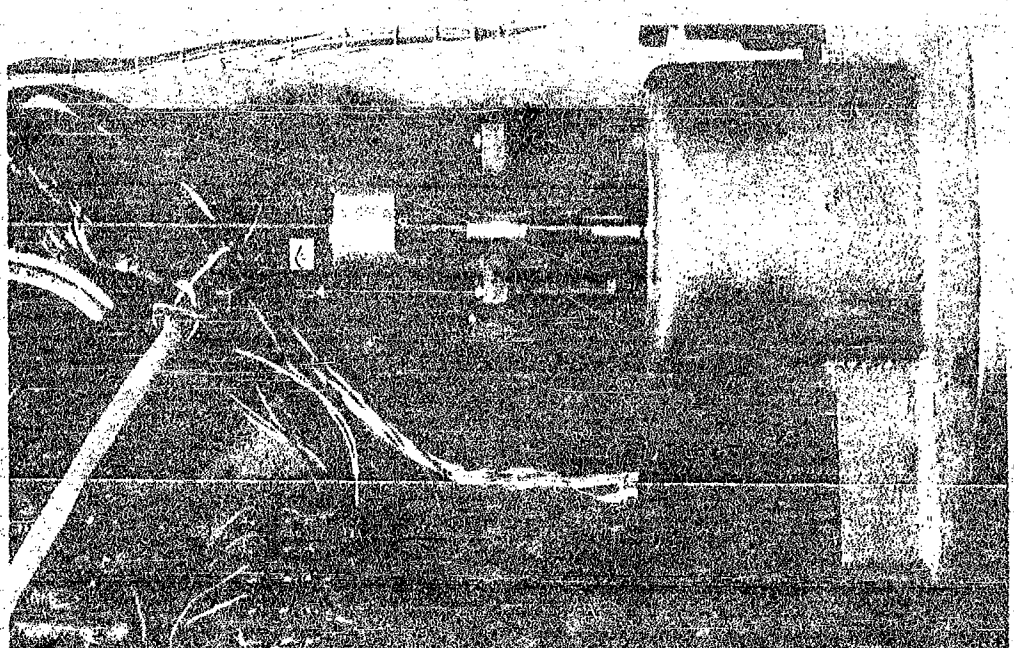

FIGURE 36 POTENTIOMETER OUTPUT-POSITION TRANSDUCER, MODEL EHD-3

	Sinusoidal	Results shown in	Square wave	Results shown in
J_L(kg-m)	0	Figure 37 Table XV	0	Figure 39
	0.1	Figure 38		
	0.4			
T_L	0		0	
f (cps)	0.1, 1, 10, 14, 20		1, 5, 20, 30	

TABLE XIV - MODEL EHD-3 FREQUENCY RESPONSE SUMMARY

Table XIII indicates that the armature's preference to rotate CW but not CCW reduces the allowable speed.

With the loading equipment utilized (magnetic clutch) it was not possible to apply a large torque load without also applying a sizeable inertia, so power output was not measured directly. In future work, special prony brakes of low inertia might be employed to measure power for short instances, if care is given to prevent overheating.

With time-varying inputs (Table XIV) peak input voltage was varied because of the loading on the audio oscillator. Voltage was converted to theoretical peak output speed without attenuation. Peak output amplitude was measured with a film-type potentiometer. This was converted to peak speed by multiplying by the frequency. The ratio of output to input represented the gain, and comparison of input and output waves on the dual trace oscilloscope represented the phase shift. Current was varied somewhat. It was seen that the value of inertial load had no effect upon the frequency response. It should be pointed out that since the potentiometer measures output position this automatically produces 90° of phase shift from the input signal. Thus the measured phase shift is reduced by 90° to obtain that due to the actuator. Phase shift was about 50° at 20 cps in all cases, and about 80° at 30 cps for the the square wave. Although the capability of responding to these high input frequencies was demonstrated, doubt must be raised about the validity of the phase shift data. The measured break frequency of around 20 cps results in an actuator time constant τ_M of around .008 sec. which is far below the EHD's inherent capability, as the τ_M of .00037 obtained in Section 6 would indicate. The actual τ_M is believed to be much lower. This is borne out by the transient performance, where step time was roughly measured by a limited - sensitivity, potentiometer method, as of the order of .001 to .002 seconds.

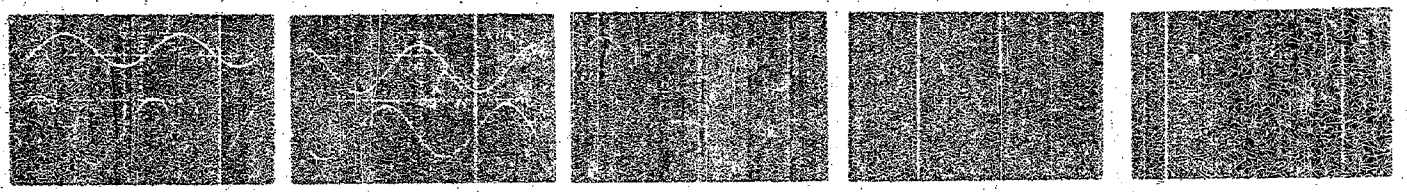

f = 0.1 cps, 5 volts/cm | f = 1 cps, 1 volt/cm | f = 10 cps, 0.2 volt/cm | f = 14 cps, .05 volt/cm | f = 20 cps, 0.10 volt/cm

FIGURE 37 SINUSOIDAL FREQUENCY RESPONSE, EHD-3, $J_L = 0$

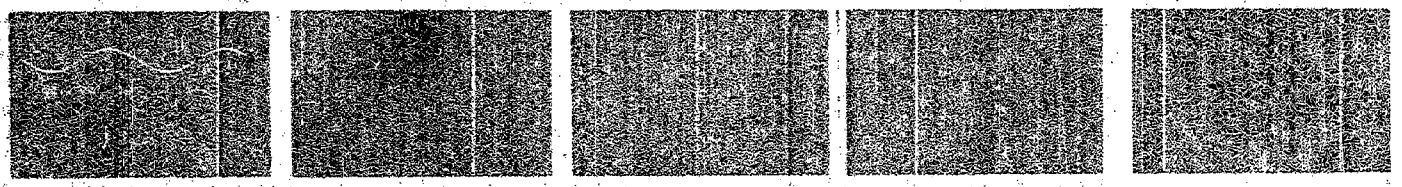

f = 0.1 cps, 5 volts/cm | f = 1 cps, 1 volt/cm | f = 10 cps, 0.2 volt/cm | f = 14 cps, 0.2 volt/cm | F = 20 cps, 0.1 volt/cm

FIGURE 38 SINUSOIDAL FREQUENCY RESPONSE, EHD-3, $J_L = 0.1$ KG-M^2

Calibration - Both Axes

Vertical Axis - Top trace: 10 volts/cm - Signal voltage to the analog to digital converter (input)

Bottom trace: Given beneath each photograph - Potentiometer signal (output)

Horizontal Axis - All traces: Time base, corresponds to frequency given beneath each photograph

Each square is one cm on a side

Note: Phase shift is the displacement between input and output trace peaks, less 90° resulting from the integration of the position feedback transducer.

Input Frequency (cps	Output		Signal Voltage Zero to Peak	DC Level of Peak Velocity (Rad/Sec.)	Velocity Gain		Phase Shift (Degrees)	Current per Magnet (Amps DC)
	Zero to Peak Amplitude (Radians)	Peak Velocity (Rad/Sec.)			(Ratio)	(DB)		
0.1	1.1	0.7	8.0	0.7	1.0	0	0	4.5
1.0	0.16	1.0	10.0	0.86	1.26	+2.0	10	6.5
10.0	0.022	1.4	12.5	1.1	1.27	+2.1	25	6.0
14.0	0.012	1.1	12.5	1.1	1.0	0	30	5.5
20.0	0.0072	0.90	14.5	1.25	0.72	-2.8	50	5.5

Formulas

1. Calibration of control circuitry:

   K = 34 cps/volt dc

   (This is an average value since the gain was slightly higher in one direction than the other, since corrected).

2. $\dot{\theta}$ = output speed (rad/sec.) =

$$\frac{\text{Signal voltage (zero to peak)} \times 34 \text{ cps/v} \times 2\pi \text{ radians/rev.}}{\text{lo steps/input rev.} \times 156 \text{ input rev/output rev.}}$$

TABLE XV - SINUSOIDAL FREQUENCY RESPONSE, EED-3, $J_L = 0$

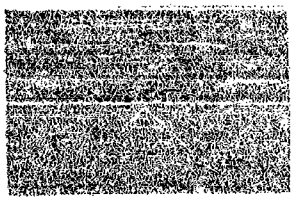

f = 1.0 cps

0.5 volt/cm

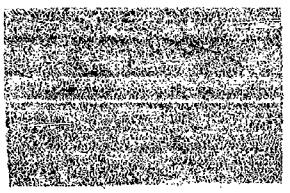

f = 5 cps

0.2 volt/cm

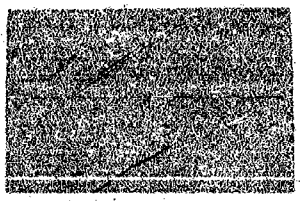

f = 20 cps

.05 volt/cm

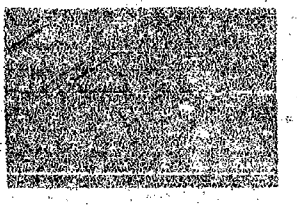

f = 30 cps

.05 volt/cm

CALIBRATION

Vertical

Top trace (input): 10 volts/cm
Bottom trace (output): Given beneath each photograph

Horizontal

All traces: Time base, corresponds to frequency given. Each square is one centimeter on a side.

Note: Phase shift is the displacement between input and output trace peaks, less 90° resulting from the integration of the position feedback transducer.

FIGURE 39 SQUARE WAVE FREQUENCY RESPONSE, EHD-3, $J_L = 0$

Top Trace - Signal voltage to the analog to digital converter (input).

Bottom Trace - Potentiometer signal (output).

Closed Loop Operation

The actuator was connected into a closed loop of the constant-rate, bistable type (also known as a "bang bang" servo, discussed further in Section 12). The feedback potentiometer was summed against a command potentiometer in a micropositioner which responded to the polarity of the error to select either a positive or negative constant-voltage input. This system eliminates the deadband at null and is very effective, accurate, easy to apply and inexpensive. It was used to demonstrate the response to manually-applied step inputs. It permitted the device to make single steps and was used for the resolution tests (covered in Section 4.6).

4.4 Electrical Controls

At the start of the program it was hoped that any actuator developed could be run directly from a 400 cycle power source normally available in aircraft type systems. It became apparent through analysis, however, that a stepping actuator was going to provide the greatest versatility and performance. Further analysis indicated that direct use of 400 cycle power with a series of silicon controlled rectifiers as power gating switches would seriously limit the high speed performance of the unit. This comes about because proper shape progression in the mechanical motion of the flexible member is best produced by overlapping of on-time in adjacent poles. For this overlap to occur, several full cycles of 400 cycle power must be switched to each pole. The analysis had indicated that the time necessary to turn on a pole and have it complete its useful motion could be as short as .001 seconds. Two full cycles at 400 cps corresponds to .005 seconds. Further delays could increase this time since switching may not always occur at a zero crossing of the alternating supply.

A further limitation for the 400 cycle type drive system is the actual rate of rise of the sinusoidal voltage, (dv/dt). The speed of response is directly related to the application of this voltage to a pole, and greater dv/dt produces faster response. Obviously, for equal peak voltages, a transistor switch and a D-C power supply can give the greatest dv/dt when operated in a cut-off to saturation type mode.

It was then decided to use a D-C power supply and power transistors to sidestep the response problem generated by use of the 400 cps system. This has worked out well. Tests show that current rise time for a single pole can be less than .002 seconds. Limitations on driving the poles at higher than 100 cps are primarily caused by the transistor voltage rating chosen for this design. Continuing improvements in transistor technology will undoubtedly increase this barrier.

The decision to go to a D-C supply over a 400 cps A-C supply was the first major decision in the control circuitry area. This involved a conflict with the objectives of the contract. However, because of the greater capability of the actuator that resulted, this appears to have been warranted. It is always possible to relax response capability and run the actuator from a 400 cps line if deemed desirable. (Obviously 400 cps could be used instead of 60 cps for powering the DC supply. 60 cps was used to save the expense of obtaining a higher power 400 cps generator than was available). It was felt that at this stage of development, the actuator itself should be the limiting feature and not the power supply or control circuitry.

After the power supply was constructed and tests started, even though current rise time was excellent (of the order of .001 to .002 seconds) it was realized that a constant current D-C power supply would provide even faster electrical response. This modification, not at all difficult, should be considered early in any future work. It is discussed further in Section 4.5 following. However, the control circuitry would operate essentially as well with either type of D-C power supply and does not impose any limitations on the actuator other than the component ratings.

The actuator is basically a digital device. To properly check out its performance a very simple analog to digital circuit was constructed. In actual use the capability of the unit should obviously not be limited by characteristics of the analog to digital converter if they can be improved. The one used for the model was made in the laboratory, is simple and inexpensive, but relatively crude. Commercial types are available and future units should include one of the more accurate varities.

To make use of commercially available transistor circuits a number of compromises were made with regard to power supplies. Presently there are three separate supplies to operate the logic circuits that do the switching, and one power supply to operate the power output stage. It is a very simple task to incorporate all of these into one compact power pack for a packaged unit for use in field applications.

In similar fashion the logic circuits themselves could be greatly reduced in size and packaged specifically for the actuator operation. Presently, many of the logic circuit boards are only partially used. This was done to allow the use of the inexpensive modules that were chosen.

The design approach taken was that the control circuit should not limit the basic capability of the actuator. Furthermore it was felt that the electronics should be as inexpensive as possible to allow greater funds to be expended on the actuator itself. The control electronics that were put together for this application have not placed a basic limitation on the unit, yet are versatile enough to accomodate a wide variety of pole configurations and pole winding characteristics. Although a great amount of analysis had gone into the design of the unit, indicating modest peak voltages, there was some doubt about the actual voltage level and coil

winding requirements, because of the non-linear magnetic circuit and the interaction of the Harmonic Drive motion referred back to the magnetic circuit. Therefore the main power supply was designed to accommodate a wide variation of possible voltages and currents. The original analysis turned out to be correct. The non-linearities were not too severe and the actuator operated at the voltage and current levels that were predicted. The versatility built into the electronics cost very little more and provided a margin for error. It is very costly to have to make major adjustments at the end of a manufacturing phase to match components at their interfaces.

With regard to the magnet poles, they were first wound with 70 turns per leg of #18 wire. An excessively long electrical time constant was the only difficulty encountered. To overcome this problem most expeditiously, without having to rewind the coils, a one (1) ohm, 25-watt resistor was placed in series with each coil pair. This decreased the electrical time constant (L/R) by about 10. All tests included the use of this resistor. Any future model would have the electrical design changed to eliminate it. This modification is an example of a quick, inexpensive means of matching at an interface.

One other merit of a transistorized digital control actuator over a proportional control actuator is the significant reduction in power consumption. In the proportional control unit the power amplifier plus actuator power consumption is almost constant with varying load and speed. In the digital control unit the driving transistors are either at cut-off or saturation and dissipate relatively little power, while the main power supply can be controlled to limit the power to the actuator with relatively lower over-all losses.

Technical assistance on the use of the digital logic circuits was provided by Tech Serv Inc. of Beltsville, Maryland. Basic circuit operations and techniques were developed by United. The final circuit configuration and implementation was a joint venture to make use of their particular form of circuit modules. The reproduction of their circuit diagrams in this report is with their permission and their cooperation is acknowledged and greatly appreciated.

It was decided early in the program that no matter what type of actuator was developed the electronic circuitry necessary to operate it successfully would be rather routine in nature. This philosophy was followed throughout. At each stage in the development of the actuator a brief look at possible control circuits was undertaken. After the over-all design was accepted and work started in manufacturing, time was then expended to develop the necessary control circuits. The major requirement placed on these circuits was that they would not limit the actuator's capabilities in any way. Now that the testing of the

unit has been accomplished it appears that the input, logic and switching circuits did not adversely affect the unit's performance. It is considered important to emphasize that little attempt was made to design circuits specifically for this application, and no attempt was made to package the circuits for minimum size and weight. Pictures showing the power supplies and logic circuits are apt to be deceiving unless this point is brought out. The pictures do not give any reasonable basis for judgement as to what the final component package size might be if a concerted effort for optimization and miniaturization were undertaken. Any specific application requires tailoring of the control functions to meet that application. Therefore each application might require modifications of the control circuits to varying degrees. Any time thus spent in optimization and miniaturization at this stage of development is not warranted. Because of the versatility of the actuator a number of different control circuits could be used. It will require an investigation of the proposed application to determine which type of control circuit is best suited to do the job.

The requirements for the control circuit function to complement the actuator were worked out and are now briefly described.

The actuator necessitated the development of an electronically controlled, balanced, rotating magnetic force field. This field had to act in an outward radial direction. The force couple is mated with Harmonic Drive speed reducer techniques as explained in Section 3. A series of sixteen "U" shaped magnet poles was located in a circular configuration. (See Figure 12) These poles had to be actuated in such a manner that not only were opposite poles energized, but adjacent poles were overlapped, with the overlap time dependent on input signal. The pole switching sequence also was to be capable of being reversed.

Input power available was 3 phase, either 60 or 400 cps, 115 volts line to neutral. Control signals for the device were analog in nature with polarity sensing necessary to control the direction of rotation of the magnetic field.

The following discussion of the electronics is best understood by referring to Figure 40. A simple analog to digital circuit consisting of complementary NPN-PNP transistors connected in common base configurations is used to determine the polarity. The conducting transistor then charges a capacitor which in turn triggers a one-shot multivibrator at a predetermined voltage level. The two channel, polarity-sensitive pulse trains so developed drive a three stage, up-down counter chain, i.e. divide by 8. The up-down counters are inter-connected to a series of eight "And" gates to develop eight sequential signal paths (0 through 7). These signal paths are connected to eight flip-flops as loads. To achieve the desired overlap the turn on of the flip-flops is determined by the corresponding "And" gate signal, but turn-off is accomplished by connecting through a series of "Or" gates to the pole two steps behind, in time, independent of the direction of rotation of the sequence. Thus, for pole 4 being turned on by "And" gate 4, this signal would also turn off pole

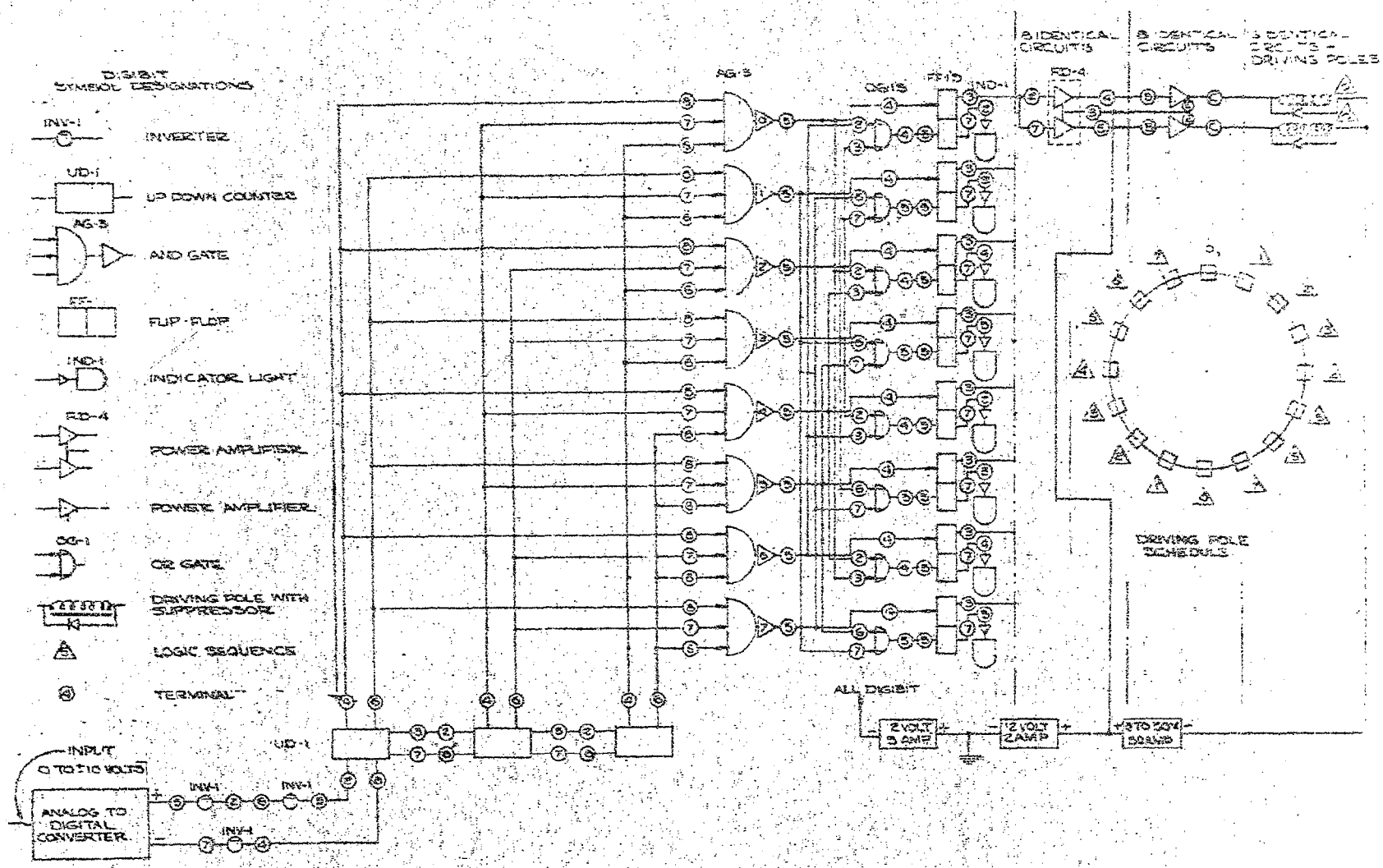

FIGURE 40 CONTROL CIRCUIT BLOCK DIAGRAM, MODEL EHD-3

2 or 6 depending on which one was on. The "Or" gate merely prevents false signal paths inadvertently turning on other poles by insufficient isolation of turn-on and turn-off functions.

Figures 41 through 49 show the circuit schematics. Figure 50 shows a figure of a typical "Digibit" logic circuit card.

Limited tests with this system in conjunction with the constant voltage power supply resulted in stable operation out to frequencies greater than 30 cps, for both sine and square wave inputs, with and without load inertia. Actual measurements on individual poles indicated accurate response with peak speeds of greater than 100 round trip excursions per second (approximately .025 in. total travel). Analysis using a constant current source indicates even higher stepping rates can be achieved. With an individual step for each pulse developed by the analog circuit the actuator is a very precise stepping unit. Overshoot for each step was seen to be small due to good damping and it was estimated that the ringing occurred at frequencies well above 200 cps.

Figure 51 shows the entire model in test, actuator with 0.1 kg-m^2 inertia load, rear of input, logic and switching circuitry and their power supplies, 16 1-ohm resistor bank, and the main power supply. Figures 52 and 53 show front and rear detail views of just the input, logic and switch circuitry and their power supplies. Figure 54 shows the main power supply in detail.

4.5 Discussion of Maximum Speed and Response

It was recognized early in the project that limits on maximum output speed would result from various factors, partially introduced in the last section.

(a) Dynamics of the flexible member and attached armature mass.
(b) Voltage capabilities of semiconductors.
(c) Time required to magnetize the circuit.

For a stepping device, there is a close connection between maximum speed (stepping rate) and transient response, which is itself closely related to frequency response.

Item (a) includes two effects. First, if the natural frequency is exceeded by the applied frequency, the deflection changes direction and diminishes rapidly in magnitude for the same impressed deflection force, there being a phase shift approaching 180°; thus, to achieve the proper deflection, progressively larger forces are required as the frequency increases. Operation at the natural frequency may represent an efficient condition, but the rapid changes in phase shift as it is approached would probably result in non-linear performance through this speed range. Natural frequency calculations (Appendix IX) indicate that, without armature mass, natural frequency is around 500 cps, and that armature mass reduces this by two or more. A value of about 200 cps is estimated, which corresponds to a speed of 39 rpm. Since the maximum speeds in test were considerably

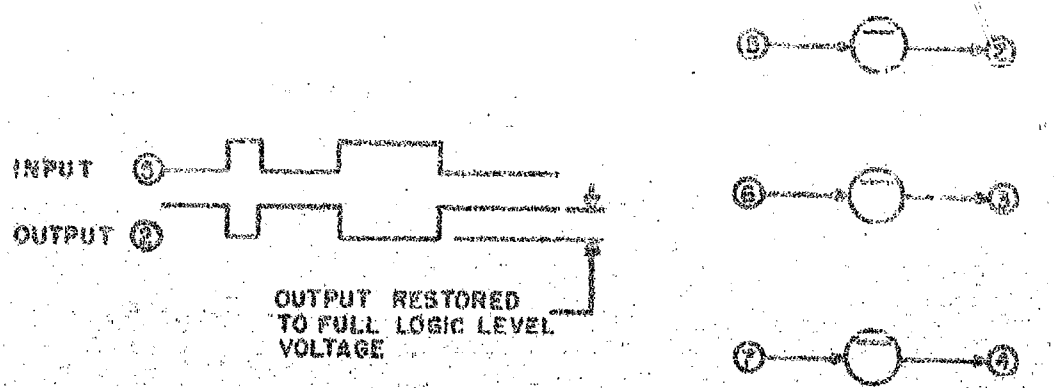

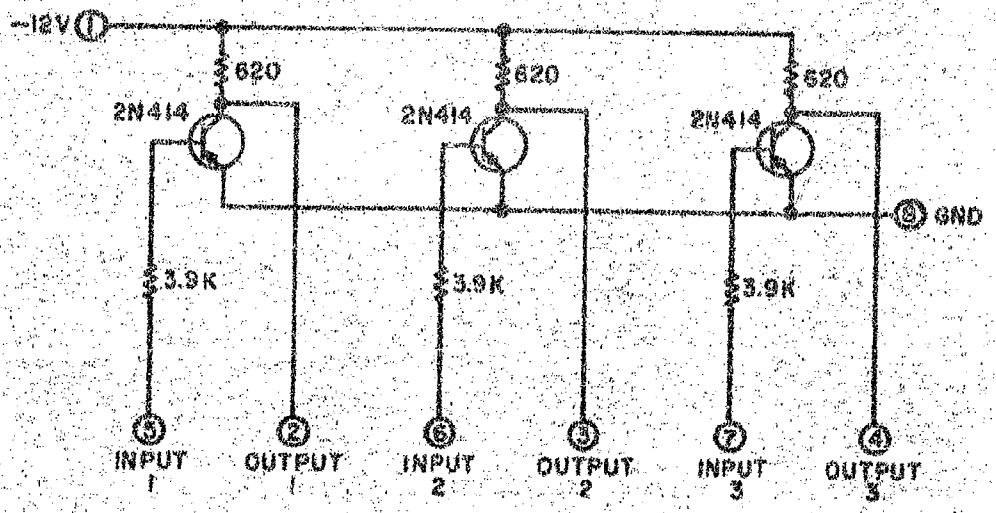

FIGURE 41 INV-1 INVERTER DIGITAL COMPONENT, MODEL EHD-3

Data hereon is proprietary and shall not be disclosed, used, or duplicated, for procurement or manufacturing purposes without written permission of Tech Serv, Inc.

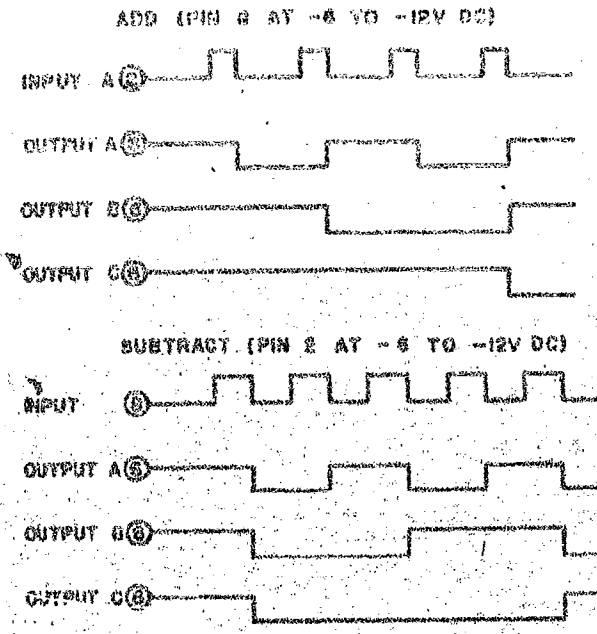

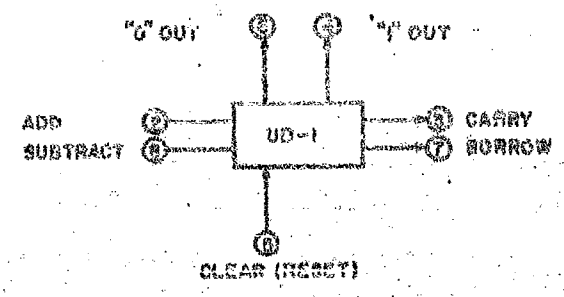

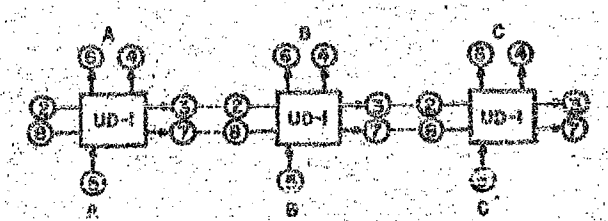

TYPICAL 3 STAGE ADD-SUBTRACT COUNTER

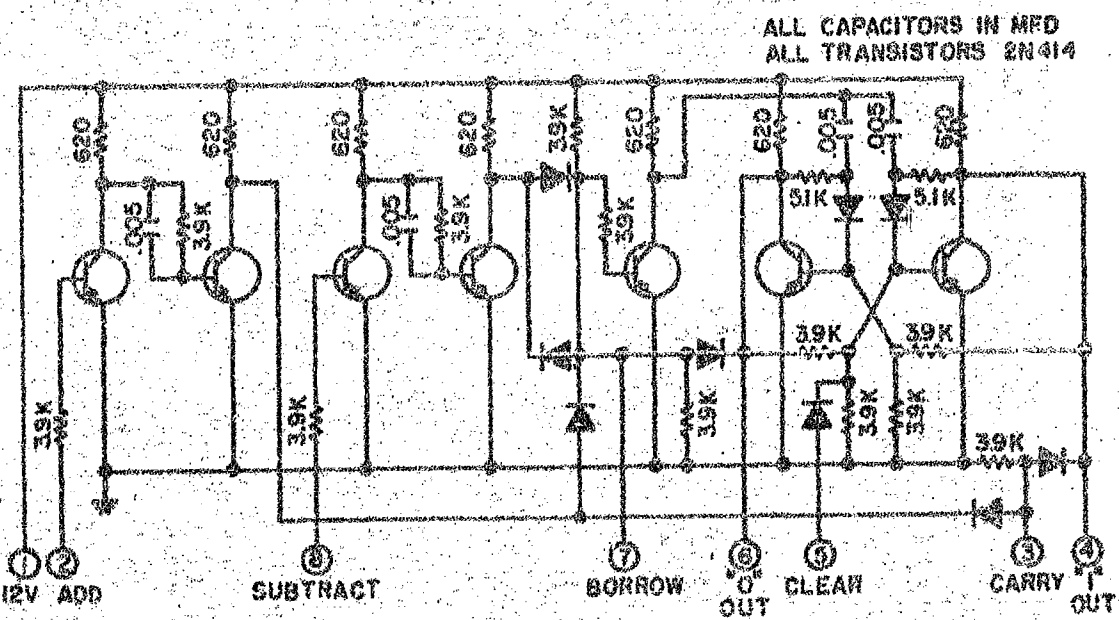

FIGURE 42 UD-1 SINGLE STAGE ADD-SUB-COUNTER DIGITAL COMPONENT, MODEL EHD-3

Data hereon is proprietary and shall not be disclosed, used, or duplicated, for procurement or manufacturing purposes without written permission of Tech Serv, Inc.

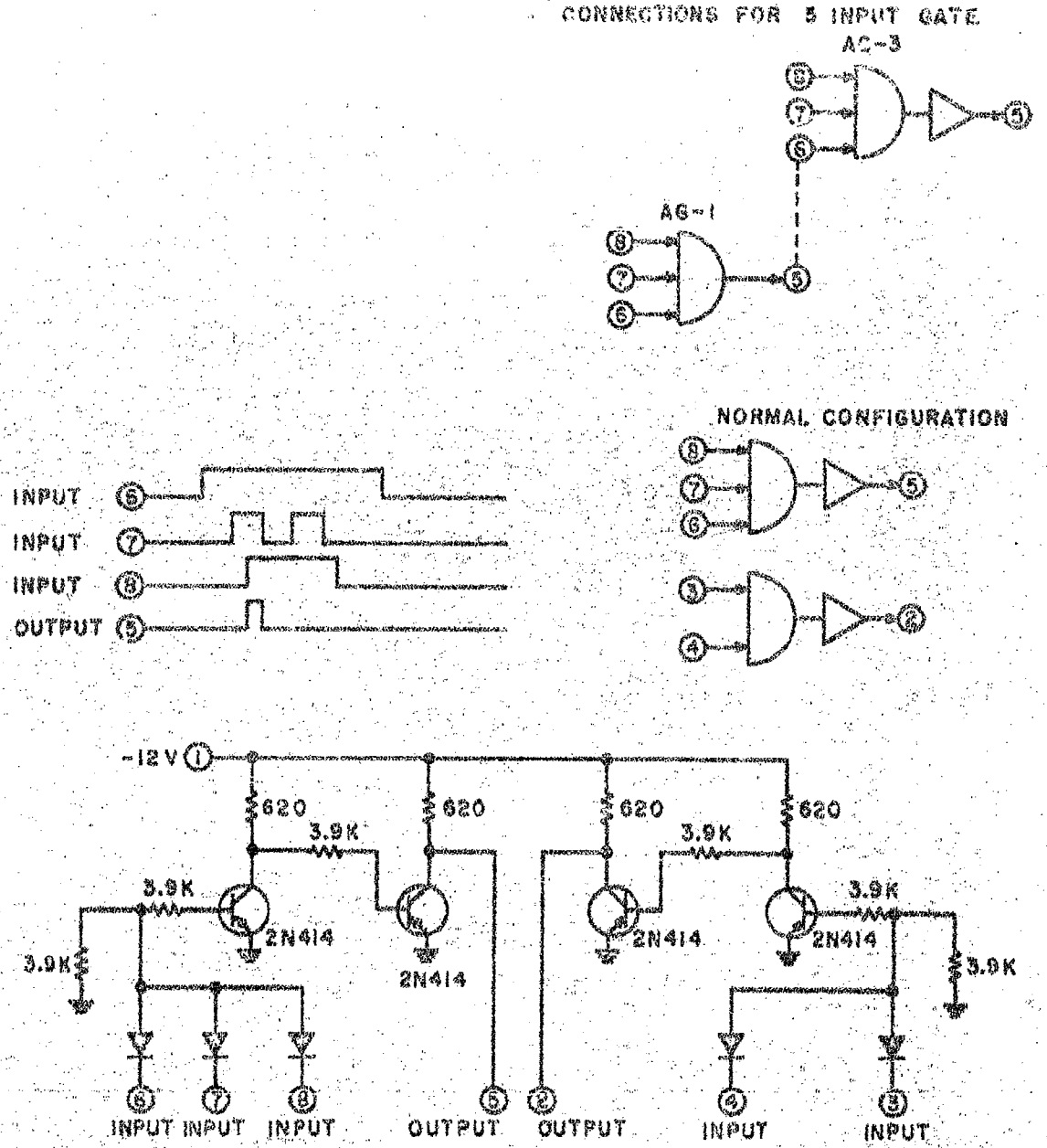

FIGURE 43 AG-3 DIODE "AND" GATE DIGITAL COMPONENT, MODEL EHD-3

Data hereon is proprietary and shall not be disclosed, used, or duplicated, for procurement or manufacturing purposes without written permission of Tech Serv, Inc.

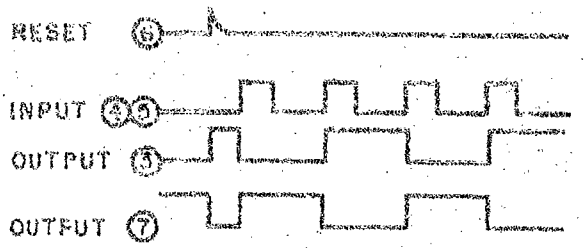

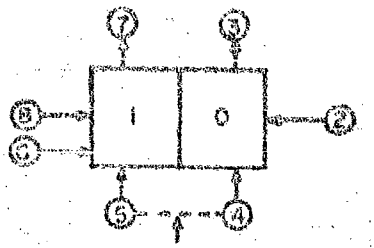

T OPERATION

LEVEL OPERATION

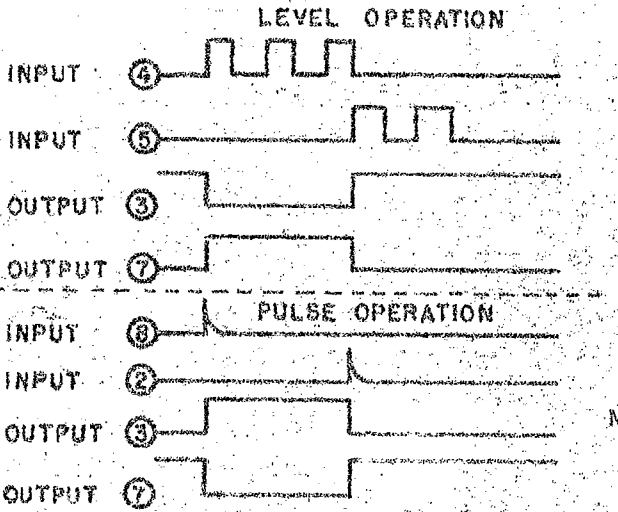

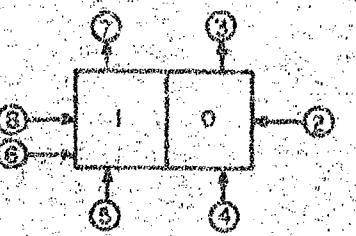

R-S OPERATION

NOTE

INPUT TO PINS 8 AND 2 MUST BE CAPACITOR - COUPLED (AS FROM AG-2). THIS SAME REQUIREMENT EXISTS FOR RESET PULSES ON PIN 6.

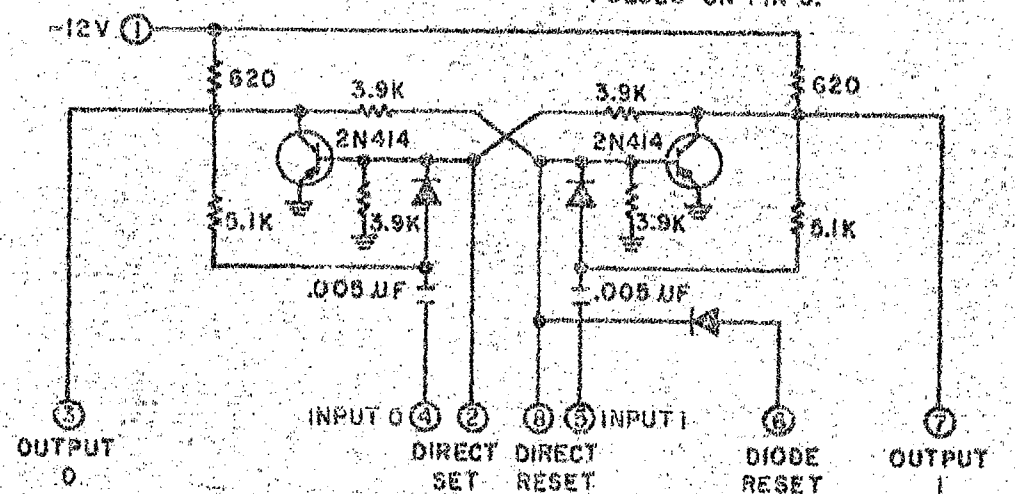

FIGURE 44 FF-1 FLIP-FLOP DIGITAL COMPONENT, MODEL EHD-3

Data hereon is proprietary and shall not be disclosed, used, or duplicated, for procurement or manufacturing purposes without written permission of Tech Serv, Inc.

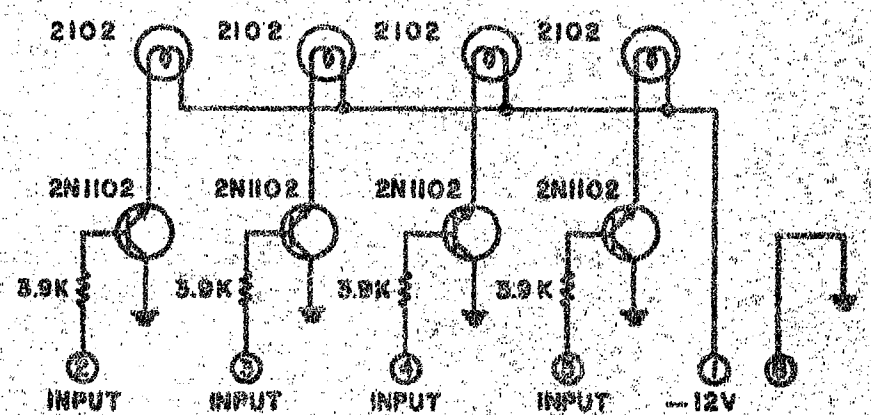

FIGURE 45 IND-1 INDICATOR DIGITAL COMPONENT, MODEL EHD-3

Data hereon is proprietary and shall not be disclosed, used, or duplicated, for procurement or manufacturing purposes without written permission of Tech Serv, Inc.

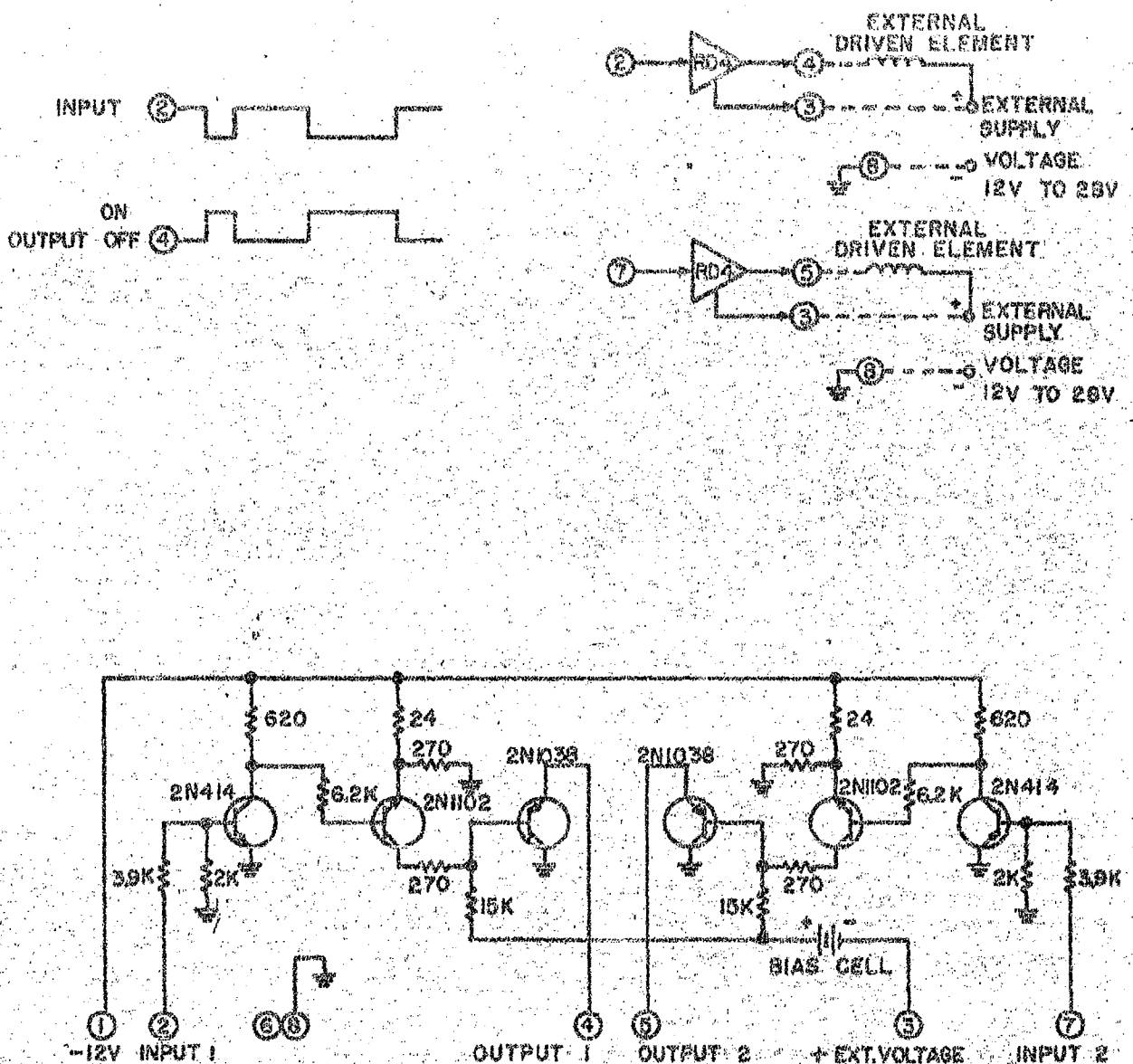

FIGURE 46 RD-4 RELAY DRIVER DIGITAL COMPONENT, MODEL EHD-3

Data hereon is proprietary and shall not be disclosed, used, or duplicated, for procurement or manufacturing purposes without written permission of Tech Serv, Inc.

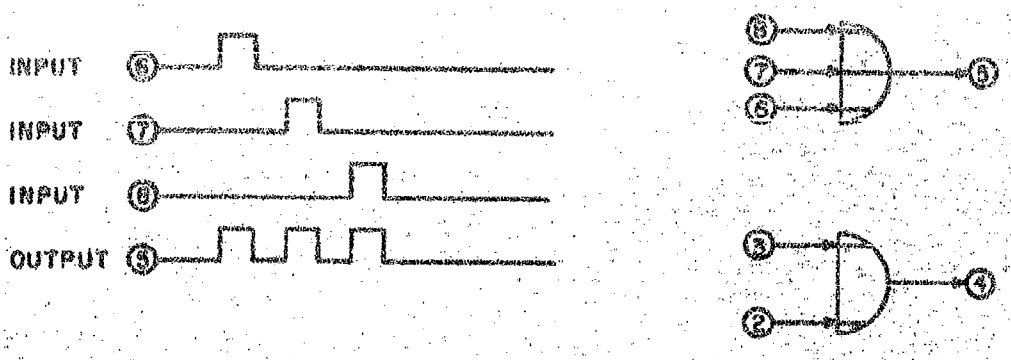

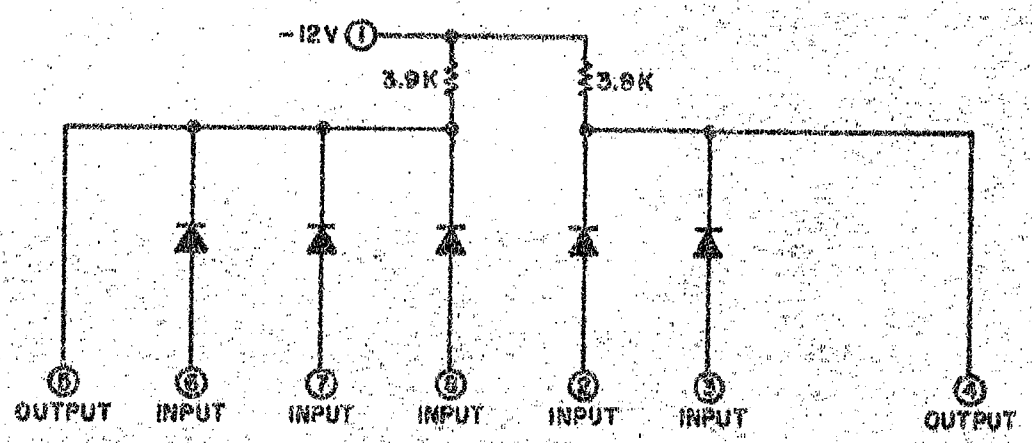

FIGURE 47 DIODE "OR" GATE DIGITAL COMPONENT, MODEL EMD-3

Data hereon is proprietary and shall not be disclosed, used, or duplicated, for procurement or manufacturing purposes without written permission of Tech Serv, Inc.

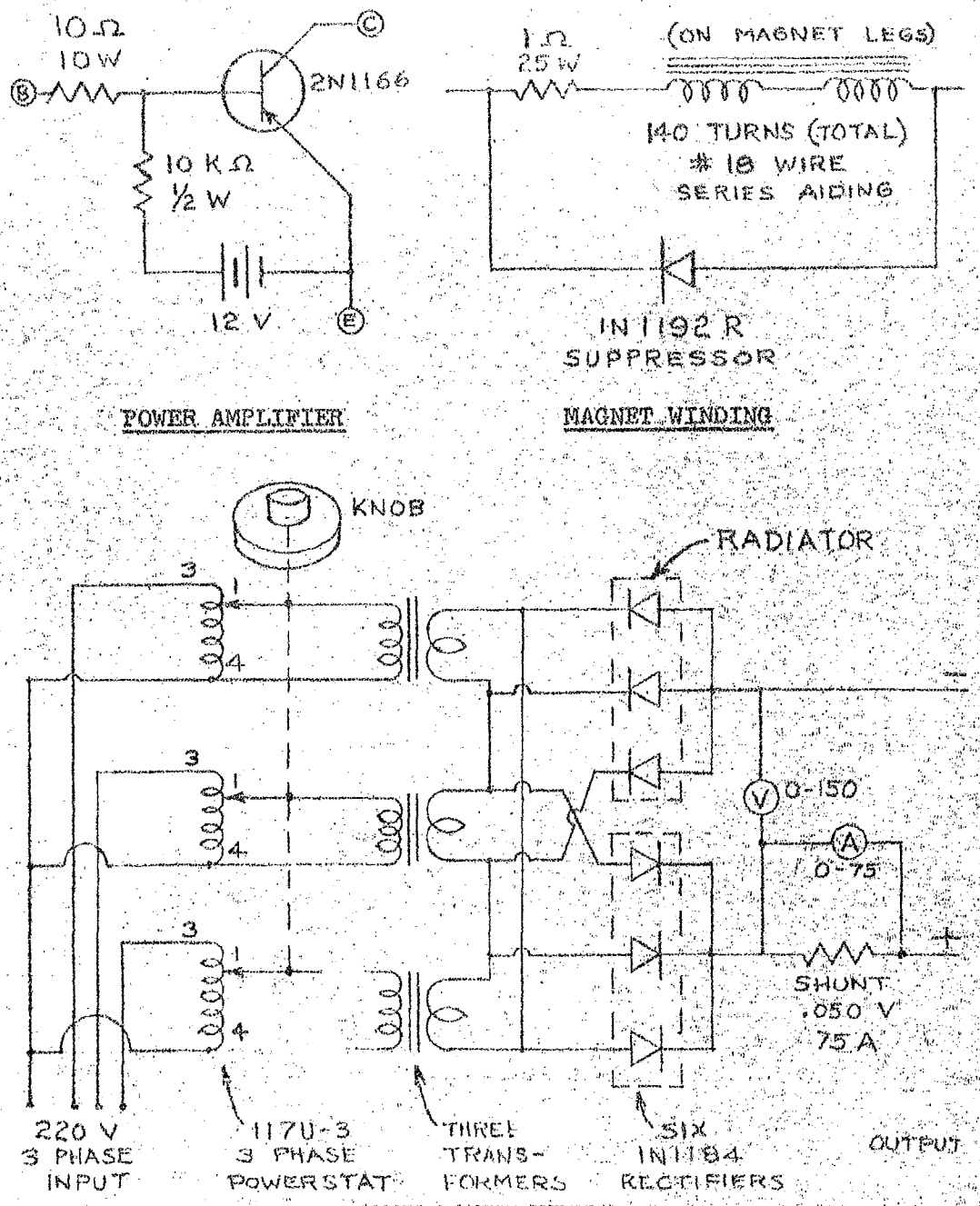

FIGURE 48 POWER AMPLIFIER, MAGNET WINDING AND MAIN POWER SUPPLY CIRCUITS, MODEL EHD-3

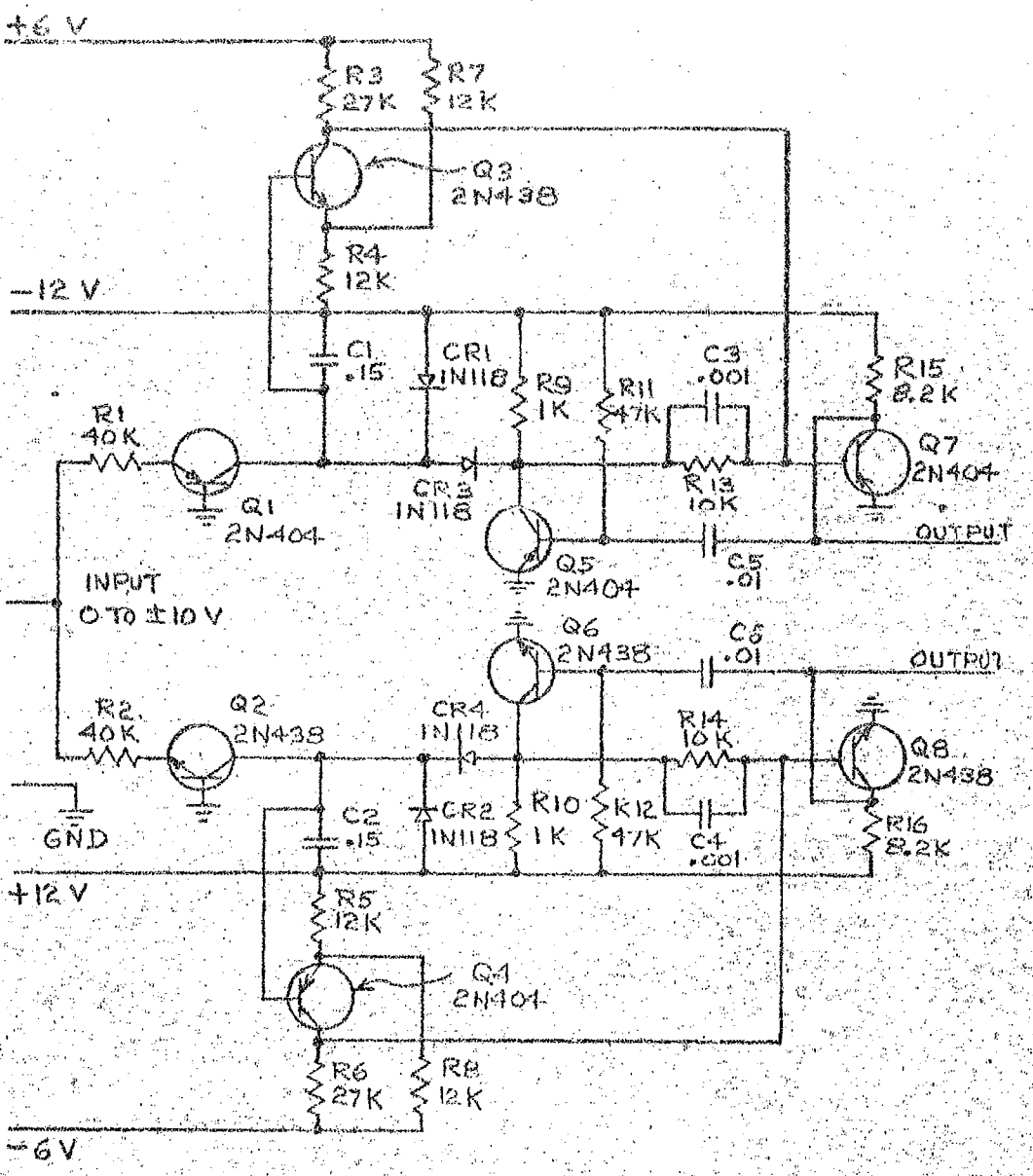

FIGURE 49 ANALOG TO DIGITAL CONVERTER CIRCUIT, MODEL EHD-3

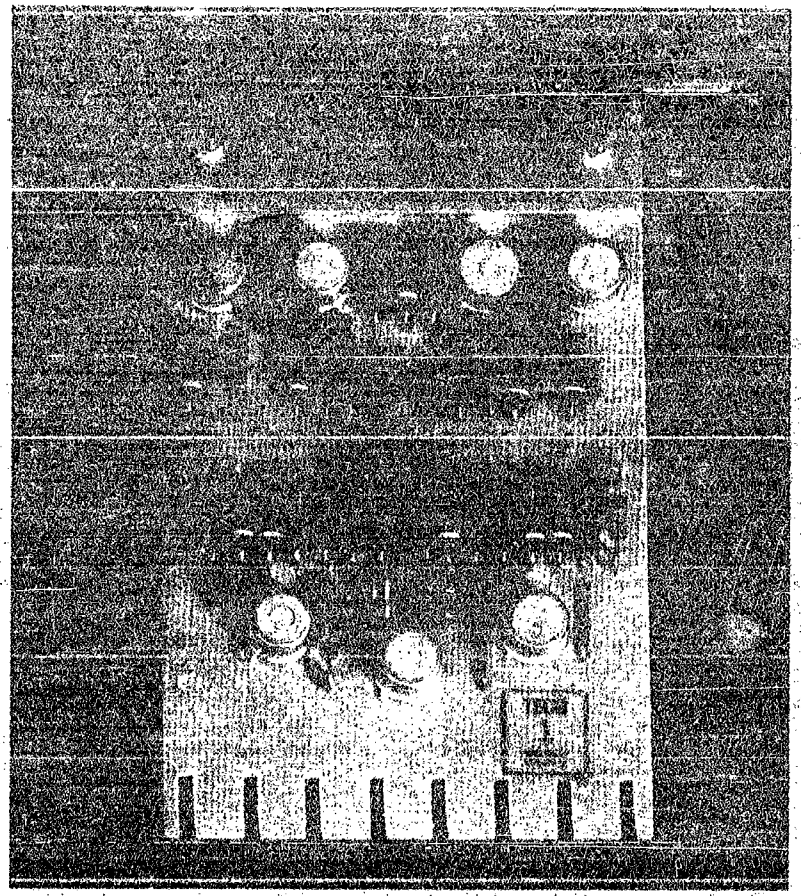

FIGURE 50 TYPICAL "DIGIBIT" LOGIC CIRCUIT CARD

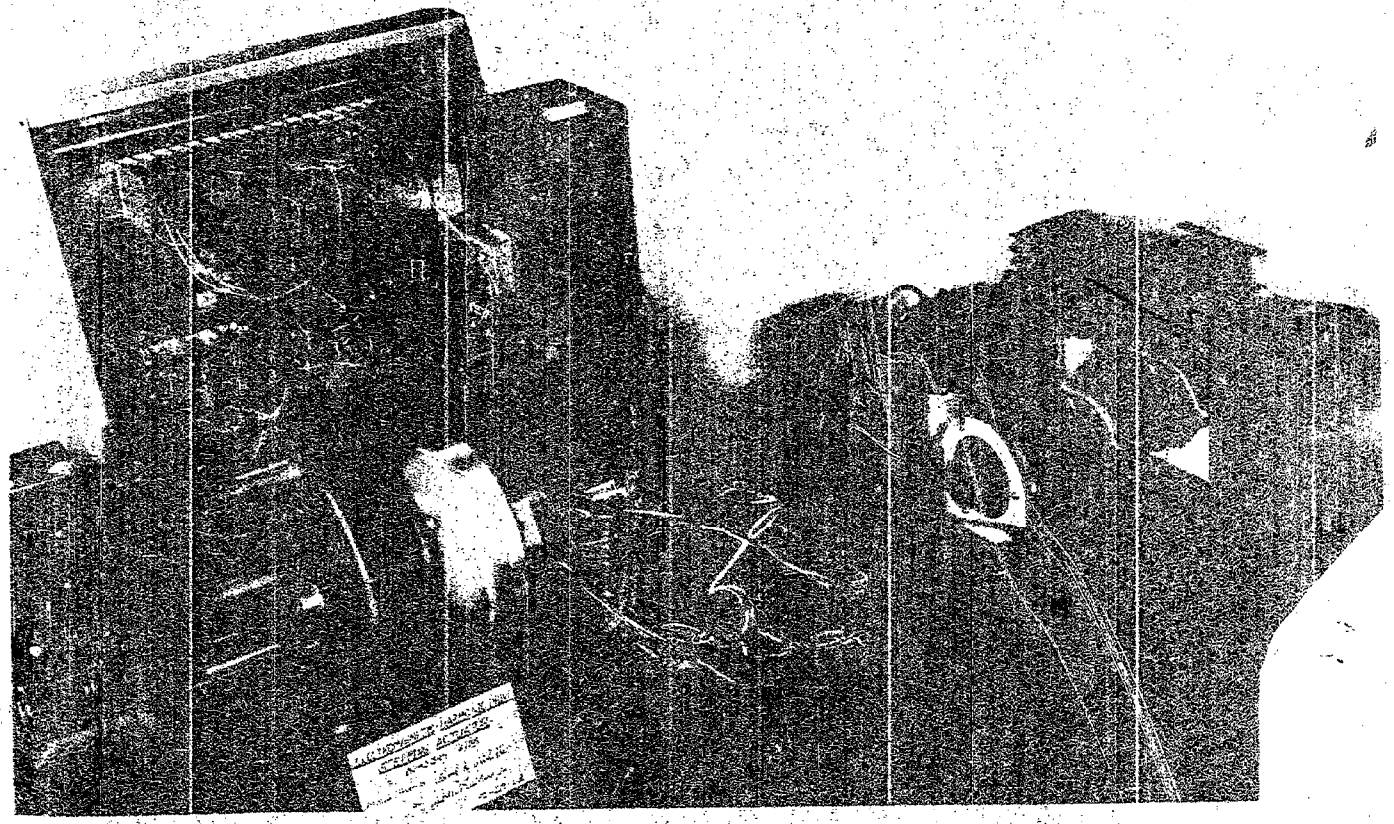

FIGURE 51 ENTIRE EHD-3 MODEL INCLUDING CONTROLS AND 0.1 KG-METER^2 LOAD

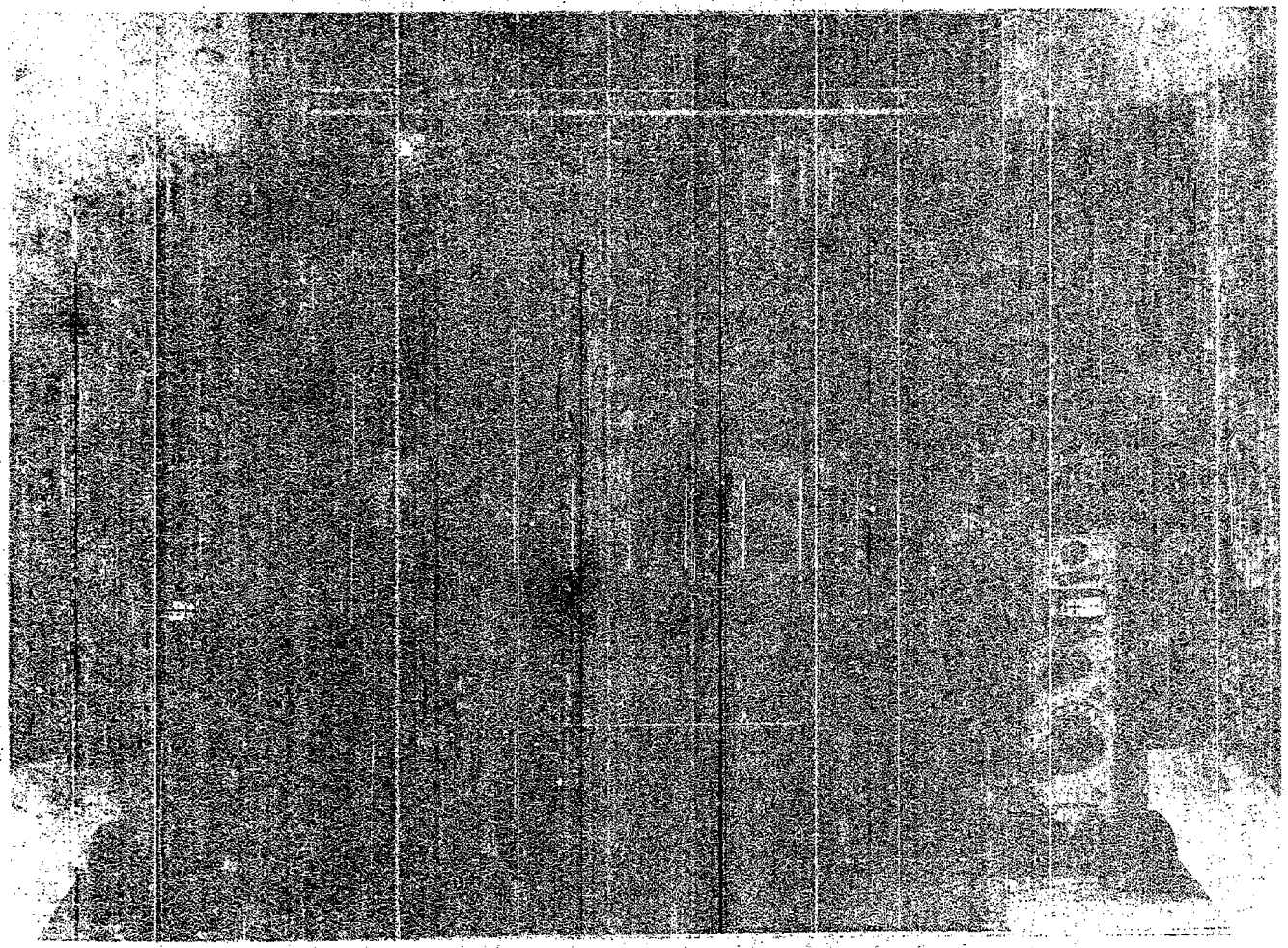

FIGURE 52 INPUT, LOGIC AND SWITCHING CIRCUITRY AND POWER SUPPLIES, FRONT VIEW, MODEL EHD-3

FIGURE 54 MAIN POWER SUPPLY, MODEL EHD-3

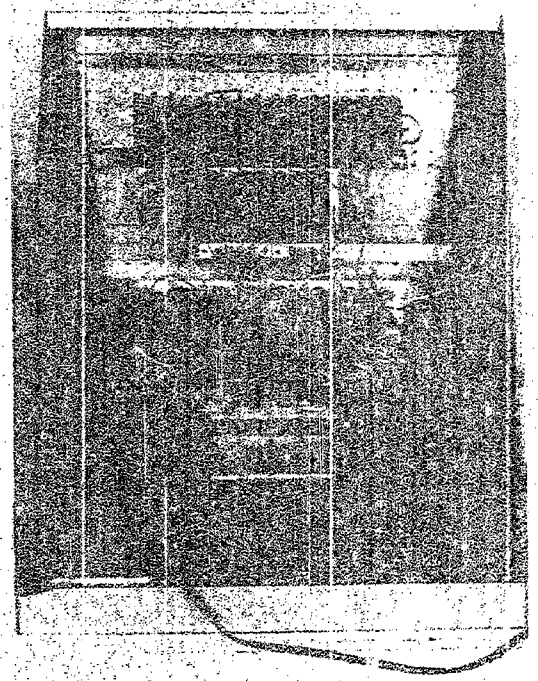

FIGURE 53 INPUT, LOGIC AND SWITCHING CIRCUITRY AND POWER SUPPLIES, REAR VIEW, MODEL EHD-3

lower (18 rpm), it is believed that nautral frequency was not limiting.

As discussed in Section 4.3, if the EHD-3 were stepped two magnets at a time, output speed would double for constant input frequency. This might be possible if, due to tooth friction or dynamic effects the teeth remained engaged when the power angle approached 45°.

The back-emf voltage that the power stage semiconductors work against increases with input frequency. With the EHD-3 tests, this was purposely limited to 800 cps where peak voltage was about 60 volts, even though the power transistors are rated for 100 volts.

Magnetization time, or the time required to reach operating flux density, involves the complications that arise in the study of the dynamics of electromagnetic devices. The power supply should ideally have a constant current characteristic. Then, MMF would follow the impressed currents. To the extent that the circuit's L/R ratio becomes significant, there will be a corresponding delay to the current and MMF build-up. First consider the constant current case. When the device is first turned on, depending upon the gap at the point of peak MMF, a certain flux density results and for the power angle corresponding to this gap, a certain torque is produced, which begins to accelerate the total inertia, the initial position response following that of Figure 30*. If the commanded speed is relatively low, and inertia high, flux density increases rapidly as power angle decreases but little, and a large torque is produced.

If the inertia is low, acceleration is greater so that the gap and the reluctance decreases faster. This results in faster increase of flux density toward saturation but, also, a faster decrease in power angle so that torque produced may be less. For in-between values of inertia, the rates of reluctance and power angle change are counterbalancing.

As the commanded speed increases, the condition is approached wherein the MMF at that point falls (gradually with the RF type, step-wise with SF type) before the device has made sufficient movement, power angle exceeds it's safe value, and tooth disengagement occurs. Obviously, this limiting speed decreases as load inertia is increased and acceleration decreased.

With an essentially constant voltage supply (high L/R ratio) which pertained to the models, flux density is proportional to the time integral of the impressed voltage (Faraday's Law), and the maximum power angle will increase with command frequency, thereby establishing a limit upon speed.

---

* For "normal" operation, as opposed to Figure 67 which represents "slew" operation (discussed in Section 11.2.1).

As a result of these interrelationships, measurements of response time for current are not considered so significant as for flux density which would indicate the force, torque, and motion. The difficulties involved in measuring the dynamic flux and torque were not considered justified. A series of current and voltage dynamic measurements were taken for the EHD-3, showing about .001 to .002 seconds to the end of armature movement and .002 to .004 seconds total rise time, for two different peak voltage inputs, 30 and 15 respectively (Figure 55).

This bears out Faraday's Law, and indicates further that the load inertia (0.1 kg-m^2), plus the speed (2.9 rpm), was so small that the step was completed before flux saturation was reached. An alternate possibility is that the reluctance is lower than expected and saturation is reached at only partial current. Both of the above effects may be acting together.

The time to move the armature gives insight into the potential slew-speed capability of the device, if the dynamics permits it. If one considers that the working stroke time, t_p could last as long as half the time between steps, $t_s/4$, then, referring to Figure 30, and based upon

$$t_p = 3.4 \times 10^{-4} \text{ sec (From Appendix VI)} \quad (4\text{-}50)$$

$$t_s = 4\, t_2 = 1.35 \times 10^{-3} \text{ sec} \quad (4\text{-}51)$$

and

$$\dot{\theta}_o = \frac{1}{2R_g}\left(\frac{1}{2t_s}\right) 2\pi = \frac{\pi}{2R_g t_s} = 7.4 \text{ rad/sec} = 70 \text{ rpm} \quad (4\text{-}52)$$

4.6 Other Characteristics

4.6.1 Resolution and Minimum Speed

The model, when stepped one magnet at a time, has a resolution of

$$\theta_M = \frac{1}{nMR_g} = 4 \times 10^{-4} \text{ rev} = 8.7 \text{ minutes of arc} \quad (4\text{-}53)$$

Over a series of steps the average variation was measured as about $\pm$ 10%. It was operated at a fairly smooth, continuous average speed of about 1/10 rpm (4 steps/sec). However, it should be realized that the actuator itself is a stepping device capable of as low an average speed that is commanded by the controls. No attempt was made to obtain an unusually low average speed.

4.6.2 Holding Torque

With no input current the holding torque due to residual magnetism is negligible. With steady state coil current the stall torque obtained, as a function of current, is given in Figure 33. This

J_L = 0.1 kg-m^2
I = 40a
Voltage calibration 10 v/cm
e_m = 15-20
e_{DC} = 3

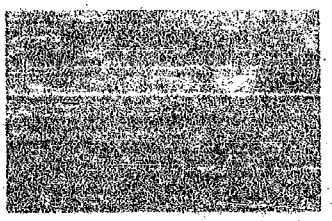

J_L = 0.1 kg-m^2
I = 60a
Voltage calibration 20 v/cm
e_m = 30
e_{DC} = 4

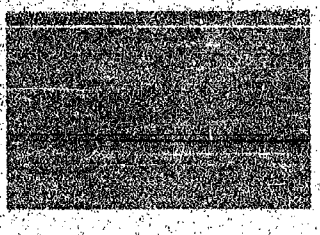

J_L = 0
I = 40a
Voltage calibration 10 v/cm
e_m = 15-20
e_{DC} = 3

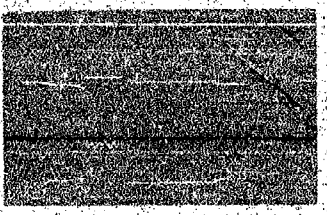

J_L = 0
I = 60a
Voltage calibration 20 v/cm
e_m = 30
e_{DC} = 4

FIGURE 55 MAGNET COIL VOLTAGE AND CURRENT WAVE FORMS, EHD-3
Speed = 2.9 rpm
Top trace-voltage (calibration varies, given above)
Bottom trace-current (10 amps/cm)

represents a well-aligned set of magnets, the results for other combinations are lower. (Estimated to vary by 25%. See Appendix VIII).

4.6.3 Backlash

Measured backlash was negligible, not measurable, employing a small torque reversal and a dial indicator.

4.6.4 Size and Weight

The weight of the research model actuator is 22 lbs. The housing is an aluminum casting.

4.6.5 Efficiency, Losses, Temperature Rise

Stepping devices and indeed servo motors in general are not characterized by high efficiency. Their accelerating capability and, for stepping devices, stepping rate versus load inertia, being more significant. Nevertheless, the efficiency of the model is very good, surpassing competitive types. The possible power losses in the actuator itself, excluding the external control circuitry, result from the I^2R loss in the coils, hysteresis and eddy current losses. The material used has hysteresis properties which are generally equivalent to that of regular electrical steel, so for a tractive magnet this can be neglected relative to the I^2R loss. By the use of laminations in all of the iron paths, the eddy current loss was made negligible also.

The final configuration of the model, placing the magnets outboard of the flexspline, was primarily selected in order to eliminate having a section of the flexspline transverse to the flux. This would have constituted a shorted turn and incurred a high eddy current loss. This would also contribute a sizeable time delay, limiting the maximum speed capability.

The I^2R loss is given by

$$P_R = 8\, P_c \qquad (4\text{-}54)$$

where P_c, the loss in one coil, is

$$P_c = i_m{}^2 R_c \qquad (4\text{-}55)$$

since, neglecting transient effects, four magnets composed of two coils each are concurrently energized.

Before specifying current, it is necessary to calculate the required MMF. Consider the magnet at the start of its excitation. The MMF required is essentially dependent on the reluctance of the air gap across which the design flux density must be established. This reluctance is directly proportional to the gap length. The wedge shape of the gap greatly complicates the calculations, so the simplification will be made that the reluctance depends upon the gap length at the midpoint of the magnet's pole face.

For the first trial, consider that the magnet's power angle (from the major axis to the midpoint of the magnet) is 45°. (The actuator's power angle due to the other set of magnets is 33 3/4°). For the ideal flexspline shape (no distortion) the gap, "g", at the plane of the teeth, is

$$g = \frac{d}{2} \tag{4-56}$$

Since $d = \frac{2}{F_D}$ for two lobe Harmonic Drive (4-57)

$$g = 1/F_D \tag{4-58}$$

Using $F_D = 96$ (4-59)

$$g = 1/96 = .0104" = 2.6 \times 10^{-4}_m \tag{4-60}$$

Neglecting the reluctance of the iron relative to the air path

$$\mathcal{F} = \frac{\beta_m g}{\mu_o} \tag{4-61}$$

Take

$$\beta_m = 2.2 \text{ w/m}^2 \tag{4-62}$$

Due to the lever action of the back-up armature pieces, the gap is greater at each of the magnet's gaps by the mechanical advantages Kma_1 and Kma_2.

For the in-board gap

$$g_1 = kma_1 g = \frac{3.3}{2.5} g = 3.4 \times 10^{-4}_m \tag{4-63}$$

For the out-board gap

$$g_2 = kma_2 g = \frac{4.3}{2.5} g = 4.5 \times 10^{-4}_m \tag{4-63}$$

$$\mathcal{F}'_1 = \frac{\beta_m g_1}{\mu_o} = 590 \text{ a-t} \tag{4-65}$$

$$\mathcal{F}'_2 = \frac{\beta_m g_2}{\mu_o} = 790 \text{ a-t} \tag{4-66}$$

Total MMF, $\mathcal{F}'_3 = 1380$ a-t (4-67)

For an actuator power angle of 27°, the power angle of the magnet under consideration would be

$$\delta = 27^\circ + 22\tfrac{1}{2}^\circ = 38^\circ \tag{4-68}$$

$$\therefore g_3 = g\left[1 - \sin 2(45^\circ - 38^\circ)\right] = 2.0 \times 10^{-4}\text{m} \qquad (4\text{-}69)$$

and total MMF would be less.

However, there are two factors that tend to make the gap larger. First, there may be some distortion in the shape of the flex-spline, which would increase the curvature ahead of the flex-spline. Second, the above analysis is based on the magnet pole face being circular; however, for the Model EHD-3, to conserve manufacturing time and cost, the faces had flat faces. This makes the average gap greater than if it were rounded. For the diameter of the model, the increase in gap at the ends is .011", so the average is about .006" more.

The previous total MMF is thus adjusted by the factors:

$$\mathcal{F}_4 = \mathcal{F}_3 \times \frac{2.0}{2.6} \times \frac{.0104" + .006"}{.0104"} = 1680 \text{ a-t} \qquad (4\text{-}70)$$

To allow for the effect of shape distortion, an increase of as much as 50% (to 2500 a-t) was anticipated.

Knowledge of the capabilities of the semi-conductors to be employed indicated that the current limit should be about

$$\left.\begin{aligned} &i_m = 10 \text{ to } 15\text{a} \\ &\text{with } i_m = 11\tfrac{1}{4}\text{a, design value (45a total for 4 poles)} \end{aligned}\right\} \qquad (4\text{-}71)$$

So that the required number of turns is

$$N = \frac{\mathcal{F}_4}{i_m} = 150 \text{ turns} \qquad (4\text{-}72)$$

or 75 turns per coil. However, the design was completed when the design flux density was 2.0 w/m^2, which results in 140 turns. The resistance of one coil, using 70 turns of #18 AWG wire, the largest that could be fitted in, is approximately

$$R_c = 0.1\ \Omega \qquad (4\text{-}73)$$

at room temperature, by calculation and measurement. Thus, the range of power loss is

$$P_c = 8(0.1)(10)^2 = 80 \text{ watts}, \quad i_m = 10\text{a} \qquad (4\text{-}74)$$

to

$$P_c = 8(0.1)(15)^2 = 180 \text{ watts}, \quad i_m = 15\text{a} \qquad (4\text{-}75)$$

with $$P_c = 8(0.1)(11.25)^2 = 100 \text{ watts}, \quad i_m = 11.25\text{a} \qquad (4\text{-}76)$$

Little attention was given to cooling in this feasibility model. An analysis of how temperature rise can be estimated is given in Appendix X. For the EHD-3 the radiating area is taken as

$$A = 1\ 7/8"\ (\pi)6" + 2\frac{\pi}{4}\left[(6)^2-(4)^2\right] = 66\ in^2 \qquad (4\text{-}77)$$

Hence

$$Q = hA\Delta t = .0035(66)85 = 20 \text{ watts} \qquad (4\text{-}78)$$

For the two power dissipation values, the theoretical steady state temperature would be, at room temperature ambient,

$$t = 20 + \frac{80}{66(.0035)} = 370^{\circ}C,\ P_R = 80 \text{ watts} \qquad (4\text{-}79)$$

$$t = 20 + \frac{180}{66(.0035)} = 800^{\circ}C,\ P_R = 180 \text{ watts} \qquad (4\text{-}80)$$

which would indicate the need for improved cooling. A heat run test, without any supplementary cooling, was performed to measure temperature rise, using thermocouples wedged against the coils with a wooden block. Results are given in Figures 56 and 57 for two current levels. In order to prevent damage to the insulation, the tests were discontinued at 200° F (93°C).

Assuming a liberal "hot-spot" allowance of 20°C, the comparative results are shown in Table XVI.

Current per magnet (amps)	11.2	15
Time to reach 200°F (minutes)	27	6
Measured steady state (°C)	100	*
Hot-spot allowance (°C)	20	20
Assumed measured wire steady state (°C)	120	--
Theoretical wire steady state (°C)	370	800

*Test discontinued at 93°C.

TABLE XVI-TEMPERATURE RISE DATA, EHD-3.

The much better cooling that was achieved is believed to result from motion of the elements which greatly increases the heat transfer coefficient. Appendix X explains that NEMA B insulation

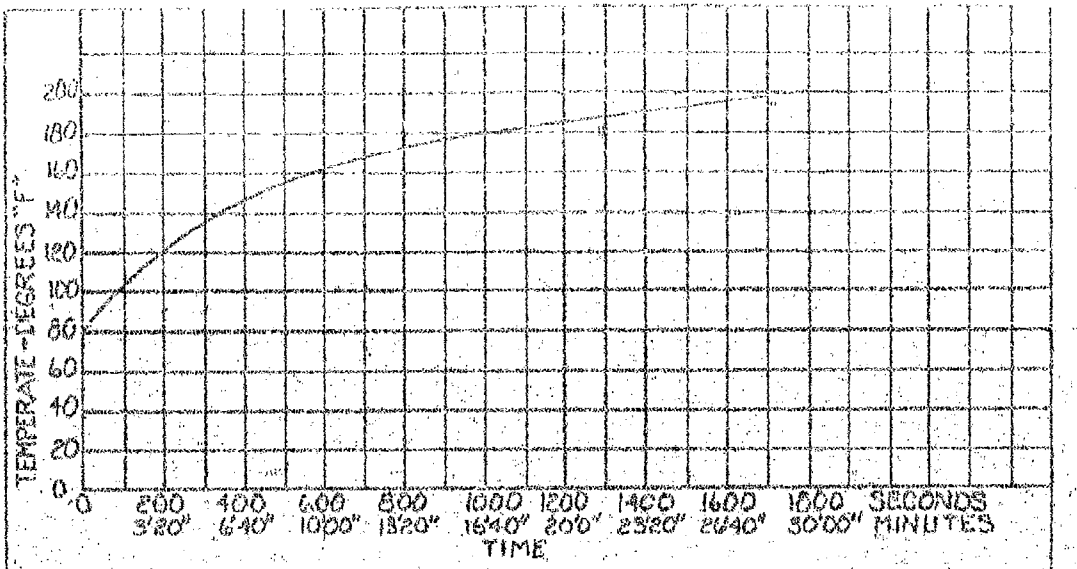

FIGURE 56 MEASURED TEMPERATURE RISE, MODEL EHD-3, 11.1 AMPS PER MAGNET, 4 RPM

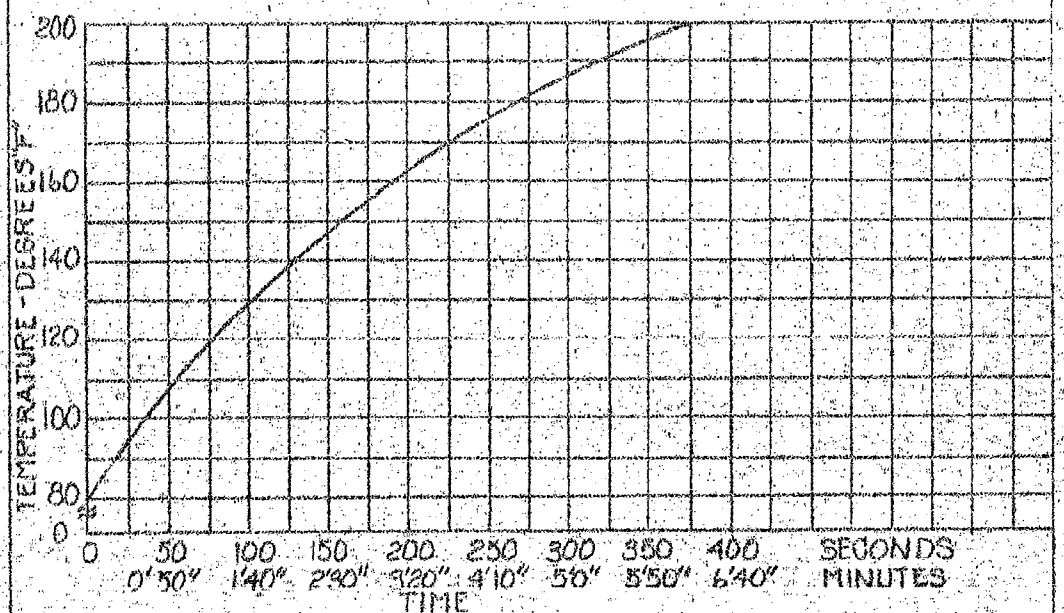

FIGURE 57 MEASURED TEMPERATURE RISE, MODEL EHD-3, 15 AMPS PER MAGNET, 6 RPM

has a long-life winding temperature limit of 130° C, so that the model could be run indefinitely at 11 amps per magnet for the 0.1 kg-m^2 load at 2.9 rpm.

4.6.6 Repeatibility

During a period of about one month (December 1962) the model was operated nearly daily, and less frequently for the following month. No degradation in performance was observed. After the first few days of operation, the unit was disassembled. Except for a slight interference between the armatures and the housing, which was corrected, there was no evidence of accelerated wear.

4.6.7 Acoustic Noise

A measurement was made of the acoustic noise of the actuator. At a distance of three feet directly in front of the magnet end of the device, the measured levels of Table XVII were obtained, varying with speed and current. These levels are not excessive for electromechanical devices in general.

DIRECTION *	SPEED (RPM)	TOTAL CURRENT (AMPS)	ACOUSTIC NOISE (DB) **
CCW	6	30	71
CCW	6	45	74
CCW	6	60	76
CCW	12	30	85
CCW	12	45	87
CCW	12	60	88
CW	6	30	74
CW	6	45	76
CW	6	60	78
CW	12	30	84
CW	12	45	86
CW	12	60	88

*Viewing output (magnet) end
**Scale "A" reading, General Radio Model 1551-C Noise Meter, 3 feet away along the rotation axis.

TABLE XVII - ACOUSTIC NOISE MEASUREMENT, EHD-3

Ambient level 55 db (room quiet)
Viewing hole of the actuator plugged up
Actuator mounted on a felt pad

ROTATING FIELD TYPE - DETAILED ANALYSIS AND TECHNICAL EVALUATION OF DESIGN

5.1 General

The rotating field type is characterized by constant speed, constant torque output for a fixed input frequency and voltage. There are two variations of this type (see Figure 11) denoted by differences in the flux path:

Circumferential flux, characterized by:

- -Fixed iron magnetic path.
- -Flux density limitation due to threading of flux.
- -Additional air gaps between the links.
- -Forces at the link interfaces which tend to increase deflection force and friction losses.

Radial flux characterized by:

- -Increasing iron magnetic path, giving a moderate loss in force.
- -Powder gap requiring considerable MMF.

For both types, if the flexspline is metal, it also carries flux but tends to degrade the entire operation due to eddy current and rotor copper loss.

Furthermore, for the preferred configuration of locating the stator field outside of the armature, the metal flexspline acts as a high-resistance rotor at stall, producing a counter torque from induction motor action. This decreases the net output torque. With the alternate configuration of placing the stator field inside the armature, the induction motor torque reinforces the Harmonic Drive torque. However, considerably less space is available inside, so that net torque-to-volume would be less than for the preferred configuration, even though efficiency might be somewhat greater.

Since flux density in the air gap is considerably lower for both of the RF types than with the stepping field type and since torque is proportional to the second power of flux density in the gap, the torque is reduced considerably from that obtainable in the stepping device. The best calculated maximum air gap flux density is about one third of the SF type, so the output torque is thus about $(1/3)^2 \approx 1/10$. Despite this effect, the power rate to power loss ratio and other performance characteristics are still considerably better than is obtainable from conventional electrical actuators not employing separate clutching mechanisms.

In this Section, there is given first a physical description of the various models, then a detailed analysis of predicated performance including derivations of formulas for analyzing the electrical, torque and inertia characteristics. In the accompanying Appendix (XI), there is an analysis of the EHD-2 model that

was made and tested, including detailed calculations to substantiate the losses. There is then presented an analysis of the performance which can be expected if certain improvements are made; in particular, eliminating the metallic flexspline. For a non-conducting flexspline, the theoretical efficiency increases from less than 1% to 40% and the torque from 2.2 lb. in. to 72 lb.in. The characteristics of these types are summarized in Table XVIII.

Tests results for the RF types are combined with the analysis as explained in the Introduction.

5.2 Description

The secondary or rotating field model acts as a synchronous motor. In general, its electrical design is considerably less complex than the stepping type. In fact, models were constructed using parts from a conventional three-phase induction motor (see Figures 16 and 17). The basic concept is that superposition of two or three sine wave currents, properly phased, results in a smoothly rotating flux field, as with any AC polyphase motor. This field is combined with reluctance action by using an armature means that moves radially outward to close the air gap. This outward motion also deflects the flexspline into progressive engagement with the circular spline. The reduction and integration action of the splined members is basically the same as with the stepping type. The key difference between the two types is that, with the rotating field type, there is essentially only one closed loop of flux for the entire device, as opposed to four loops for the stepping field type. Due to the distributed windings, this one loop has a flux density distribution that varies, approximately sinusoidally, and spreads over a 180° segment.

There is also a fundamental difference in the two variations of armature. The first (EHD-4) utilizes a flexible chain of rigid links (see Figures 14 and 19) positioned just inside the flexspline. The flux passes through the flexspline and threads circumferentially around the chain in two parallel magnetic paths. Because of convergence, the flux density will be greater inside the flexspline. The portion of the chain positioned 90° to each side of the maximum flux density position will carry the highest flux density. This, in general, leads to a flux density in the air gap which is less than the saturation level of the magnetic material.

The second armature variation (EHD-2) (see Figure 13) utilizes a powder of iron or other permeable material plus a rigid laminated core that does not flex, but rather rotates with the flexspline. The flux emanates primarily from the pole tips, passes through the flexspline and then through a "frozen bridge" of powder, on into the core. Most of it enters at the slot tips due to the lower reluctance path offered there. Even the finest size powder has a reluctance several orders of magnitude greater than solid magnetic iron, thus focussing the flux as stated above. The slots

of the core provide space for the powder to move into when the flux field is located elsewhere. This action has been studied and verified with high-speed movies. The major drawback to this scheme appears to be higher minimum reluctance, due to the necessity for clearance space in which the powder bridge forms and the low permeability of powder relative to solid material. Thus, for the same input current as the link variation or the stepping type, a much lower torque is expected; or conversely, to get high torques a greater current is required. However, because the powder type has no internal element of significant path length limiting the flux density, such as the link, it is expected that its torque capability would be greater than for the link type, but at a progressively lower efficiency. It is also likely that heat dissipation would prevent its torque approaching that of the stepping type except for possibly short-time transient peaks.

In order to obtain steady state holding torque from the rotating field types, there would be required a means of supplying direct current to one of the windings. This is considered feasible.

5.3 Analysis

The analysis is based upon the radial flux configuration; in particular, Model EHD-2.

In performing an electric and magnetic analysis on a polyphase AC machine, such as the device under consideration, it is best to initially view the machine as single phase. At an appropriate later point the phases are recombined to ascertain the device's performance.

Consider first the magnetic circuit. In schemetic form the magnetic circuit for one phase is shown in Figure 58. For a magnetic circuit in which the flux is changing, the relationship between flux and voltage is given by Faraday's Law. This states that the voltage induced in a magnetic circuit is, at all times, given by:

$$e = N \frac{d\Phi}{dt} \qquad (5\text{-}1)$$

In the case of all the Rotating Field actuators, the impressed voltage has a sinusoidal variation with time; i.e.,

$$e = e_m \cos \omega t \qquad (5\text{-}2)$$

Due to the winding configuration, this voltage, impressed on a single phase, will produce a flux which should approach a variation that is sinusoidal in space. That produced by the other phases will be thesame, but phased differently of course. However, the voltage actually involved in the calculation is not the line or terminal voltage, but rather the voltage which, when vectorily added to other voltages in the circuit, such as the resistance voltage drops, equals the terminal voltage. So, first, the value

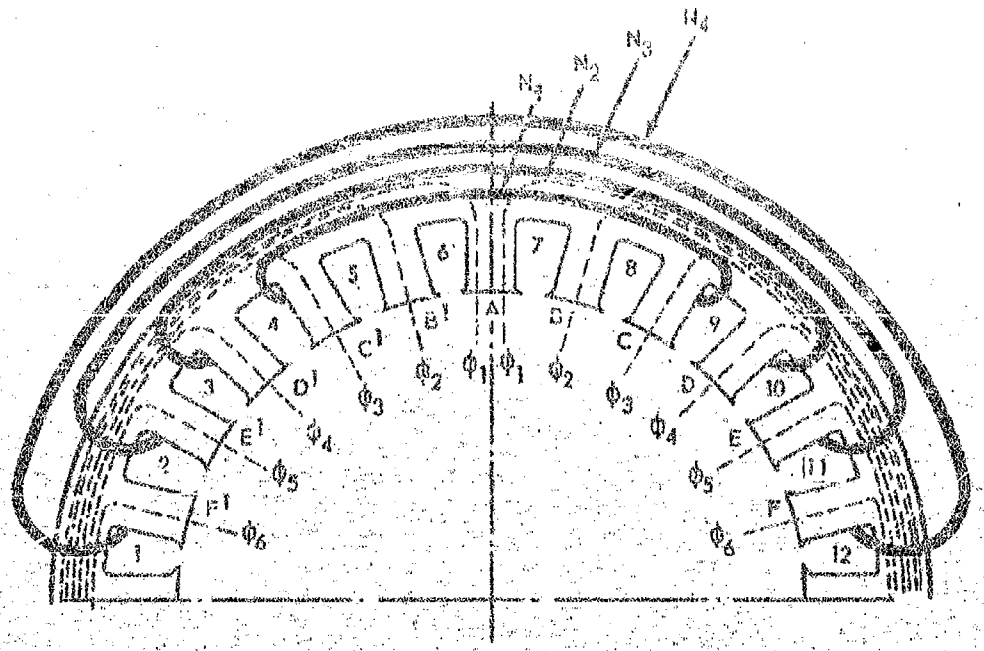

FIGURE 58 - FLUX LINKAGES OF MODEL EHD-1, 2, 4 ROTATING FIELD STATOR (24 POLE TEETH)

One side of one phase is shown. The coils on the other side are identically placed. All coils of a phase are wired in series. For the second phase of this three-phase device, the coils would be shifted by 120° (8 stator pole teeth). The third phase is shifted by another 120°.

N = Number of turns in coil designated
Φ = Lines of flux in stator pole tooth
1,2,3...Identification number of slot
A,B,B',...Identification number of stator pole tooth

of voltage to be used in Equation (5-1) must be found. An equivalent circuit is very helpful (Figure 59). This is the same as an induction motor circuit because, in essence, the device can be considered as an induction motor operating at full slip (1.0). Actually, the slip is equal to

$$s = 1 - \frac{\dot{\theta}_o}{R_g \dot{\theta}_o} \tag{5-3}$$

But since, with output taken from the flexspline, R_g is negative (there is a reversal in direction),

$$s = 1 + \frac{1}{R_g} \tag{5-4}$$

For R_g, typically, of 100 or more

$$s \approx 1.0 \tag{5-5}$$

For simplication in nothtion, define

$$e_3 = e_{x_e} \tag{5-6}$$

which is the voltage across the exciting inductive reactance. In order to find e_3 in terms of e_t, the terminal voltage which can be measured, an approximate solution is to assume that the ratio of resistance to reactance for the parallel combination of Z_2 and Z_e is the same as for Z_1.

Hence,

$$e_{z_e} = e_t - I_t Z_1 = e_t (R_1^2 + X_1^2)^{\frac{1}{2}} \tag{5-7}$$

Actually, this relation is considered good for the no-load case ($I_2=0$), but may be somewhat inaccurate when I_2 exists and is added (vectorily) to I_e with a metal flexspline. It is very difficult to make a no-load test, as a flexible rotor element is unavoidably deflected to produce Harmonic Drive action (toothed or frictional) thereby acting as a high-torque load.

Power factor is found from the basic measurements as

$$\text{Power Factor } (\cos \theta_e) = \frac{P_1}{E_t I_t} \tag{5-8}$$

Then e_3 is found from

$$e_3 = e_{z_e} \sin \theta_e \tag{5-9}$$

Now Faraday's Law can be applied. In terms of the equivalent circuit

$$e_3 = e_{3_m} \cos \omega t \tag{5-10}$$

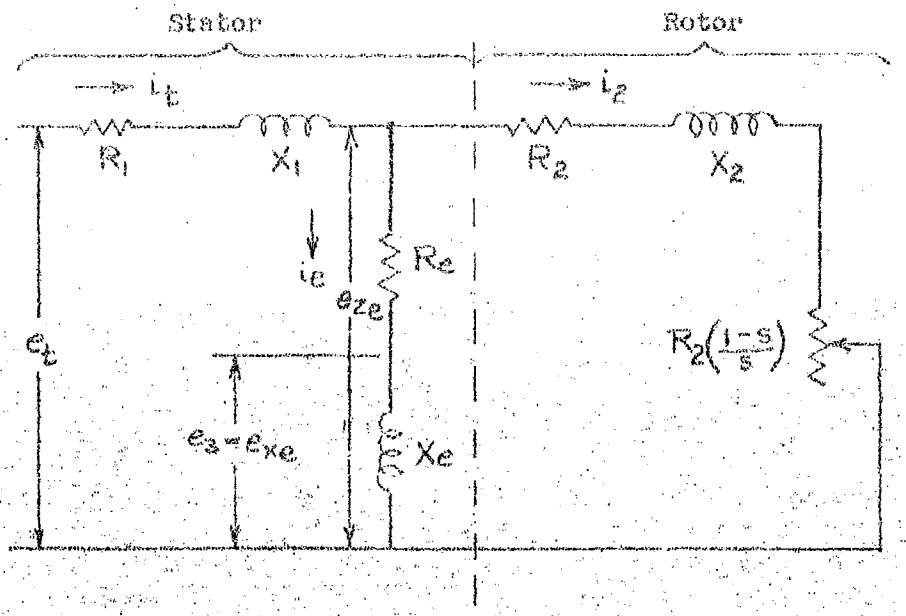

Subscript Notation	
1	stator
2	rotor
e	magnetizing
t	terminal

Vector Definitions

$$Z_1 = R_1 + jX_1$$

$$Z_2 = \frac{R_2}{s} + jX_2$$

$$Z_e = R_e + jX_e$$

FIGURE 59 EQUIVALENT ELECTRIC CIRCUIT FOR A ROTATING FIELD ACTUATOR

This is for one of the phases only, hence for a three phase device e_t is the line to neutral voltage.

Power absorbed by $R_2\left(\frac{1-s}{s}\right)$ represents the shaft power.

R_1 and R_2 account for the stator copper losses.

R_e accounts for the core loss (hysteresis plus eddy current).

X_1 and X_2 account for the leakage reactances.

X_e accounts for the exciting reactance.

Faraday's Law should be applied to each coil separately. For coil N_1

$$(e_{3_m})_{N_1} \cos\omega t = N_1 \frac{d}{dt}(2\phi_1 + 2\phi_2 + 2\phi_3) \tag{5-11}$$

Hence

$$\phi_1 + \phi_2 + \phi_3 = \frac{(e_{3_m})_{N_1}}{2N_1} \int \cos \omega t \, dt = \frac{(e_{3_m})_{N_1}}{2\omega N_1}(\sin \omega t + C_1) \tag{5-12}$$

Consider that

$$\left.\begin{aligned} &\phi_1 + \phi_2 + \phi_3 = 0 \quad \text{when } t = \frac{n\pi}{\omega} \quad n = 0, 1, 2 \ldots \\ &\therefore C_1 = 0 \quad \text{and} \quad \phi_1 + \phi_2 + \phi_3 = \frac{(e_{3_m})_{N_1}}{2\omega N_1} \sin \omega t \end{aligned}\right\} \tag{5-13}$$

The maximum value is the amplitude

$$(\phi_1 + \phi_2 + \phi_3)_m = \frac{(e_{3_m})_{N_1}}{2\omega N_1} \tag{5-14}$$

Likewise for coil N_2

$$(e_{3_m})_{N_2} \cos\omega t = N_2 \frac{d}{dt}(2\phi_1 + 2\phi_2 + 2\phi_3 + 2\phi_4) \tag{5-15}$$

$$(\phi_1 + \phi_2 + \phi_3 + \phi_4)_m = \frac{(e_{3_m})_{N_2}}{2\omega N_2} \tag{5-16}$$

and also for the other two coils

$$(\phi_1 + \phi_2 + \phi_3 + \phi_4 + \phi_5)_m = \frac{(e_{3_m})_{N_3}}{2\omega N_3} \tag{5-17}$$

$$(\phi_1 + \phi_2 + \phi_3 + \phi_4 + \phi_5 + \phi_6)_m = \frac{(e_{3_m})_{N_4}}{2\omega N_4} \tag{5-18}$$

Summing for all coils, realizing that for coils in series

$$e_{3_m} = (e_{3_m})_{N_1} + (e_{3_m})_{N_2} + (e_{3_m})_{N_3} + (e_{3_m})_{N_4} \tag{5-19}$$

and that

$$(\phi_1 + \phi_2)_m = \phi_{1_m} + \phi_{2_m}, \text{ etc.} \tag{5-20}$$

since all fluxes are functions of the same frequency and phase, there is obtained

$$\begin{aligned} e_{3_m} = 2\omega\big[&N_1(\phi_{1_m} + \phi_{2_m} + \phi_{3_m}) + N_2(\phi_{1_m} + \phi_{2_m} + \phi_{3_m} + \phi_{4_m}) \\ &+ N_3(\phi_{1_m} + \phi_{2_m} + \phi_{3_m} + \phi_{4_m} + \phi_{5_m}) + N_4(\phi_{1_m} + \phi_{2_m} + \phi_{3_m} + \phi_{4_m} + \phi_{5_m} + \phi_{6_m})\big] \end{aligned} \tag{5-21}$$

In the stator design the coils are wound so that the values approach a sinusoidal distribution in space. With this particular motor there is a rather long flat-top shape since the shortest-span coil spans past 4 spaces, per Figure 58. But it still matches the sine wave fairly well, as shown in Figure 60.

How well the centers of the other flux values fall on the curve remains to be seen. (In a design problem or synthesis, the number of turns would be unknown, and expressions can be written for the Φ's in terms of the maximum value, from which the turns are eventually found). So, in this case

$$\Phi_{3_m} = \Phi_{2_m} = 2\,\Phi_{1_m} = \Phi_m \qquad (5\text{-}22)$$

There are, so far, four unknown values of flux and two independent equations. Consider the MMF analysis for the other equations. Since, in general,

$$\mathcal{F}\text{ - MMF} = Ni_e = \mathcal{R}\Phi \qquad (5\text{-}23)$$

for each of the air gaps, considering the reluctance of the iron paths negligible and $\mathcal{R}$ the reluctance of one air gap in a half phase, there is written

Gap No.	Peak MMF Required
A	$2\mathcal{R}\Phi_m$
B	$\mathcal{R}\Phi_m$
B'	$\mathcal{R}\Phi_m$
etc.	

Since the coils are all in series, the same current flows through each, so Kirchhoff's circuit laws can conveniently be applied to an equivalent circuit (Figure 61) in which each resistor is the reluctance of one gap.

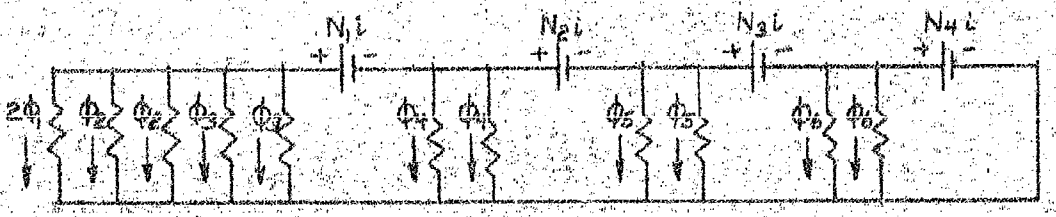

$$\mathcal{R}\Phi_{6m} - N_4 i_{e_m} = 0 \qquad (5\text{-}24)$$

$$\mathcal{R}\Phi_{5m} - N_3 i_{e_m} = \mathcal{R}\Phi_{6m} \qquad (5\text{-}25)$$

$$\mathcal{R}\Phi_{4m} - N_2 i_{e_m} = \mathcal{R}\Phi_{5m} \qquad (5\text{-}26)$$

$$\mathcal{R}\Phi_{3m} - N_1 i_{e_m} = \mathcal{R}\Phi_{4m} \qquad (5\text{-}27)$$

FIGURE 61 . MAGNETIC EQUIVALENT CIRCUIT

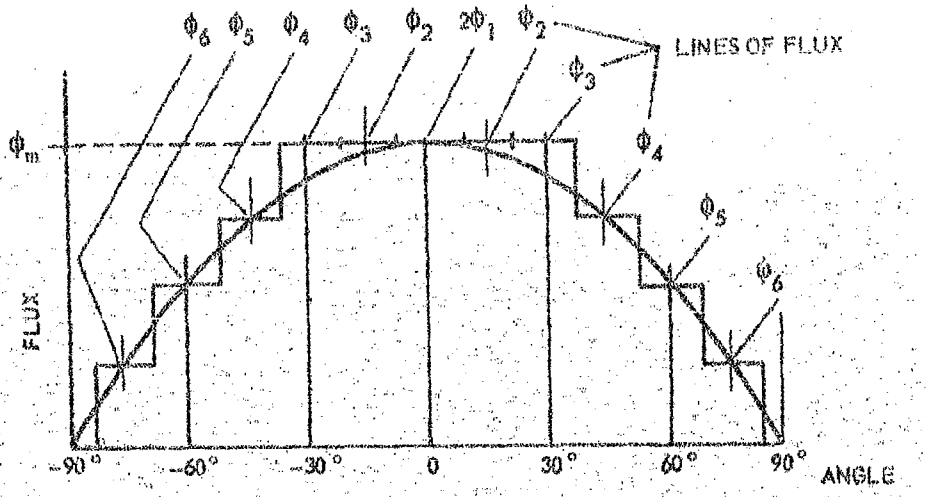

FIGURE 60 MATCHING OF FLUX AT STATOR POLE TEETH AIR GAPS TO A SINUSOIDAL DISTRIBUTION, FOR MODEL EHD-1, -2, -4 ROTATING FIELD STATOR (24 POLE TEETH).

This results in four equations and two more unknowns, $\mathcal{R}$ and i_{e_m}, so the equation can be solved for the three variables e_{3_m}, i_{e_m}, and $\mathcal{R}$ in terms of each other, to give:

$$e_{3_m} = \frac{2\omega\, i_{e_m}}{\mathcal{R}} \left[\frac{5}{2}(\Sigma N)^2 + 3N_4^2 + 2N_3^2 + N_2^2 + 4N_4N_3 + 2N_4N_2 + 2N_3N_2\right] \quad (5\text{-}28)$$

From the equation and a calculation of $\mathcal{R}$, the values of flux can be found using for $\mathcal{R}$ the expression

$$\mathcal{R} = \frac{1}{A_Q}\left[\frac{X_1}{\mu_1} + \frac{X_2}{\mu_2}\right] \quad (5\text{-}29)$$

From Φ is found the magnetic force F_Q at each stator pole tip from the magnetic force formula. This is used with the torque and supporting force formulas of Section 3.

$$F_T = 2\sum_{180^\circ} F_p \sin 2\theta_p \quad (5\text{-}30)$$

$$T_1 = F_T D_p \eta_T \quad (5\text{-}31)$$

$$F_R = \sum_{180^\circ} F_p \cos 2\theta_p \quad (5\text{-}32)$$

As discussed in Section 3, the maximum torque load that can be applied without causing the teeth to disengage is roughly that for which

$$\theta_p = \delta_m = \frac{1}{2}\arctan\frac{1}{2\tan\phi_a} \quad (5\text{-}33)$$

for the pole tip where β has its maximum value β_m. Total torque for the device is derived as follows: For a three-phase device, instantaneously when the torque in one phase is maximum, the flux in the other two phases is each at 1/2 its maximum value. These combine vectorily to produce a net flux in phase with the first phase. Since all phases are 120° apart, the added flux is

$$2\left(\frac{\Phi_m}{2}\cos 60^\circ\right) = \frac{\Phi_m}{2} \quad (5\text{-}34)$$

Hence, the total flux is $1\frac{1}{2}$ times that due to one phase, and the force is greater by the ratio $(1\frac{1}{2})^2 = 2.25$.

Hence, $T_2 = 2.25\, T_1$ (5-35)

There is also a counter torque T_3 produced by currents induced in the flexspline, if it is metal, in conjunction with the flux field (induction motor action). If the values of the rotor resistance and reactance were obtained in conjunction with these values for the stator discussed earlier, then the counter torque could be calculated using the usual induction motor equations.

The net torque output would be the gross Harmonic Drive torque minus the induction motor torque.

$$T_4 = T_2 - T_3 \tag{5-36}$$

Resistance of the windings is calculated from knowledge of the wire size and mean length of turn. Hence, I^2R loss can be obtained. It should be realized that

$$I_1 = I_e + I_2 \quad \text{(vector addition)} \tag{5-37}$$

as discussed before, so several I^2R losses are involved. The core loss, P_c can be found as

$$P_c = I_e^2 R_e \tag{5-38}$$

Thus, total losses could be found.

Also, inertia could be found by using the expressions of Section 3 considering the effective mass of powder that is moved equal to the mass of the rectangular solid defined by ΔQ times x_2. The output speed is obviously the input frequency divided by ratio.

$$\dot{\theta}_M = \frac{\omega}{R_g} = \frac{2\pi f}{R_g} \tag{5-39}$$

so that power output is

$$P_o = T_4 \dot{\theta}_M \tag{5-40}$$

Knowing the weight the usual significant performance characteristics can be found. Appendix XI derives the specific values for the various models.

SECTION 6
COMPARISON OF EHD WITH OTHER DEVICES

6.1 Comparison of Ratings

The results of the evaluations of Sections 4 and 5 are given in Table XVIII for all EHDtypes. The data is a combination of theoretical and measured values for reasons discussed in Sections 1, 4 and 5. The SF type EHD-3 is representative of the highest power rates that can be achieved, but the RF types, important for their simplicity, also possess very good power rates. In order to compare this data with the state-of-the-art for conventional electric high response actuators, Table XIX was prepared. This compares the performance characteristics of greatest importance.

The Minertia DC motor is a very new type for which the weight could not be ascertained. It is seen that its high theoretical power rate is obtained at an extremely high pulse current level. This severely limits the pulse length and duty cycle, and the weight of the power supply required would be very high. It is listed as an example of the extremes to which conventional types of actuators, in which the gap remains constant, are expected to be carried through research.

The power rate of the Printed Circuit motor is in the same range as the EHD-3 model (the maximum theoretical performance SF type described in Section 4.3.1 would be greater), but as with the Minertia type, its power rate is achieved at a pulse current that represents a much greater I^2R loss and power supply requirement. Stepping or synchronous types are not given because none exist with high power, low inertia characteristics comparable to the others of Table XIX.

The actuators should also be compared on the basis of allowable duty cycle or pulse duration, and temperature rise as it affects life and reliability. These are important factors in most applications. In general, the higher the power rate of the conventional actuator, the shorter its duty cycle and pulse duration. For the EHD types, with a reasonable amount of cooling, duty cycle would be essentially continuous.

T_M for the conventional types is taken from the manufacturer's data sheets where given. In two cases this is not given, so T_M is calculated as defined in Section 2 at the following speeds:

-Inland Torque motor-30 rpm (1/2 maximum rating).

-Diehl motor-5000 rpm corresponding to peak P_M.

PHYSICAL CHARACTERISTICS	STEPPING FIELD EHD-3	ROTATING FIELD EHD-2 (as built)	ROTATING FIELD EHD-3 (Mod)	ROTATING FIELD EHD-4 (Mod)
δ_m (deg)	27	20	20	20
D	96	96	96	96
D_p	3.25	2.6	2.6	2.6
N_g	156	128	128	128
Flexspline Mat'l.	Metal	Metal	Plastic	Plastic
δ_w (deg)	20	30	30	30
η_T	0.80	0.60	0.70	0.70
η_s	1.0	1.0	1.0	1.0
β_{ia} (w/m2	2.2	0.45	0.8	0.72
N_Q	32	24	24	24
b (inch)	0.5	1.625	1.625	1.625
w (inch)	0.4	0.250	0.250	0.250
s_g (stacking factor)	0.8	0.9	0.9	0.9
V (cubic inches)	240	190	95	95
Wt (lbs.)	22	16	8	8
PERFORMANCE CHARACTERISTICS				
T_m (lb-in)	1060	2.2	72	58
T_M (lb-in)	530	2.2	72	58
) (n-m)	60	0.25	8.2	6.6
J_m (kg-m^2	1.2×10^{-2}	9.0×10^{-4}	9.0×10^{-4}	1.9×10^{-3}
ω_m (rpm)	18	28	28	28
e (voltage)	*	120 rms, phase	290 rms, phase	———
I (current amps)	60 Total	1.9 rms, phase	0.46 rms, phase	0.46 rms, phase
I^2R (watts)	180	204	5	5
Eddy current loss (watts)	0	83	21	21
total electri- P_T cal loss (watts)	180	287	26	26
P_m (kw/sec.)	310	0.1	75	24
P_L (watts)	115	1	24	19
η_M (%)	35	0.2	40	36

* High peak during switching, up to 50 to 100v, and low DC level (3 to 5v) between steps. See Section 4.

TABLE XVIII-EHD CHARACTERISTICS

	Electromagnetic Harmonic Drive							
		Rotating Field Type						
	Stepping Field Type (1)	Powder and Core Armature (2)	Link Armature (3)	G.E. D.C. Servo Motor (4)	Inland D.C. Torque Motor (5)	Diehl A.C. Servo Motor (6)	Printed Circuit Torque Motor (7)	Minertia D.C. Motor (8)
Pitch Diameter (in.)	3.25	2.6	2.6	---	---	---	---	---
Power Rate (kw/sec)	310	75	24	86	35.3	14	390	7000
$\frac{\text{Power Rate (kw/lb.sec)}}{\text{Weight}}$	14	4.4	1.5	5.7	1.1	0.33	6.8	Weight Not Known
$\frac{\text{Power Rate (sec}^{-1})}{I^2R \text{ Loss}}$	1700	2900	920	45	38.4	2.6	39	120
$\frac{\text{Power Rate (sec}^{-1})}{\text{Cont. Power Output}}$	2700	3100	1300	340	100	18	260	7000
τ_M Motor Time Constant (sec.)	.00037	.00032	.00077	.009	.003	0.21	.020	.0043
Weight (lbs.)	22	16	16	15	32	42	57	Not Known
I^2R Loss (watts)	180	26	26	1900	920	5400	10,000	60,000
Cont. Power Output (watts)	115	24	19	250	350	750	1500	1000

(1) EHD-3
(2) EHD-2 with plastic flexspline
(3) EHD-4 with plastic flexspline
(4) Type 5BC28HC1, 250 watt rated output, calculated at stall (19 times rated) torque.
(5) Type T-8001-A, 350 watt rated output at 100 rpm, calculated at saturation.
(6) Type ZP-162-2209-1, 400 cps, 750 watt rated output, calculated at stall (2.1 times rated) torque at 150% rated control voltage.
(7) Type 1028, 1500 watt rated output, calculated at 5 times rated current.
(8) New Development, Control Engineering, November 1962, page 57, 1000 watt rated output calculated at 10 times rated torque.

TABLE XIX - COMPARISON OF EHD AND CONVENTIONAL LOW INERTIA ELECTRIC ACTUATORS

τ_M for the EHD types is calculated at the rated speeds given in Table XVIII.

It should be realized that for a specific peak load speed, τ_M may be different, depending on the load speed and gearing if any, but P_M would also vary in the same manner, so the usefulness of the actuator for fast response remains relatively the same, provided that the gearing does not introduce serious time lags or non-linearities.

The comparison between an EHD actuator and a conventional electrical servo device can be usefully presented by a graph such as Figure 62, which compares an Inland Torque motor operated with 5:1 gearing to match its peak speed to a load speed of 12 rpm, a no-slip value for the present EHD-3 model. The data for Figure 62 are given in Table XX.

The Inland motor is selected for comparison because it provides the highest power rate for conventional devices characterized by a high duty cycle and none or little required output gearing for matching to the load.

Following the approach presented in Section 2, the ratios of P_M/P_L for each actuator are plotted as a function of load time constant τ_L. It is seen that for load requirements characterized by τ_L less than .00048 sec. (designated the "extreme performance servo region") there is a 25 to 1 advantage for EHD-3 compared to the conventional actuator. For example, at τ_L = .0004 sec. which represents $\ddot{\theta}_L$ = 3100 rad/sec^2, the Inland motor requires a P_M of 58 P_L, whereas the EHD-3 requires a P_M of 2.4 times P_L, (58/2.4 = 25). Even though (from Table XX) the conventional electrical actuator has a power output 2.8 times that of the EHD-3 at this particular load speed, it is quite evident that the EHD-3 can drive a larger load.

Figure 62 also shows that for τ_L between .00048 sec. and .012 sec. (the so-called "high performance" servo region) the P_M/P_L advantage for the EHD-3 falls gradually from 25:1 to approximately 2:1. Thus it is seen that EHD offers very significant advantages wherever large load accelerations relative to load speeds are required. It is most significant to compare the two devices on the basis of weight of the size actuator required to drive a particular load. Actuator peak power output P_M is approximately proportional to weight for a certain type of actuator, within reasonable speeds. Hence, the ratio of P_M/Wt is divided into the P_M/P_L ratio to give a Wt/P_L ratio, which is also plotted in Figure 62. For this particular case the ratios of Wt/P_L (Weight per load power of the conventional type to the EHD-3) are unity at a breakeven point of τ_L = .012 sec. and indicates that on a weight basis the EHD-3 requires less weight for all applications except the "low performance" servo region. (It is a coincidence that this is also the τ_L for which τ_M/τ_L = 1/2 for the Inland Motor). The weight advantage (ratio of Wt/P_L for the two actuators) is constant at 12.7 in the extreme performance region and falls gradually to unity at the breakeven

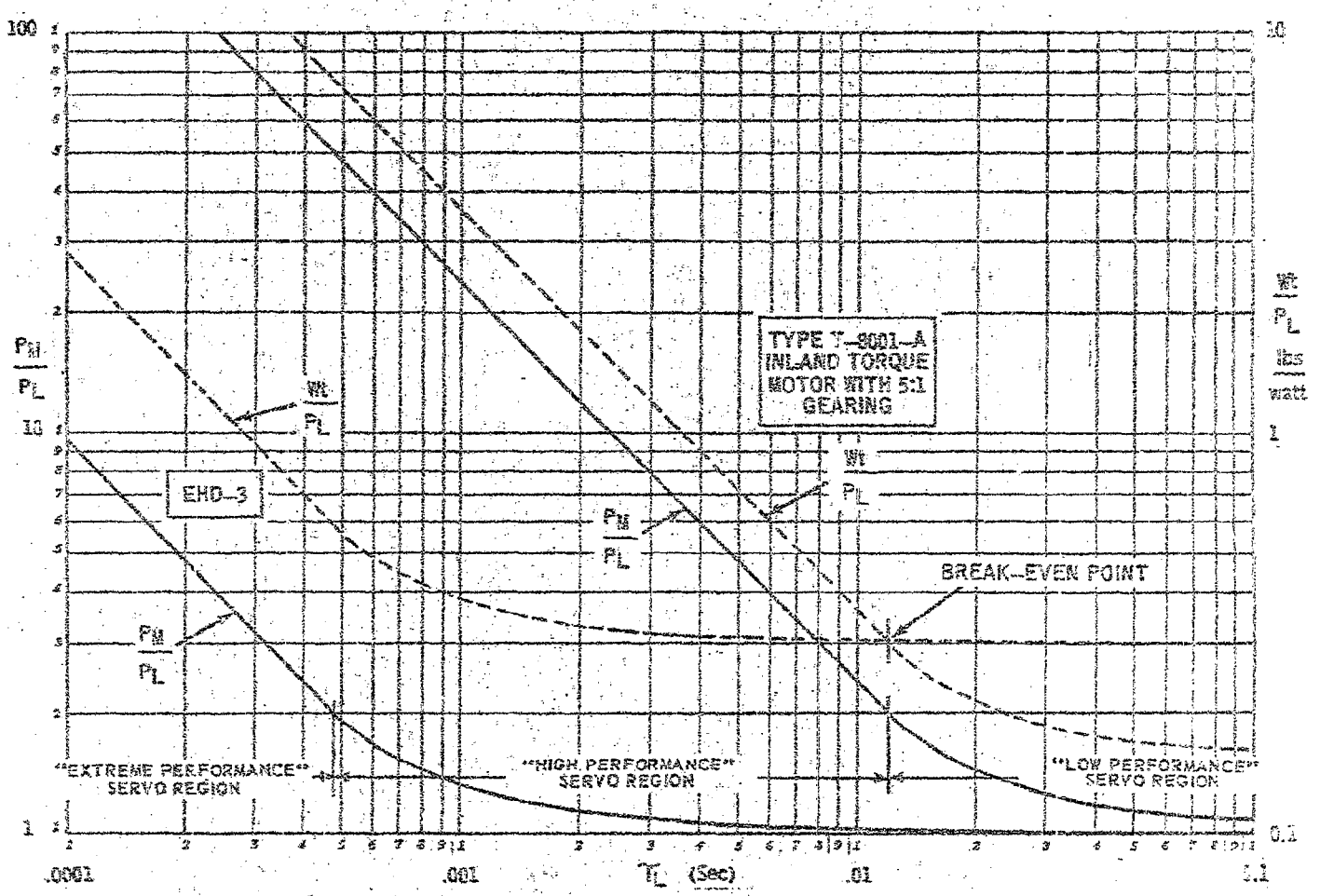

FIGURE 62 - EHD-3 AND CONVENTIONAL ACTUATOR COMPARED AS A FUNCTION OF τ_L AT $\dot{\theta}_L$ = 12 RPM.

Load Peak Speed, $\dot{\theta}_L$ = 12 rpm = 1.26 rad/sec.

Load Time Constant, τ_L, varied.

EHD-3	T-8001-A*
$\tau_M = \frac{1.26(.0112)}{60} = .00024$ sec.	$\dot{\theta}_M$ = 60 rpm = 6.3 rad/sec. 5:1 gearing used. gearing inertia neglected, also frictional loss. $\tau_M = 6.3\ \frac{(.024)}{25} = .006$ sec.
P_M = 60 (1.26) = 76 watts	$P_M = 25 \times 12 \times 0.113 \times 6.3 =$ 214 watts
W_t = 22 lbs.	W_t = 32 lbs.
$P_M/W_t = \frac{76}{22} = 3.4$	$P_M/W_t = \frac{214}{32} = 6.7$

*Inland Torque Motor

TABLE XX - DATA FOR FIGURE 62

point. For an intermediate τ_L of, for example, .003 sec., peak acceleration is

$$\ddot{\theta}_L = \frac{\dot{\theta}_L}{\tau_L} = \frac{12\ (2\pi/60)}{.003} = 420 \text{ rad/sec}^2 \qquad (6\text{-}1)$$

and the comparison is as shown in Table XXI.

CHARACTERISTICS	EHD-3	T-8001-A Inland Motor	Ratio of T-8001-A to EHD-3
P_M/P_L	1.1	8	7.3
Wt/P_L(lbs./watt)	0.32	1.2	3.8
Actuator Weight (lbs.) for P_L = 100 Watts	32	120	3.8

TABLE XXI - EHD-3 COMPARED TO A CONVENTIONAL ACTUATOR AT τ_L = .003 SEC.

Although the effect of the gearing used with the Inland motor has been neglected, there will be the weights of the controls for each to be considered, so the above is useful primarily as a guide.

The EHD models are synchronous devices, in which output speed is proportional to input frequency. During transient starting periods, the actual output lags the commanded output by a finite amount before synchronism is reached. The maximum lag permissible without losing synchronism determines the maximum load inertia and torque than can be accelerated for a particular commanded speed.

The problem of achieving synchronous operation is not peculiar to EHD; it is characteristic of synchronous devices in general. Conventional synchronous motors operate as induction motors during startup. Conventional steppers can be operated with special feedback controls that produce a self-stepping action in which succeeding steps start only after the output has responded sufficiently to reduce the lag to a specified value. The action is analogous to a DC motor. Inertia of EHD is much less than conventional devices, so that for most applications no problem with achieving synchronism occurs. However, for an extreme application, to exploit the maximum response capability of the EHD, special electronic techniques can be used. The stepping field type is most suitable in this case, wherein self-stepping can be utilized. By this means the actuator would continue to accelerate the load up to commanded speed, producing a positive output torque regardless of the extremity of the input command, and succeeding steps would be initiated in accordance with the response.

For the high performance servo applications, the weight advantage offered by low inertia actuators is so large that actuators of this type, such as hydraulic and clutching servo devices, are invariably used. This is the area where EHD would be of greatest value, since it would give dynamic performance similar to hydraulic and clutching servo actuators but with the advantages inherent with variable speed electrical devices combined with Harmonic Drive precision speed reduction.

With regard to hydraulic actuators, they involve problems with reliability, sensitivity to contamination, severe temperature limitations of hydraulic fluids, and the weight and power losses of their power supplies. The reliability of clutching types of electrical servo actuators has been a concern in many cases. Also the magnetic particles often limit the angle at which they may be fully applied. The cases when it is justified to design an actuator specifically for the application will generally be for the high or extreme performance servo applications, where low weight is very important. The major objective might be to provide a power rate that just exceeds the minimum requirement by a suitable safety margin, and if T_M/T_L drops near 1/2 or below, then increasing importance must be given to maximizing power output. It should be pointed out that maximizing torque is beneficial to both power rate and power output.

It is re-emphasized that power rate is the significant parameter with regard to advancing state-of-the-art of servo actuators. With regard to power rate to weight, EHD is about 2 to 10 times improved over conventional forms of electrical actuators.

6.2 Comparison of Model EHD-3 and Typical Conventional Electrical Actuators under the Same Conditions as the EHD-3 Tests.

In Table XXII is presented a comparison of the measured performance of model EHD-3 with an Inland DC torque motor that would be required to do the same job with the same loading factor.

As shown by Table XXII the Inland torque motor has about twice the I^2R loss and 1 1/2 times the weight of the EHD-3. Another factor is that the EHD-3 gives stepping action which is capable of greater resolution and accuracy than the DC motor.

Also shown in Table XXII are the characteristics of one of the higher power, minimum inertia conventional stepping motors, (the largest of this manufacturer's line) which is shown to be inadequate to drive the load.

6.3 Applicability to Flight Control Actuation Systems

Surveys were made of typical flight control actuation systems, including data obtained from representatives of the Flight Control Laboratory, ASD. As a result it was seen that a typical load might be similar to the load used for the EHD-3 tests except with a higher load acceleration which is more typical of a high performance application as defined in Section 2.2. However, in order to just meet

the load capability of the conventional actuator chosen (Inland Torque motor type T-10004-A) an inertia of 70% of the test inertia is used. The EHD-3 is moderately underloaded.

LOAD CHARACTERISTICS

J_L = 0.1 kg-m^2 = 1.0 lb.in.sec.^{2}

T_L = 0

$\dot{\theta}_L$ = 1.0 rad/sec. = 9.6 rpm

$\ddot{\theta}_L$ = $2\pi f \dot{\theta}_L = 2\pi(30)1 = 190$ rad/sec.^{2} (based on f = 30 cps)

τ_L = $\dot{\theta}_L/\ddot{\theta}_L$ = .0053 sec.

P_L = $J_L\ddot{\theta}_L\dot{\theta}_L$ = 19 watts

$\dot{P}_{M_{min}}$ = (minimum power rate required) = $4J_L\ddot{\theta}_L^2$ = 14.5 kw/sec.

ACTUATOR CHARACTERISTICS

	EHD-3	Inland Torque Motor T-8001-A*	Slo-Syn Stepping Motor X250-P1**
τ_M(sec)	.00037	.003	.006
τ_M/τ_L	.07	0.57	0.75
P_M/P_L	1.08	2.25	3
P_M required(watts)	20	43	37.5
P_M available(watts)	62	120	5
$\frac{P_M \text{ required}}{P_M \text{ available}}$	0.32	0.36	7.5
I^2R Loss(watts)	80	160	---
Weight (lbs.)	22	32	7.8

*Includes gearing of $\frac{30}{9.6}$ = 3.1

**Includes a 4 1/3:1 planetary gearhead. I^2R loss not calculated as actuator is inadequate powerwise.

TABLE XXII - COMPARISON OF MODEL EHD-3 AND TWO CONVENTIONAL LOW INERTIA ELECTRIC ACTUATORS UNDER THE SAME TEST CONDITIONS.

Table XXIII presents a comparison of the two actuators. The assumption is made here that the gearing required by the Inland Actuator (a ratio of 3.1 to 1) has a negligible effect upon total actuator inertia and backlash-derived non-linearities. This may not be true, but since the EHD has a form of gearing, this provides a conservative comparison. The large advantage in regard to weight and I^2R loss for the EHD are shown by the table.

LOAD CHARACTERISTICS

J_L = 0.07 kg-m^2 = 0.62 lb.in.sec.^{2}

T_L = 12 nm = 100 lb.in.

$\dot{\theta}_L$ = 1.0 rad/sec. = 9.6 rpm

Closed loop response ± 1 db at 20 cps

τ_L = .0024 sec.

$\ddot{\theta}_L$ = 420 rad/sec.^{2}

P_L = 41 watts

$\dot{P}_{M\ min}$ = (minimum power rate required) = 69 kw/sec.

ACTUATOR CHARACTERISTICS

	EHD-3	Inland Torque Motor T-10004-A*
τ_M (sec.)	.00037	.006
τ_M/τ_L	0.154	2.5
P_M/P_L	1.18	10
P_M required (watts)	48	410
P_M available (watts)	62	425
$\frac{P_M \text{ required}}{P_M \text{ available}}$	0.77	0.96
I^2R	80	1050
Weight (lbs.)	22	110

*Based on neglecting the inertia and backlash effect of supplementary gearing of 30/9.6 = 3.1 for a speed of 30 rpm.

TABLE XXIII - COMPARISON OF MODEL EHD-3 AND INLAND TORQUE MOTOR FOR A TYPICAL AERONAUTICAL SYSTEM APPLICATION

EHD was also compared to Diehl AC servo motors, which would require high-ratio gearing, for three applications, representative of one low performance servo (Antenna-Drive) where EHD offers no advance and two high performance types where it does (computer memory drum drive and a missile flap drive). An analysis was made explaining why EHD has a power rate several orders of magnitude greater, due to the fundamental difference between radial and lateral armature motion in the air gap. (See Appendix I)

SECTION 7

OTHER DESIGN AND PERFORMANCE PARAMETERS

7.1 General

This section covers various supplementary considerations that are more or less common to all EHD types but not fundamental enough to be included in Section 3.

7.2 Ratio and Gap

Reduction ratio R_g is related to the total radial deflection of a point "d"

$$R_g = \frac{D_p}{d} \qquad (7\text{-}1)$$

But "d" is dependent upon the diametral tooth pitch

$$d = \frac{2}{P_D} \qquad (7\text{-}2)$$

Thus

$$R_g = \frac{(P_D)R_g}{2} \qquad (7\text{-}3)$$

The air gap of the magnet is proportional to "d".

It is desirable to have a small "d" because this:

(1) Reduces the reluctance and hence the MMF
(2) Reduces the deflection force F_D

However, if the "d" is too small, tolerances and distortions from the ideal shape become more significant and poor tooth action may result. Also, higher ratio results in lower output speed for a particular output speed.

Harmonic Drive has been successfully made at 180 pitch and higher, but 100 or under is more commonly used. After consideration of the various factors, the values selected for the EHD models were as shown in Table XXIV.

	EHD-1, 2, 4	EHD-3
P_D	96	96
d (in.)	.0208	.0208
D_p (in.)	2.66	3 1/4
R_g	128	156

TABLE XXIV - HARMONIC DRIVE DATA FOR MODELS

7.3 Magnetic Force and Material Study and Sample Pole Tests

Basic magnetic circuit properties show that magnetically produced force is a function of flux density squared. With this fact in mind, early investigation was undertaken to find material that operated at high flux densities, but required low magnetomotive force. Typical β^2 versus H curves for a variety of magnetic materials were studied. One of the more modern materials developed by the Bell Laboratories called Vanadium Permendur (Reference 3) appeared to have the best overall characteristics. This is shown in Figure 63, which gives typical curves for the magnetic material most commonly used in similar applications. It was decided that some testing of the material should be undertaken to determine if it was adaptable to the proposed use in the actuator. Being a relatively new material, little literature was available relative to its properties in actual applications. The primary source, Arnold Engineering, produces small quantities but has limited application data, such as was required for this program (Reference 1). Certainly, no information about its idiosyncrasies was readily available such as is the case with the grain oriented silicon sheet steels, which are so-called magnetic circuits workhorse.

In an attempt to use the material properly, it was decided to build up a sample pole piece with standard configurations so that useful measurements could be made. Any discrepancies between theoretical and actual figures could then be studied and a determination made as to the significance of the discrepancy. The pole shape chosen was an "E" stack with a central coil of 100 turns (see Figure 64). The "I" Keeper was mounted on a moving rod. The rod was then attached to a spring scale so that force measurements could be made. Measurements of current versus force-to-close, for various airgap lengths, were made. Figure 65 shows the results, together with the theoretical force to-open curve.

Initial tests did not agree with the theoretical results by a wide margin as can be seen in Figure 65, and a conference was held between the Arnold Engineering staff at Morengo, Illinois and a representative of United Shoe Machinery. The results of this conference was that Arnold suspected degradation from the handling technique used on the annealed pieces by the transformer company which had done the sample pole assembly work. Arnold had previously determined that annealed Vanadium Permendur laminations must be carefully bonded at sub-freezing temperatures in order to maintain their superior magnetic properties. The Arnold Engineers further indicated that a flux density of at least 2.2 webers/sq. meter would be readily obtainable with proper treatment and care of the finished parts. United accepted this explanation and decided to have Arnold do all future treating and assembly of magnetic material. Thus, the sample pole tests were most useful in pointing out a basic consideration that otherwise might not have been discovered in time to factor into the laboratory model.

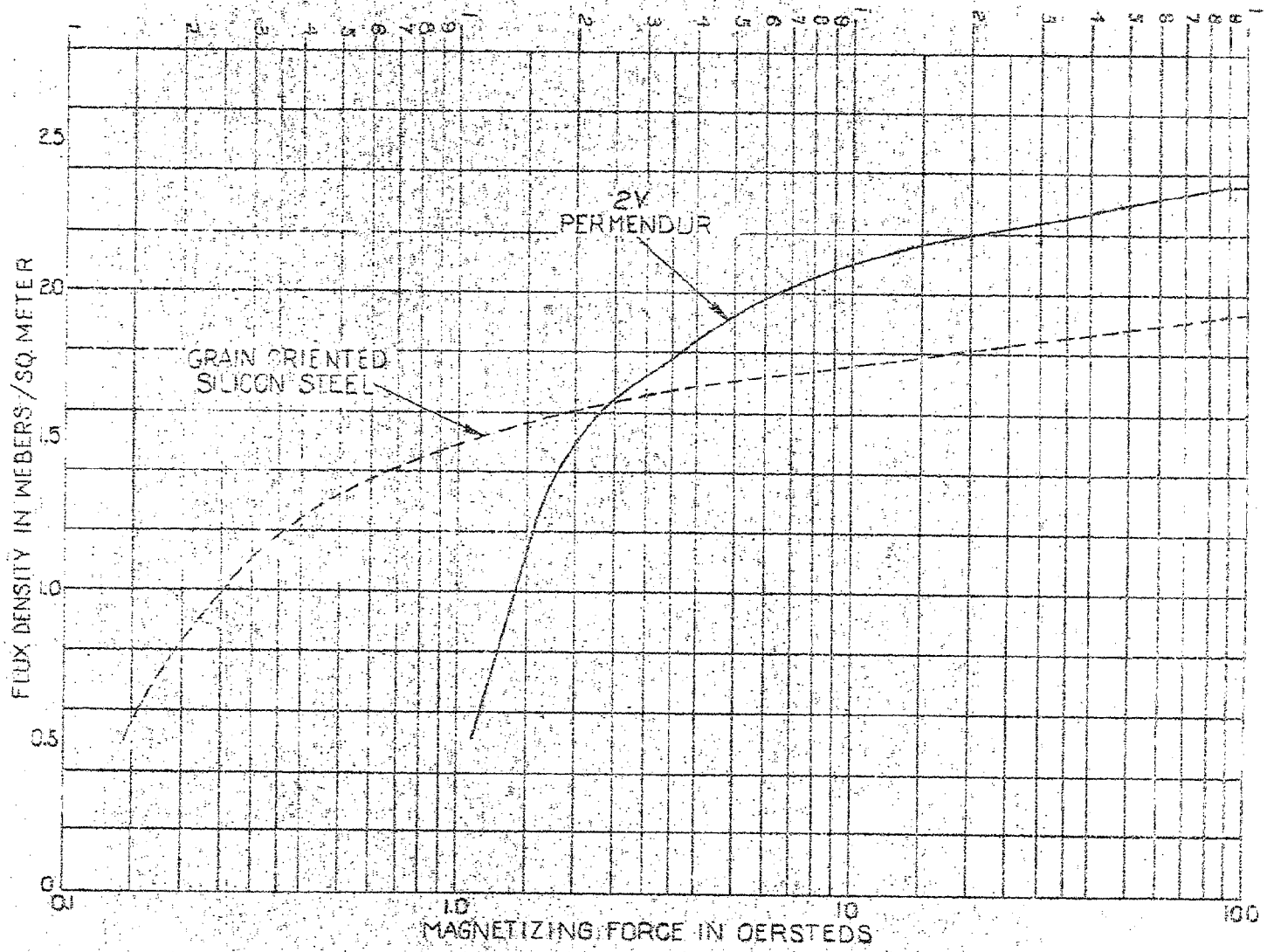

FIGURE 63. MAGNETIC MATERIAL PROPERTIES

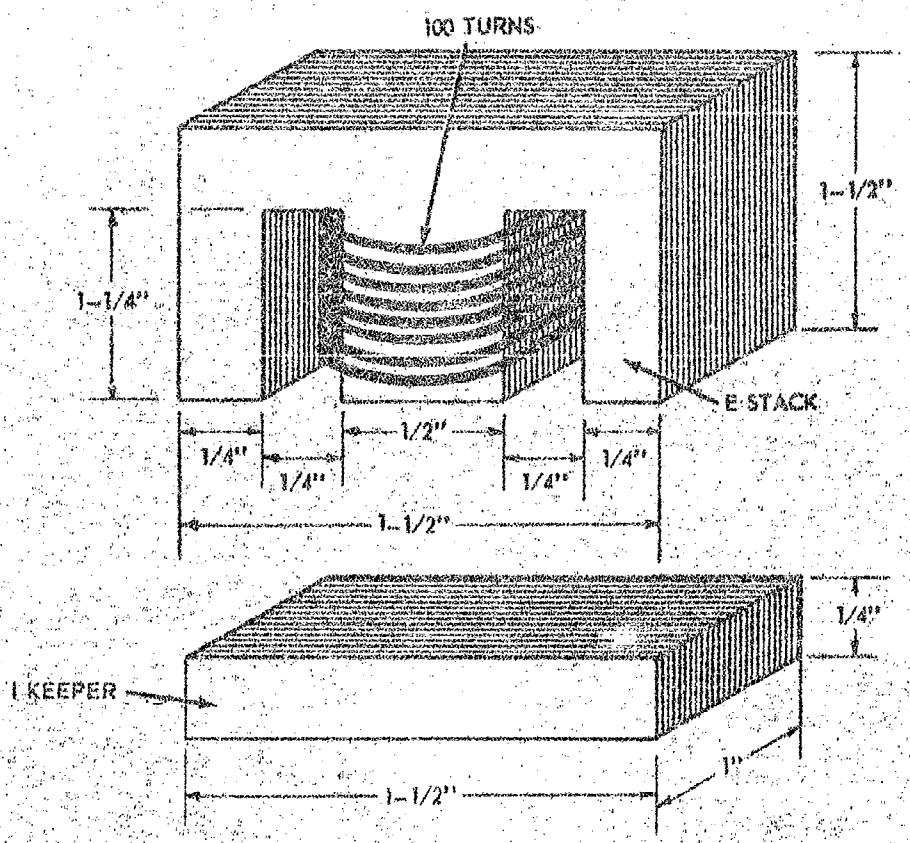

FIGURE 64 SAMPLE POLE CONFIGURATION
Material: Vanadium Permendur

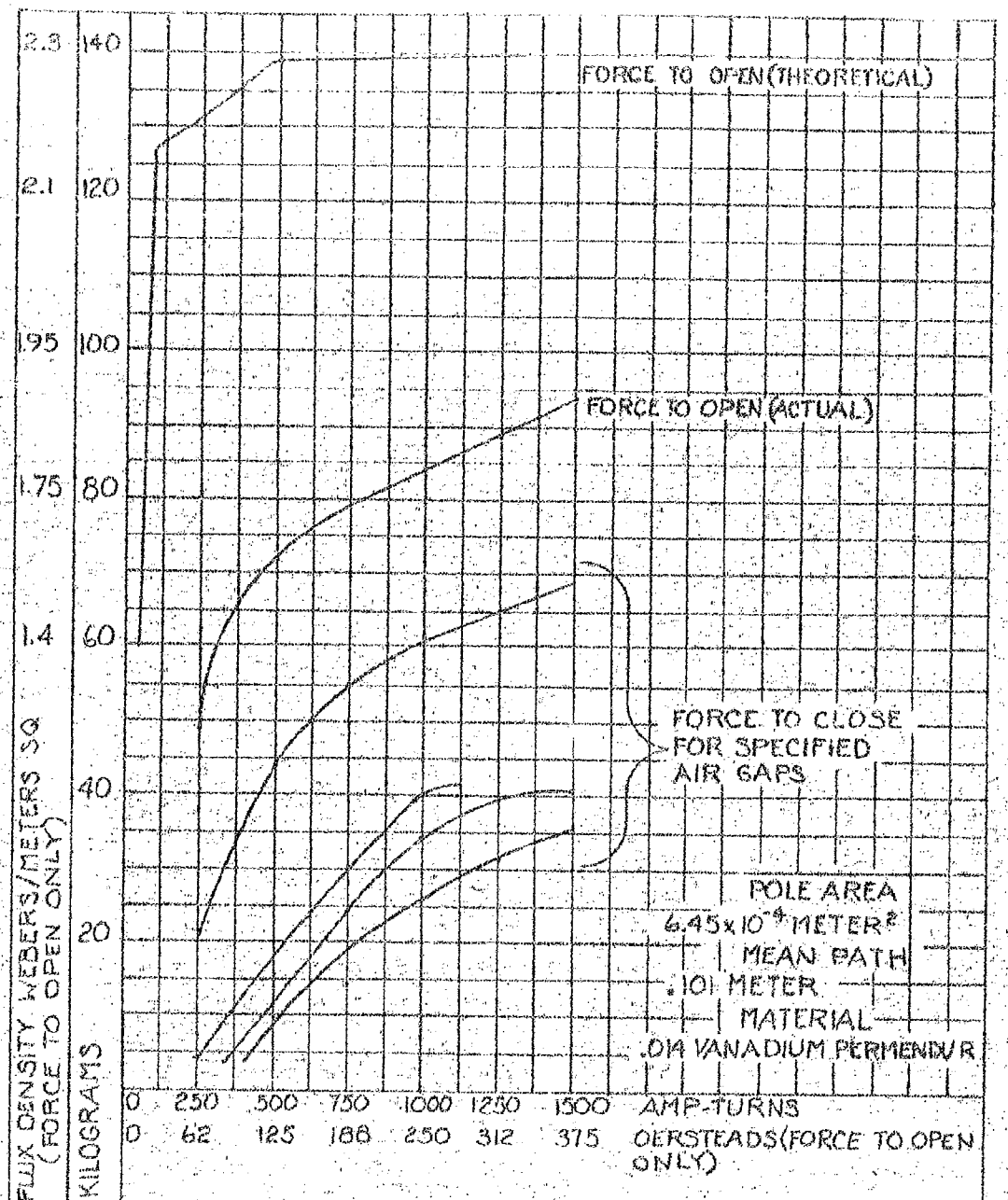

FIGURE 65 SAMPLE MAGNETIC POLE TEST RESULTS

Other facts that were first thought to have changed the magnetic properties of the sample pole are as listed below:

(1) Surface grinding of mating surfaces
(2) Fringing and leakage flux
(3) Improper heat treating
(4) Poor pole configuration

It now appears that none of these items affect the magnetic properties to any significant amount. This is borne out by the high-stall torque the actuator exhibits, which is an indirect measurement of the static magnetic circuit properties.

7.4 Speed and Power Output

7.4.1 Maximum Speed and Power Output - Maximum speed capability of the SF type is discussed in Section 4.5.

The RF types are much simpler electrically as standard AC power is directly applied for constant speed applications or on-off type servos. Models EHD-1 and 2 were tried at 400 cps and 115 V but did not operate. (Possibly, higher voltage might have helped, but was not tried). Therefore, the other available frequency (60 cps, 1/7 of 400) was used. If the increased speed warrants the complexity in the future, circuits might be used that generate 120 cps or other harmonics of 60 or the 200 cps sub-harmonics of 400. Square wave inputs that such circuits would probably entail should not degrade performance.

When higher speeds are attained, the same factors that limit the SF type come to bear, as discussed in Section 4.5.

Power output is given by

$$P_o = T_M \dot{\theta}_M \qquad (7\text{-}4)$$

Up to the point where T_M is independent of speed P_o obviously is directly increased by increases in speed. After this point, due to the effects of increased speed and inertia discussed above, it is expected that T_M would decrease, and that approximately constant P_o might be expected. This assumption enables calculating torque and power rate for any desired speed. The testing done was not sufficient to determine the point of changeover.

7.4.2 Minimum Speed - As all EHD devices discussed up to this point are synchronous actuators, minimum speed depends only upon the input frequency or pulse repetition rate, which is capable of being reduced to as small a value that could be desired, depending on the type of frequency standard employed.

7.4.3 Variable Speed - For the RF type, variable speed requires a source of variable frequency polyphase power, whose voltage increases with frequency to produce constant flux. If the device is two-phase, this might be done with a free-running multivibrator circuit with feedback voltage adjustment.

Since the SF type is a digital actuator requiring logic circuitry, this requires only a means of changing the input pulse repetition rate.

The exception to synchronous action would be the use of a self-stepping mode of operation, discussed in Section 10.2.

7.5 Output Element

There are two major factors determining whether the flexspline or the circular spline should be the output element. These are predicated upon the constraint that if the magnetic forces are unidirectional, the teeth should be on the same sides of the flexspline as the magnets.

(1) There is considerably more space outside the flexspline to place the fixed parts of the magnetic circuit, and thus the flexspline was designed with external teeth, making the circular spline lie around it. It is far easier and results in less total inertia to attach the circular spline to the housing and couple the flexspline to the output shaft.

(2) It is considered desirable to have relatively little tangential motion between the magnet pole faces and the particular armature elements with which they are working. This is dependent upon the maximum power angle. Flexspline tangential velocity is the sum of its harmonic variation from zero to twice output velocity plus the circular spline velocity. Thus, relative to the housing which holds the magnets, it varies as shown in Table XXV.

	Fixed Circular Spline		Fixed Flexspline	
Variation of the flexspline tangential velocity relative to the housing	0 at $\delta = 0$ to $2\dot{\theta}_o$ at $\delta = 90°$		$-\dot{\theta}_o$ at $\delta = 0$ to $+\dot{\theta}_o$ at $\delta = 90°$	
Pressure Angle	$20°$	$30°$	$20°$	$30°$
Maximum power angle, δ_m	$27°$	$21°$	$27°$	$21°$
Variation of the flexspline tangential velocity relative to the housing up to the maximum power angle	0 at $\delta=0$ to $0.4\dot{\theta}_o$ at δ_m	0 at $\delta=0$ to $0.72\dot{\theta}_o$ at δ_m	$-\dot{\theta}_o$ at $\delta=0$ to $-0.1\dot{\theta}_o$ at δ_m	$-\dot{\theta}_o$ at $\delta=0$ to $-0.28\dot{\theta}_o$ at δ_m
Average flexspline tangential velocity relative to housing	$0.45\dot{\theta}_o$	$0.36\dot{\theta}_o$	$0.55\dot{\theta}_o$	$-0.64\dot{\theta}_o$

TABLE XXV - RELATIVE VELOCITIES OF HARMONIC DRIVE ELEMENTS

The fixed circular spline is somewhat better, but either would probably be satisfactory in this regard.

If the above constraint need not be adhered to, it might be possible to use internal flexspline teeth. In this case, the flexspline teeth would contact an internal circular spline at the minor axis, and the driving forces would be acting in a direction radially opposing the direction in which the shape deflects into tooth engagement. Use of an internal circular spline and making it the output member results in somewhat less inertia than if the flexspline or an external circular spline are the output members. However, the reduction in inertia is not great, and the possibility of shape distortion makes experimentation with this concept questionable.

SECTION 8

MODEL DESIGN AND MANUFACTURING

8.1 Configuration and Sizing

The RF type configurations were selected and designed to utilize standard purchased motor stators and housings, thereby saving on cost. For models EHD-2 and 4 a bell-shaped metal flexspline was used to obtain parallel motion and constant deflection at the teeth and within the air gap. Another advantage of the bell shape propounded by some authorities, but not as yet confirmed, is that it resists shape distortion. Using an available structure, it was necessary to have the field rewound to provide space for placing the circular spline as near to the stator as possible. Model EHD-1, made to observe general powder action, used this same stator and a simple toothless flexcup made of a plastic sheet rolled and welded.

The configuration selected for the SF model (EHD-3) was the result of comparing many alternate approaches. The design eliminates metallic flexspline material from the air gap and provides force magnification, but at a resulting magnification in gap size. A cup shape was used because its coning conformed to the levers and is easier to manufacture. The size was generally selected based upon the analysis for a power output of approximately 100 watts. A standard Harmonic Drive pitch diameter of 3 1/4" was used. Other configurations considered were:

(1) Magnets positioned to pull through the flexspline. This results in high eddy current problems unless a plastic flexspline is utilized. For this case, response and speed would have to be reduced and losses would be greater.

(2) Magnets positioned to pull against T-shaped armature pieces that project through slots in the flexspline. This only partly eliminates the eddy current problem due to the maximum practical size of slot. Further, it is quite complicated design-wise.

(3) Concept (1) or (2) above plus magnets positioned to pull directly upon an extension of the same armature that work with the other magnets. This allows the magnets to be staggered, thereby decreasing the torque fluctuation for steady-state load applications.

(4) One similar to concept (3) except that the flexspline has a so-called castellated coupling or dynamic spline connected to the output shaft through a rigid diaphragm containing slots for the armatures. (See Figure 66-A).

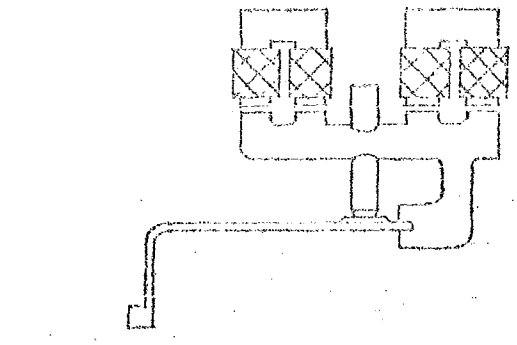

(B) BIDIRECTIONAL CRANK OUTSIDE

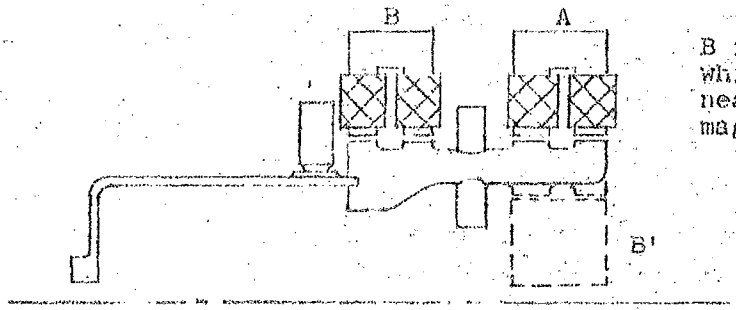

B is preferred to B' which does not have nearly so much total magnet volume.

(C) BIDIRECTIONAL CRANK AT END

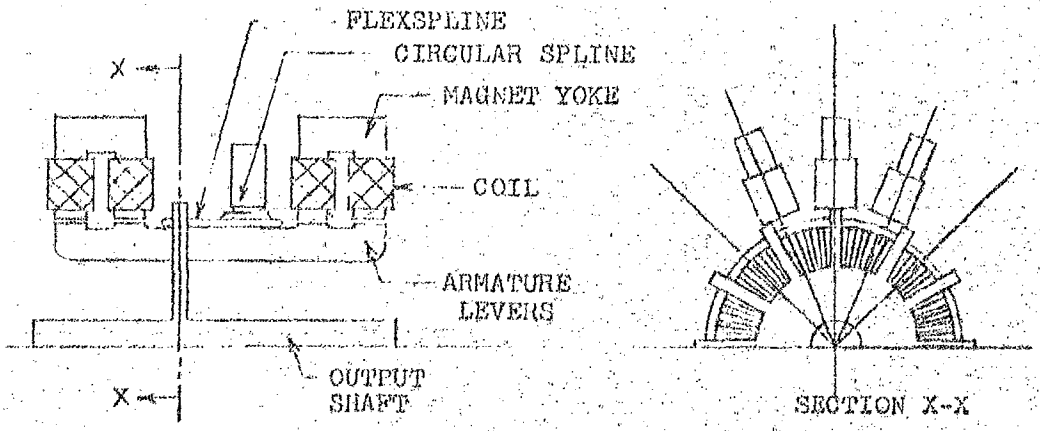

(A) CASTELLATED COUPLING

FIGURE 66 ALTERNATE CONFIGURATIONS

(5) A crank type of armature (such as Figure 66 B and C), which offers the possibility of exerting bidirectional forces. This concept lies between the external polarized armature configuration (see Section 3) and the armature integrated with the flexspline which gives the preferred distributed forces. The torque loading produced by practical size armatures due to the doubling of forces may produce excessive shape distortion. Also, it is considerably more complicated designwise and is likely to have greater dynamic problems (resonances and shock and vibration vulnerabilities).

(6) Magnets positioned to pull against small armature slugs containing slots at each end of which the shell of the flexspline and the cylindrical portion containing the teeth are respectively placed.

(7) An entirely different concept in which the flexible element is not a cup or bell shape, but just a deformed disc containing teeth on either or both sides. These are made to mate with one or more rigid face gears when deflected axially by magnets which attract armature material attached to the outer diameter of the disc. A careful study was made of this approach as it might reduce the size of the actuator and produce high-torque output due to its large-diameter, pancake-type configuration. This appears as Appendix XIII. The analysis indicated that the axial motion must be quite large in order to use teeth. To keep stresses reasonable, a very thin disc is therefore required, which would have a very low torque rating.

Deflection can be less if teeth are not used but torque, accuracy, and linearity would fall off as occurs when reliance is placed on a friction drive.

8.2 Magnet Design - SF Type

In addition to the considerations covered in Section 4, attention was given to:

(1) Mechanical properties of vanadium permendur.
(2) Pole tip clamps.

Fortunately, vanadium permendur has good mechanical properties even in the annealed state and is suitable for being used as the armature of power magnets at considerable stress levels. Investigation also disclosed that impact, such as occurs between the armature and the pole face, does not degrade its magnetic properties. The parallel flux paths through the lamination produce repulsion forces. To keep the laminated pole tips from separating, a series of non-magnetic clamps were placed between the legs of each magnet. This has worked out well.

8.3 Armature Design - RF Type

The RHD-2 type, utilizing powder and a laminated core, involved consideration of:

(1) Size and material of powder particles
(2) Lubricant addition to the powder
(3) Clearance between flexspline and core
(4) Shape of "teeth" on the core
(5) Restriction of the powder to the gap

It has been found from test that particles of about 5 mils in diameter, much coarser than carbonyl E (0.1 to 0.5 mil size) tried initially, performs best. Very small particles pack together and jam the operation. It is believed that about 3 mil would be even better, and preferably spherical-like carbonyl powder, as opposed to the random shapes of the coarse-grit powder used. Lubricant additions (oil and/or molybdenum disulphide) were tried and improved operation with the coarse powder, but gave no detectable improvement with the fine. The core "teeth" were shaped with a flat top about 0.100" wide. Radial clearance was about .080", although it is believed that a smaller clearance would be an improvement. To maintain the powder in the gap spaces, thereby preventing it from either getting into the air gap or stiffening the flexible shell (both problems were encountered), diaphragms composed of a flexible rubber ring over a disk were used on each side of the gap. They did not appreciably stiffen the flexspline.

The EHD-4 type utilising the linked armature, involved manufacturing a multiple number of identical links with mating concave/convex ends and outer edges rounded to fit the flexspline. To provide the highest air gap flux density, they were made from vanadium permendur. They were first stamped by a die, then bonded. The individual laminations did not remain aligned and there was also extra flash from the bonding operation. To improve the surface, hand scraping was tried. It is believed that the portions of the adhesive that remained aided in preventing higher frictional forces. As assembled, the model had a total circumferential clearance between links of about 3/16 inch, which undoubtedly affected the performance obtained during test. The selection of radial thickness and number of links was based on good design proportions, as well as the analysis relating flux density at the gap to the radial thickness of the links. After initial operation, the unit was disassembled to experiment with additions of lubricant. It was observed that the laminations had become considerably detached, to the degree that it was not practical to reassemble them without additional assembly fixtures. Repulsion forces created by the parallel flux paths, plus impact and vibration, probably caused this detachment. The type of bonding that is required to avoid degrading the magnetic properties does not give a strong bond.

One improvement that might be considered is to lay the die-stamped laminations side by side, without bonding, in a staggered fashion thereby distributing the inter-link air gaps, using end disks and an inner spool to keep the assembly together.

8.4 Harmonic Drive Reduction Ratio

The reasons for the selection of pitch diameter, pressure angle, diametral pitch, and tooth length have been covered in other sections of this report.

6.5 Packaging

The output shafts of all EHD types were made double-ended to enable fastening transducers to one end, with the load attached to the other.

The housing of the EHD-3 was designed as an aluminum casting to simplify manufacture and reduce weight. Even-so, conservatism in design was used to avoid having problems with the housing. It is believed that significant light-weighting for this size unit can be done. Standard servo mounting features were incorporated in the model. The shaft extension at the magnet end was selected to be used for attaching to the load for two reasons: a mounting flange at this end can have a larger diameter, which increases mounting rigidity; and the weight overhanging the mounting support is less. However, the 5/8", 10" long shaft permits considerable wind-up which, in conjunction with high load inertia, can result in cut-off frequencies that tend to limit dynamic performance. The solution involves either stiffening the shaft, a minor change, or revising the design to attach loads to the other end.

SECTION 9

TESTING AND TEST METHODS

As explained in the introduction, test results are integrated with the theory in Sections 4 and 5. This section briefly describes the tests, test equipment, and methods in general.

Because the EHD-3 SF type is the primary model all five contractually-specified tests were performed on it, as well as others that were considered worthwhile. Methods and results are discussed in Section 4.

All EHD models were tested for output speed; hysteresis and other losses, input voltage, current and power at various torque loads including the maximum steady torque load allowable without ratcheting; winding resistance; and weight. As previous discussion has stated, acceleration of the inertia of the loading device significantly increases the torque load on the SF type. However, with the RF types, which are synchronous, not stepping, devices, this inertia does not contribute to the total load for constant speed testing.

With the RF types measurements were made at 60 cps input, after 400 cps was seen to be excessive for these particular designs. Results are discussed in Section 5.

The test methods and equipment used all followed modern engineering practices, so only brief descriptions will be given. These have also been discussed in Sections 4 and 5. It is believed that from this discussion the tests and results could be duplicated by other workers.

For the SF type (EHD-3) only

Test	General Method and Equipment
Frequency Response	Input-audio oscillator; output transducer-film type potentiometer, dual beam oscilloscope, camera.
Resolution	Light beam reflected off a mirror fastened to the output shaft, angle measured at about 30 feet.
Repeatability	(1) The variation in output position, measured in the resolution test, for different number of steps, final step selection, and direction of approach. (2) Any change in the general operating capability at different times following periods of non-operation and/or disassembly.

Temperature Rise	Thermocouple wedged against the coil.
Backlash	Change in the reading of a dial indicator which bears against a lever attached to the output shaft, when the shaft is moved through its free-play angle.
Holding Torque with constant DC input	Application of static torque to a lever, attached to the output shaft, through a spring scale.
Acoustic Noise	Acoustic noise meter
<u>For Both the SF type (EMD-3) and the RF types</u>	
Output speed	Timing of 5 to 10 revolutions by a stop watch
Hysteresis and other losses, input voltage, current, and power, at various torque loads.	Magnetic particle clutch with dynamometer scale, electrical meters.
Winding resistance	Ohmmeter
Weight	Weighing scale

SECTION 10

SCALING

Calculations of the significant performance characteristics of the two basic types of EHD actuators are covered in Sections 4 and 5. In this section it is shown that these characteristics can be related to pitch diameter in a generalized form whereby approximate performance predictions can be made for actuators of any practical size. The results appear in Table XXVI as a function of pitch diameter. In applying these scaling factors, values of performance at some basic diameter are required. For the SF type, the performance of Model EHD-3 is used except that stepping rate is raised to 1000 step/sec., representing 125 cycles/sec. magnet frequency and 22½ rpm output. This is believed practical through further development. For the RF type, the theoretical performance of Model EHD-2, modified as discussed in Section 5, is used.

The following basic constraints hold for any D_p. These, plus the values of the scaling constraints, are shown in Table XXVII.

(1) Deflection "d" (and hence diametral pitch) remains the same as the laboratory models; thus, ratio Rg is directly proportional to Dp, and output speed varies inversely with Dp for constant input frequency.

(2) Peak current remains the same as present models.

(3) Wire size remains the same

(4) Flux density remains the same (taken as 2.2 webers/m.^{2} for the SF type, 0.80 for the RF type).

(5) η_s (shape factor) = 1.

(6) There are 16 magnets for the SF type and 24 stator pole teeth for the RF type.

(7) The circumferential clearance between magnets or poles is 0.250" for the SF type and 0.170" for the RF type.

In general, to obtain peak torque, the approximate order of magnitude will result if mean torque T_M is doubled.

Voltage given is peak for the SF types and RMS for the RF types. It is only approximate due to various uncertainties discussed earlier in the report.

If it is advisable to consider the special design of a RF type for 400 cps input frequency, the compromises required to obtain such speed would upset the scaling factors given, and a separate analysis should be made.

U	=	$1-k_1/D_p$ (utilization factor)
T_M	=	$k_2UD_p^3$
J_M	=	$k_3D_p^5$
$\dot{\theta}_M$	=	k_4/D_p
i_m^2R	=	$k_5UD_p^3$
E	=	$k_6D_p^2$
V	=	$k_7UD_p^3$
Wt	=	$k_8UD_p^3$
P_M^o	=	$T_M^2/J_M = k_2^2U^2D_p/k_3$
P_M	=	$T_M\dot{\theta}_M = k_2k_4UD_p^2$
η_M	=	$\frac{P_M}{P_M/\eta_T+i_m^2R} = \frac{k_2k_4UD_p^2}{\frac{k_2k_4UD_p^2}{\eta_T}+K_5UD_p^3}$
P_M^o/P_M	=	$K_2U/k_3K_4D_p^2$
P_M^o/i_m^2R	=	$k_2^2U/k_3K_5D_p^2$
P_M^o/Wt	=	$k_2^2U/k_3k_8D_p^2$
T_M/V	=	k_2/k_7
T_M/Wt	=	k_2/k_8

TABLE XXVI - SCALING RELATIONSHIPS FOR ERD ACTUATORS, FOR USE WITH SECTION 10. Values of the scaling constants and basiccharacteristics assumed are given in Table XXVII.

BASIC CONSTRAINTS	UNITS	STEPPING TYPE: SINGLE STEP	STEPPING TYPE: DOUBLE STEP	ROTATING FIELD TYPE
P_D		96 →	→	→
$d = \frac{2}{P_D}$ (iron)	m	5.2×10^{-4} →	→	→
$\mathcal{B}_m$	w/m^2	2.2 →	→	0.8
Φ_a	deg.	20 →	→	30
δ_m	deg.	$22\frac{1}{2}$	45	20
η_T		0.8 →	→	0.7
f		1000 steps/sec. →	→	60 cps
$Rg = Dp/d$		1900 Dp →	→	→
SCALING CONSTANTS				
k_1		3.3×10^{-2} →	→	→
k_2		1.8×10^{5}	2.1×10^{5}	5.6×10^{4}
k_3		3.2×10^{3} →	→	7.2×10^{2}
k_4		0.21	0.42	0.20
k_5		5.2×10^{5} →	→	3.4×10^{4}
k_6		1.2×10^{4} →	→	6.7×10^{4}
k_7		11 →	→	10
k_8		2.7×10^{4} →	→	5.6×10^{3}

TABLE XXVII - SCALING FACTORS FOR USE WITH TABLE XXVI

Note that power rate is normally expressed in kw/sec so that a 10^3 factor enters.

The practical limits to which units may be scaled include these factors:

(1) Input frequency should not exceed natural frequency, which decreases with D_p. (See Appendix IX.) This should be checked for any design of interest.

(2) Deflection force becomes very significant below D_p of 1 5/8". (See Appendix III.)

As an example of how these scaling factors are used, Table XXVIII presents the theoretical characteristics of a 5-inch diameter stepping type actuator. A power rate of 1100 kw/sec., for a single step, is indicated.

	SINGLE STEP		DOUBLE STEP	
	Mks Units	English Units	Mks Units	English Units
D_P	0.127 m	5.0 in.	0.127 m	5.0 in.
R_g	241			
U	0.74			
T_M	350 n-m	3100 lb.in.	410 n-m	3600 lb.in.
J	0.11 kg-m^2	1.0 lb.in.sec^2	0.11 kg-m^2	1.0 lb.in.sec^2
$\dot{\theta}_M$	1.6 rad/sec		3.2 rad/sec.	
$i_m^2 R$	1000 w			
E_-	191 v			
V	.021 m^3	0.74 $ft.^3$	.021 m^3	0.74 $ft.^3$
wt.	54 kg	120 lbs.	54 kg	120 lbs.
$\dot{P}_M$	1100 kw/sec.		1500 kw/sec.	
P_M	560 w	0.75 hp	1300 w	1.75 hp
η_M	33%		50%	
$\dot{P}_M/P_M$	2000 sec^{-1}		1150 sec^{-1}	
$\dot{P}_M/i_m^2 R$	1100 sec^{-1}		1500 sec^{-1}	
$\dot{P}_M/wt.$	20 kw/kg-sec.	9.2 kw/lbs.sec	28 kw/kg-sec.	12.5 kw/lbs.sec.

TABLE XXVIII - STEPPING FIELD ACTUATOR ESTIMATED RATINGS, AS AN EXAMPLE OF USE OF SCALING FACTORS OF SECTION 10.

SECTION 11

ADVANCED DESIGN CONCEPTS

11.1 General

This section covers suggestions for improvements. They are placed in two categories:

1. Ideas generated from testing, evaluation of tests, and continuing analysis during the project, that might improve the laboratory models.

2. Ideas that were purposely not included in the models because of the objective of proving feasibility, not meeting secondary objectives such as military environments and low cost.

Although some of these have been introduced earlier in this report, they are summarized here for completeness.

11.2 Modifications to Laboratory Models

11.2.1 Self-Stepping - In the present form, both the SF and RF devices are designed to operate at a constant average output speed, for fixed input frequency, from zero up to rated load. Thus they are both synchronous devices. Most conventional synchronous motors (reluctance, hysteresis and wound rotor) have the capability of acting as induction motors to accelerate up to synchronous speed under some load. Most stepping motors can lose step and still not be damaged. However, it is not understood what damaging effects might occur if the Harmonic Drive devices, due to load, were to operate below synchronous speed. One possibility is that the teeth may disengage, with the unit running as a friction drive during this transient period. Possibly friction in the teeth might maintain engagement, or the tooth may ratchet and fail. This subject is particularly important for it helps determine the accelerating capability under load.

In some applications, a torque source rather than a speed source is often desired. For example, a negative torque-speed characteristic provides damping for stabilization of closed loop servomechanisms. Providing this characteristic with conventional stepping devices has been done, by use of internal feedback to initiate each step such that output torque is maintained approximately equal to load torque. The speed automatically adjusts itself in accordance with load changes, increasing as the load torque decreases. For the SF EHD device performance of the feedback function electrically by operation on the coil current or voltage waveshape should be practical. This would eliminate space, alignment and sensitivity problems that might result from utilization of internal electromechanical transducers. In Section 4 it was shown that when there is a negligible steady torque load, model EHD-2 must step to a zero power angle, and therefore the maximum power angle after switching is only $22\frac{1}{2}^{\circ}$ for single step operation. With self-

stepping, for the same load and for a single step, power angle need not fall to zero, and a variation, for example 10° to 32½°, would be achieved. Thus the output torque would be considerably more constant and approximate a linear torque-speed characteristic. The device would be designed so that a specified maximum power angle and speed could not be exceeded.

When self-stepping is not used, it is possible to calculate the lowest τ_L that can be achieved in a slewing mode. This was done and it was seen that minimum τ_L is approximately the reciprocal of the magnet pulse rate. This is derived in Figure 67. As shown, it was assumed that the power angle can instantaneously increase to 1½ steps (or 33 1/3°) at the initiation of the second step, slightly exceeding the maximum value calculated in Section 4 of about 27°. Notice that the curvature of the θ_0 curve changes with the polarity of the torque. Even though the curvature is slightly greater during the start of the second step, it is assumed that this portion does not determine the maximum response because torque available for acceleration is greater at that point. Using this result, in reference to the performance of Figure 62 for which f_p = 500 pulses per second, there is obtained

$$\tau_L = \frac{1}{f_p} = .002 \text{ sec.} \qquad (11\text{-}1)$$

Since τ_M = .00037 sec. (Section 6)

$$\tau_M/\tau_L = 0.18 \qquad (11\text{-}2)$$

and

$$\frac{P_M}{P_L} = \frac{1}{1 - \tau_M/\tau_L} = 1.2 \qquad (11\text{-}3)$$

For the conventional actuator of Figure 62,

τ_M = .006 sec. and at the same τ_L

$$\tau_M/\tau_L = 3 \qquad (11\text{-}4)$$

$$\frac{P_M}{P_L} = 4\,\frac{\tau_M}{\tau_L} = 12 \qquad (11\text{-}5)$$

At τ_L = .002 sec., there is an advantage for the EMD-3 of

$$\frac{P_{M_{HD}}}{P_{M_C}} = \frac{12}{1.2} = \frac{10}{1} \qquad (11\text{-}6)$$

Therefore, in Figure 62 the entire region to the right of τ_L = .002 sec., where $P_{M_{HD}}/P_{M_C}$ varies from 10/1 downwards, is achievable without resorting to self-stepping.

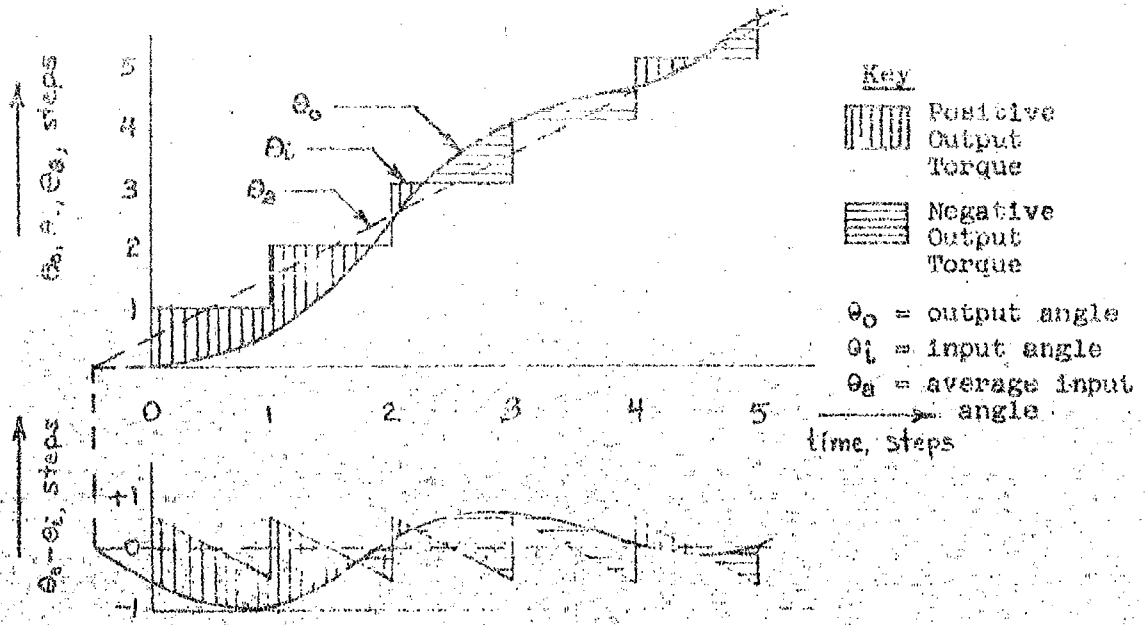

Assume that the θ_o response is $\frac{1}{4}$ cycle of a sinusoid starting from an imaginary origin at $t = -\frac{1}{3}$ step, with an amplitude of -1 step, as shown above. The frequency of this waveform is

$$f = \frac{1}{1\frac{1}{3}} \times \frac{1}{4} \times f_p = \frac{f_p}{6}$$

where f_p = magnet step rates (pulses per second)

since

$$\dot{\theta}_o = 2\pi f\ \theta_o$$
$$\ddot{\theta}_o = (2\pi f)^2\ \theta_o$$

Then

$$T_L = \frac{\dot{\theta}_o}{\ddot{\theta}_o} = \frac{1}{2\pi f} = \frac{3}{\pi f_p} \approx \frac{1}{f_p}$$

FIGURE 67 TYPICAL SLEWING MOTION OF MODEL EHD-3 WITH NEGLIGIBLE STEADY TORQUE LOADING

$T_L = 0$

Flux Rise Time Neglected

That Figure 67 is a valid representation, is shown by its excellent correlation with the RRD-3 test results.

Using data from Section 4, and applying Figure 67 to determine $\ddot{\theta}_{M_m}$

$$T_m = 86 \text{ n-m} \quad (11\text{-}7)$$

$$f_p = 500 \text{ cps} \quad (11\text{-}8)$$

$$\theta_{M_S} = 2.52 \times 10^{-3} \text{ rad.} \quad (11\text{-}9)$$

$$\ddot{\theta}_{M_S} = (2\pi f)^2 \theta_{M_S} = \left(\frac{\pi}{3} f_p\right)^2 \theta_{M_S} \approx (500)^2 \theta_{M_S}$$

$$= 630 \text{ rad/sec}^2 \quad (11\text{-}10)$$

$$J_{M_1} = 1.12 \times 10^{-2} \text{ kg-m}^2 \quad (11\text{-}11)$$

$$T_L = 22 \text{ n-m} \quad (11\text{-}12)$$

Peak torque available for accelerating the external load, T_{a_m}, is therefore

$$T_{a_m} = T_m - J_M \ddot{\theta}_{M_m} - T_L = 86 - 7 - 22 = 57 \text{ n-m} \quad (11\text{-}13)$$

$$\therefore J_L = \frac{T_{a_m}}{\ddot{\theta}_{M_m}} = \frac{57}{630} = .09 \text{ kg-m}^2 \quad (11\text{-}14)$$

The test load was 0.1 kg-m^2.

11.2.2 Power Angle - Increase of the power angle beyond that which theoretically provides for constant and reliable tooth engagement would increase the torque and power rate. For the SF type, study of double step operation can be made after minor wiring modifications. As there is a problem with measuring torque, a torque traneducer might be employed to measure the peak values. With the RF types the torque can be a steady load permitting direct measurement of maximum torque and indirectly of power angle. The problem here is that the torque efficiency may drop more than with the SF type due to extended deflection over 180° and friction within the powder or links.

11.2.3 Pressure Angle - Recent success with operating a hydraulic Harmonic Drive actuator having 14½° pressure angle teeth indicates that this might be successfully applied, probably to the SF type only.

11.2.4 Increase in Torque Loading in Relation to Reliability and Life - The ratings of torque and power rate listed for the laboratory models are believed to be compatible with the general design life objective of such devices although this should be proved by life testing in future programs. If it is desired to increase the ratings, such as by changes in the magnet polar area, the increased torque loading effects should be given further study, analytical and experimental, to assess the probable life, as well

as what special materials, heat treatments, force distribution, etc., should be considered to maximize life. With the RF type, the optimum performance capabilities of plastic flexsplines would merit additonal attention.

11.2.5 Other Stepping Field Improvements - A constant-current power supply has been discussed as a means of increasing the electrical response so that the limitations become that of the mechanical elements. Another advantage of this type of supply is that operation down to and including stall would be possible without voltage adjustment as is required for the present research model. In the interests of simplicity and to save time, the present model was made with flat pole faces. If these were curved to match the armature, the mean air gap length and hence the reluctance should be decreased significantly. The difference in radial distance between an arc of 1 5/8 inch radius and a chord 1/2 inch long (as in the present design) is .011 inch.

It appears that if the fulcrum were separated from the output shaft by a bearing, the armatures would have considerably less net rotation, thereby decreasing the inertia (as discussed in Section 3.6).

11.3 Refinements and Optimum Packaging to Meeting Environment Requirements and other Productization Requirements

11.3.1 Environmental Requirements - Packaging is most often thought of in terms of weight, volume, shock and vibration, but all of the applicable military requirements such as are given in MIL-STD-446 and MIL-E-5272 must be given consideration in final design. Although the present actuators (exclusive of the EHD-3 electronics) fall within the program objective of weight and volume, obviously the further that reductions in weight and size can be carried, the better for aerospace uses. It is felt that considerable savings can be made in reducing the actuators themselves, by use of lighter density materials in some places, thinner castings, and compacting dead spaces. At the same time, the devices must not be allowed to become susceptible to fatigue failure through vibration, impact failure through shock, or thermal failure. In addition, some long thin elements, such as the poles of the stepping type, must be investigated for vibration resistance and redesigned as necessary.

Attention to thermal design would be necessary. Limiting the temperature to certain levels in relation to insulation and other components is necessary for high reliability. The duty cycles expected in typical operation will help determine the type of cooling, heat sink, forced convection, radiation, or the like, that might be utilized in configuration development.

It is felt that the control circuitry, power amplifier, and power supply can all be made suitable for use with any reasonable environment presently compatible with transistors and diodes.

11.1.2 Reliability Aspects - In the PF devices, attention is required to provide a more positive containment for the powder if used. Possibly a flexible plastic diaphragm could be welded to the plastic flexpillar.

In the SF devices, the effects of the impacting of the armatures upon the magnets should be studied, and if there are indications of accelerated wear some means of protection, such as a thin layer of some absorbent, durable material, may be required.

SECTION 12

IMPLICATIONS UPON ELECTRICAL CONTROL SYSTEMS

12.1 General

The high power rates of all EHD devices together with the digital characteristics of the stepping type and the synchronous speed characteristic of the rotating field types, means that unique and highly advantageous control system performance is obtainable. Because of these unique characteristics the possible systems themselves become broadened in scope and advanced in sophistication and performance. These factors are discussed in this section.

12.2 Stepping Field Types

With the control circuits developed for operation with this device it is possible to obtain the following variations in system design:

(1) Direct operation from a pulse train produced by a digital computation system and thus the attainment of high torque digital actuation.

(2) The capability to start and stop in extremely short periods of time allows for higher-performance bang-bang servo systems. With the increase in power rate, basic motor time constant is substantially decreased and the stability problem inherent in the design of bang-bang systems is diminished. If constant speed is used, the control system becomes quite simple, requiring only a reversible, constant repetition rate, pulse train.

(3) By the analogue to digital converter, directly apply the actuator and its associated electronics in analogue systems. The converter is utilized where linear analogue signals are available. When introduced into the circuitry it will produce a pulse train with frequency proportional to amplitude of the input analogue signal.

(4) Being digital in nature, the electronic circuitry can also be designed to provide for more suitable relay servo control. By introducing to the actuator different levels of pulse train frequency which are easily turned on or off by relay control, dual-mode operation can be obtained. For example, one might provide a combination of a fast, constant-speed slew with a narrow range of analogue control. This allows for higher performance systems operating in a minimum of time with a minimum of overshot following the input signal.

The system design versatility allowed by this actuation means is thus very unique. Knowing the load inertia and acceleration requirements, the required power rate can be determined.

This power rate, independent of gearing, must then be supplied by the motor. Performance requirements of aerospace actuators generally involve power rate requirements which have dictated the utilization of hydraulic motors primarily for their high acceleration capabilities. In order for an electric actuator to meet these high power rate requirements it is required that a motor of present day design have a horsepower rating 4 to 10 times the actual steady state horsepower requirements of the load. Since EMD has, for a given power output, power rates equivalent to that found in present day actuators (excluding the low duty cycle types) having 4 to 10 times the power output, or more, it is possible to increase the band width of electric systems working under wide ranges of input signal variations. It is significant to point out here that the attainment of very wide band width in present day electrical systems is quite possible, but at a sacrifice in amplitude of the signals, which decreases sharply with an increase in input signal frequency. What is needed, therefore, is a device which has the power rate capabilities allowing for increased magnitude of input signals over the frequency range or band width desired for the system. Required band width, after all, is dictated primarily by the requirements of the system to respond to step inputs.

During the course of the initial investigations it has become obvious that the development of any actuator of this type, with radically different characteristics, might produce extreme requirements upon the electronic driving circuitry. At the present, this has been shown to be true. The high electrical load requirements imposed upon the driving circuits have indicated the need for special consideration. There may be limitations in the attainment of very high power rate actuators due to limitations of the solid-state power stage components. Rather substantial efforts and accomplishments have been performed to date in providing for circuits suitable for demonstrating the inherent capabilities of the actuator being developed. Any continuing program should include further study and development of the implications upon the electronics of these new classes of actuators.

One very noteworthy advanced control concept would be self-stepping operation using internal feedback. As discussed previously in this report, this would convert the actuator to a torque source.

12.3 Rotating Field Types

The more simple rotating field device is capable of operating from any two or three phase source. It does however, represent a constant speed device unless one is able to develop a suitable polyphase variable frequency system. However, the attainment of a high response constant speed device, capable of rapid acceleration and decelerations, makes it more fruitful to study the implications and compatibility of this device with bang-bang or contactor systems, where such a device is needed. The resulting characteristics of systems utilizing this device in a bang-bang fashion would, we believe, have very significant advantages negating the requirement to develop a variable frequency source. Although not having the power rate capabilities of a stepping field type of actuator, the rotating field device does have, in relation to its output power,

a power rate capability upwards to an order of magnitude better than equivalently rated existing electric devices.

SECTION 13

CONCLUSIONS

As a result of the analytical and experimental work of this project, the following conclusions have been reached.

(1) Feasibility of Electromagnetic Harmonic Drive (EHD) has been demonstrated, in two different forms.

(2) Analytical methods for understanding and predicting performance and designing EHD actuators were devised and substantiated by close correlation with experimental results.

(3) As an electrical actuator, EHD provides a drastic reduction in inertia, which results in advancing the state-of-the-art for fast response electrical servo actuators, not employing separate clutching and braking. This results in some radical implications for control systems.

(4) The key parameter characterizing the capability for fast response is shown to be power rate (torque squared to inertia). EHD provides large advances in power rate to weight and power rate to electrical loss ratios from which the overall improvement in system weight and duty cycle capability follows.

(5) The type of servo application (extreme, high, and low performance) is important when comparing actuators.

(6) Compared to a typical conventional DC torque motor with gearing, the weight saving of a EHD actuator would be as much as 13:1 depending on the application.

(7) EHD has excellent overall efficiency.

(8) Fundamental analyses were derived which provide a firm analytical foundation for all future work in this area. Both ideal and practical aspects are covered.

(9) A magnetic force distributed over the flexspline member by use of magnets placed integral with a continuous flexible armature is superior to coupled external magnets producing point forces on the flexspline.

(10) Power angle and shape distortion are the most significant parameters determining maximum operating torque.

(11) The calculation of effective inertia contributed by the short-stroke motion of the flexible elements can be routinely done by methods explained in this report. However, deviations from ideal motion paths increase

these values. Experimental verification of inertia is not straight forward, yet useful results are obtained.

(12) The primary model made to fulfill specific contract objectives was a stepping actuator, with essential characteristics of 115 watts power output, 310 kw/sec. power rate, 35% overall efficiency, 22 lbs. weight, 240 cubic inch volume, using a 3½ inch Harmonic Drive pitch diameter. Electrical control is provided by digital logic and switching circuitry, transistorized and of modular construction for high versatility, including an analog to digital converter to utilize DC inputs. Solid state components are necessary to achieve the inherent high response of the actuator. Other characteristics are:

- Bidirectional operation
- Variable speed
- Open loop frequency response demonstrated to 30 cps
- Maximum speed about 18 rpm
- Maximum inertial load about 400 lb.in.^{2} in conjunction with a torque load of 200 lb.in.
- Holding torque about 1300 lb.in.
- Resolution of 8.7 minutes of arc (one step) demonstrated by a closed-loop laboratory setup.
- Repeatability about 10%
- Minimum speed dependent only on the controls
- Essentially zero backlash
- Highest known power output for a stepping actuator
- 6 minutes time for temperature to reach 200° F, which was nearly steady-state, with a high inertial load at 6 rpm
- 60 cps, 3 phase, 220 V power input rectified to DC, adjustable over approximately 0 to 70 volts, and capable of 70 amps current.

(13) The theoretical maximum power rate for the 3½ inch size stepping actuator is about 2000 kw/sec. but practical considerations may not allow this to be fully realized.

(14) For a hypothetical application, believed typical of aeronautical systems, the EHD stepping actuator would

provide a 5:1 weight saving and 13:1 electrical loss saving compared to conventional DC torque motors.

(15) The EHD stepping actuator is capable of fulfilling requirements for a typical missile control surface or flap drive and the arm drive of a computer disc file memory unit, for which a 200 watt conventional AC servomotor has far insufficient power rate.

(16) Using scaling factors developed in the study, a 5 inch pitch diameter stepping actuator, based on the same design approach as the lab model, is predicted to have a power rate of 1100 kw/sec., 33% efficiency, develop 0.75 horsepower and weigh 120 lbs.

(17) The secondary model made was a synchronous actuator which operates directly from a polyphase AC supply and economically utilizes standard motor parts. Response capability (approximately 50 kw/sec. power rate) exceeds conventional synchronous actuators, and number of parts is less. Basic flexspline action and inertia reduction characteristics are like the stepping actuator.

(18) Use of superior magnetic materials, such as vanadium permandur, permits significant increases in power rate.

(19) Using the flexspline as the output member of EHD was shown to be more favorable than the circular spline.

(20) Lubricants are not needed for the EHD.

(21) Excellent performance in hard vacuum and high temperature environments is anticipated.

The following problem areas or matters deserving of greater study were recognized. There is not necessarily a problem, but further study is considered advisable.

(1) Relationship of maximum torque and speed to life, reliability and loss of step or synchronism. For the stepping actuator, use of self-stepping through internal feedback would increase performance even further but at the expense of greater complexity. Double stepping might also improve performance.

(2) The constant voltage power supply places a limitation on response due to its time constant, whereas a constant current supply would not.

(3) The acoustic noise of the stepping actuator, although not considered excessive, indicates that material or design changes might improve life, response and/or efficiency capability.

(4) Optimization of the armature and magnet shape should improve performance somewhat.

(5) The synchronous actuator was not optimized with regard to materials, electrical windings, air gap and in particular, armature design. It does not provide variable speed, although this is not required in a simple bang-bang servo for which it might be well suited.

(6) Tooth pressure angle, if reduced, may increase performance.

(7) The output shaft of the stepping actuator has marginal stiffness, and may be affecting dynamic performance.

SECTION 14

RECOMMENDATIONS

Further analytical and experimental work should be devoted to optimizing the performance, in relation to realistic life and environmental requirements, in the areas of:

- Armature and magnet design
- Constant current power supply
- Tooth pressure angle
- Packaging (light-weighting, shock and vibration analysis, thermal design, output shaft stiffness)
- Materials, in particular for the flexspline, magnets and armature
- Study the effects of double stepping and self stepping (stepping actuator only)

Following optimization and design for more specific field environments, life tests should be conducted. After successful life testing, design of hardware for specific application would be in order.

In general, the aspects to be studied break down into (1) optimization of design (2) life assurance, and (3) the usual transition from a laboratory model to a commercial model capable of operating in field environments.

List Of References - Referred To In The Report

1. Allegheny Ludlum Corporation, "Vanadium Permandur", Bulletin EM-23.

2. Cameron, C. F. and D. D. Lingelbach, "The Dynamics of Relays," Electronic Industries, September, October, November, 1959.

3. Gould, H. L. B. and D. N. Wenny "Supermendur - A New Rectangular - Loop Magnetic Material," Electrical Engineering, March, 1957.

4. Harris, H. "A Comparison of Two Basic Types of Servo-Mechanisms," A.I.E.E. Trans., 66 (1947) Page 83-92.

5. Ham, C. W. and E. J. Crane, "Mechanics of Machinery," McGraw-Hill, New York, 1948.

6. Kojima, Zen-Ichiro, "Sleeve Rotor gives Servo Motor fast response," Control Engineering, January 1963, Page 95.

7. Newton, G. C. Jr. "What Size Motor for Proper Operation of Servo-Mechanisms," Machine Design, 22 (1950), Page 125-130.

8. Newton, G. C. Jr. and R. W. Rasche, "Can Electric Actuators Meet Missile Requirements?" A.I.E.E. Trans. - Pt. II, 80 (1961), Page 306-311.

9. Rabinowicz, Ernest "Practical Approach To Friction Coefficients," Product Engineering, September 26, 1960, Page 62.

10. Rotors, H. C., "Electromagnetic Devices," Wiley, N.Y., 1941.

11. Singer, F. L. "Engineering Mechanics," Harper and Brothers, New York, 1943.

12. Wiles, J. F. British Patent No. 1576, "Electro-magnetic Engines," 1870.

13. Yaskowa, J. and T. Fukuda, "Slotless Armature - Key to Motor's Low Inertia," Control Engineering, November, 1962, Page 87.

List of Supplementary References-Consulted But Not Referred To In The Report.

14. Bailey, S. J. "Incremental Servos," Parts 1 through 4, Control Engineering, October 1960 through March 1961.

15. Ritter, Francis, "Strong Magnets," International Science and Technology, April, 1962, Page 58.

16. Blackburn, J. F., G. Reethof, and J. L. Shearer, editors, "Fluid Power Control," Wiley, New York, 1960.

17. Bozarth, Richard M. "Ferromagnetism," Van Nostrand, N.Y., 1951.

18. Chubb, B. A. and R. Grau, "The Magnetic Particle Clutch, A Versitile Control Element for Rocket Systems," Lear, Inc. Engineering Report No. GR EM 101 presented at the Institute of Aerospace Sciences, American Rocket Society, Los Angeles, June 13-15, 1961.

19. Douglas, J. F. H. "Reluctance Motors for High Torque Specifications," A.I.E.E. Paper No. CP 61-222, presented at the A.I.E.E. Winter General Meeting; N.Y., January 29-February 3, 1961.

20. Electro-Technology, May, 1962 "Drives and Drive Systems-A Selective Bibliography."

21. Fitzgerald and Kingsley, "Electric Machinery", McGraw-Hill, New York, 1952.

22. Fitzgerald and Higginbotham, "Basic Electrical Engineering", McGraw-Hill, New York, 1959, Pages 168-189, 192-214.

23. Gardner, Annesta R., "What You Can Do With Flexible Magnets," Product Engineering, January 2, 1961, Page 77.

24. Gardner, M.F. and J. L. Barnes, "Transients in Linear Systems," Volume I, Wiley, N.Y., 1942.

25. General Electric Company, "Silicon Controlled Rectifier Manual," second Edition, 1961.

26. Greenblatt, H. C. "A Transient-Current Solenoid Driver," Electro-Technology, October, 1961, Page 132.

27. Iron Age, "Adhesive-Bonds Form Magnets", December 3, 1959, Page 112.

28. Littlemann, M.F. "Application of Magnetic Materials," Journal of Metals, March, 1960, Page 220.

29. Machine Design, "The Electric Motor Book," December 21, 1961.

30. M.I.T. Staff Publication, "Magnetic Circuits and Transformers," Wiley, N.Y., 1943.

31. McAdams, W.H., "Heat Transmission," McGraw-Hill, N.Y., 1954.

32. Merrill, F. W. "Permanent-Magnet Excited Synchronous Motors," A.I.E.E. Paper 54-412, Presented at the A.I.E.E. Fall General Meeting, Chicago, Ill., October 11-15, 1954.

33. Musser, C.W. "Breakthrough in Mechanical Drive Design-The Harmonic Drive," Machine Design, April 14, 1960, Page 160.

34. O'Brien, D. G., "Hydraulic Stepping Motors," Electro-Technology, April, 1962, Page 91.

35. Parziale, A. J. and P. D. Tilton, "Characteristics of Some Magnetic-Fluid Clutch Servo Mechanisms," A.I.E.E. Winter General Meeting, N.Y. New York, January 30-February 3, 1950.

36. Philco Corporation, Application Notes on Transistors and Silicon Controlled Rectifiers, 1959 through 1961.

37. Richards, R. K. "Arithmetic Operations in Digital Computers," Van Nostrand, Princeton, N.J., 1955.

38. Ritow, I. "The Role of Response in Specifying Servo Drives," Electrical Manufacturing, March, 1956, Page 82.

39. Schwartz, S. Editor, "Selected Semiconductor Circuits Handbooks," Wiley, N.Y., 1960.

40. Seeley, S. "Electron Tube Circuits," McGraw-Hill, N.Y., second edition, 1958.

41. Strong, E. M. "Electrical Engineering-Basic Analysis", Wiley, New York, 1943.

42. Stout, M. B. "Basic Measurements," Prentice Hall, N.Y., 1950; Page 360-393.

43. Texas Instruments Co., Application Notes on Transistors and Silicon-Controlled Rectifiers, 1959 through 1960.

44. Tustin, A. "Direct Current Machines for Control Systems," MacMillian Co., N.Y., 1952.

45. U. S. Bureau of Standards Preferred Circuits, sections 210, 213, 221, 222, N 17, U. S. Government Printing Office.

46. Veinott, C. G. "Theory and Design of Small Induction Motors," McGraw-Hill, New York, 1959.

APPENDIX I

REPORT OF ELECTROMAGNETIC HARMONIC DRIVE WITH STEPPING FIELD ACTUATOR

I-1 Introduction and Summary

This Appendix summarizes some of the major aspects of the writer's study of the electromagnetic Harmonic Drive with a stepping field actuator. This report is concerned with servo applications of this type of electromagnetic Harmonic Drive.

In Part I-2 of this Appendix it is shown that electric servomotors when used in high performance applications, should have higher torque-squared-to-inertia ratios than are obtained with conventional designs if they are to have reasonable power ratings relative to the load power requirements. Next, a brief study of lateral versus variable-gap movement of magnet armatures indicates a distinct advantage for the variable-gap configuration insofar as force-squared-to-inertia ratios are concerned. Thus, it is seen that the electromagnetic Harmonic Drive uses a magnet configuration which is well adapted to the achievement of high torque-squared-to-inertia ratios or power rates. The characteristics of the electromagnetic Harmonic Drive are then compared with conventional servomotors. Performance data on both the laboratory model that has been built as well as estimated characteristics for a design representing maximum theoretical performance are presented along with corresponding information for two-phase induction servomotors. This comparison shows that the electromagnetic Harmonic Drive is characterized by power rates which are orders of magnitude higher than those of conventional servomotors. This means that the electromagnetic Harmonic Drive can be almost selected on the basis of an approximate match of the motor power capability to the load power requirement. This is in distinct contrast to conventional electric servomotors that frequently have to have a much higher power rating than would be indicated on the basis of the load power requirement.

Part I-2 of this Appendix continues with a discussion of several possible applications for the electromagnetic Harmonic Drive. A drive for a radar antenna to be used in a space vehicle is found to require so little power and acceleration capability that both conventional motors and electromagnetic Harmonic Drives can be used providing they can be built small enough. In another possible application the electromagnetic Harmonic Drive is shown to have bright prospects whereas a conventional electric motor would not be feasible. This application is the arm drive for a disc file (intermediate-access-time-memory device) for a digital data processing system. The third application is represented by the flap actuator for an air-to-air missile. In this application the electromagnetic Harmonic Drive is found to be capable of meeting the requirements with far less weight and space than a conventional electric servomotor. The general conclusion drawn from this study of the electromagnetic Harmonic Drive characteristics in relation to typical applications is that it has a unique advantage over conventional electric servomotors for driving loads requiring high accelerations but not requiring high velocities.

* This appendix was prepared by Dr. G. C. Newton, Jr.

The breadth of its field of application can be increased if the maximum speed of the output shaft can be increased, either through lower reduction ratios in the Harmonic Drive elements or through higher pulse frequencies for the magnets or both.

Appendix VII discusses in some detail certain design considerations for electromagnetic Harmonic Drives. A study is made of configurations of the magnets for use with a Harmonic Drive employing a 3.25 inch diameter flexspline. This study shows that a large amount of iron, relative to the amount of copper, theoretically should be used in the magnets in order to achieve maximum power rate.

I-2.1 Preferred Motion in Reluctance-Type Electromagnetic Actuators

In this section we explain the advantage, with respect to the achievement of high power rates, of the variable-gap reluctance type actuator, as used in the electromagnetic Harmonic Drive, over the constant-gap actuator used in other devices. Figure 68 shows a magnet configuration similar to that used in the electromagnetic Harmonic Drive (EHD). In this figure (A) is an end view showing the armature free to move in the lateral direction with the gap maintained constant. (B) is another end view corresponding to vertical motion of the armature such that the gap is variable. View (C) is a side view of the magnet. In all three views the coils are omitted. The legs will be assumed to have square cross sections of dimension b. The force acting on the armature at one pole for lateral motion will now be compared with a corresponding force for vertical motion. In making this comparison it is assumed that the core material has negligible reluctance relative to the gaps and that the magneto-motive force available $\mathcal{F}_m$ that is available from the coil produces a flux density just equal to $\mathcal{B}_m$, the saturation flux density of the core material, when the gap has a value g. For the case of lateral motion a force will be computed with the armature covering one half of a pole. (The force in this case is independent of the armature position to the degree that fringing effects are absent). For the vertical motion case the force is computed with the pole fully covered by the armature and the gap at the value g.

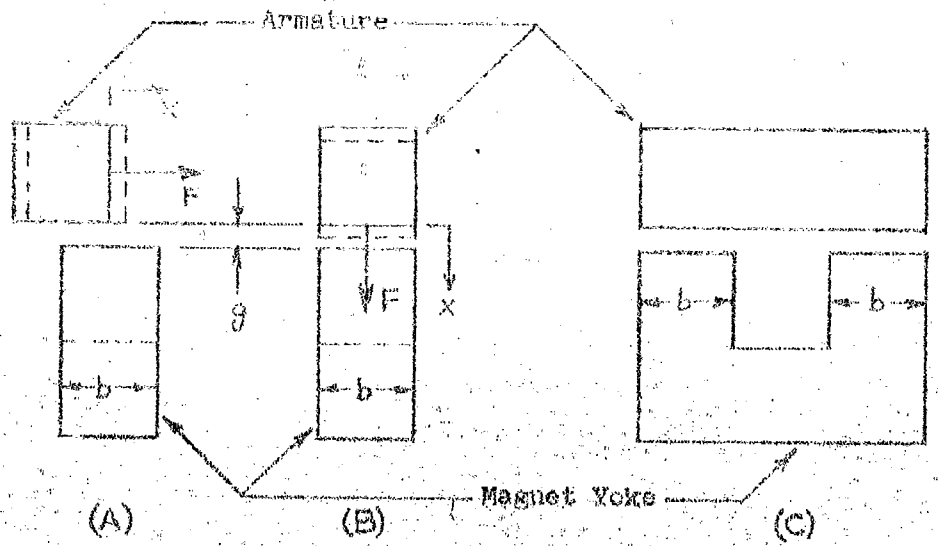

MAGNET AND TWO POSSIBLE ARMATURE MOTIONS

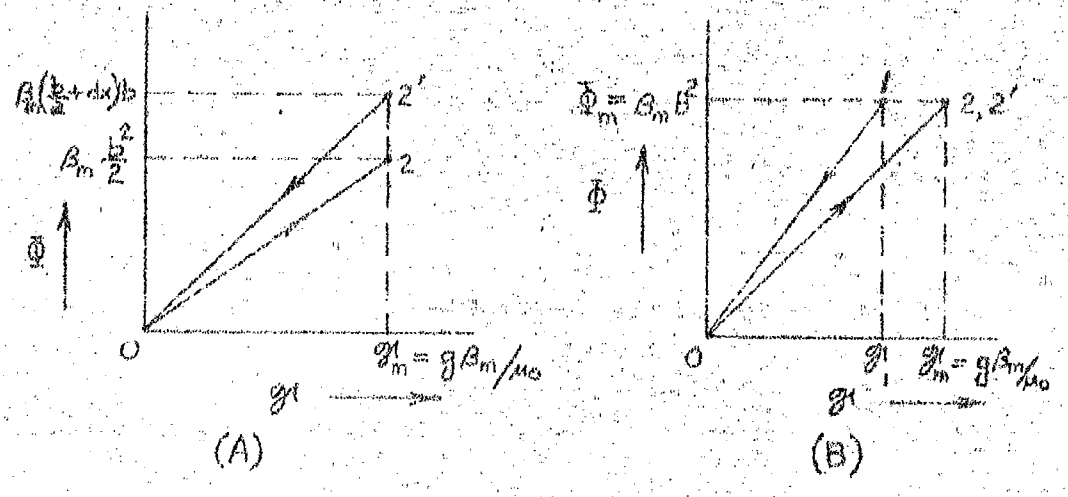

F = force
b = dimension of magnet
g = gap
x = direction of motion
$\mathcal{B}$ = flux density
$\mathcal{F}$ = magnetomotive force
Φ = lines of flux
μ_0 = permeability of free space (air)

FIGURE 68 - FLUX VERSUS MMF TRAJECTORIES FOR THE TWO FUNDAMENTAL TYPES OF ARMATURE MOTION

In general, the force acting on the armature can be computed from the area enclosed by the flux versus magnetomotive force trajectory. For a suitably chosen trajectory the area corresponds to the mechanical work produced. The electromechanical force is found by dividing the mechanical work by the incremental distance that the armature moved in order to form the loop in the trajectory. Figure 68 (A) and (B) show the trajectories for lateral and vertical motions of the armature. These trajectories are formed by raising the magnetomotive force (mmf) from zero to a maximum value, allowing a small motion dx to occur and then returning the magnetomotive force to zero. In the case of the lateral motion of the armature the flux increases from point 2 to 2' while the magnetomotive force is constant at its maximum value. For vertical motion of the armature the flux does not change and points 2 and 2' lie on top of one another. Until the magnetomotive force decreases to compensate for the gap reduction the iron remains saturated and the flux remains constant until point 1 is reached.

For lateral motion the mechanical work done by the armature on its environment is the area enclosed in the flux versus MMF trajectory of Figure 68 (A). That is, the mechanical work in a consistent set of units is equal to the area of the triangle symbol 0, 2, 2'. The equation for this area is

$$dW_m = 1/2\,(d\phi)\,\mathcal{F}_m' \qquad \text{(A1-1)}$$

Substituting in values for the flux change $d\phi$ yields

$$dW_m = 1/2\,(B_m\, b\, dx)\, g\, B_m/\mu_o \qquad \text{(A1-2)}$$

Dividing the work by the displacement dx gives the magnetic force F_m tending to drive the armature in a direction to increase x. This force is

$$F_m = 1/2\,\frac{B_m^2}{\mu_o}\, b g \qquad \text{(A1-3)}$$

In the case of vertical motion of the armature the flux density initially stays constant at its saturation value ϕ as explained above. Then as the magnetomotive force is further reduced the flux goes from point 1 in the figure to zero. The value of this magnetomotive force $\mathcal{F}_1$ that is necessary to produce saturation flux density across the reduced air gap is given by

$$\mathcal{F}_1 = (g - dx)(B_m/\mu_o) \qquad \text{(A1-4)}$$

The mechanical work done for the incremental displacement is the area of the triangle 0, 1, 2. Thus the mechanical work can be expressed as

$$dW_m = 1/2\,\phi_m(-d\mathcal{F}') \qquad \text{(A1-5)}$$

This can be expressed as

$$dW_m = 1/2\,B_m b^2\,\frac{B_m}{\mu_o}\,dx \qquad \text{(A1-6)}$$

so that the magnetic force tending to drive the armature in a direction to reduce the air gap becomes

$$F_m = 1/2 \frac{B_m^2}{\mu_o} b^2 \qquad (A1-7)$$

Comparison of the force for lateral motion (given by Equation A1-3) with that for vertical motion (given by Equation A1-7) shows that the former is smaller than the latter by the ratio of the gap dimension g to the leg width b. With a typical magnet, such as for the laboratory model of the electromagnetic Harmonic Drive, g is of the order of 0.020" and the leg width is of the order of 0.40". Thus the force level that is achievable with lateral motion is of the order of 1/20 of that which can be achieved by vertical motion. Since the armature mass is substantially the same for both kinds of motion it is evident that the force-squared-to-inertia ratio, or power rate, can be improved by a factor of the order of 400 by going from lateral motion to vertical motion for a typical magnet geometry.

This simplified example shows why conventional rotating electrical machinery with slotted iron rotors cannot possibly achieve power rates comparable to those possible with simple magnets of the variable-gap variety. The slots of the rotor moving past those of the stator in conventional machines are analogous to the lateral motion of the armatures of a plurality of magnets like those discussed above.

The knowledge that very high power rates can be achieved by limited-range, variable-gap movement of magnet armatures together with the fact that the Harmonic Drive converts limited-range, oscillatory motion into continuous rotation led to the proposed use of Harmonic Drive with electromagnetic actuation as a high power rate servomotor.

I-2.2 Characteristics of Electromagnetic Harmonic Drive Compared with Conventional Servomotors

Table XXIX compares electromagnetic Harmonic Drive data with information for two conventional servomotors.

	EHD, Stepping Field Type, Dp = 3¼ Inch		Diehl, Low Inertia 400 cps, 2 phase servomotors	
	EHD-3*	Maximum Theoretical Performance**	FFF-85-16-1 100 Watt	ZF105-2217-1 200 Watt
Average Stalled Torque, T_m (nm)	120	173	0.339	0.735
Average Torque T_M (nm)	60	129	0.226	0.530
Peak Speed, $\dot{\theta}_M$ (rad/sec)	2	2	523	534
Inertia, J_M (kg-m^2)	.0012	.0123	0.394×10^{-4}	1.21×10^{-4}
Peak Power P_M (watts)	115	260	118	283
Power Rate $\dot{P}_M$ (kw/sec)	310	1355	1.30	2.32
I^2R Loss (watts)	180	100	122	297
Total Mass (kg)	9	9	5.22	6.58

*Leg width of 0.5 inch
**Leg width of 0.8 inch - discussed in Section 4.3.1.

TABLE XXIX-COMPARISON OF EHD AND DIEHL SERVOMOTOR-EHD based on $\mathcal{P}_m = 2.0$ w/in^3

The characteristics shown in this table are those that are particularly useful for determining the size of servomotor required to drive a given load. The first column in this table gives data for the laboratory model that has been deduced from actual measurements. The second column lists the characteristics of a design for an electromagnetic Harmonic Drive which is representative of the maximum theoretical performance. Both designs use a 3.25 inch diameter flexespline. The basis for the second design is given in Appendix VII. The third and fourth columns of Table XXIX show the characteristics of typical low inertia servomotors of the 100 and 200 watt sizes, respectively.

The first row of Table XXIX lists the average stalled torque. In the case of the EHD devices the term average refers to the mean value over power angles between switching points. In view of the finite number of magnets, the power angle of the

device changes by discrete values each time a magnet is switched on. Between switching points the torque varies somewhat as the flexspline moves toward the position of the next switching point. The average stalled torque is the mean value of this variation with respect to angle. The second line in the table shows the average torque that is available at the peak speed rating shown in the third line. The peak speed for the EHD devices is related to the peak pulse frequency that can be used with the magnets. This frequency is established by the volt-ampere ratings of the semiconductor devices that are used for switching the magnet currents. For purposes of Table XXIX a 100 pulse per second frequency is assumed. This is the frequency that was actually achieved in the laboratory model. For two-phase servomotors the average torque and peak speed ratings are based on the point in the static torque-speed characteristic that corresponds to maximum power output. Somewhat higher power rates could be obtained with these motors by choosing a point on the torque-speed characteristics corresponding to a higher torque and a lower speed but this would be done at the expense of a reduced power rating. The line corresponding to the I^2R loss is the power dissipated in the magnets in the case of the electromagnetic Harmonic Drive. For the typical servomotor this figure corresponds to the total loss at maximum power output. The last line in the table gives the weight of the servomotors exclusive of electronics. For the electromagnetic Harmonic Drives the 9 kilogram figure is approximately the actual weight of the laboratory model. The "maximum theoretical" design will tend to be heavier on account of the larger amount of iron in the magnets but compensating changes can be made in the housing by thickness reduction so that the anticipated total weight will be substantially unchanged from the laboratory model.

From Table XXIX one observes that the electromagnetic Harmonic Drives tend to be low-speed, high torque devices when compared with typical servomotors. The power ratings of the EHD devices are comparable with Diehl type servomotors. With respect to power rate, however, the electromagnetic Harmonic Drives enjoy a marked advantage; this advantage is in the range of a factor of 100 to 200 in favor of the Harmonic Drives. Also, the I^2R loss of the Harmonic Drives can be made smaller than the corresponding loss in the two-phase servomotors without sacrifice of power rate or peak power. On the other hand, the electromagnetic Harmonic Drives compared to these servomotors are at a slight disadvantage with respect to weight.

The above comparison may be somewhat questionable since the EHD devices are basically stepping motors and therefore have a characteristic, not shown in Table XXIX, that is very different from the induction servomotors. This is the stepping action which makes the electromagnetic Harmonic Drives act something like synchronous motors except that they can go down to zero speed. Logical circuits have to be used to control the EHD

magnet currents. These logical circuits can be arranged to control the electromagnetic Harmonic Drives in a variety of ways. Open-loop incremental digital control of motor position can be used. Another alternative is to control the output speed by varying the frequency of an alternating input signal. With such an arrangement it is possible to form a closed-loop control of output position by using an error signal to control, either linearily or nonlinearily, the frequency of the signal put into the logical circuits.

In conclusion, the stepping characteristic of the electromagnetic Harmonic Drives can be a distinct advantage in situations involving digital control of shaft position or velocity. However, in other situations it may be a disadvantage because of the more complex motor control circuitry that is required.

I-2.3 Examples of Applications

In this section three possible applications for the electromagnetic Harmonic Drive are presented in order to gain insight into the applicability of this device to positional control systems. For each application the information needed to calculate servomotor size is assembled. Also for each application an estimate for the servo bandwidth is given. In the light of this information, the potential of the electromagnetic Harmonic Drive for each application is discussed.

The first application is an antenna drive for a space vehicle such as might be used for radar mapping of the Earth's surface or that of a nearby planet such as Venus. In order to map the surface the radar antenna must move through a scanning sequence of positions. In the particular example under consideration the antenna moves in discrete jumps of the order of a degree in angle between transmit pulses and is held approximately stationary during the transmission and reception of a pulse. In order to carry out this scanning sequence a servomechanism is used to drive the antenna. The load on this servomechanism is primarily the antenna inertia since the load torque caused by friction and windage is expected to be negligible in the space environment.

Table XXX, Column 1 gives the pertinent information concerning the antenna drive application.

	Antenna Drive	Arm Drive*	Missile Fin Drive
Inertia, J_L (kgm^2)	5.0	0.20	1.09×10^{-3}
Peak non-inertial torque, T_L (n-m)	Negligible	Negligible	51.5
Peak Acceleration, $\ddot{\theta}_L$ (rad/sec)	0.25	139	625
Peak Velocity, $\dot{\theta}_L$ (rad/sec)	0.10	8.33	10
Time Constant T_L (sec)	0.4	.0575	.016
Peak Load Power P_L (watts)	0.125	232	522
Minimum Motor Power Rate, $\dot{P}_{Mmin}$ (kw/sec)	1.25×10^{-3}	15.5	130.4
Bandwidth required, (rad/sec)	25	167	100
(cps	4	27	16

*Data for a hinged arm.

TABLE XXX - SPECIFICATIONS FOR THREE APPLICATIONS

The arm drive of a disc file memory unit is considered as the second possible application. Disc files (such as the IBM 1301) are used as random access memories for digital data processing systems. They have an access time intermediate to that of magnetic cores and magnetic tape. A typical disc file consists of a number of continuously rotating discs with magnetic material on the top and bottom surface of each. These are stacked with space between each on a common shaft. An arm or "comb" is used to position read-write heads at a selected radius above or below the surface of each disc. A positional servomechanism is used to select the appropriate tracks on the surfaces of the discs for writing in or reading out information. Of the order of 10^8 bits of information can be stored in approximately 100 track positions among the several discs. Access times of the order of 180 milliseconds are realized. In order to achieve access times of this order it is necessary to be able to position the arm from one extreme to the other in less than 120 milliseconds. The IBM 1301 file uses a fluid power servo drive which moves the arm in a linear fashion radially outward from the axis of rotation. Estimates of the peak power requirement for this type of control run in the neighborhood of 2 kilowatts. It appears that a considerable reduction in the peak power requirement can be achieved by arranging the

arm to rotate about a hinge point at a radius beyond the edge of the disc. The heads would then travel along an arc in a manner similar to a photogeneph pickup. Assuming that the arm is hinged, the specifications for the arm drive becomes as shown in column 2 of Table XXX.

As a third application a missile control surface or flap drive is considered. Data for an air-to-air missile is presented in column 3 of Table XXX. These data are those listed as Requirement B of Reference 8.

On the basis of the data presented in Table XXX, it is evident that the antenna drive can be handled readily by conventional electric motors as well as by the electromagnetic Harmonic Drive. The basic problem in this application is how to build a Harmonic Drive that would be small enough. For the antenna drive the stepping characteristic of the Harmonic Drive could be a distinct advantage since direct digital control could be used without the need for a feedback loop. This advantage might offset the excess size of the Harmonic Drive if it was found that it could not be scaled down to the power level indicated in Table XXX. Also, it should be noted that there is no difficulty in meeting the specified bandwidth of 25 radians per second.

The arm drive turns out to be an application requiring a relatively large power rate for the power level of the load. From Table XXIX it is seen that, provided some means of velocity matching is done, the "maximum theoretical" design of electromagnetic Harmonic Drive would more than meet the requirements of the arm drive application as shown in Table XXX. On the other hand, from these same tables it is seen that the Diehl low inertia servomotors in the 100 and 200 watt sizes cannot handle this application because of insufficient power rate. Thus the arm drive represents an application for which the electromagnetic Harmonic Drive appears to have a unique advantage since it can do the job within space and weight limitations that cannot possibly be met by conventional motors. Furthermore, direct digital control may be possible with the further advantage of eliminating the positional feedback loop. The only question concerning the use of the electromagnetic Harmonic Drive in this application is bandwidth. The bandwidth required is slightly greater than has been demonstrated to date on the laboratory model. However, further development may yield a bandwidth that will handle this application.

With respect to the third application, the missile flap drive, the information of Table XXX indicates a peak load power requirement of the order of 1/2 kilowatt. Conventional motors of this size would have inadequate power rates whereas the Harmonic Drive would possess more than adequate power rates. This means that the EHD will not need much excess power over the load power requirement in order to handle this load. This would be in distinct contrast to the conventional electric motor which would require a motor power rating many times the load power requirement in order to handle this application.

APPENDIX II

CENTRIFUGAL FORCE ON THE FLEXSPLINE

Centrifugal Force on the flexspline due to rotation of the mass of the armature, in those cases where it rotated, is given by

$$F_c = mr\dot{\theta}_M^2 \qquad \text{(A2-1)}$$

For the SF type SHD-3, at $\dot{\theta}_M$ = 30 rpm, for example

$$M = \alpha_M W_a = 2.08 \text{ kg} \qquad \text{(A2-2)}$$

$$r = \frac{Dp-b}{2} = 1.38" = 3.5 \times 10^{-2} \text{m} \qquad \text{(A2-3)}$$

$$\dot{\theta}_M = 30 \text{ rpm} = 3.15 \text{ rad/sec} \qquad \text{(A2-4)}$$

$$\therefore F_c = 0.23 \text{ n} = .051 \text{ lbs.} \qquad \text{(A2-5)}$$

which is negligible.

This will in general be true in all cases.

APPENDIX III

DEFLECTION FORCE

To calculate deflection force of a Harmonic Drive cup shape flexspline, the following basic formula can be used (All values here are in English units).

$$F_D = 0.56\, d\, E_y\, l\, w^3 \qquad \text{(A3-1)}$$

where $E_y = 30 \times 10^6$ (psi) for steel

l = length of a component segment (inch)

w = thickness of a component segment (inch)

This formula holds for two-lobe Harmonic Drive, which is planned for this device, but not three-lobe. The following calculations are for EHD-3. The value of d used will be for $P_D = 96$ pitch, and two-lobe Harmonic Drive.

$$d = \frac{2}{P_D} = \frac{2}{96} = .0208'' \qquad \text{(A3-2)}$$

The thickness of the topth bed, w_b, to avoid excessive stresses, is selected as

$$w_b = .030'' \qquad \text{(A3-3)}$$

It is believed that a tooth length of

$$l_b = \frac{D_p}{6} \qquad \text{(A3-4)}$$

is adequate, even when loaded to an average torque of $40D_p^3$. For the model the average torque is lower and the conclusion is even more conservative.

As F_D is seen to be inversely proportional to some positive power of D_p, not determined, whereas the magnetic force produced, F_M, is approximately directly proportional to D_p^2, in order to find the maximum value of F_D/F_M, the smaller D_p's should be examined. The values of F_D are obtained to be

	F_D	F_M	F_D/F_M
$D_p = 1\ 5/8''$	3.8	28	0.14
$D_p = 2''$	2.5	42	0.06

F_M was calculated for Dp = 3¼ inches in Section 4.3. It is here scaled down by the ratio of the diameters squared. For greater values of Dp, the ratio F_D/F_M becomes smaller and F_D even more negligible.

Because of possible shape distortion in the flexspline resulting in loss of deflection, it is wise to consider that F_D may have to be slightly greater. In the case of type EHD-3, the rubber tubing increases the stiffness slightly more. Allowing a margin of about 70% for these effects, the following ratios of F_D/F_M are believed adequate:

$$F_D/F_M = 0.1 \qquad 2'' \leqslant D_p \qquad \text{(A3-5)}$$

$$F_D/F_M = 0.25 \qquad 1\tfrac{5}{8}'' \leqslant D_p < 2'' \qquad \text{(A3-6)}$$

For Dp below 1 5/8", F_D/F_M rises at a steep rate.

Calculations for the RF types would be very similar.

APPENDIX IV

INERTIAL FORCE ON THE FLEXSPLINE

A distributed inertia force is produced on the flexspline due to the acceleration of its equally distributed mass. The force has sinusoidal distribution when there is true harmonic motion, with the maximum value in the outward direction occurring at the major axis. This force counteracts the tooth separating and deflection force which also have maximum values at the same point. The value of inertia force is directly proportional to the square of the speed and the first power of the mass and the ratio. The inertia force is greater than for conventional Harmonic Drive units. It was realized that the torque output is proportional to the mass of the armatures which move with the flexspline, and to obtain useful torques this mass is, in general, greater than the mass of the outer race and other elements that move with the flexspline. For example, at 30 rpm, a unit with the characteristics of the model EHD-3 would experience an average inertia force of 8 pounds at the major axis, derived as follows

$$r = \frac{D_p}{2} + \frac{d}{2} \sin 2 R_g \dot{\theta}_o t \qquad \text{(A4-1)}$$

$$r = \frac{D_p}{2} + \frac{D_p}{2R_g} \sin 2 R_g \dot{\theta}_o t \qquad \text{(A4-2)}$$

$$\ddot{r} = -\frac{D_p}{2R_g} (2 R_g \dot{\theta}_o)^2 \sin 2 R_g \dot{\theta}_o \qquad \text{(A4-3)}$$

$$\ddot{r}_m = -2 D_p R_g \dot{\theta}_o^2 \qquad \text{(A4-4)}$$

$$\dot{\theta}_o = 30 \text{ rpm} = 3.15 \text{ rad/sec.} \qquad \text{(A4-5)}$$

$$R_g = 156 \qquad \text{(A4-6)}$$

$$D_p = 3.25" = .0825 \text{ m} \qquad \text{(A4-7)}$$

$$\therefore \ddot{r}_m = 260 \text{ m/sec}^2 \qquad \text{(A4-8)}$$

The mass of the armature laminations associated with one magnet is, from Figure 69

$$M_a = 0.13 \text{ kg} \qquad \text{(A4-9)}$$

Thus, the inertia force for these elements centered at the major axis is somewhat less than

$$F_I \approx \ddot{r} M_a = 34 \text{ n} = 8 \text{ lbs.} \qquad \text{(A4-10)}$$

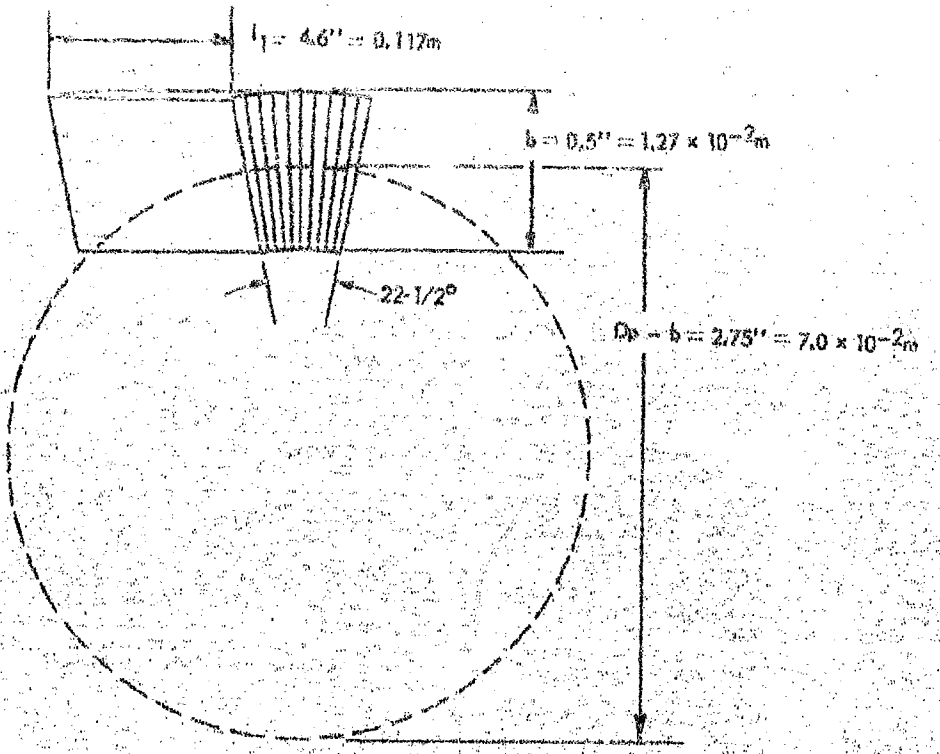

Mass of this element, $Ma = \rho\, Va$

Volume of this element, $Va = l_1\, b\, (Dp - b)\, S_3$

Stacking Factor, $S_3 = \frac{Dp-2b}{Dp-b} = \frac{2.25}{2.75} = 0.8$

Density, ρ for iron laminations = 7.82×10^3 kg/m^3

$Ma = \rho\, S_3\, l_1\, b\, (Dp-b) = 0.13$ kg

FIGURE 69 MASS OF THE ARMATURE ELEMENT ASSOCIATED WITH ONE MAGNET, MODEL EHD-3

APPENDIX V

DERIVATION OF THE MAGNETIC FORCE FORMULA

In general the magnet may be considered to consist of a fixed yoke which, by the impressed current through its coils, is a source of MMF, and a movable armature. The space between one pole face of the magnet and the armature is air with permeability μ_0, between the other pole face and the armature is a powder of permeability μ_1. See Figure 70 (A). As a special case the armature may hinge so that as the air gap closes there is no enlarging space behind. See Figure 70 (B). For this case, the same formulas hold when one takes the limit as $\mu_1 \sim \mu_0 \rightarrow \mu_1$.

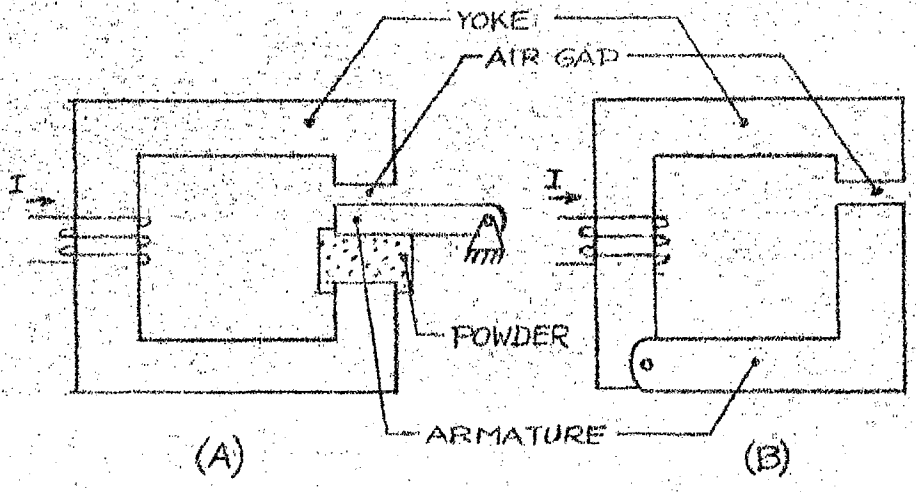

FIGURE 70 TWO BASIC TYPES OF ELECTROMAGNETS

The following derivation is based on Reference 10, pages 196-202. The simplifying assumption is made that armature movement is negligible during the increase of MMF up to the level of consideration. First consider the special case.

The current I flowing through the coil of N turns creasts MMF equal to

$$\mathcal{F} = N I \qquad \text{(A5-1)}$$

This magnetomotive force creates magnetic lines of flux Φ in accordance with the relation

$$\Phi = \frac{\mathcal{F}}{\mathcal{R}} \qquad \text{(A5-2)}$$

For air gaps greater than a few thousands of an inch and small yokes of reasonable cross-sectional area and highly permeable

material, virtually no MMF is dropped within the yoke so that the air gap reluctance determines the flux. As current changes, so does MMF and Φ. Due to armature movement and hysteresis of the iron the changes describe a path such as is shown in Figure 71. The energy within the circuit is equal to the area under the

$\mathcal{F} - \Phi$ curve.

In reference 10, the author explains that dW_{mg}, the area of the loop, can rather laboriously be shown to be equal to

$$dW_{mg} = \tfrac{1}{2}(\mathcal{F}_c + \mathcal{F}_m)\, d\Phi \qquad (A5\text{-}3)$$

Realizing that

$$\mathcal{F}_c \ll \mathcal{F}_m \qquad (A5\text{-}4)$$

and that, for fringing neglected,

$$d\Phi = A_Q\, dB \qquad (A5\text{-}5)$$

Equation A5-3 can be written

$$\frac{dW_{mg}}{dx} = \frac{A_Q}{2}\, \mathcal{F}_m\, \frac{dB}{dx} \qquad (A5\text{-}6)$$

Using the definition of permeance

$$\mathcal{P} = \frac{\Phi}{\mathcal{F}} = \frac{BA_Q}{\mathcal{F}} \qquad (A5\text{-}7)$$

or in differential form for constant MMF

$$d\mathcal{P} = \frac{d\Phi}{\mathcal{F}} = \frac{A_Q\, dB}{\mathcal{F}} \qquad (A5\text{-}8)$$

and

$$F_1 = \frac{dW_{mg}}{dx} \qquad (A5\text{-}9)$$

where F_1 is the instantaneous magnetic force, one obtains the general force formula

$$F_1 = \tfrac{1}{2}\, \mathcal{F}^2\, \frac{d\mathcal{P}}{dx} \qquad (A5\text{-}10)$$

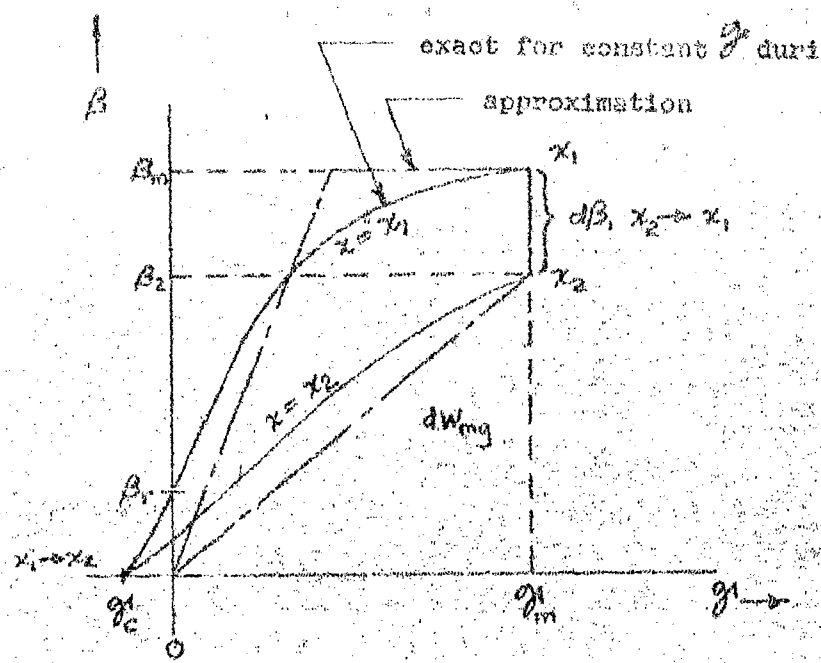

W_{mg} = work done by the magnet
$\mathcal{F}$ = magnetomotive force
$\mathcal{B}$ = flux density
x = distance
$\mathcal{F}_c$ is the reverse MMF force necessary to remove the residual flux density

FIGURE 71 FLUX DENSITY VERSUS MMF LOOP FOR DERIVING THE MAGNETIC FORCE, BASED ON CONSTANT MMF DURING MOTION

The numbers represent the armature posotions referred to in the report. For approximate analyses the simplier approximation is often taken, based on constant permeability up to $\mathcal{B}_m$ and zero incremental permeability thereafter.

For the special case of parallel plane surfaces with flux passing normally between the surfaces, with fringing neglected, for a specific air gap of x_2

$$\mathcal{P} = \frac{\mu_0 A_a}{x_2} \tag{A5-11}$$

$$\frac{d\mathcal{P}}{dx} = -\frac{\mu_0 A_a}{x_2^2}\frac{dx_2}{dx} \tag{A5-12}$$

Now, in order to produce output work from the magnetic cycle, it is necessary that the gap decrease while the MMF is acting, hence:

$$dx_2 = -dx \tag{A5-13}$$

Use is made of the fundamental relationship between magnetic field intensity and flux density.

$$\beta = \mu_0 H = \frac{\mu_0 \mathcal{F}}{x_2} \tag{A5-14}$$

which can be applied here assuming that the gap x_2 is large enough that the reluctance of the iron path is negligible and all the MMF is dropped in the gap.

Combining these expressions one obtains:

$$F_1 = \frac{\beta^2 A_a}{2\mu_0} \tag{A5-15}$$

which is the desired result.

It should be noted that β increases during the stroke so that F_1 will also. If fringing again is neglected, the above formulas show that $\mathcal{P}$ and β increase linearly with decreasing gap, and so F_1 should increase parabolically. From this concept a value for average force could be obtained. Considering the many approximations made, it is worth while to make one more and assume that during the working stroke

$$d\beta \to 0 \tag{A5-16}$$

which is the limit approached with a magnetic material which has a very sharp break in $\mathcal{B}$ vs. $\mathcal{F}$ at the knee of the curve. Then the average force would be equal to the instantaneous force given above. This approach will be followed with constant realization of the assumptions made. Thus $\beta = \beta_m$ and

$$F_{a_1} = \frac{\beta_m^2 A_a}{2\mu_0} \tag{A5-17}$$

Now if consideration is taken for when μ is not $\gg \mu_0$, there is a loss of force due to the fact that additional iron must be magnetized as the air gap decreases. Note that this is not the case when the path length of the powder stays the same, as with a solenoid type device in which the flux makes a small loop through powder behind and moving with a keeper piece.

The loss of forces is given by: (Reference 10, page 200)

$$F_{Q_2} = A \int_0^{B_m} H \, dB \qquad \text{(A5-18)}$$

This formula is derived for the case of iron plungers, where fringing outside the plunger is negligible and is considered discontinous at the boundary of A. Since μ for the powder is much closer to μ of air than of iron, there is no distinct boundary, and if A is taken as A_Q, F_{Q_2} may be less than actually is obtained. Furthermore, the integral is a function of how close to saturation is the value of B_m. To simplify the above and to attempt to retain approximate accuracy, also in recognization of the generally expected spacing between stator poles and the axial length of the stator, consider that:

1. The integral is taken as the area of a triangle of value

$$\int_0^{B_m} H \, dB = \int_0^{B_m} B/\mu_1 \, dB = B_m^2/2\mu_1 \qquad \text{(A5-19)}$$

where μ_1 is the slope of line from the origin to the saturation point. (See Figure 72)

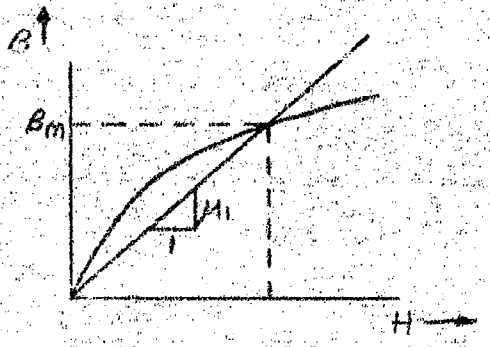

FIGURE 72 - MAGNETIC DIAGRAM FOR FORCE-LOSS CASE

2. Take $A = A_Q$ (A5-20)

Hence $F_{Q_2} = \dfrac{B_m^2 A_Q}{2\mu_1}$ (A5-21)

Note that F_{Q_1} and F_{Q_2} are not directly dependent on the gap lengths. However, this figures in the requirement for ϕ'. The net force is thus, for a decrease in air gap:

$$F_{Q_3} = F_{Q_1} - F_{Q_2} = \frac{\beta_m^2 A_Q}{2}\left[\frac{1}{\mu_0} - \frac{1}{\mu_1}\right] \qquad (A5\text{-}22)$$

$$= \frac{\beta_m^2 A_Q}{2\mu_0}\left[\frac{\mu_1 - \mu_0}{\mu_1}\right]$$

or $$F_{Q4} = K_1 F_{Q_1} \qquad (A5\text{-}23)$$

where $K_1 = \frac{\mu_1 - \mu_0}{\mu_1}$ a modifying factor which is < 1. (A5-24)

This Document Reproduced From Best Available Copy

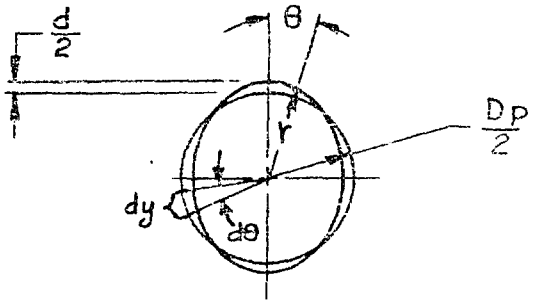

y = CIRCUMFERENCE OF ELLIPTOID FOR ANGLE θ
y_o = CIRCUMFERENCE OF CIRCLE FOR ANGLE θ
$\Delta y = y - y_o$
D_P = PITCH DIAMETER
d = HARMONIC DRIVE TOTAL RADIAL DEFLECTION
r = RADIUS AT ANY POINT

FIGURE 73 NOMENCLATURE FOR DERIVATION OF TANGENTIAL COMPONENT OF HARMONIC MOTION

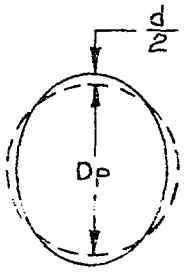

(A) "IDEAL" SHAPE

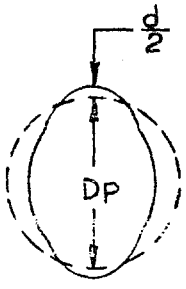

(B) DISTORTED SHAPE

FIGURE 74 FLEXSPLINE SHAPES

Preceding Page Blank

It can be shown that the position of the particle in the tangential direction is as follows:

$$dy = r\,d\theta = \left(\frac{D_p}{2} + \frac{d}{2}\cos 2\theta\right) d\theta \qquad \text{(A6-6)}$$

$$y = \int_0^\theta r\,d\theta = \frac{D_p}{2}\theta + \frac{d}{2}\int_0^\theta \cos 2\theta\, d\theta$$

$$= \left[\frac{D_p\theta}{2} + \frac{d}{4}\sin 2\theta\right]_0^\theta \qquad \text{(A6-7)}$$

Define

$$y_o = \left[\frac{D_p}{2}\theta\right]_0^\theta \qquad \text{(A6-8)}$$

$$\therefore \Delta y = y - y_o = \left[\frac{d}{4}\sin 2\theta\right]_0^\theta \qquad \text{(A6-9)}$$

which can be written as

$$\Delta y = \frac{d}{4}\sin 2(\psi - R_g\theta_M) \qquad \text{(A6-10)}$$

The time derivative is

$$\frac{d\Delta y}{dt} = \dot{y} = \frac{-d}{2}\cos 2\theta = \frac{-d}{2}R_g\cos 2(\psi - R_g\theta_M)\dot{\theta}_M \qquad \text{(A6-11)}$$

The generalized velocity of a point on the pitch line would then be

$$\dot{z} = (\dot{r}^2 + \dot{y}^2)^{1/2} =$$

$$= d^2R_g^2\dot{\theta}_M\left\{\left[\sin 2(\psi - R_g\theta_M)\right]^2 + \frac{1}{4}\left[\cos 2(\psi - R_g\theta_M)\right]^2\right\}^{1/2} \qquad \text{(A6-12)}$$

This mean kinetic energy associated with a particular magnet armature is the kinetic energy averaged with respect to ψ. The total mean kinetic energy W for a group of n_M armatures spaced at equal angles around the flexspline is n_M times the mean kinetic energy of one. Thus

$$W = \frac{n_M}{2\pi}M_a\int_{-\pi/2}^{\pi/2}\dot{z}^2(\psi, \theta_M)\,d\psi \qquad \text{(A6-13)}$$

Substituting the value for $\dot{Z}$ into equation A6 13 yields

$$W = \left\{ \frac{n_M}{2\pi} M_a R_g^2 d^2 \int_{-\frac{\pi}{2}}^{\frac{\pi}{2}} \left[\sin 2(\Psi - R_g \theta_M) \right]^2 + \frac{1}{4} \left[\cos 2(\Psi - R_g \theta_M) \right]^2 \right\} \dot{\theta}_M^2 \qquad \text{(A6-14)}$$

The integral evaluates to be $\frac{5\pi}{8}$ so that

$$W = \frac{5}{16} n_M M_a R_g^2 d^2 \dot{\theta}_M^2 \qquad \text{(A6-15)}$$

and

$$J = \frac{2W}{\dot{\theta}_M^2} = \frac{5}{8} n_M M_a R_g^2 d^2 \qquad \text{(A6-16)}$$

Noting that for Harmonic Drive $R_g d = D_p$ one obtains

$$J = \frac{5}{32} n_M M_a D_p^2 \qquad \text{(A6-17)}$$

or

$$J = \frac{5}{8} \rho V D_p^2 \qquad \text{(A6-18)}$$

where $V = n_M V_a$ (A6-19)

is the circumscribing volume of the entire cylinder of flexible elements.

In the absence of accurate information on distorted wave shapes, the following wave shape, under condition of full load torque, has been used for purposes of calculating forces.

$$\left.\begin{aligned} f(\theta) &= -1, && -\tfrac{\pi}{2} < \theta \leq -\tfrac{5\pi}{16} \\ f(\theta) &= \cos 4\left(\theta + \tfrac{\pi}{16}\right), && -\tfrac{5\pi}{16} < \theta \leq -\tfrac{\pi}{16} \\ f(\theta) &= +1, && -\tfrac{\pi}{16} < \theta \leq 0 \\ f(\theta) &= \cos 4\theta, && 0 < \theta \leq \tfrac{\pi}{4} \\ f(\theta) &= -1, && \tfrac{\pi}{4} < \theta \leq \tfrac{\pi}{2} \end{aligned}\right\} \qquad \text{(A6-20)}$$

For angles outside this range the function is given by

$$f(\theta) = f(\theta - \pi) \qquad \text{(A6-21)}$$

Figure 74 shows the "ideal" and distorted flexspline shapes. The various functions of the above equations are then substituted into the expression for kinetic energy, which, in this case, is simplified by neglecting the $\dot{y}$ component of $\dot{Z}$. The new integral evaluates to be π, so that

$$W = \frac{1}{2} n_M M_a R_g^2 d^2 \dot{\theta}_M^2 \qquad \text{(A6-22)}$$

$$J = n_M M_a R_g^2 d^2 = \rho V D_p^2 \qquad \text{(A6-23)}$$

which, based upon the simplifying assumption, can be considered roughly twice that for the ideal shape. We, therefore, conclude that the moment of inertia at the output shaft that is contributed by the magnet armatures is a function of the flexspline shape and that distortion caused by load forces may increase the effective inertia considerably.

In order to account for variations in flexspline shape, the moment of inertia of the magnet armatures will be expressed as

$$J_a = \frac{5}{8}\eta_S n_M M_a R_p^2 d^2 = \frac{5}{8}\eta_S \rho V D_p^2 \qquad (A6-24)$$

where η_S is a factor (larger than 1) that accounts for the increase in the inertia that is associated with distortion from the "ideal" shape.

Lever Type Elements

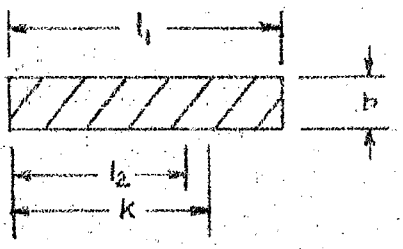

FIGURE 75 - LEVER TYPE ELEMENT

Consider that each lever of length l_1 and width b pivots at its left end, bearing against the inside of the tooth bed at l_2 (Figure 75). The inertia of the element rotating at the pivot is, by the transfer theorem

$$J_p = J_o + M\left(\frac{l_1}{2}\right)^2 \qquad (A6-25)$$

Where J_o is the inertia through the centroid, which is at $l = l_1/2$ for the symmetrical shape assumed. From texts on mechanics (Reference 11)

$$J_o = \frac{1}{12} M(l_1^2 + b^2) \qquad (A6-26)$$

Hence

$$J_p = \frac{1}{12} M(l_1^2 + b^2) + \frac{1}{4} M l_1^2 \qquad (A6-27)$$

The radius of gyration, k, is calculated as

$$k = \left(\frac{J_p}{M}\right)^{1/2} = \left[\frac{1}{12}(l_1^2 + b^2) + \frac{1}{4} l_1^2\right]^{1/2} = \left[\frac{1}{3} l_1^2 + \frac{1}{12} b^2\right]^{1/2} \qquad (A6-28)$$

For model EHD-3

$$l_1 = 4.6" \tag{A6-29}$$

$$b = 0.5" \tag{A6-30}$$

So that the term containing b is negligible, and

$$k = \frac{\sqrt{3}}{3} l_1 = 0.578\, l_1 = 2.66" \tag{A6-31}$$

Inertia of a Prestressed Ring

A similar type of analysis can be made of the prestressed ring to calculate its inertia. Inertia is a function of the fifth power of the pitch diameter. Its relative magnitude is somewhat greater than the other elements of EHD, but far less than conventional devices.

Increase in Inertia Due to Excessive Kinetic Energy

The magnetic forces developed by the various EHD models produce forces which are other than harmonic in wave form. They do not give true harmonic motion to the armature. For the SF type the forces are more nearly constant, after the flux rise time, resulting in high terminal velocities when the gap closes, and excessive kinetic energy over what is required. For the RF types the forces act over twice the 90° angle required for ideal harmonic motion. A calculation of this is carried out here for model EHD-3. Refer to Figure 76 for a comparison of the two wave forms and the kinetic energies of each during their respective working strokes.

In both wave forms the unidirectional magnetic forces do not start to act until the flexspline is past mid-deflection (depending on the maximum allowable power angle). But the simplifying assumption is made that the acceleration upon the armature is sinusoidal during the entire return stroke for both wave forms. Since the armature levers are connected somewhat by the rubber tubing as well as by the flexspline this is a reasonable approach. The tangential component of velocity during the step-force motion is also neglected.

A power angle of $\sigma_m = 27°$ is used as in Section 4.3.2

For the sinusoidal-force wave form the working stroke t_{w_1} is taken as

$$t_{w_1} = \frac{\sigma_m}{45°}\left(\frac{t_s}{2}\right) = 0.3\, t_s \tag{A6-32}$$

$$\therefore W_1 = \frac{0.3 t_s}{2\, t_s}\left(\frac{1}{16}\right) J_a \theta_M^2 = 4.7 \times 10^{-3} J_a\, \delta_M^2 \tag{A6-33}$$

SINUSOIDAL FORCES

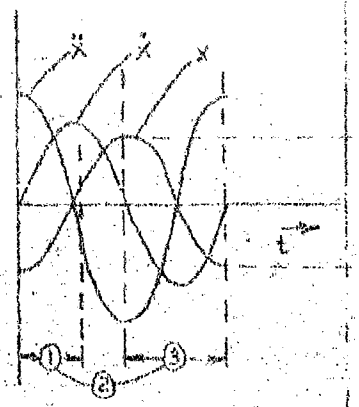

$$W_1 = \frac{t_{W1}}{2t_s} \times \frac{1}{16} \times \frac{J_a \dot{\theta}_m^2}{2}$$

STEP FORCES

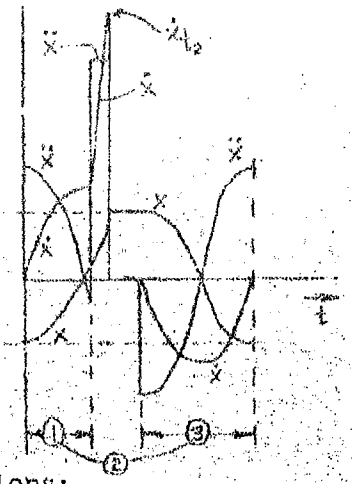

Assumptions:

- Flux rise time is neglected
- The average velocity $\bar{\dot{x}}$ is $\frac{1}{2}$ the maximum velocity at impact

$$\bar{\dot{x}} = \tfrac{1}{2}\dot{x}_m$$

$$\bar{\dot{x}}^2 = \tfrac{1}{4}\dot{x}_m^2$$

$$W_2 = \tfrac{1}{2} M_a \bar{\dot{x}}^2$$

but $$\dot{x}_m^2 = \frac{2F_M}{M_a} x t_{W_2}$$

Hence $$W_2 = \tfrac{1}{4} F_M x t_{W_2}$$

Definitions and Assumptions

1. Working Stroke, t_W
2. Return stroke
3. One half a harmonic period, t_s

W_1 is the kinetic energy of the armature associated with one magnet during the sinusoidal working stroke.

W_2 is the kinetic energy of the armature associated with one magnet during the step-force working stroke.

It is assumed that the kinetic energy during the return stroke is the same for each case - 16 magnets.

FIGURE 76 KINETIC ENERGY OF ARMATURE ELEMENTS FOR MODEL EHD-3 AS AFFECTED BY THE WAVEFORM OF MOTION

From Section 4.3.2

$$J_a = 89 \times 10^{-4} \text{ Kg-m}^2 \tag{A6-34}$$

$$\therefore W_1 = 4.2 \times 10^{-5} \dot{\theta}_M^2 \text{ n-m} \tag{A6-35}$$

For the step-force waveform, for $\delta_m = 27^\circ$

$$x_{t_{W_2}} = \frac{d}{2} \cos 2\delta_m \tag{A6-36}$$

The average d per air gap is about .030" = 7.6×10^{-4} m

$$\therefore x_{t_{W_2}} = 2.2 \times 10^{-4} \text{m} = .008" \tag{A6-37}$$

From Section 4.3.2 $F_M = 500$ newtons

$$\therefore W_2 = \frac{1}{4} F_M x_{t_{W_2}} = 2.8 \times 10^{-2} \text{ n-m} \tag{A6-38}$$

However, as there are 8 working strokes for the entire device per a harmonic period, the time between start of strokes is $t_s/4$, and the average kinetic energy is given by

$$\overline{W_2} = \frac{t_{W_2}}{t_{s/4}} (W_2) \tag{A6-39}$$

To find t_{W_2} use

$$x_{t_{W_2}} = \frac{F_M}{M_a} \frac{t_{W_2}^2}{2} \tag{A6-40}$$

Hence $$t_{W_2} = \left[\frac{2 M_a x_{t_{W_2}}}{F_M} \right]^{1/2} \tag{A6-41}$$

From Figure 69

$$Ma = 0.13 \text{ kg} \tag{A6-42}$$

$$\therefore t_{W_2} = 3.4 \times 10^{-4} \text{ sec.} \tag{A6-43}$$

t_s depends on operating speed.

$$t_s = \frac{1}{2} \left(\frac{1}{f} \right) = \frac{1}{2 R_g \left(\frac{\dot{\theta}_M}{2\pi} \right)} = \frac{\pi}{156 \dot{\theta}_M} \tag{A6-44}$$

$$\overline{W_2} = 4.7 \times 10^{-4} \dot{\theta}_M \tag{A6-45}$$

The increase in kinetic energy, for all 16 magnets, is

$$\Delta W = 16(\bar{W}_2 - W_1) = 7.5 \times 10^{-3} \dot{\theta}_M - 6.7 \times 10^{-4} \dot{\theta}_M^2 \qquad \text{(A6-46)}$$

Hence the increase in inertia is

$$J = \frac{2\Delta W}{\dot{\theta}_M^2} = \frac{1.5 \times 10^{-2}}{\dot{\theta}_M} - 1.3 \times 10^{-3} \ kg\text{-}m^2 \qquad \text{(A6-47)}$$

It is seen that this depends on speed. For typical speeds of interest Table XXXI presents the results.

$\dot{\theta}_M$ rad/sec	RPM	ΔJ	New Ja	Percent of Ja for Sinusoidal Force
1	9.5	1.4×10^{-2}	2.3×10^{-2}	260%
2	19	0.6×10^{-2}	1.5×10^{-2}	167%
3	29	0.4×10^{-2}	1.3×10^{-2}	145%
4	38	0.2×10^{-2}	1.1×10^{-2}	122%

TABLE XXXI - INCREASE IN INERTIA DUE TO EXCESSIVE KINETIC ENERGY

This means that the inertia associated with radial motion of the armatures based on step forces is 2.6 times as large at 9.5 RPM, 1 2/3 rds as large at 19 RPM, the approximate rated speed, and 1.45 as large at 29 RPM.

Experimental Methods of Calculating Inertia

The following discussion relates to model EHD-3. The procedure is to perform a transient test either loaded or unloaded, and make certain measurements for use with the following formulas.

By basic definition of velocity and acceleration

$$\dot{\theta}_M = \frac{d\theta_M}{dt} \qquad \text{(A6-48)}$$

thus

$$\dot{\theta}_M = \int \ddot{\theta}_M \, dt \qquad \text{(A6-49)}$$

and for the condition $\dot{\theta}_M = 0$ at $t = 0$

$$\dot{\theta}_M = \int_0^{t_1} \ddot{\theta}_M \, dt \qquad (A6\text{-}50)$$

Because $\dot{\theta}_M$ is more likely to be zero at the start of a step (i.e., end of the succeeding step), when there is no load inertia, this is probably an advantage of making the test this way. Now

$$\ddot{\theta}_M = \frac{T_a}{J} \qquad (A6\text{-}51)$$

T_a = accelerating torque
J = inertia

So that

$$\dot{\theta}_{M_{t_1}} = \int_0^{t_1} \frac{T_a}{J} \, dt \qquad (A6\text{-}52)$$

Even though, due to non-harmonic motion of the armature pieces under the influence of constant accelerating forces, inertia may fluctuate, the primary concern is with its effective value during operation; thus it will be treated as a constant.

Hence

$$J = \frac{1}{\dot{\theta}_{M_{t_1}}} \int_0^{t_1} T_a \, dt \qquad (A6\text{-}53)$$

Thus, to proceed further, a value for torque is needed. This is determined as a function of the following:

1. The flux density taken for saturation, provided that the MMF is sufficient.
2. The current and flux rise time.
3. The angular movement during the rise time.
4. Existence of a frictional load, and whether or not it is coulomb or viscous or both.
5. Shape distortions that may increase the effective power angle and influence fringing and increase reluctance, during dynamic operation.

The simpler case is that of no or negligible frictional load, which is thus a wise choice for the inertia measurement.

In this case, the torque versus angle function for a 15 magnet device, neglecting current rise time, is as shown in Figure 77, where the device steps to produce zero torque output.

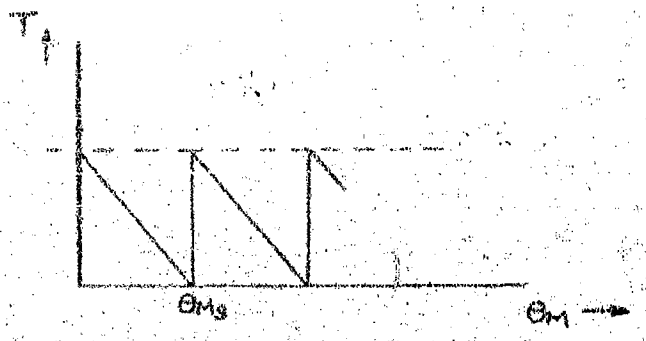

FIGURE 77 - TORQUE VS. ANGLE FUNCTION

If this were the torque acting, the resulting motion would be that of a damped sinusoid; where the response after t_s is rather indeterminant due to non-linearities, the motion would appear as in Figure 78.

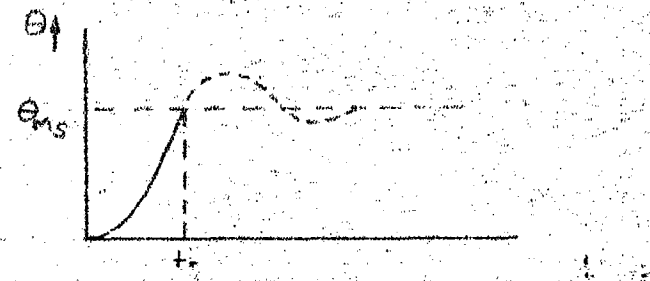

FIGURE 78 - DAMPED SINUSOIDAL MOTION

Using the expression

$$Ta = T_p\left(1-\frac{\theta_M}{\theta_{M_s}}\right) \qquad \text{(A6-54)}$$

Tp = peak torque

θ_{M_s} = one step angle

there results

$$J = \frac{T_p}{\dot{\theta}_{M_{t_s}}}\left[\int_0^{t_s}\left(1-\frac{\theta_M}{\theta_{M_s}}\right)dt\right] = \frac{T_p}{\dot{\theta}_{M_{t_s}}}\left[t_s - \frac{1}{\theta_{M_s}}\int_0^{t_s}\theta_M\,dt\right] \qquad \text{(A6-55)}$$

By the use of a good linear variable differential transformer, if the response of θ versus t were obtained, the area under the curve up to t_s, the end of the step, would equal the above integral. $\theta_{M_{t_s}}$ could be measured as the slope of θ_M versus t at t_s. A value of Tp is selected as discussed before.

Next consider the effect of flux rise time. There will be some motion during this time, and as a result, the maximum torque at the end of the rise must be somewhat less than if there were no motion. Since torque depends on flux, which itself depends on current as well as gap length (up to saturation), it should be possible to plot torque versus time during the rise. Current versus time for fixed inductance would be exponential, but inductance increases as the gap closes ($L = N \frac{d\phi}{dt}$); also reluctance decreases, increasing flux; torque is proportional to flux density squared. It is seen that this becomes rather complex. If the flux produced by specific currents at specific gaps were known, a measurement of current rise time could be used with a measurement of step angle versus time to give the angle at the end of the rise, and thus the peak torque could be taken from the proceeding relationship of torque to position. The procedure then might be to break the integral into two parts:

1. Assume some function (most simply straight line) of T versus t during the rise time.
2. Measure $\int \theta_M dt$ for the remaining portion and manipulate as discussed above.

A simpler approach is as follows. The θ_M versus t response curve will not depart drastically from a sinusoid, even with current and flux rise time considered, since the angle at the end of the rise will not be a large percentage of a step for rise time not greater than about 1/2 the total step time. (Figure 79). This seems to be a reasonable situation based on the potentiometer-measured response and current measurements.

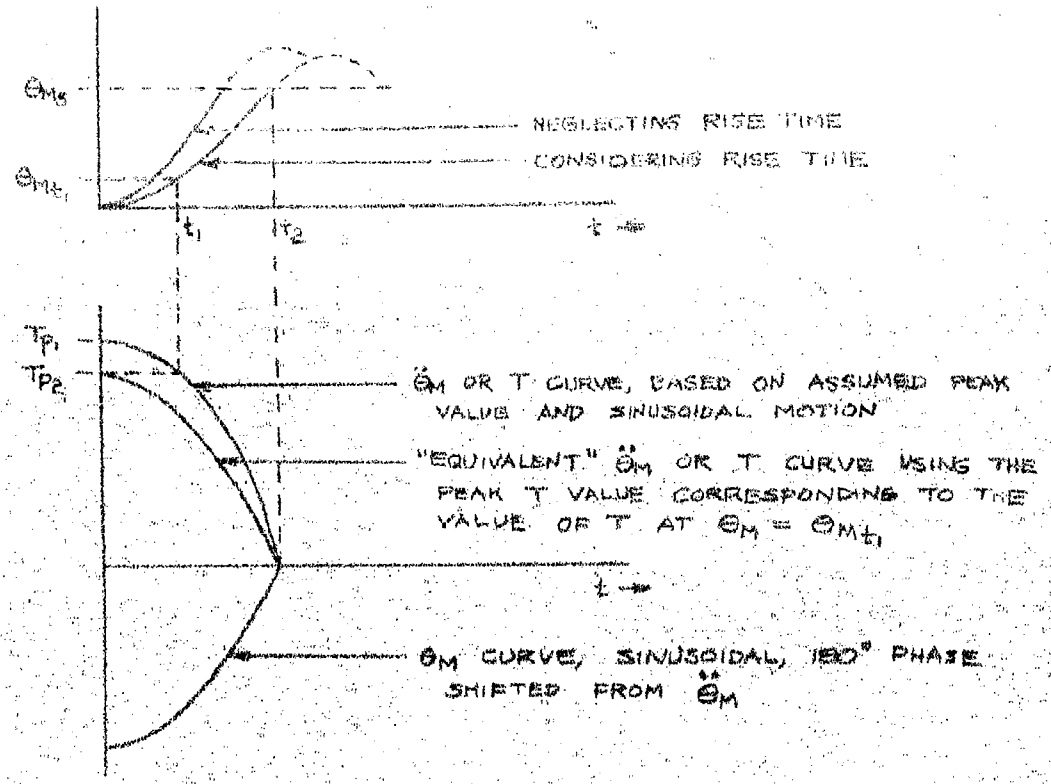

FIGURE 79 - SINUSOIDAL APPROXIMATIONS

The method used for measuring output position with a potentiometer, even though it is an infinite resolution film type, is limited in its capability to indicate the time for a single step which is necessary for the analysis, but approximate responses were obtained.

For example, for a step response time of

$$t_2 = .002 \text{ sec} \tag{A6-56}$$

Assume that peak torque is

$$T_{P_1} = 83 \text{ n-m} = 740 \text{ lb-in} \tag{A6-57}$$

Flux rise time was typically

$$t_1 = .001 \text{ sec} \tag{A6-58}$$

From Figure 30

$$\theta_{M_{t_1}} \approx \frac{1}{5} \theta_{M_S} = 4.5^\circ \tag{A6-59}$$

From Figure 32

$$T_{p_2} = \frac{2.1}{2.5} T_{p_1} = 70 \text{ n-m} = 620 \text{ lb-in} \qquad \text{(A6-60)}$$

Hence

$$T = 70 \cos 2\pi f t \qquad \text{(A6-61)}$$

$$f = 1/4t_2 = \frac{1}{.008} = 125 \text{ cps} \qquad \text{(A6-62)}$$

$$T = 70 \cos 2\pi (125) t \qquad \text{(A6-63)}$$

$$\therefore \int_0^{t_2} T\,dt = \frac{70}{250\pi} = 0.09 \qquad \text{(A6-64)}$$

But

$$\theta_{M_S} = 22.5^\circ \left(\frac{\pi}{360}\right) \frac{1}{R_g} = 2.52 \times 10^{-3} \text{ rad.} \qquad \text{(A6-65)}$$

$$\theta_M = -\theta_{M_S} \cos 250\pi t \qquad \text{(A6-66)}$$

$$\dot{\theta}_M = 250\pi \theta_{M_S} \sin 250\pi t \qquad \text{(A6-67)}$$

$$\dot{\theta}_{M_m} = 250\pi \theta_{M_S} = 2.0 \text{ rad/sec.} \qquad \text{(A6-68)}$$

$$\therefore J = \frac{1}{\dot{\theta}_{M_m}} \int T\,dt = 4.5 \times 10^{-2} \text{ kg-m}^2 \qquad \text{(A6-69)}$$

which is several times greater than the theoretical value. If the above calculation is repeated for t_2 = .001 sec. and t_1 = .0005 sec the result is

$$J = 1.1 \times 10^{-2} \text{ kg-m}^2 \qquad \text{(A6-70)}$$

which is slightly less than the theoretical.

As J depends greatly on measurement of ts, better measurements are required to improve the validity of this calculation.

Inertia of a Standard Ball-Bearing Harmonic Drive Unit

Nomographs have been prepared for the average inertia to be expected for a conventional Harmonic Drive Unit. From these, for D_p = 3 1/4 inch.

$$J = 1.0 \text{ kg-m}^2 \qquad \text{(A6-71)}$$

Inertia of the Swash Plate Wave Generator
The following analysis applies to a wave generator represented by Figure 80.

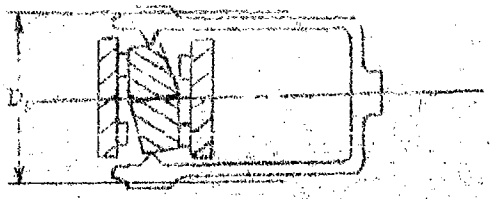

FIGURE 80 - SWASH PLATE WAVE GENERATOR

Kinetic energy due to axial harmonic motion of the plate is equal to

$$Wp = \frac{1}{2} J_p (\dot{\theta}_{p_m})^2 \qquad (A6\text{-}72)$$

where

Wp = kinetic energy

Jp = inertia of the plate rotating around a centroidal axis perpendicular to the devices' axis.

$\dot{\theta}_{p_m}$ = maximum axial velocity.

This is based on the concept that this maximum velocity applies to the locus of the ends of the minor axis (90° phase shift from the ends of the major axis).

$$\dot{\theta}_{p_m} = 2\pi f \theta_{p_m} \qquad (A6\text{-}73)$$

where θ_{p_m} = single amplitude of angular motion of plate

and

$$f = Rg\ \dot{\theta}_o \qquad (A6\text{-}74)$$

where $\dot{\theta}_o$ = output speed of device

Rg = Harmonic Drive ratio

$$W_p = \frac{1}{2} J_p (2\pi R_g \dot{\theta}_o \theta_{p_m})^2 = (4\pi^2 J_p R_g^2 \theta_{p_m}^2) \frac{\dot{\theta}_o^2}{2} \qquad (A6\text{-}75)$$

But

$$W_p = \tfrac{1}{2} J_{p_o} \dot{\theta}^2 \qquad (A6\text{-}75A)$$

J_{p_o} = effective inertia of the plate at the output due to axial motion.

Equating values of W_p

$$J_{p_o} = 4\pi^2 \, J_p R_g^2 \theta_{p_m}^2 \qquad (A6\text{-}76)$$

Jp is found as follows:

To simplify, make the approximation that the plate is a homogeneous right circular cylinder, (See Figure 81), for which

$$J_{z\text{-}z} = 1/4 \, MR^2 + 1/12 \, MC^2 \qquad (A6\text{-}77)$$

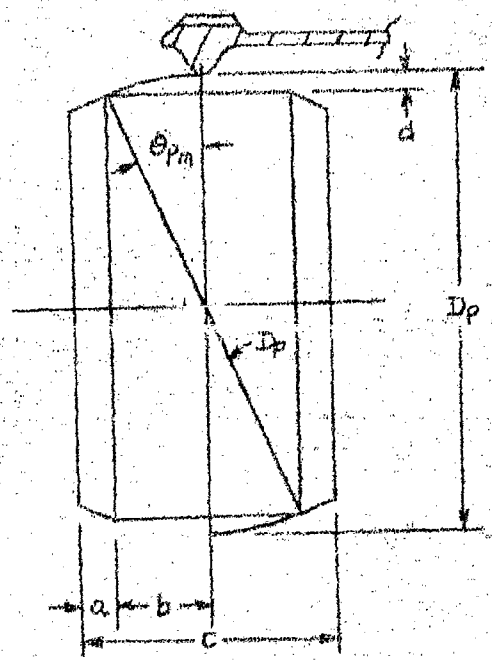

FIGURE 81 - SWASH PLATE SIMPLIFIED MODEL

Since R $\approx \frac{Dp}{2}$ (actually less by the bed thickness, dedendum, and inertia bearing point.)

$$J_{z-z} = M\left[\frac{Dp^2}{16} + \frac{c^2}{12}\right] \quad (A6\text{-}78)$$

$$M = \rho \frac{\pi}{4} Dp^2 C \quad (A6\text{-}79)$$

Where ρ = mass density

C is found as follows:
From the diagram of motion of the plate, again considering the lengths as Dp:

$$a = \frac{Dp}{2} \theta p_m \quad (A6\text{-}80)$$

b is the increase in width to assure deflection in the face of variations in tolerances and excessive axial motion.

$$\text{Take } b = 1/4\ a \quad (A6\text{-}81)$$

Then
$$C = 2(a+b) = 2.5a = 1.25\ Dp\theta p_m \quad (A6\text{-}82)$$

$$M = \frac{1.25\pi}{4} \rho Dp^3 \theta p_m = 0.98 \rho Dp^3 \theta p_m \quad (A6\text{-}83)$$

and

$$J_{z-z} = 0.98 \rho \theta p_m Dp^5 \left[\frac{1}{16} + \left(\frac{1.25\theta p_m}{12}\right)^2\right] \quad (A6\text{-}84)$$

As will be shown, θp_m is of the order of 5° to 10°, or 0.1 to 0.2 radians, so that

$$1/16 \gg \left(\frac{1.25\theta p_m}{12}\right)^2 \quad (A6\text{-}85)$$

Thus
$$Jp = J_{z-z} = \frac{0.98}{16} \rho \theta p_m Dp^5 = .0613 \rho \theta p_m Dp^5 \quad (A6\text{-}86)$$

where Jp is used for easier notation

$$\therefore J_{P_b} = 4r^2 R_g^2 \theta p_m^2 (0.0613 \rho \theta p_m Dp^5) = 2.42 \rho R_g^2 \theta p_m^3 Dp^5 \quad (A6\text{-}87)$$

Now from Figure 81

$$d = \frac{Dp}{2}(1 - \cos \theta p_m) \quad (A6\text{-}88)$$

$$\theta p_m = \cos^{-1}\left(1 - \frac{2d}{Dp}\right) = \cos^{-1}\left(1 - \frac{2}{R_g}\right) = \cos^{-1}\left(\frac{R_g - 2}{R_g}\right) \quad (A6\text{-}89)$$

For the right triangle (see Figure 82)

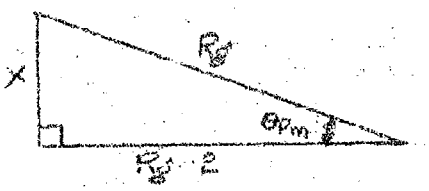

FIGURE 82 - SWASH PLATE CALCULATION TRIANGLE

$$X = \left[R_g^2 - (R_g-2)^2\right]^{\frac{1}{2}} = \left[4R_g - 4\right]^{\frac{1}{2}} = 2\sqrt{R_g - 1} \qquad \text{(A6-90)}$$

Normally

$$R_g \gg 50 \qquad \text{(A6-91)}$$

so that

$$X \approx 2\sqrt{R_g} \qquad \text{(A6-92)}$$

$$\therefore \theta_{pm} = \sin^{-1}\frac{X}{R_g} = \sin^{-1}\frac{2\sqrt{R_g}}{R_g} = \sin^{-1}\frac{2}{\sqrt{R_g}} \qquad \text{(A6-93)}$$

For small angles less than 10°,

$$\theta \approx \sin\theta \qquad \text{(A6-94)}$$

$$\theta_{pm} \approx \frac{2}{\sqrt{R_g}} \qquad \text{(A6-95)}$$

$$J_{p_o} = 2.42\rho R_g^2 D_p^5\left(\frac{2}{\sqrt{R_g}}\right)^3 = 19.4\rho\sqrt{R_g}\,D_p^5 \qquad \text{(A6-96)}$$

This is about 7 times that for a conventional ball bearing type. For example, for $D_p = 3.25$ inch, $R_g = 156$, steel armature:

$$J_{p_o} = 74 \text{ kg-m}^2 \qquad \text{(A6-97)}$$

the conventional $J_c = 1.0$ kg-m^2 (Equation A6-71)

$$\therefore \frac{Jp_o}{Jc} = 7.4 \qquad \text{(A6-98)}$$

It is believed that this results from the wedging action. That is, to develop a certain deflection of the flexspline requires a much larger motion of the periphery of the swash plate. In the above example, the corresponding peripheral motion is

$$l \approx \frac{D_p}{\sqrt{R_g}} = 0.26" \qquad \text{(A6-99)}$$

and the deflection is:

$$d = \frac{D_p}{R_g} = .0208" \qquad \text{(A6-100)}$$

and

$$\frac{l}{d} = \sqrt{R_g} = 12.5 \qquad \text{(A6-101)}$$

Other sizing factors account for the difference between 7.4 and 12.5

There is additional inertia if the swash plate also rotates around the device's axis. This is not necessary however.

It is also necessary to check that the width C is sufficient.
- to make the plate essentially rigid
- to carry the necessary flux

For the example used

$$C = 1.25\ D_p\theta_{p_m} \qquad \text{(A6-102)}$$

$$\theta_{PM} = \frac{s}{\sqrt{R_g}} = 0.160 \text{ rad} = 9.15^\circ \qquad \text{(A6-103)}$$

$$\therefore C = 1.25(3.25)\ 0.16 = 0.65 \text{ inch} \qquad \text{(A6-104)}$$

which should satisfy both requirements.

APPENDIX VII

THEORETICAL ANALYSIS OF POWER RATE, MAGNETOMOTIVE FORCE, AND POWER OUTPUT FOR THE STEPPING ACTUATOR

This appendix was prepared by
Dr. G. C. Newton, Jr.

The average torque developed by the EHD-3 can be calculated from the work done by the "n" magnets for one revolution of the output shaft divided by 2π. This figure is multiplied by the torque efficiency η_T in order to account for friction in the Harmonic Drive. The work done per cycle by a magnet is denoted by W_{mg}. Thus the average output torque T_M is given by

$$T_M = \frac{\eta_T R_g n_m W_{mg}}{\pi} \qquad (A7\text{-}1)$$

A factor of 2 in the numerator and denominator has been cancelled. The numerator factor of two arose from the fact that for each revolution of the output shaft, each magnet executes $2R_g$ cycles of operation where R_g is the reduction ratio of the Harmonic Drive. This assumes a flexspline shape with two points of contact with the ring gear. The denominator factor of 2 that has been cancelled came from the 2 factor used to change revolutions to radians.

How the magnets should be designed depends upon what parameter is being maximized and what constraints are being imposed on the design. For purposes of this report it is assumed that the goal is to maximize the torque-squared-to-inertia ratio or power rate P_M subject to limitations on the width, volumes and I^2R loss of the magnets. The limitation on width arises from the chosen method of driving the flexspline, viz., driving with internal levers having armatures for the magnets located at the ends. For a given flexspline size and a given number of magnets, this means that there is a specified amount of peripheral length of the flexspline that can be associated with each magnet as its width dimension. Also, for the given conditions, there is a limited volume that reasonably can be associated with each magnet as well as a maximum I^2R loss. Although in practice there may be other constraints, such as current and voltage limitations on the semi-conductor devices used to control the magnet currents, these are assumed not to be binding in the analysis of this appendix.

An alternate goal to the maximizing of the power rate is maximizing the output power of the EHD. Such a goal is more complex than the power rate consideration since speed limitations imposed by switching and back emf considerations

come into play. However, to the extent that maximizing the magnet work W_{mg} per cycle is equivalent to maximizing output power, it will be seen that maximizing the power rate will come close to maximizing output power. This comes about since torque or force enters the power rate expression as a squared quantity whereas the inertia enters as a quantity raised to the inverse first power.

The power rate is given by

$$\dot{P}_M = \frac{T_M^2}{J_M} \qquad \text{(A7-2)}$$

Considering the various components of inertia, it is found that the power rate can be expressed as

$$\dot{P}_M = \frac{\eta_T^2 R_g^2 n^2 W_{mg}^2}{\pi^2 \left[J_s + J_r + 0.5\eta_s R_g^2 n d^2 M_a \right]} \qquad \text{(A7-3)}$$

The force-squared-to-inertia ratio F_a^2/M_a or power rate of an individual magnet is

$$\frac{F_a^2}{M_a} = \frac{(W_{mg}/d)^2}{M_a} \qquad \text{(A7-4)}$$

since W_{mg}/d is the average force developed by the magnet during its working stroke. From Equation A7-3 it is seen that maximizing the power rate of the Harmonic Drive would be equivalent to maximizing the force-squared-to-inertia of the individual magnets if the moment of inertia J_s+J_r of the flexspline assembly were negligible.

Having formulated an expression for the power rate, the next step is to establish the magnet configuration that maximizes the power rate within the limitations imposed by the specified constraints. Figure 28 shows the key dimensions of a typical magnet for the general arrangement that has been chosen for the laboratory model of the stepping field actuator. This figure assumes that the coils can be tapered in order to get the maximum amount of copper into them. It this were done in the laboratory model, the volume V_{mg} of a magnet (indicated by the dashed lines) would be approximately 6.05 cubic inches or 0.99×10^{-4} meters^3. This volume appears to yield a reasonable overall size for the magnet assembly relative to the flexspline dimensions. It is therefore taken as the first of the specifications in determining the ideal magnet design. In terms of Figure 28 this volume is related to the key dimensions as follows:

$$V_{mg} = \frac{\pi(D_p + c + b)}{n}\left[\frac{2\pi(D_p + 2c + b)}{n} + 2b - 2w\right](c + 3b) \qquad \text{(A7-5)}$$

It is proposed to step the currents in the coils in such a way that 4 magnets out of the 16 will be excited at any one time. For purposes of power rate calculation, the "power" angle between the flexspline major axis and the magnets is assumed to be such that the magnet gap changes from its mid-value to its minimum value while excited. This condition corresponds to an elliptical shape for the flexspline and maximum work (output torque) from the magnets. For the distorted flexspline shape discussed in Section 3.3, a larger amount of work can be obtained from a magnet during its excited period because the "power" angle can be selected so that the magnet gap changes by a greater amount than when the ideal shape for the flexspline is maintained. This will partially compensate for the increase in the inertia caused by flexspline distortion.

In summary, the power rate will be calculated for the ideal flexspline shape with the knowledge that it will diminish as the flexspline distorts but not as rapidly as the inertia increases. Also, it will be assumed that the coil currents reach their steady values in times that are short compared to the "on-time" period. Thus the power rate that is computed corresponds to the upper limit on power rate as the speed approaches zero and the shape of the flexspline approaches its ideal form.

The second specification of the magnet design is the power that is to be dissipated as I^2R losses in the coils. In the laboratory model it is estimated that 100 watts of heat can be dissipated from the magnets. This means the I^2R loss per coil P_Q can be 100/2x4 or 12.5 watts since there are two coils per magnet and 4 magnets are excited at any instant.

The problem of maximizing is equivalent to finding how the fixed magnet volume should be shared between the iron and the copper. Obviously, either too much copper or too much iron will yield reduced power rate through reduction of the available magnetic force. For the laboratory model of the EHD-3 the flexspline dimensions are fixed with D_p = 3.25 inches and d=0.0208 inches. This means that the dimensions "a", "b" and "w" of Figure 28 are to be chosen, thereby fixing the ratio of iron to copper. However, the volume constraint implies a relationship among these dimensions so that, effectively, only two are free for the designer to manipulate. In order to further simplify the analysis, "w" will be assigned an arbitrary value of 0.8 "b" thereby leaving only the magnet leg width "b" as a free variable. It is reasonable to make "w" somewhat less than "b" in view of the magnet width limitation imposed by the requirement of fitting 16 of them around the periphery of the flexspline.

The procedure for adjusting "b" for maximum power rate $\dot{P}_M$ is to calculate the later as a function of the former and find the maximum. This is done numerically in view of the algebraic complexity of the relations. For a given "b" the

coil dimensions are established and, for the specified coil power dissipation P_c, this establishes the available MMF as follows:

$$\mathcal{F}_m = 2\sqrt{\frac{P_c A_c}{\rho_c L_c}} \qquad (A7\text{-}6)$$

where A_c is the coil's cross sectional area, L_c its mean turn length and ρ_c is the effective resistivity of the copper allowing for the winding space factor and insulation. A resistivity of 3.44×10^{-8} ohm-meters is used in the numerical calculations; this is based on the winding cross section being approximately 50 percent copper. The factor of 2 corresponds to two coils connected series-aiding.

From Figure 28 the mean turn length and cross section area of a coil are estimated as, respectively

$$L_c = \pi\left[\frac{\pi(D_p + c + b)}{2n} - \frac{w}{2}\right] + 2b + 2w \qquad (A7\text{-}7)$$

and

$$A_c = \left[\frac{\pi(D_p + c + b)}{2n} - \frac{w}{2}\right] c \qquad (A7\text{-}8)$$

With the MMF established, the mechanical work W_{mg} done by the magnet in closing the gap from x_2 to x_1 is computed. This is done by considering the iron to be infinitely permeable up to saturation and incrementally impermeable after saturation; also, fringing in the air gap is neglected. Knowing that the mechanical work is given by the area traced by the magnetic operating point in the flux-MMF plane, expressions are developed for it on the assumption that the MMF reaches full value rapidly compared to the time required for the gap to close. Three different cases arise depending upon whether or not and when the magnet saturates. These cases and the corresponding equations for W_{mg} are given in Figure 83. In these graphs "$\mathcal{B}$" is the magnetic flux density and

$$\mathcal{B}_2 \triangleq \mu_c \frac{\mathcal{F}_m}{x_2} \qquad (A7\text{-}9)$$

$$\mathcal{F}_1 \triangleq \frac{\mathcal{B}_m}{\mu_c} x_1 \qquad (A7\text{-}10)$$

where μ_c is the permeability of free space (or air) and $\mathcal{B}_m$ is the saturation flux density of the iron (assumed to be 2 webers per meter^2 in calculations or approximately 130,000 lines per square inch).

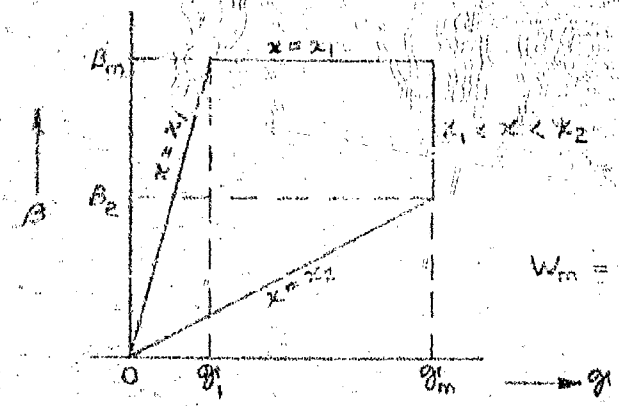

$$W_m = bw\left(B_m \mathcal{F}_m - \frac{B_m \mathcal{F}_1}{2} - \frac{B_2 \mathcal{F}_m}{2}\right)$$

(A) Flux density versus mmf for $\mathcal{F}_1 < \mathcal{F}_m$, $B_2 < B_m$.

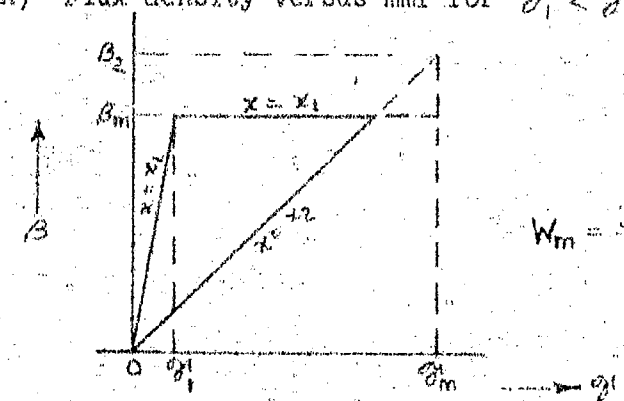

$$W_m = \frac{bw}{2}\left(\frac{B_m \mathcal{F}_m}{B_2} - \mathcal{F}_1\right)B_m$$

(B) Flux density versus mmf for $\mathcal{F}_1 < \mathcal{F}_m$, $B_2 > B_m$.

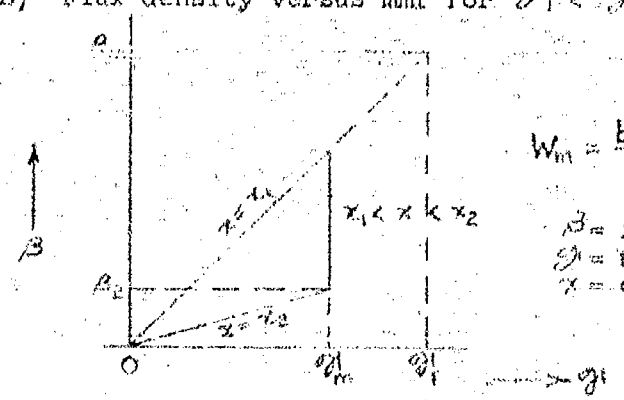

$$W_m = \frac{bw}{2}\left(\frac{B_m \mathcal{F}_m}{\mathcal{F}_1} - B_2\right)\mathcal{F}_m$$

B = flux density
$\mathcal{F}$ = magnetomotive force
x = distance

(C) Flux density versus mmf for $\mathcal{F}_1 > \mathcal{F}_m$.
(B_2 is always less than B_m for this case.)

FIGURE 83 FLUX DENSITIES VERSUS MAGNETOMOTIVE FORCES
(For Appendix VII)

The air gap is the sum of the two individual gaps shown in Figure 28. The minimum gap with the armature substantially in contact with the magnet poles is taken as $X_1 = .006$ inch to allow for the remaining gap and the discontinuity in the magnetic path. X_2 is taken as the gap corresponding to the armatures in mid position* and is calculated from Figure 28 as

$$X_2 = \frac{d}{2}\left\{ \frac{\frac{b}{2}}{0.875} + \frac{\left[\frac{\pi(D_p+2c+b)}{n} + b-w\right]}{0.875\, D_p} \right\} \qquad (A7\text{-}11)$$

The effective mass M_a of the magnet armature, to be used in Equation A7-3 is that which, if placed at the tooth bed of the flexspline, would be equivalent to the magnet armature laminations associated with one magnet. From Figure 28 this mass may be computed approximately as

$$M_a = \frac{1}{(0.875\, D_p)^2} \left\{ \int_0^{D_p + \frac{\pi}{n}(D_p + 2c + b) + \frac{3}{2} b - w} \rho\, b \left[\frac{\pi (d-2b)}{n}\right] x^2\, dx \right\} \qquad (A7\text{-}12)$$

or

$$M_a = \frac{\pi \rho b (D_p - 2b)}{3(0.875\, D_p)^2 n} \left[D_p + \frac{\pi}{n}(D_p + 2c + b) + \frac{3}{2} b - w \right]^3$$

where the interior diameter $D_p - 2b$ is used for computing the volume since the laminations comprising the armature are close packed at this diameter from which they fan out radially. ρ is the density of the armature laminations.

Finally, an expression is required for J_n. For designs similar to the laboratory test model this is the inertia that is added to the flexspline on account of the rotation of the magnet armature laminations. From Figure 28 this inertia can be approximated as

$$J_n = \frac{\pi}{4} \rho b\, (D_p - 2b) \left[D_p + \frac{\pi}{n}(D_p + 2c + b) + \frac{3}{2} b - w \right] (D_p - b)^2 \qquad (A7\text{-}13)$$

On the basis of the above equations the parameters entering into the power rate expression of Equation A7-3 are computed as functions of the magnet leg width "b". Figure 29 shows how the power rate varies with the leg width. From this figure it is seen that the leg width producing maximum theoretical performance is in the vicinity of 0.8 inch. This

*Since the coils are excited one quarter of the time, the current is on from the mid position to the minimum gap position under conditions of maximum average output torque.

is considerably larger than the 0.5 inch used in the laboratory model and results in a theoretical power rate improvement by better than a factor of four over the model. It is interesting to note that the maximum power output from the EHD-3 has a maximum at nearly the same value of "b" as does the power rate. A separate curve of output power is drawn in Figure 29 for 100 pulse per second frequency input to the coils. This corresponds to 19.2 rpm shaft speed.

Also shown in Figure 29 is a plot of total magnet ampere turns as a function of the leg width "b". The available magnetomotive force is seen to decrease almost linearly with increase in leg width. At the ideal leg width value of 0.8 inch, the available ampere turns are insufficient to produce saturation at middle armature position where the current is turned on. The flux density at this moment is 77 percent of saturation.

The reason that Figure 29 shows maxima for power rate and output power at nearly the same value of leg width "b" is that the moment of inertia J_M is almost invariant with this parameter. With a constant J_M, power rate varies as the square of the torque T_M. But the torque is proportional to the output power P_M since the speed is constant. Thus, power rate is proportional to power squared and the maxima are coincident.

The moment of inertia J_M would be expected to increase with leg width "b". However, flat rather than tapered laminations are assumed for the armature. This means that the number of laminations of a given thickness decreases as "b" increases since the inner radius of the armature decreases. The reduction in the number of laminations nearly cancels the increase in width thereby making the moment of inertia nearly constant. At b=0.8 inch, the moment of inertia J_M is 1.12×10^{-2} kilogram meter^2. The breakdown of this inertia is: flexspline J_s, 5 percent; rotational inertia J_r of armature laminations, 22 percent; and effective inertia J_a of armature laminations associated with radial motion, 73 percent.

Some idea of the proportions of the parts of the EHD-3 with a leg width of 0.8 inch can be had from Figure 28. The general conclusion drawn from this study of the magnet configuration is that more iron and less copper than would be intuitively selected theoretically yields the best design in terms of either power rate or power criteria. However, for large leg widths it would be necessary to use tapered laminations in the armature in order to avoid saturation limiting of flux by this part of the magnetic circuit. This would tend to cause the inertia to increase with "b" and to make the power rate maximum occur at a lower value of "b", perhaps in the vicinity 0.75 inches.

The power rates indicated in this study actually cannot be achieved because of saturation limiting in the armature laminations which reduces the saturation flux density in the magnets below the assumed level of 2 webers per square meter. However, use of tapered armature laminations would be expected to yield power rates not too much lower than those indicated in Figure 29; perhaps 1800 kw/sec rather than 2700 kw/sec.

A summary of the assumptions upon which is based the analysis of the magnet configuration leading to Figure 28 is given in Table VIII. The value of this analysis lies not so much in the specific results as in the general insights that have been discussed above and in the development of a method for magnet design for EHD-3 applications. The specific results can have utility only to the degree that the assumptions of Table VIII are satisfied.

APPENDIX VIII

STALL TORQUE MEASUREMENTS (EHD-3)

Figure 33 shows the data taken in performing stall torque measurements. While the test was in process, it became apparent that certain poles had higher stall torque capability than others. After this fact was noted, the remainder of the test was run using a particular set of poles. It turns out most of the test was run using this set of poles anyway because it is a preferred position as far as the electronic circuit is concerned. This preferred condition is due to interaction between power supplies, logic circuits, and the analog to digital circuit, the latter being quite voltage-sensitive.

The curve (Figure 33) is an average for all points at any particular current level and was shaped to fit a smooth configuration. Indication of saturation of the iron structure is to be noted.

APPENDIX IX

NATURAL FREQUENCY OF FLEXSPLINES

IX-1 Analysis

The mechanical natural frequency of the flexspline might limit the speed of response, and the steady state speed. It is constructive to compare the estimated natural frequency with the required frequency of the harmonic deflection. This is expected to be about 100 cps maximum.

There are two basic types of flexsplines to be considered, Figure 84 (A) and (B).

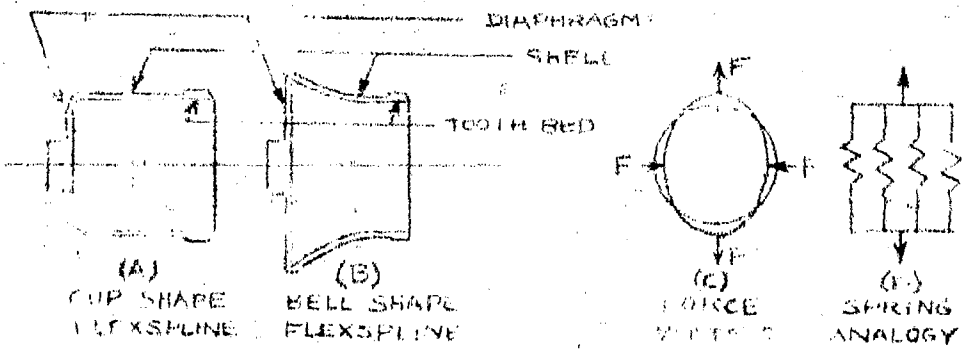

FIGURE 84 - NATURAL FREQUENCY CALCULATION MODELS

Disregard shell diaphragm, etc. In general, these should raise the ω_n due to restraining action.

Assume that the two lobe deflection, Figure 84 (C) is analogous to a spring system like that of Figure 84 (D).

With F_D applied, each of the four springs deflects a total amplitude of $d/2$. For the above, $F_D = 2F$.

Hence, considering a simple spring

$x = d/2$ $\quad$ d = Harmonic Drive deflection

$F = F_D/2$ $\quad$ F_D = Force required at ends of major axis to produce the Harmonic Drive deflection, with no force at any other point.

M = 1/4 of mass of ring.

and

$$\omega_n = \left[\frac{F/x}{M/3}\right]^{1/2} = \left[\frac{k}{M/3}\right]^{1/2} \qquad \text{(A9-1)}$$

ω_n = resonant frequency (rad/sec)

In order to experimentally measure the natural frequency, the flexsplines were hit sharply and the acoustic pitch determined.

IX.F Example

Consider a standard 3 1/3 in. pitch diameter cup shape flexspline without any attached mass:

$F_D = 12$ lbs $= 53$n (checked by measurement) (A9-2)

$x = \frac{d}{2} = .016" = 4.07 \times 10^{-4}$m (A9-3)

$k = \frac{F}{x} = 1.3 \times 10^5$ n/m (A9-4)

Take the effective length as the tooth bed only

$l = 1.0" = .025$m (A9-5)

Take bed thickness

$h = .060" = 1.52 \times 10^{-3}$m (A9-6)

$D_p = 3\ 1/3" = .0846$m (A9-7)

$$\rho = 7.82 \times 10^{3} \text{ kg/m}^3 \qquad \text{(A9-8)}$$

$$M = \tfrac{1}{4}\pi D_p^2 h l \rho = 2 \times 10^{-2} \text{ kg} \qquad \text{(A9-9)}$$

$$\therefore f_n = \frac{\omega_n}{2\pi} = \frac{1}{2\pi}\left[\frac{k}{M/3}\right]^{1/2} \approx 700 \text{ cps} \qquad \text{(A10-10)}$$

In comparison the measured value was 520 cps. Taking into account the mass of the shell portion the calculated f_n would be decreased.

With attached armature mass, the frequency would be less. If the mass of the EHD-3 armature (16 x 0.13 = 2.1 kg, see Figure 69) is considered effectively attached, the mass is about 100 times greater so that f_n is about 70 cps. Acutally the mass is not attached, so the full mass is not effective, and the result should be somewhere between 700 and 70 cps.

APPENDIX X

HEAT DISSIPATION AND TEMPERATURE RISE ANALYSIS

Analysis is desirable to determine the general heat transfer situation, whether or not forced cooling is likely to be required and to what extent. The problem is complicated primarily by the matter of whether or not a significant conduction heat transfer path will be established between the coil and the housing. If so, assuming that the ambient air temperature surrounding the device is moderate enough to permit a normal temperature rise, say 50°C, then forced cooling should not be required. This conclusion is based on the relative large surface area of the housing.

Next consider the case where there is no significant conductive heat transfer path between coils and housing. To prevent contamination of the air gaps, tight sealing of the housing is necessary. This means that the air inside will be trapped, resulting in a temperature gradient through the housing wall. If NEMA Type B insulation is used, the allowable temperature rise is 85°C based on a 40°C ambient and a 5°C hot spot allowance, giving a maximum winding temperature of 130°C. The convective heat transfer coefficient will be of the order of .003 to .004 watts/in^2 - °C, which is about half the value given by the authors of References 10 and 16 for coils exposed to still air. The ½ factor arises from the non-ventilated enclosure. This assumption was also checked roughly by calculations from Reference 31, Page 190. More detailed calculations are possible using the methods described in the latter reference.

It is assumed also that, even if the space between coils and housing is too small for good convection, the conductive transfer through the air makes up the difference. Hence, the area is taken as the surface area of the annular ring of the coils, excluding the inside against the flexspline.

APPENDIX XI

PERFORMANCE ANALYSIS OF THE ROTATING FIELD TYPES

XI-1 Calculations for Model EHD-2

$$\cos \theta_e = \frac{P_i}{E_t I_t} \qquad \text{(A11-1)}$$

$$P_i = 97 \text{ watts} \qquad \text{(A11-2)}$$

$$E_t = 120 \text{ volts} \qquad \text{(A11-3)}$$

$$I_t = 1.81 \text{ amps} \qquad \text{(A11-4)}$$

$$\therefore \cos \theta_e = 0.423 \qquad \text{(A11-5)}$$

$$Z_1 = \frac{R_1}{\cos \theta_e} = \frac{R_1}{0.423} \qquad \text{(A11-6)}$$

By measurement:

$$R_1 = 4.1\ \Omega \qquad \text{(A11-7)}$$

$$\therefore Z_1 = 9.7\ \Omega \qquad \text{(A11-8)}$$

$$e_{ze_m} = e_{t_m} - i_m Z_1 \qquad \text{(A11-9)}$$

$$e_{t_m} = \frac{1}{2}(1.414)120 = 85 \text{ V for half of one phase} \qquad \text{(A11-10)}$$

$$i_m = 1.414(1.81) = 2.7 \text{ a.} \qquad \text{(A11-11)}$$

$$\therefore e_{ze_m} = 85 - 2.7(9.7) = 59 \text{ V} \qquad \text{(A11-12)}$$

$$e_{s_m} = e_{ze_m} \sin \theta_e = 59(0.905) = 54 \text{ V} \qquad \text{(A11-13)}$$

Coil Number	No. of Turns
N_1	69
N_2	70
N_3	74
N_4	66
Total	279

(A11-14)

$$\omega = 2\pi 60 = 377 \text{ rad/sec} \qquad \text{(A11-15)}$$

$$\alpha_m = \frac{1}{2} \tan^{-1} \frac{1}{2 \tan \bar{\varphi}_a} \qquad \text{(A11-16)}$$

$\Phi_D = 30°$ was taken as the pressure angle after rework of the original 20° angle which, including some tooth manufacturing errors, did not perform well.

$\therefore \phi_{m1} = 22°$ (A11-17)

$X_1 = \frac{d}{2}\left[1 - \sin(45° - \phi_m)\right] = \frac{d}{2}(0.382)$ (A11-18)

$d = 2/P_D$ (A11-19)

$P_D = 50$ (A11-20)

$\therefore d = .0400"$ (A11-21)

Now refer to Figure 85.

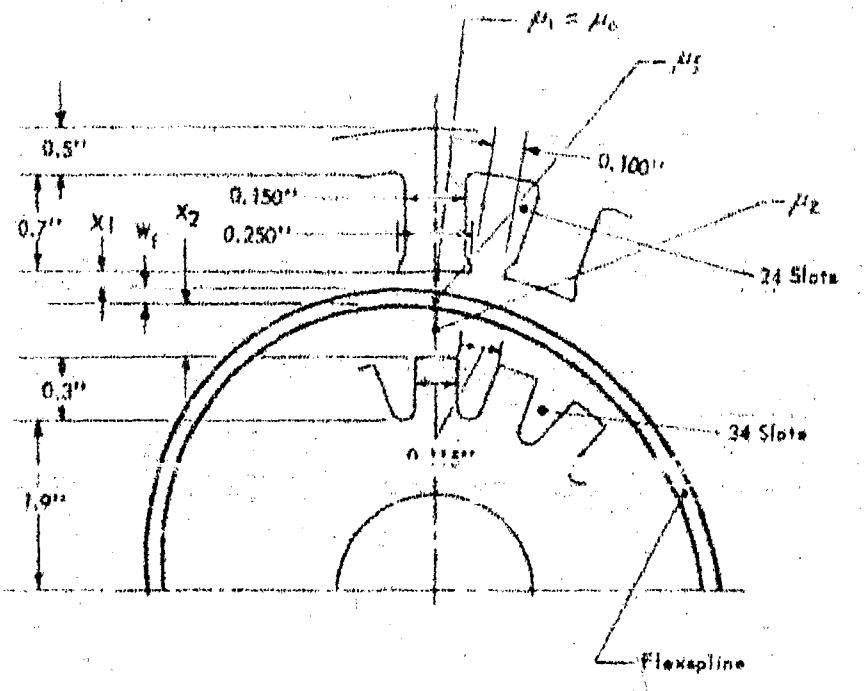

μ = Permeability
μ_0 = Permeability of Air
X,W = Distance

FIGURE 85 DETAILS OF THE MAGNETIC CIRCUIT, MODEL EHD-2
End View - Axial length is 1.0"

$X_1 = .006" = 1.5 \times 10^{-4}$ m (A11-22)

$X_1 + X_2 + t_f = 0.107"$ for this model (A11-23)

and $t_f = 0.014"$ (A11-24)

$X_2 = .087" = 2.2 \times 10^{-3}$ m (A11-25)

Take $\mu_2 = 2.2 \times 10^{-5}$ W/a-t-m (A11-26)

But $\mu_1 = \mu_0 = 4\pi \times 10^{-7}$ w/a-t-m (A11-27)

as in this case μ_1 is the same as the permeability of air, since there is no material in the X_1 gap.

μ_2 is 1/2 that used in a well-engineered magnetic-particle clutch.

$$\mathcal{R} = \frac{1}{A_Q}\left[\frac{x_1}{\mu_0} + \frac{x_2}{\mu_2}\right] \quad \text{(A11-28)}$$

$$A_Q = \frac{1}{4}" \times 1\frac{5}{8}" = 2.62 \times 10^{-4}\ m^2 \quad \text{(A11-29)}$$

$$\therefore \mathcal{R} = 43 \times 10^5\ w/a\text{-}t\text{-}m \quad \text{(A11-30)}$$

$$\therefore e_{3m} = \frac{2\omega}{\mathcal{R}} i_{em}(2.63 \times 10^5) = 46\, i_{em} \quad \text{(A11-31)}$$

$$\therefore i_{em} = 1.2\ a. \quad \text{(A11-32)}$$

$$I_e = 0.85\ a \quad \text{(A11-33)}$$

$$x_e = \frac{e_{3m}}{i_{em}} = \frac{54}{1.2} = 45\ \Omega \quad \text{(A11-34)}$$

$$z_e = \frac{e_{zem}}{i_{em}} = \frac{59}{1.2} = 49\ \Omega \quad \text{(A11-35)}$$

$$\therefore R_e = (z_e^2 - x_e^2)^{1/2} = 19.2\ \Omega \quad \text{(A11-36)}$$

The eddy current loss is

$$P_1 = I_e^2 R_e = (0.85)^2 19.2 = 13.8 \text{ watts per half phase.} \quad \text{(A11-37)}$$

Total eddy current loss for all three phases

$$P_1 = 3(2)13.8 = 83\ w \quad \text{(A11-38)}$$

which is high due to the eddy currents.

The stator copper loss is:

$$P_2 = (I_1)^2 R_1 = (1.91)^2 4.1 = 15 \text{ watts per half phase} \quad \text{(A11-39)}$$

For all three phases

$$P_2 = 3(2)\,15 = 90\ w \quad \text{(A11-40)}$$

The peak air gap flux is calculated as follows:

		Percent	
$2\Phi_{1m} = \Phi_{2m} = \Phi_{3m}$	$= 7.70 \times 10^{-5}\ w$	100	(A11-41)
Φ_{4m}	$= 5.86 \times 10^{-5}\ w$	76	
Φ_{5m}	$= 3.94 \times 10^{-5}\ w$	50	
Φ_{6m}	$= 1.85 \times 10^{-5}\ w$	24	

which agrees very favorably with the desired sinusoidal flux distribution.

Peak air gap flux density at the center is thus:

$$\beta_m = \frac{\Phi_m}{A_g} = 0.30\ w/m^2 \quad \text{(A11-42)}$$

Multiplying by 1-1/2 to account for the other phases

$$\beta_{m_t} = 1.5(0.30) = 0.45\ w/m^2 \quad \text{(A11-43)}$$

This is below the saturation level of the powder.

Due to the necked shape of the pole tip in the stator pole and the stacking factor of the lamination, for the iron

$$\beta = 0.45\left(\frac{0.250}{0.1750}\right)\frac{1}{0.90} = 0.84\ w/m^2 \quad \text{(A11-44)}$$

This is far below the saturation of the material used (silicon steel).

If μ_2 was neglected

$$F_{1}/A_g = \beta_m^2/2\mu_0 = 3.6 \times 10^4\ n/m^2 = 5.2\ lbs/in^2 \quad \text{(A11-45)}$$

Considering μ_2

$$k_1 = \frac{\mu_2 - \mu_0}{\mu_2} = 0.41 \quad \text{(A11-46)}$$

$$F_M/A_g = k_1 F_1/A_g = 1.48 \times 10^4\ n/m^2 = 2.2\ lbs/in^2 \quad \text{(A11-47)}$$

Assuming that the flux distribution is sinusoidal, use of the expression for finding F_T for a number of F_M at various angles from the major axis and $\delta_m = 20^0$, there results:

$$\sum_{180^0} \sin 2\theta_k = 1.92 \qquad \text{(A11-48)}$$

$$F_M = 3.9\,n \qquad \text{(A11-49)}$$

$$F_T = 2 F_M \sum_{180^0} \sin 2\theta_k = 15\,n \qquad \text{(A11-50)}$$

$$T_1 = F_T D_p \eta_T \qquad \text{(A11-51)}$$

$$D_p = 2.6'' = 6.6 \times 10^{-2}\ m \qquad \text{(A11-52)}$$

$$\therefore T_1 = 0.99\,\eta_T \text{ per phase} \qquad \text{(A11-53)}$$

$$\text{and } T_2 = 2.25\,T_1 = 2.23\,\eta_T \text{ for the device} \qquad \text{(A11-54)}$$

η_T to be determined later.

Now consider a power bookkeeping analysis for the device:

Power Input	97 x 3 =	291 watts	(A11-55)
Power Losses			
Eddy current loss, P_1	83		
Stator copper loss, P_2	90		
Subtotal		173	
Balance to be accounted for		118	

The measured shaft output power was negligible

$$T_M = 0.25\ n\text{-}m = 2.2\ lb\text{-}in \qquad \text{(A11-56)}$$

$$\dot{\theta}_M = 2.9\ rad/_{sec} = 28\ rpm \qquad \text{(A11-57)}$$

$$\therefore P_M = T_M\ \dot{\theta}_M = 0.7\ watts \qquad \text{(A11-58)}$$

Hence, 117 watts must be divided between two places, the losses associated with the Harmonic Drive elements and the induction motor power output which appears as heat in the rotor (rotor I^2R loss). A no-load test was not run,* so calculations of induction motor power were not made. It is likely to be considerable, since the gap is nearly as large as for the motor before it was modified, due to the continued presence of the laminated core, and the flexspline acts as a squirrel-cage rotor with shorted end, etc. On the other hand, the losses for the Harmonic Drive action may be

* This requires use of a non-metallic rigid plug to keep the flexspline from deflecting.

higher than their usual low figure, due to at least two factors: (1) Sliding of the flexspline against the stator. When run without teeth, the units run about 17% low in speed, so that the deflection in the air gap is not quite matched to the teeth.

(2) Tooth gliding. Due to the extended arc of deflection, produced by the 180° sinusoidal flux distribution, there may be departures from the proper harmonic shape, resulting in greater tooth losses.

The power output theoretically available from the Harmonic Drive is only

$$P_{HD} = 2.23\ \eta_T\ (2.9) = 6.5\ \eta_T \qquad \text{(A11-59)}$$

and, even if η_T is taken relatively high, such as $\eta_T = 0.6$

$$P_{HD} = 6.5\ (0.60) = 3.9 \text{ watts} \qquad \text{(A11-60)}$$

whereby losses in the Harmonic Drive are

$$P_{HD_L} = 6.5\ (1.0-0.60) = 2.6 \text{ watts} \qquad \text{(A11-61)}$$

The balance, 117 - 2.6 - 114 watts, must be copper losses in the rotor. This is indicative of an induction motor with a high resistance rotor, whose characteristic is as shown in Figure 86.

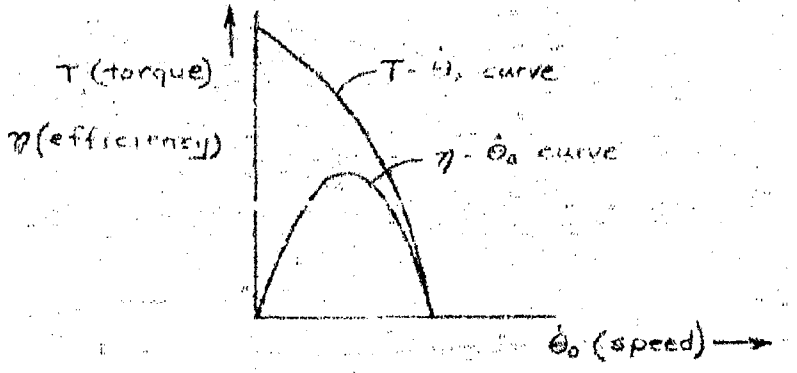

FIGURE 86 - INDUCTION MOTOR CHARACTERISTIC

Near stall, where this device is operating, efficiency is very low. The value of induction motor torque is the theoretical torque output less the actual

$$T = 2.23\ \eta_T - 0.25 = 1.1 \text{ n-m} \qquad \text{(A11-62)}$$

Apparently, the drop-off in torque, as speed increases, is so rapid that there is insufficient torque to overcome the tooth action and cause rotation in the other direction. It is reasonable to believe that the material and shape of the flexspline do result in a high resistance rotor.

Looking at it another way, this is a 1/2 h.p. motor, or 373 watts. For a peak efficiency of, say, 40% for a high resistance rotor at 1/2 synchronous speed, or 1800 rpm, and assuming that its efficiency with its usual rotor is 80%, torque output at 1/2 speed would be

$$T = \frac{\frac{373}{0.85}(0.30)}{1800\left(\frac{2\pi}{60}\right)} = 0.69 \text{ n-m} \qquad \text{(A11-63)}$$

and for an essentially straight-line torque-speed curve, at stall the torque would be

$$T = 2(0.69) = 1.38 \text{ n-m} \qquad \text{(A11-64)}$$

which is very close to the figure of 1.1 obtained above.

The above may constitute a reasonable explanation of the behavior of this device.

Overall efficiency is only

$$\eta_M = \frac{0.72}{291} = 0.2\% \qquad \text{(A11-65)}$$

It should also be mentioned that the torque output of the model, with the same voltage input, varied quite widely from as much as 0.7 in-lb down to the 0.2 in-lb obtained in the November, 1962 tests. In line with the above analysis, it does not seem that this could be entirely accounted for by a change in η_M, but a change in μ_2 is believed to have occurred. One of the problems, of course, is how to design the powder gap, core slots, and powder material so that it can move freely in and out of the gap and produce a high permeability when linked by flux.

XI-2 Optimization

Consider next what might be obtained if various of the negative aspects could be over come. Assume that the flexspline is made of plastic, that the powder has a permeability equal to that obtained in magnetic clutches, that the powder gap is decreased so that its minimum value, at which point flux is very low, is

equal to the Harmonic Drive deflection, that the powder is magnetized to its saturation point of 0.8 w/m^2 (beyond that would lower efficiency at a rapid rate), and that the stator bore is modified to give $\eta_m = 0.7$. The same number of turns will be retained. Then, for a three-phase device

$$\beta_m = \frac{2}{3}(0.8) = 0.53\ w/m^2 \quad \text{for one phase} \qquad \text{(A11-66)}$$

$$F_1/A_Q = \beta_m^2/2\mu_o = 1.1 \times 10^5\ n/m^2 \qquad \text{(A11-67)}$$

$$k_1 = \frac{4.4 - 0.4\pi}{4.4} = \frac{3.1}{4.4} = 0.70 \qquad \text{(A11-68)}$$

$$F_3/A_Q = k_1 F_1/A_Q = 7.8 \times 10^4\ n/m^2 \qquad \text{(A11-69)}$$

$$F_3 = 20.4\ n \qquad \text{(A11-70)}$$

$$F_T = 2 F_3\ 1.92 = 78\ n \qquad \text{(A11-71)}$$

$$T_1 = F_T D_p/\eta_T = 3.6\ n\text{-}m \qquad \text{(A11-72)}$$

$$T_2 = 2.75 T_1 = 9.1\ n\text{-}m = 82\ lb\text{-}in \qquad \text{(A11-73)}$$

This value gives $T/D_p^3 = 4.1$ which is considered satisfactory for plastic. Since there is no induction motor counter torque, useful power output is:

$$P_M = T_2 \dot{\theta}_M = 24\ watts \qquad \text{(A11-74)}$$

At the minor axis:

$$X_1 = X_2 + t = .0208 + .0208 + .014 = .056" \qquad \text{(A11-75)}$$

At $\theta_p = 20^\circ$

$$X_2 = .056 - .014 - .006 = .036" = 9.2 \times 10^{-4} m \qquad \text{(A11-76)}$$

$$\mathcal{R} = \frac{1}{A_Q}\left[\frac{X_1}{\mu_o} + \frac{X_2}{\mu_2}\right] = 12.6 \times 10^5\ w/a\text{-}t\text{-}m \qquad \text{(A11-77)}$$

Per phase

$$\Phi_m = 0.53(2.62 \times 10^{-4}) = 1.39 \times 10^{-4}\ w \qquad \text{(A11-78)}$$

For sinusoidal flux distribution

$$\Phi_{6m} = 0.24\,\Phi_m = 0.34 \times 10^{-4}\ w \qquad \text{(A11-79)}$$

$$i_{6m} = \frac{\mathcal{R}\,\Phi_{6m}}{N_4} = 0.65\ a \qquad \text{(A11-80)}$$

$$I_e = 0.707\ i_{6m} = 0.46\ a \qquad \text{(A11-81)}$$

$$e_{3m} = \frac{2\omega}{\mathcal{R}}(2.63 \times 10^5)\, i_{6m} = 102\ v \qquad \text{(A11-82)}$$

$$\therefore E_3 = 0.707\, e_{3m} = 72\ v.\ \text{for a half phase} \qquad \text{(A11-83)}$$

Since $I_2 = 0$ $\quad I_4 = I_e = 0.46\ a$ (A11-84)

and the stator copper loss per phase is:

$$P_2 = (0.46)^2\ 4.1 = 0.86\ \text{watts} \qquad \text{(A11-85)}$$

and the total is:

$$P_2 = 3(2)0.86 = 5.1\ \text{watts} \qquad \text{(A11-86)}$$

The main unknown factor is the eddy current loss. This should be far less than before optimization. Let us take it as 1/4 of the previous value.

$$P_1 = \frac{83}{4} = 21\ \text{watts} \qquad \text{(A11-87)}$$

Thus, the input power required is:

Eddy current loss P_1		= 21 watts
Stator copper loss, P_2		= 5.1 watts
Harmonic Drive output		= 24 watts
Harmonic Drive frictional loss	$= 0.30\frac{(24)}{0.7}$	= 10.3 watts
Total		60 watts

(A11-88)

Overall efficiency $\eta_2 = \frac{24}{60} = 40\%$ (A11-89)

which is a vast improvement over the model. This is based on the validity of the above assumptions, of course. One problem is that the voltage required may be greater than

provided by a 220^{V} (line to line) main, even though power is less than previously. A possible way to overcome this is to use a larger wire size, decreasing the resistance and the number of turns. It is not believed that performance would be degraded, based on study of the design equations of this analysis.

$$Re = P/I_e^2 = \frac{21/6}{(0.46)^2} = 16.6\ \Omega \qquad \text{(A11-90)}$$

$$Xe = E_e/I_e = \frac{\quad}{0.46} = \qquad \text{(A11-91)}$$

$$Ze = (Re^2 + Xe^2)^{1/2} \approx Xe = 313\ \Omega \qquad \text{(A11-92)}$$

Taking R_1 and X_1 the same as for the present model.

Then

$$R_1 + Re = 4.1 + 16.6 = 20.7\ \Omega \qquad \text{(A11-93)}$$

From before

$$X_1 = (Z_1^2 - R_1^2)^{1/2} = (8.7^2 - 4.1^2)^{1/2} = 8.2\ \Omega \qquad \text{(A11-94)}$$

$$X_1 + Xe = 8.2 + 313 \approx 313\ \Omega \qquad \text{(A11-95)}$$

The impedance of the entire circuit is

$$Z_t = [(R_1 + Re)^2 + (X_1 + Xe)^2]^{1/2} = 313\ \Omega \qquad \text{(A11-96)}$$

$$\therefore E_t = Z_t I_t = 313(0.46) = 144^{V} \text{ per half phase} \qquad \text{(A11-97)}$$

$$\text{and } E_t = 2(144) = 288^{V} \text{ per phase} \qquad \text{(A11-98)}$$

As this is more than the line to neutral voltage, a redesign with less turns, requiring more current is desirable.

$$\text{Power factor } (\cos \theta_e) = \frac{R_1 + Re}{Z_t} = \frac{20.7}{313} = .07 \qquad \text{(A11-99)}$$

XI-3 Inertia

The significant components are due to harmonic motion of the armature.

$$Ja = \tfrac{5}{16}\pi \rho\, b\, x_2 (D_p - x_2) D_p^2 \qquad \text{(A11-100)}$$

$$X_2 = 2.2 \times 10^{-3}\ m \qquad \text{(A11-101)}$$

$$\therefore J_a = 3.0 \times 10^{-4}\ kg\text{-}m^2 \qquad \text{(A11-102)}$$

and output-speed rotation of the armature (powder) and core

$$J_r = \pi/32\ \rho b\ D_p^{\ 4} = 5.0 \times 10^{-4}\ \text{kg m}^2 \qquad \text{(A11-103)}$$

giving a total inertia

$$J_M = 9.0 \times 10^{-4}\ \text{kg-m}^2 \qquad \text{(A11-104)}$$

XI-4 Performance Characteristics

The power rate and other important characteristics are given in Table XVIII.

XI-5 Model EHD-4

Briefly, the torque capability is only slightly less than that of the EHD-2 with the selected radial thickness of the link,

$$X_0 = 0.34" \qquad \text{(A11-105)}$$

Referring to Figure 14, equating the value of flux crossing the air gap in a 90° segment to the flux in the critical, most highly magnetized link

$$\sum_{90^\circ} \frac{B}{\beta m_{gap}}\ w\, b\, \beta m_{gap} = 0.34\, b\, \beta m_{link} \qquad \text{(A11-106)}$$

For 24 poles and a sinusoidal flux distribution

$$\sum_{90^\circ} \frac{B}{\beta m_{gap}} = 3.8 \qquad \text{(A11-107)}$$

Taking $\beta m_{link} = 2.0\ w/m^2$

$$\beta m_{gap} = 0.72\ w/m^2 \qquad \text{(A11-108)}$$

Thus,

$$T_M = \left(\frac{0.72}{0.80}\right)^2 8.1 = 6.6\ \text{n-m} = 58\ \text{lb-in} \qquad \text{(A11-109)}$$

The measured torque was 46% of the EHD-2, but voltage was only 83%. The lower torque results from the saturation effect and the reduced voltage. Basing total inertia on the following main components:

$$J_a = 1.8 \times 10^{-3}\ \text{kg-m}^2 \qquad \text{(A11-110)}$$

$$J_r = 4.2 \times 10^{-7}\ \text{kg-m}^2 \qquad \text{(A11-112)}$$

J_r is negligible and there is obtained

$$J_M = 1.8 \times 10^{-3}\ \text{kg-m}^2 \qquad \text{(A11-112)}$$

The measured current was 18% of the EHD-2, presumably due to the greater than expected air gap within the ring. However, it is believed that net reluctance could be made at least as low as the Improved EHD-2. Therefore, for the purposes of comparison, the same current will be used in Table XVIII.

APPENDIX XII

CALCULATIONS FOR SECTION 6

Load Characteristics For Section 6.2

From the open loop response with model EHD-3, at approximately 45° actuator phase shift

$$f = 30 \text{ cps} \qquad (A12-1)$$

$$\dot{\theta}_L = 10 \text{ rad/sec} \qquad (A12-2)$$

$$\ddot{\theta}_L = 2\pi(30)\dot{\theta}_L = 190 \text{ rad/sec}^2 \qquad (A12-3)$$

$$\tau_L = \dot{\theta}_L/\ddot{\theta}_L = 5.3 \times 10^{-2} \text{ sec} \qquad (A12-4)$$

Load Characteristics For Section 6.3

Assume a desired closed loop response of ± 1 db to 20 cps. This corresponds to about 70° to 75° phase margin at cross-over, or 15° to 20° phase shift. Thus the ratio of cross-over frequency to the reciprocal of the break frequency should be about 0.3. Hence the break frequency must be about 1/0.3 times, so that approximately

$$\tau_L = \frac{0.3}{20(2\pi)} = 2.4 \times 10^{-3} \text{ sec} \qquad (A12-5)$$

EHD 1 Data

At 9.6 rpm, rated power output is taken as

$$\frac{9.6}{18} \times 115 = 62 \text{ watts}$$

Current for these tests was 10 amps per magnet or less, so 10 amps is used in Sections 6.2 and 6.3.

Inland Torque Motor Type T-8001-A Data

The manufacturer's data states that the maximum speed should be "under 1 rev/sec." Consider a value of 1/2 this, or 30 rpm for the basis of calculating τ_M. Since T_M = 300 lb. in. for its general rating

$$\tau_M = \frac{\dot{\theta}_m J_M}{T_M} = 3 \times 10^{-3} \text{ sec} \qquad (A12-6)$$

For the comparison of Section 6.2, $\dot{\theta}_L = 9.6$ rpm, so the use of gearing is indicated to allow $\dot{\theta}_M$ to be 30 rpm. Thereupon power available in this application is

$$P_M = T_M \dot{\theta}_M = 120 \text{ w} \qquad (A12\text{-}7)$$

The motor is thus loaded down to about the same degree as the EHD-3.

The required P_M is 43 watts, for which

$$T_M = \frac{P_M}{\dot{\theta}_M} = 14 \text{ n-m} = 125 \text{ lb-in} \qquad (A12\text{-}8)$$

At this torque, I = 5 amps so that

$$I^2R = (5)^2 6.5 = 160 \text{ w} \qquad (A12\text{-}9)$$

This compares well with the EHD-3. Inertia and friction of the gearing have been neglected.

Slo-Syn Type X250-P1 Stepping Motor Data

The manufacturer's data states that the Slo-Syn motors can start and stop in .025 sec., so a τ_M of .006 sec. will be used. A reasonable velocity match is given by the integral planetary gearhead (4-1/3 to 1 ratio), for which maximum output speed is 16.6 rpm and torque is 41 lb-in. Thus at 9.6 rpm power output is 4.6 watts.

Size1-2F-162-2209-1 Servo Motor Data

The manufacturer's data shows:

$$\dot{\theta}_M = 5000 \text{ rpm at peak } P_M \qquad (A12\text{-}10)$$

$$T_M/J_M = 2440 \text{ rad/sec}^2 \qquad (A12\text{-}11)$$

$$\tau_M = \frac{\dot{\theta}_M J_M}{T_M} = 0.21 \qquad (A12\text{-}12)$$

Inland Torque Motor Type T-10004-A Data

For Section 6.3, this higher-rating unit is required. As with the smaller type, a $\dot{\theta}_M$ of 30 rpm will be used. Hence

$$\tau_M = 6 \times 10^{-3} \text{ sec.} \qquad (A12\text{-}13)$$

$$T_M/T_L = 2.5 \qquad (A12\text{-}14)$$

$$P_M/P_L = 4\, T_M/T_L = 10 \qquad (A12\text{-}15)$$

$$P_m = T_m \dot{\Theta}_m = 425 \text{ w} \qquad \text{(A12-16)}$$

Assuming that P_M required = P_M available, allowing for the gear friction loss peak current required is 16.2 amps and I^2R loss is

$$I^2R = (16.2)^2 4 = 1050 \text{ w} \qquad \text{(A12-17)}$$

APPENDIX XIII

DEFORMED-DISC HARMONIC DRIVE

Given a disc which is buckled, or deformed, into a lobe pattern as shown in Figure 87 (A), it can be mathematically shown that the orbit of motion of a particle on the surface at radius r_o is a figure-of-eight of geometry shown by Figure 87 (B).

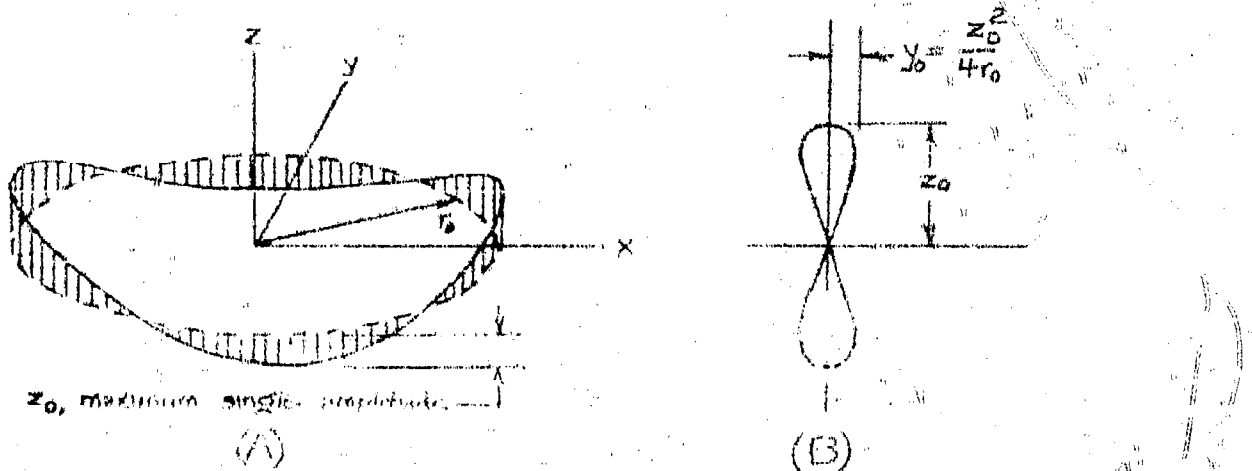

FIGURE 87 - DEFORMED DISC HARMONIC DRIVE

From Figure 87(B)

$$\frac{y_o}{z_o} = \frac{z_o}{4r_o} \qquad (A13\text{-}1)$$

But for such a disc

$$z_o \ll r_o \qquad (A13\text{-}2)$$

In general, then

$$\frac{y_o}{z_o} \ll 1 \qquad (A13\text{-}3)$$

and the circumferential shift, y_o, is small. Of course, operation as a friction device producing Harmonic Drive appears possible, but linearity and accuracy would be poor as with any friction drive involving deflections. In order to put teeth on the disc, it is necessary for:

$$y_o = \tfrac{1}{2} P_c \qquad (A13\text{-}4)$$

where P_c circular pitch $= \pi / P_D$ (A13-5)

P_D diametral pitch

As a practical measure, teeth finer than 150 Dp are expensive and of questionable reliability. But these are not fine enough to be useful here; so let us consider an even finer pitch of 256.

$$P_c = \pi/P_D = \pi/256 = .012" \quad (A13\text{-}6)$$

$$y_0 = .006" \quad (A13\text{-}7)$$

$$z_0^2 = 4 r_0 y_0 = .024 r_0 \quad (A13\text{-}8)$$

$$z_0 = 0.155 \sqrt{r_0} \quad (A13\text{-}9)$$

Since

$$R_g = \frac{N}{\Delta N} = \frac{N}{2} \quad \text{for } \Delta N = 2 \quad (N, \text{ number of teeth}) \quad (A13\text{-}10)$$

and

$$N = D_p P_D = 2 r_0 P_D = 512 r_0 \quad (A13\text{-}11)$$

Then

$$R_g = \frac{512 r_0}{2} = 256 r_0 = P_D r_0 \quad (A13\text{-}12)$$

Consider three possible sizes, as shown in Table XXXII

	P_R		
	100:1	200:1	400:1
r_0	0.39	0.78	1.56
$\sqrt{r_0}$	0.62	0.88	1.25
z_0	0.96	0.136	0.194
z_0/r_0	0.246	0.175	0.125

TABLE XXXII - DEFORMED DISC HARMONIC DRIVE PARAMETERS

The practicability of obtaining these amounts of deformation is doubted, for other than extremely thin material which would not have the capability of very high torque.

APPENDIX XIV

CALCULATIONS OF SCALING FACTORS

K_1 and Utilization Factor, U

This factor represents the proportion of the gross pole area that can be used for a magnet, when a constant clearance, u, between magnets is used.

For the SF type, u is taken as 1/4 inch. (6.4×10^{-3}m) and the number of magnets is taken as 16 for all sizes. Thus:

$$U = \frac{\frac{\pi D_p}{16} - u}{\frac{\pi D_p}{16}} = 1 - \frac{16u}{\pi D_p} = 1 - \frac{3.3 \times 10^{-2}}{D_p} \qquad (A14\text{-}1)$$

$$\therefore K_1 = 3.3 \times 10^{-2} \qquad (A14\text{-}2)$$

For the RF type, u is taken as 0.170" (4.32×10^{-3}m) and the number of stator pole slots as 24, corresponding to model EHD-2, for all sizes.

Thus:

$$U = 1 - \frac{24u}{\pi D_p} = 1 - \frac{3.3 \times 10^{-2}}{D_p} \qquad (A14\text{-}3)$$

$$\therefore K_1 = 3.3 \times 10^{-2} \qquad (A14\text{-}4)$$

K_2 and Mean Torque, T_M

It is first shown that T_M varies as the product of U and D_p^3. Assume that b (leg axial width) increases linearly with D_p, w (magnet circumferential width) is proportional to $D_p U$, and the lever's mechanical advantage remains constant.

The produce of these is A_Q which is proportional to F_M for constant β.

T_M is proportional to $F_M D_p$.

Therefore:

$$T_M = K_2 U D_p^3 \qquad (A14\text{-}5)$$

For model EHD-3, with a single step

$$T_M = 60 \text{ n-m}, \quad D_p = 8.25 \times 10^{-2} \text{ m}, \quad U = 1 - \frac{3.3 \times 10^{-2}}{8.25 \times 10^{-2}} = 0.6 \qquad (A14\text{-}6)$$

$$K_2 = \frac{60}{241}$$

$$\therefore K_2 = 1.75 \times 10^5 \qquad \text{(A14-7)}$$

with a double step, T_M = 73 n-m and

$$K_2 = \left(\frac{73}{50}\right) 1.75 \times 10^5 = 2.14 \times 10^5 \qquad \text{(A14-8)}$$

For model EHD-2 (modified)

$$T_M = 8.2 \text{ n-m}, \; D_p = 6.6 \times 10^{-2} \text{ m}, \; U = 0.50 \qquad \text{(A14-9)}$$

$$\therefore K_2 = \frac{T_M}{U D_p^3} = 5.6 \times 10^4 \qquad \text{(14-10)}$$

K_3 and Inertia, J_M

It was shown in Section 3 that J_M varies substantially as D_p^5.

For EHD-3, $J_{M_1} = 1.2 \times 10^{-2}$ kg-m^2, $D_p = 8.25 \times 10^{-2}$m

$$\therefore K_3 = \frac{J_{M_1}}{D_p^5} = 3.2 \times 10^3 \qquad \text{(A14-11)}$$

For EHD-2 (modified) $J_{M_1} = 9.0 \times 10^{-4}$ kg-m^2

$$\therefore K_3 = \frac{J_{M_1}}{D_p^5} = 720 \qquad \text{(A14-12)}$$

K_4 and Output Speed, $\dot{\theta}_M$

For EHD-3, with a single step, based on $\dot{\theta}$ = 100 steps/sec.

$$\dot{\theta}_M = 1000 \frac{\text{steps}}{\text{sec.}} \times \frac{\text{input rev.}}{16 \text{ steps}} \times \frac{\text{output rev.}}{Rg \text{ input rev.}} \times 2\pi \frac{\text{rad.}}{\text{rev.}}$$

$$\text{But } Rg = 1900 \, D_p$$

$$\dot{\theta}_M = 0.21/D_p \qquad \text{(A14-13)}$$

$$\therefore K_4 = 0.21 \qquad \text{(A14-14)}$$

For the double step $\dot{\theta}_M$ and K_4 double.

For RF types

$$\dot{Q}_M = \frac{f}{R_E}$$

$$R_E = 1900\ D_p$$

For f = 50 cps

$$\dot{Q}_R = 2.1 \times 10^{-2}/D_p = \frac{60(27)}{1900\ D_p} = 0.20/D_p \qquad (A14\text{-}15)$$

$$\therefore K_4 = 0.21 \qquad (A14\text{-}16)$$

K_5 and i_m^2 R loss

Assume that MMF is proportional to Dp. Since i_m is to be constant, N is proportional to Dp. The mean length of turn is porportional to A_Q or U D_p^2. Using a constant wire size, R is therefore proportional to U D_p^3. Thus i_m^2 R is also proportional to U D_p^3. For EHD-3, $(i_m^2 R)_m$ = 180 watts

$$\therefore K_5 = 5.2 \times 10^5 \qquad (A14\text{-}17)$$

For EHD-2 (modified) i_m^2 R = 5 watts

$$\therefore K_5 = 3.4 \times 10^4 \qquad (A14\text{-}18)$$

K_6 and Voltage, E

This is a function of the IR drop plus the back-emf voltage, combined properly for the waveforms or phase angles involved. As voltage varies for the SF type with the angle, and is quite complex for the RF type, only an order of magnitude is calculated here, based on the assumption that voltage varies with D_p^2 (Both resistance R and inductance roughly vary in this way).

For EHD-3, an approximate peak voltage of 80 volts is estimated for this speed. Thus:

$$K_6 = 1.2 \times 10^4 \qquad (A14\text{-}19)$$

For EHD-2 (modified) E = 290 V rms. Thus:

$$K_6 = 6.7 \times 10^4 \qquad (A14\text{-}20)$$

K_7 and Volume, V, also K_8 and weight, Wt

From one viewpoint volume and weight would scale as D_p^3. However, there are certain elements that possess a minimum size regardless of the actuator size, and these would not increase at quite so large a rate. Hence for simplicity consider that volume and weight scale the same as torque, i.e. the ratio of torque to volume and torque to weight remains constant. Furthermore, an assessment is made of the reduction in size and weight that should be obtained with the present models through design refinement.

These constants are calculated as follows:

For the EHD-3, $V = 240\ in^3 = 3.9 \times 10^{-3} m^3$, Wt = 22 lbs. = 10 kg

Assume that both can be reduced by 10%

$$\therefore K_7 = \frac{K_2}{T_M} V \times 0.90 = 1.1 \qquad \text{(A14-21)}$$

$$\therefore K_8 = \frac{K_2}{T_M} Wt \times 0.90 = 2.7 \times 10^4 \qquad \text{(A14-22)}$$

For EHD-2 (modified) $V = 190\ in^3 = 3.1 \times 10^{-3}\ m^3$

$$Wt = 16 \text{ lbs} = 7.2 \text{ kg}$$

Assume that both can be reduced by 50%, considered a reasonable figure since no attention was given to light - weighting or miniaturization in the project.

$$\therefore K_7 = \frac{K_2}{T_M} V \times 0.50 = 10 \qquad \text{(A14-23)}$$

$$\therefore K_8 \quad \frac{K_2}{T_M} Wt \times 0.50 = 2.8 \times 10^3 \qquad \text{(A14-24)}$$

Aeronautical Systems Division, Flight Control Lab, Wright-Patterson AFB, Ohio.
Rpt No. ASD-TDR-63-486. ELECTROMAGNETIC HARMONIC DRIVE LOW INERTIA SERVO ACTUATOR. Final report, Dec 63, 144 p. incl illus., tables, 46 refs.

Unclassified Report

The feasibility of a new type of low inertia electrical servo actuator, designated Electromagnetic Harmonic Drive, is determined. Drastic reduction in inertia, compared to conventional electrical devices, advances the state-of-the-art in regard to power rate to weight, and power rate to electrical loss characteristics, which are shown to best determine the usefulness of an actuator for fast

(over)

1. Actuators
2. Servomechanisms
3. Electromagnetic Drives
4. Control Systems
5. Digital Systems

I. APCS Project 8225, Task 822503
II. Contract AF 33(657)-7753
III. United Shoe Machinery Corp.
Harmonic Drive Division
Beverly, Mass.
IV. Hertog, D. F.
Proctor, R. W.
Spring, W. B.
Newton, G. C., Jr.
V. Not avail fr OTS
VI. In ASTIA collection

Aeronautical Systems Division, Flight Control Lab, Wright-Patterson AFB, Ohio.
Rpt No. ASD-TDR-63-486. ELECTROMAGNETIC HARMONIC DRIVE LOW INERTIA SERVO ACTUATOR. Final report, Dec 63, 144 p. incl illus., tables, 46 refs.

Unclassified Report

The feasibility of a new type of low inertia electrical servo actuator, designated Electromagnetic Harmonic Drive, is determined. Drastic reduction in inertia, compared to conventional electrical devices, advances the state-of-the-art in regard to power rate to weight, and power rate to electrical loss characteristics, which are shown to best determine the usefulness of an actuator for fast

(over)

response, light weight, efficient servo systems. A fundamental analysis is made of the requirements for optimizing these parameters.

Two forms offer the most promise. The first is a stepping device which offers all the advantages of digital control systems and the higher response capability. The second is a synchronous device with constant torque output but a somewhat lower response capability.

Following detailed analyses of both types, models were designed, manufactured, tested and evaluated in comparison with conventional devices. Examples of applications are given, typical of aeronautical systems as well as other fields. Implications upon electrical control systems, resulting from the advance in performance provided by the new device, are discussed.

response, light weight, efficient servo systems. A fundamental analysis is made of the requirements for optimizing these parameters.

Two forms offer the most promise. The first is a stepping device which offers all the advantages of digital control systems and the higher response capability. The second is a synchronous device with constant torque output but a somewhat lower response capability.

Following detailed analyses of both types, models were designed, manufactured, tested and evaluated in comparison with conventional devices. Examples of applications are given, typical of aeronautical systems as well as other fields. Implications upon electrical control systems, resulting from the advance in performance provided by the new device, are discussed.

1. Actuators
2. Servomechanisms
3. Electromagnetic Drives
4. Control Systems
5. Digital Systems

I. APCS Project 8225, Task 822503
II. Contract AF 33(657)-7753
III. United Shoe Machinery Corp.
Harmonic Drive Division
Beverly, Mass.
IV. Hertog, D. F.
Proctor, R. W.
Spring, W. B.
Newton, G. C., Jr.
V. Not avail fr OTS
VI. In ASTIA collection